University of Strathclyde
Department of Pure and Applied Chemistry

Simultaneous Detection of Multiple Explosives Using Surface Enhanced Raman Scattering

By Rachel Norman

A thesis submitted to the Department of Pure and Applied Chemistry, University of Strathclyde, in fulfilment of the requirements for the degree of Doctor of Philosophy.

March 2016

This thesis is the result of the author's original research. It has been composed by the author and has not been previously submitted for examination which has led to the award of a degree. The copyright of this thesis belongs to the author under the terms of the United Kingdom Copyright Acts as qualified by University of Strathclyde Regulation 3.50. Due acknowledgement must always be made of the use of any material contained in, or derived from, this thesis.

Signed: Date:

Acknowledgements

Abstract

There remains a continuing threat of terrorist/insurgent attacks on military/civilian personnel and key strategic infrastructures both within the UK mainland and in operational theatres. The development of a novel, innovative, low cost, field deployable bionanosensor, which will have the capability to detect low levels of explosive in a multiplexed fashion is required. The use of the specific interaction between small molecules and biological capture molecules such as antibodies coupled with the detection technique of surface enhanced Raman scattering (SERS) allows a 'one shot' analysis.

This research makes use of antibody functionalised silver nanoparticles for the detection of the explosives TNT, RDX and PETN by surface enhanced Raman scattering (SERS). Commercially available antibodies specific for TNT and RDX have been modified to specifically orientate 'flat' on the surface of silver nanoparticles bringing the target close enough to the metal surface to allow an intrinsic SERS signal of the target molecule to be obtained. Quantitative detection of TNT and RDX explosives was achieved, with pM sensitivity demonstrated for RDX. Furthermore, TNT was detected in two different types of dirt, natural and synthetic dirt in order to mimic a more realistic matrix in which TNT would be found in the field.

However, for the detection of PETN, it was required to develop a method to modify a PETN antibody in-house, to specifically orientate 'flat' on the nanoparticles surface similarly to the commercially available antibodies. This was achieved by using carbodiimide chemistry and the antibody was purified by cartridge centrifugation and HPLC. The PETN modified antibody was then functionalised onto silver nanoparticles and detection of PETN was achieved by SERS. In addition, PCA was used to allow

multiplexed analysis based on unique Raman bands for the three different explosives which could be clearly identified in the SERS spectra.

Finally, TNT was detected by using magnetic nanoparticles which were functionalised with a terminal amine group in combination with FITC modified TNT antibody functionalised silver nanoparticles. This assay was designed to allow for the formation of a Meisenheimer complex in the presence of TNT, between the amine functionalised magnetic nanoparticles and the TNT. Furthermore, the TNT antibody functionalised silver nanoparticles also binds to TNT, aggregating the nanoparticles. The magnetic nanoparticles were subsequently used to remove the nanoparticle assembly from the matrix, resulting in a concentrated sample on the magnet, resulting in an increase in SERS.

Abbreviations

Ag@MNPs	silver coated magnetic nanoparticles
$AgNO_3$	silver nitrate
AgNP	silver nanoparticles
BCA	bicinchoric acid
BSA	bovine serum albumin
CCD	charge-coupled device
CT	computer tomography
DNA	deoxyribonucleic acid
DLS	dynamic light scattering
DNT	2, 6 – dinitrotoluene
DTT	dithiothreitol
EDC	1 – ethyl – 3 – (3 – dimethylaminopropyl)carbodiimide hydrochloride
EDTA	ethylene diamine tetraacetic acid
F_{ab}	fragment, antigen binding domain
FAM	fluoroscein
F_c	fragment, crystallisation domain
FITC	fluorescein isothiocyanate
FRET	Förster resonance energy transfer
FT	Fourier transform
FWHM	full width half maximum
HCl	hydrochloric acid
HMTD	hexamethylene triperoxide diamine
HPLC	high performance liquid chromatography

IgG	immunoglobulin G
MIPs	molecular imprinted polymers
NaCl	sodium chloride
NaBH$_4$	sodium borohydride
NaOH	sodium hydroxide
NHS	N- hydroxysulfosuccinimide
NIR	near infra-red
PBS	phosphate buffered saline
PEG	polyethylene glycol
PETN	pentaerythritol tetranitrate
QCL	quantum cascade lasers
RDX	research department explosive (1, 3, 5 - trinitroperhydro – 1, 3, 5 – triazine)
RP	reverse phase
Rpm	revolutions per minute
SEC	size exclusion chromatography
SERS	surfaced enhanced Raman spectroscopy
SERRS	surfaced enhanced resonance Raman spectroscopy
(L)SPR	(local) surface plasmon resonance
SWCNT	single wall carbon nanotube
TATP	triacetone triperoxide
TMDD	tetramethylene diperoxide dicarbamide
TNT	2, 4, 6 - trinitrotoluene
UV	ultraviolet
UV-vis	ultraviolet visible

Contents

1.   Introduction

1.1   An Introduction to Explosives

There remains a continuing threat of terrorist/insurgent attacks on military/civilian personnel and key strategic infrastructures both within the UK mainland and in military operational theatres. Many such attacks involve the use of military, commercial or home-made explosives. The Office for Security and Counter Terrorism have updated our national security to severe, meaning 'the threats we face now are more diverse than ever before.'[1] The nature of this threat is constantly evolving; therefore it is becoming more difficult to detect explosive threats. A state of the art, rapid and portable method is required to detect trace explosive materials in real time.

Legislation defines an explosive as '*a substance or mixture of substances which may be made to undergo a rapid chemical change without an outside supply of oxygen, with the liberation of large quantities of energy, generally accompanied by the evolution of hot gases.*'[2]

There are four basic types of explosion; mechanical, chemical, nuclear and electrical. Chemical explosions are the most common and this thesis will focus on chemical explosions. When an exothermic chemical reaction proceeds slowly, the release of energy will be dissipated to the surrounding medium, therefore only a very small change in the environment will be observed.[3] However, when an exothermic reaction proceeds very rapidly, and the energy is confined to a small volume, it will manifest itself by expansion of hot gases. This will create a shock wave and propel any objects in the vicinity at high speed.[4] The majority of the energy evolved in an explosive reaction is from the oxidation process; therefore the amount of oxygen available is crucial. The speed at which the material is oxidised allows the explosives to be classified as either high or low explosives. High explosives react very violently, resulting in detonation; this involves the expansion of gas travelling at supersonic speeds, typically greater than 7000 meters per second.[5] Examples of high

explosives include 2, 4, 6 – trinitrotoluene (TNT), 1, 3, 5 – trinitroperhydro – 1, 3, 5 –triazine (RDX) and [3-nitrooxy-2,2-bis(nitrooxymethyl)propyl] nitrate (PETN). Low explosives react more slowly and deflagrate at subsonic speeds, usually lower than 2000 meters per second. Examples of low explosives include gun powder and fireworks. Rates of detonation between 2000 and 7000 meters per second are classified as industrial explosives, more commonly known as detonators or blasting agents. These include dynamite, emulsion and slurry. Although the oxidation process produces the largest amount of energy involved in the explosion, there is usually an initial input of energy required, this is known as a detonator. Depending on the stability of the material, mechanical impact or force can supply enough energy to detonate, in other cases higher energy, such as heat, is required. The energy required to detonate an explosive further classifies the material: primary explosives,[6] which are very sensitive and secondary explosives, which require larger amounts of energy to detonate.[7]

A detonator is a compact device which initiates a larger explosion.[8] The two main forms of detonators are chemical and electrical. Chemical detonators are usually unstable explosive materials which upon detonation will then initiate the larger explosion. Typical chemical detonators are dynamite, blasting gelatine, emulsion and slurry. Dynamite consists of a blend of nitroglycerine and nitroglycol.[9] An oxidiser, such as ammonium nitrate and a fuel, such as sawdust or wax is required. Nitrocellulose is then used as a thickening agent in dynamite to bind all the components together. Dynamite can then spontaneously detonate, or can be mechanically detonated with a plunger attached to a fuse which will trigger a spark, or by simply lighting it. Blasting gelatine is an explosive material, consisting of nitrocellulose dissolved in nitroglycerine, mixed with sodium or potassium nitrate. Emulsion explosives are a mixture of oxidisers and fuels which exists as a finite dispersion in oil. A slurry is mixture of fine explosive materials in a semi liquid matrix. Electrical detonators are slightly more sophisticated, as they can be designed to detonate the explosive at a specific time. The most common type of electrical detonator uses batteries. When switched on, current from the batteries heats up a

high resistance wire which then ignites a fusehead. This results in the detonation of the larger explosive.

1.2   Explosive Materials

The first documented explosive material discovered was gun powder, originating in China in the 10th century.[10] Gun powder is composed of a mixture of potassium nitrate, sulfur and carbon. It is a classic example of a low explosive, in which an oxidant and combustible substance is required to produce heat, light and sound which typically propels projectiles and rockets.[11]

High explosives on the other hand cover a range of materials and can be further divided into primary and secondary. Primary explosives are extremely sensitive to stimuli such as electromagnetic radiation, friction, heat or impact.[6] Examples of primary explosives include molecular azides,[12] peroxides and xenon based solutions.[13, 14] However, secondary explosives require substantially more energy to detonate, therefore they are usually more stable than primary explosives, hence they require a more powerful detonation.[7] It is for this reason that secondary explosives are used in wider applications such as demolition,[15] mining[16] and military purposes.[4]

Explosives can also be classified further by their chemical structure: inorganic salts, oxidising/reducing agents, organic peroxides and nitro based organics. Inorganic explosive devices have been used in many attacks, and more importantly these inorganic precursors are readily available, affordable and can be purchased legally.[17] Inorganic devices mainly comprise a mixture of strong inorganic oxidisers for example: nitrate, sulfate or chlorate [17] and a fuel such as diesel or sugar.[18] Another class of explosives are organic peroxides. These explosives are classed as primary explosives as they are typically unstable and as a result have unpredictable behaviour, but are easily manufactured. Triacetone triperoxide (TATP), hexamethylene triperoxide diamine (HMTD) and tetramethylene diperoxide dicarbamide (TMDD) are examples of these high energy dangerous materials.

A major class of explosives are nitro based compounds. Nitro explosive compounds decompose with a large excess of energy upon detonation,[19] and this class can be further sub divided into aromatic nitro compounds, nitrate esters and nitramines. Nitroaromatics are mutagenic and carcinogenic substances which are dangerous to mammalian systems.[20] After detonation, nitroaromatics are present in the environment, which can then be taken up by soil or human skin. This is detrimental to our ecosystem, as the mutagenic and carcinogenic substances can be uptaken by plants.[21] Moreover, 17,000 cases of nitroaromatic poisoning were reported after the First World War, with 500 people reported dead due to liver damage and anaemia.[22]

TNT is a nitroaromatic molecule which was used in the First World War. TNT was first discovered in 1863 and was used as a yellow dye.[23] It was not until 20 years later its explosive properties were known. TNT is commonly used today in applications such as underwater blasting,[24] for military purposes such as missiles and weapons, landmines[25] and in bombs.[26] TNT is a small molecule with a molecular weight of only 227.13 g/mol, as shown in Figure 1.1.
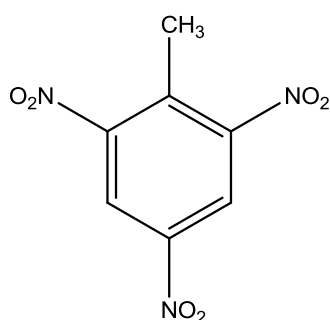
Figure 1.1: Structure of 2, 4, 6-trinitrotoluene.

Trinitrotoluene is widely used as an explosive because of its stability and it is insensitive to shock therefore it can be safely stored until required, which means it requires a detonator in order to cause an explosion.[27] Upon detonation TNT undergoes the following decomposition:

$$4\ C_7H_5N_3O_6 \rightarrow 6\ N_2 + 10\ H_2O + 7\ CO_2 + 21\ C \quad \text{or}$$
$$4\ C_7H_5N_3O_6 \rightarrow 6\ N_2 + 10\ H_2O + 14\ CO + 14\ C$$
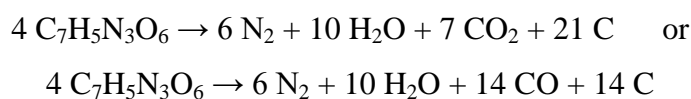
At high temperatures or pressure the equilibrium favours CO_2/CO formation and a high energy explosion is produced. The reaction is exothermic but also has a high activation energy. The driving force for the reaction is the formation of the major gaseous products, H_2O, N_2 and CO. The decomposition of TNT depends on the temperature or pressure used to detonate, lower temperatures/pressures results in a slower release of energy which favours the formation of solid products, such as diamond and graphite rather than gas.

As previously mentioned, indiscriminate use of TNT is occurring more frequently around the world due to war and terrorist activities. The use of TNT in landmines is becoming increasingly common, with the ultimate impact of landmines ending lives or inflicting life limiting injuries. It is estimated that there are 150-300 million landmines scattered around the world, and huge amounts of money is spent attempting to clear these sites.[28] For example, outside of a US military base in Kandahar, Afghanistan, insurgents surrounded their base with landmines intending to end the life of soldiers who stood on the buried explosives. Eight teams of landmine detector dogs were then employed to 'sniff' out any potential threats.[29] Sniffer dogs are highly effective at detecting explosives and it was reported by this military base in 2005, that over 2000 landmines were positively detected by sniffer dogs. However, the dogs require training, which is time-consuming and the dog may also be trained to only positively identify one explosive compound, when the reality is many explosive materials can be used in landmines. Furthermore, sniffer dogs may not always be available for out in the field detection, for example in war zones, therefore a detection method which is fast and can detect numerous threats simultaneously is highly desirable.

RDX is a nitroamine explosive that has a higher energy detonation in comparison to TNT and PETN.[30] RDX was first discovered and patented in 1898 by Georg Friedrich Henning in Germany.[31] RDX is much more stable than TNT, so much so that it is unaffected by arms fire, hence, RDX was used widely in World War II and is still used to this day as a base of a number of military explosives. RDX, which is

shown in Figure 1.2, is also used for controlled demolition of buildings. In April 2006, just 34 kg of RDX was required to demolish Jamestown Bridge, Rhode Island, which was 2100 m long.
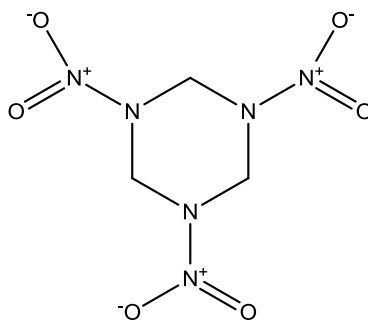
Figure 1.2: Structure of RDX.

RDX is detonated in a similar way to TNT as it also requires a high temperature or pressure, the decomposition reaction is shown below:

$$C_3H_6N_6O_6 \rightarrow 3CO + 3H_2O + 3N_2$$

As for TNT, the decomposition involves the formation of gaseous products, CO and N_2, as driving forces. As mentioned RDX, is far more stable than TNT, therefore RDX has been more widely used in terrorism. The first report of RDX being used in terrorist bombings was in the 1993 Bombay bombings.[32] Thirteen co-ordinated car bomb attacks occurred in Bombay, killing 257 people and over 1000 people were injured. This is reported to be the first ever serial blast in the world, and is the most destructive explosion in Indian history. Since 1993, many other bombings have been reported to have used RDX such as the 2004 Russian aircraft bombings,[33] 2006 Mumbai train bombings [34] and the 2010 Moscow metro bombings. Therefore a portable test which can be used to rapidly detect this dangerous material in public places is highly desired.

Another example of an explosive is pentaerythritol tetranitrate (PETN) shown in Figure 1.3.[35]
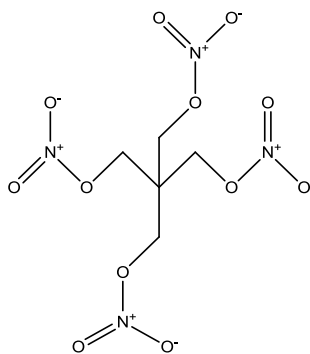
Figure 1.3: Structure of PETN.

PETN is one of the most powerful nitro based explosives. It has even more increased stability compared to TNT and RDX, therefore a stronger detonator is required as the high temperatures and pressures required for detonation of PETN are harder to achieve. Upon detonation PETN undergoes the following decomposition:

$$C_5H_8N_4O_{12} \rightarrow C_5H_8N_3O_{10}^- + NO_2$$

PETN is usually mixed with TNT or RDX as their initial explosion can then detonate PETN. When PETN is mixed with RDX in the appropriate solvent an explosive plastic mixture is formed, known as Semtex. By forming this mixture, the plastic explosive can be moulded into unusual shapes allowing it to be easily concealed therefore this approach has been used in several terrorist acts. PETN mixtures are known to have been used in several bombings such as the 'shoe bomber' in 2001.[36] This was a failed bombing attempt on an aircraft, PETN and TNT were present in the suspects shoes along with a fuse. Although the suspect had lit a match, the explosive failed to detonate due to the suspects excessive feet perspiration stabilising the explosive material. Explosives that are in liquid form are far more stable and require a higher energy detonator; this is due to the atoms being in a metastable state. More recently, in 2009, the 'underwear bomber' suspect had a six inch packet containing a mixture of PETN and acid sewn into their underwear.[37] Under a blanket the suspect lit a match on his trousers. Fortunately, a fellow passenger noticed the fire on the suspect and raised the alarm before detonation. In the 20th and 21st century an ongoing armed movement in UK and Ireland known as the Irish Republican Army (IRA), dedicated to Irish republicanism, used explosive materials. In 1930's, the IRA

attempted a bombing campaign on the UK and Northern Ireland, in which Semtex was commonly used, in the hope that Ireland would become republic. Despite officially becoming republic of Ireland in 1949, the IRA was reported as recently as 1996, being in possession of over 3 tonnes of Semtex.

TNT, RDX and PETN are commonly used as weapons of destruction by terrorists and insurgents therefore this thesis will focus on the detection of these nitro based explosive materials at trace levels with a view of integrating this approach into portable detection methods.

1.3   Current Methods of Detecting Explosives

The most common visual method of explosive detection currently used is x-ray screening.[38] This is based on the similarities of the visual form and density of the suspected explosive material to the surrounding item. This method relies on interrogating a sample with two different frequencies of x-ray and observing any visual differences in the density of the sample. However, this method depends solely on visual analysis by trained man power and a substantial difference in density of the explosive material being analysed, which is not ideal. After the attack on the world trade centres, the American Federal Government passed the Aviation and Transportation Act,[39] which requires 100% inspection of luggage passing through USA airports. Furthermore, The European Civil Aviation Conference implemented 100% screening of all luggage at all international airports in the European Union.[40] In 2002, it was estimated that 100 million suitcases were required to be scanned throughout the USA.[41] Therefore an automated system was required in order to vigilantly inspect all suitcases. X-ray diffracted computated tomography (CT) produces relatively high resolution slices of x-ray images, based on the differences in the diffraction patterns, generated by using an incident laser beam at angles from 0 to 180°.[42] The computer then assesses the x-ray image obtained and uses an algorithm to determine if the luggage requires further investigation. Whilst this automated system massively reduces the amount of trained man power required, it regularly produces false positives. False positive statistics for x-ray diffraction computed tomography are not publicly available, however, it has been suggested that an

average of 30% of suitcases produce a false positive result.[41] Items reported to give false positives are: peanut butter,[43] toothpaste, chocolate and any items the x-rays cannot penetrate, such as laptops and mobile phones.[41] Moreover, the instrument cost is around hundreds of millions of pounds and the large amount of false positives result in the requirement for a hand search by a trained individual, which further increases the cost of applying this approach. This method is most suitable to luggage in airport situations, it is not possible for in field or on individuals' detection due to the portability of instrumentation.

A more sensitive technique commonly used in airport screening is ion mobility spectroscopy.[44] This method can detect vapour or particulate samples. The sample is introduced into the system and the particulates are ionised based on their mobility in the buffer gas, separation of the ions then occurs based on mass. Therefore heavier ions are eluted more slowly and lighter ones faster. This system is widely used in airport situations as a swab can be taken from luggage and the particulates can be analysed. These systems are reported to be capable of ng detection of TNT, due to the molecules thermal and chemical stability when being ionised.[45] RDX however, is harder to prepare as a vapour due to the activation energy required to volatise it. Subsequently, less data is available for RDX. [44] PETN is the hardest challenge for explosive detection using ion mobility spectroscopy.[46] This is due to PETN having an activation energy almost three times higher than that of TNT, resulting in PETN thermally decomposing upon volatilisation. Furthermore, these systems are designed to detect explosives which have nitrogen groups present, therefore they are not able to detect home-made explosive devices containing other explosive materials. Moreover, temperature and moisture of the sample have been shown to influence the response and mobility of the sample, resulting in false positives, especially in soil samples.[44] Additionally, these systems rely on the expertise of the person running the test who normally have minimal training.

Other methods of detection use vapour collection systems to sample the air space. Vapours in trace detection of explosives are obtained by using heat to increase the volatility of explosives, known as thermal desorption, to allow separation of the

vapour from the source. A technique is then used to detect the vaporised explosive, such as gas chromatography.[47] Gas chromatography separates ions in a column depending on polarity of the molecules, detection can then be obtained by mass spectroscopy, where ions are detected dependant on the charge to mass ratio of the ion. When electron withdrawing groups, such as NO_2, elute from the column, they form a negative species. When an electron capture detector is present, a pulsed voltage is applied, in which the frequency of the pulses is changed to maintain a constant voltage in the presence of electron capturing analytes. The change in frequency is proportional to analyte concentration.

Another vapour detection technique commonly used is trained sniffer dogs.[48] It is well documented that dogs have a very sensitive nose, as they can identify odorant signatures of molecules.[49] Whilst sniffer dogs are fast and can detect low concentrations of explosives, they require intensive training and are not always reliable. They can produce many false positives, which could be a result of operator influence or non-specific identification of the explosive. These vapour collection and pressure techniques require large sample volumes, they are not explosive specific, they can only identify the presence of a class of explosive, which is also not ideal for trace material detection, especially of home-made explosives.

In 2010 Cascade Technologies installed a novel detection device in Glasgow Airport.[50] The device was designed to detect explosive gaseous vapours using quantum cascade lasers (QCL). QCL are a unique class of semi-conductor lasers designed to emit in the near IR region. In QCL, the excitation transition occurs in states given in a quantum well, opposed to between the conduction and valence band as occurs in a diode laser excitation. Subsequently, this allows for the emitted photon to tunnel into the next quantum well, resulting in multiple scattered photons from one electron. Thermal imaging can then be used to detect the explosive since each explosive compound absorbs IR light, the energy re-emitted is usually anisotropic, as heat. Each explosive will have a unique IR absorption, therefore specific images unique to each explosive can be obtained. However, the device was only successful

in detecting hydrogen peroxide and ammonia, therefore it was not ideal for detection of multiple target explosive materials.

Colourimetric sensors are widely used in the field by the military, they rely on a chemical reaction between the explosive and an indicator molecule to produce a colour change.[51] Lateral flow strips can be used for colourmetric detection of explosive materials. Typically a lateral flow strip consists of porous paper which allows the transport of fluid, to a conjugate pad on the strip. The conjugate pad has a recognition biomolecule specific for the explosive, typically an antibody, immobilised on the surface. Therefore, when a target is absorbed in the lateral flow, it will conjugate to the antibody, producing a line, this is most commonly used in pregnancy tests. However, explosives do not usually absorb in the visible spectrum. Maiolini *et al.* reported the detection of TNT by functionalising gold nanoparticles with a secondary antibody which was specific for the antibody conjugated to the pad.[52] Therefore, when the explosive was absent an intense red line, from the gold nanoparticles, was observed at the conjugation pad. When TNT was present the decrease in intensity of the red colour demonstrated the concentration of analyte present. However, this assay showed to have cross reactivity with 2 – amino - 4, 6 - dinitrotoluene and 1, 3, 5 – trinitrobenzene, as well as being a negative assay, i.e. a reduction in signal observed in the presence of TNT, which is not ideal.

Two of the most reported colourmetic test which identifies nitroaromatic molecules and nitrate anions are the Greiss test and the formation of Meisenheimer complexes.[51] A Meisenheimer complex is formed from the nucleophilic aromatic substitution of nitroaromatics.[53] For example, when a strong base is added to TNT a coloured adduct is formed, known as a Meisenheimer complex. Depending on the nitroaromatic and base used, a different coloured adducts can be obtained. The Greiss test can be used to detected nitrite anions. When a base is added to nitrate anions, nitrate amines are formed. When this is added to sulphanilamide and an arylamine, under acidic conditions, a intense azo coloured dye is formed.[54] However, these tests are not specific to explosives and will also change colour in the presence

of diazepam,[55] nitrobenzoxadiazole,[56] and in the presence of many cleaning products.

Colourimetric testing is the most portable, rapid, simple in terms of material handling and ease of interpreting results method available however, sensitivity is relatively low in comparison to other methods mentioned, and specificity is poor therefore false positives are common. False positives are a major issue as they mean that further analysis will be required which costs both time and money. In addition, due to the poor sensitivity, a negative result may be obtained when trace explosive material is present, the consequences from a false negative result are far more serious. Therefore a simple procedure to test for numerous explosives simultaneously, which has an unambiguous result, is affordable, is both sensitive and specific and can be widely deployed as an essential tool in advancing our current capability to deal with such threats is required. Bio-recognition molecules have been shown to be highly specific and selective in binding to target analytes, even in a complex matrix. Utilising the binding specificity of biomolecules for small molecules coupled with the chemical specificity of vibrational spectroscopy for the detection of explosives, is an area of great interest.

1.4   An Introduction to Biomolecules

1.4.1 Amino Acids

All proteins are made from 20 amino acid building blocks. Each amino acid consists of a different side chain, charge, hydrophobicity, and ultimately, chemical reactivity. Each unique amino acid sequence leads to great diversity of function within individual proteins. Amino acids have a common structure as shown in Figure 1.4.
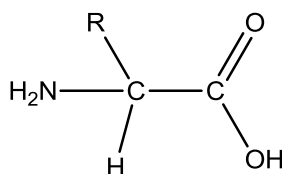
Figure 1.4: Basic structure of an amino acid.

The central carbon atom is attached to hydrogen, an amino group and a carboxyl group as well as an 'R' group. The 'R' group varies depending on which of the 20 amino acids is present, and this determines their chemical properties. Amino acids can form peptide bonds via a condensation reaction in order to form one or several polypeptide chains, known as proteins.

1.4.2 Proteins

Proteins are macromolecules which consist of one or several polypeptide chains. These chains form secondary structures as a result of the polypeptide folding which occurs due to ionic interactions, hydrophobic, electrostatic and even disulfide bridges, depending on the amino acid sequence. However, the most significant influence on secondary protein structures is hydrogen bonding. Whilst hydrogen bonding is relatively weak in comparison to other bonding, when numerous hydrogen bonds are present the following secondary protein structures can be formed: α-helix and β-sheets. α-helix and β-sheets were discovered in 1951 by Pauling, Corey and Branson.[57] An α-helix is a polypeptide chain in which every N-H bond donates a hydrogen bond to the backbone C=O group in the amino acid 4 residues earlier, hence the helical structure. β-sheets consist of polypeptide strands which are connected laterally by a minimum of 2-3 backbone hydrogen bonds, forming a twisted, pleated sheet. Furthermore, α-helix[58] and β-sheets[59] can further fold to form 3D structures, these are known as tertiary proteins.[60] Tertiary proteins are usually formed in the aqueous environment in which the protein residues consist of hydrophilic and hydrophobic regions. For example, non-ionic polar groups are usually found on the surface of the protein where they interact with the surrounding aqueous environment. However, hydrophobic groups are usually found buried in the protein, forming hydrophobic pockets, which are stabilised by Van Der Waals interactions. Furthermore, quaternary proteins occur when two or more polypeptides arrange themselves around each other to form one macromolecule.[61] Finally, proteins can be classified as globular or fibrous.[62] Globular proteins typically form a tightly folded spherical shape, whereas fibrous proteins are less complex and are elongated.

1.4.3 Antibodies

An immunoglobin, also known as an antibody, is a large 'Y' shaped glycoprotein made up of amino acids which naturally occur in living systems, specifically B cells, in which an antibody is the body's immune reaction to intruding foreign objects, known as an antigen (Figure 1.5). Antibodies are approximately 150 kDa and consist of 4 polypeptide chains: two identical heavy chains and two identical light chains connected by disulphide bridges. The light chain consists of a binding site on the tip of the 'Y', which is known as the fragment, antigen binding (Fab) region. This contains a variable amine terminated paratope that is specific for one epitope, the antigen, allowing binding between antibody and antigen to be highly specific. Therefore, the paratope of each antibody has a different composition of amino acids specific to the antigen it binds. The heavy chain, however, consists of the fragment, crystallisation (Fc) region, which does not generally vary between antibodies, despite the antibody being specific for different antigens.
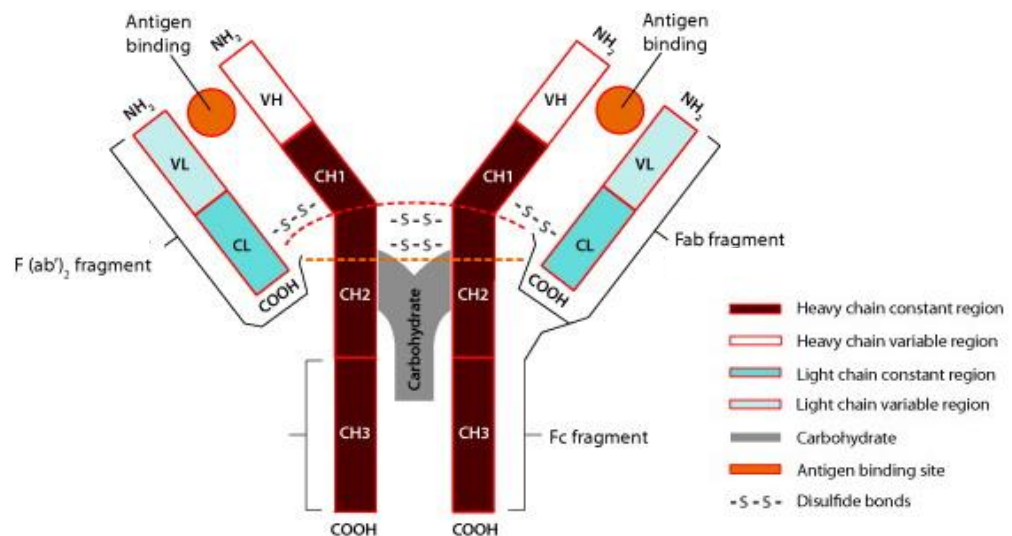
Figure 1.5: Schematic of a typical antibody.[63]

Furthermore, different varieties of antibodies can be produced, there are five common immunoglobins found in the body: IgA, IgD, IgE, IgG and IgM. These immunoglobins differ in their biological properties, functional locations and hence ability to deal with specific antigens. IgA is a dimer antibody, as shown in Figure 1.6, which is commonly used for preventing colonisation of pathogens which are

usually found on surfaces in the body that are exposed to the environment, such as ears, nose and breathing passages.[64] IgD, IgE and IgG are monomer immunoglobins,[65] IgD is a basic antibody of the dimer IgA, that co-exsists on B cells, along with IgM, however the role of IgD is still unknown.[66] IgE is found in the lungs and skin as it binds to allergens in the body to trigger the release of histamine. IgE does not allow for the Fab region of the antibody to be flexible i.e. the distance between the two binding sites cannot vary. IgG is also a monomer immunoglobin and it provides the majority of antibody based immunity from pathogens and it is the most abundant in the body and is the only antibody capable of crossing the placenta. Finally, IgM is a pentamer antibody of IgE, found on the surface of B cells, and is therefore the first active immunoglobin to the antigen site.[64] IgM and IgA consist of an extra joining chain, which comprises of 2 β-sheets folded against one another. The β-sheets are known to have at least 6 cystine residues, hence the heavy chain of these antibodies are connected via disulfide bridges.[67]
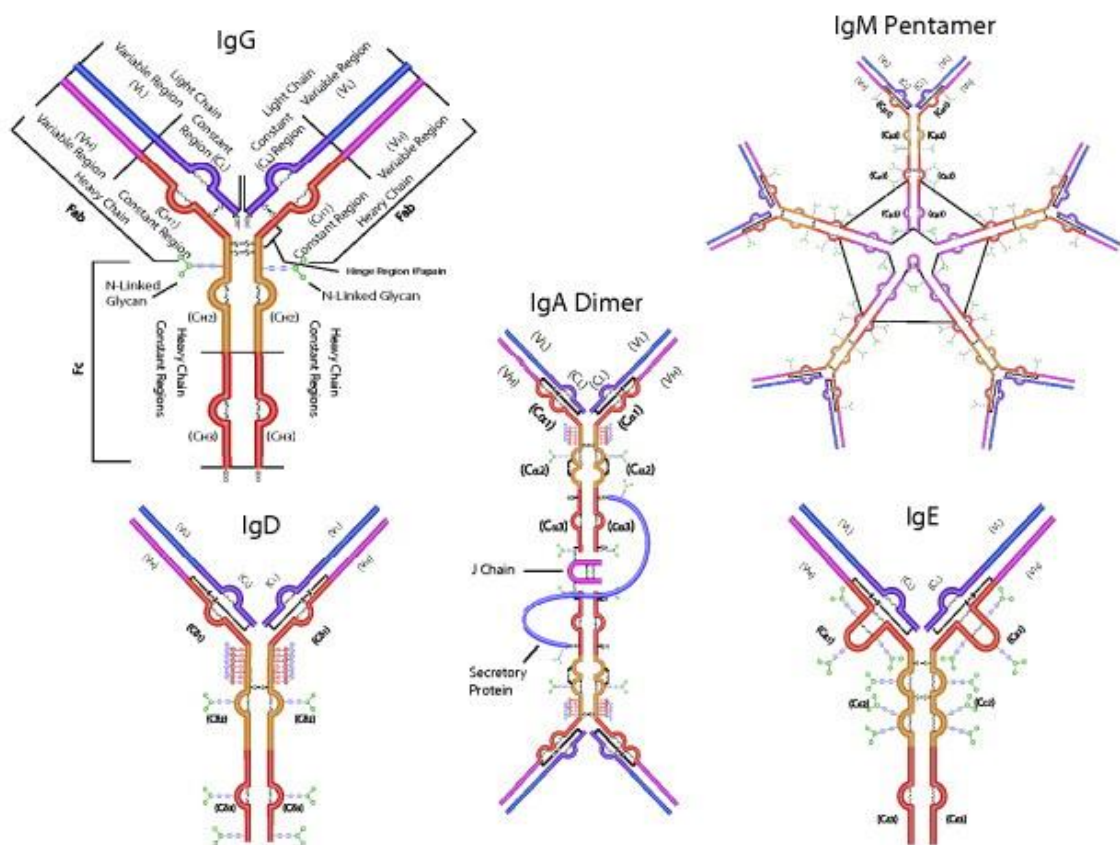
Figure 1.6: Schematic representation of different isotypes of antibody.[63]

Antibodies can be highly specific for one antigen as they are produced from an identical immune cell, these are known as monoclonal antibodies. Moreover, monoclonal antibodies have been reported to have dissociation constants, an equilibrium constant that measures the dissociation of antibody and antigen, of up to 10^{-15} M.[68] However, polyclonal antibodies are produced from different immune cells and may not be selective or specific for only one antigen.

The specificity and the selectivity of these biomolecules towards their analytes mean that biomolecules coupled assays are of great interest.

1.5 Detection of TNT using Immunoassays

TNT has recently been detected using biomolecule recognition by fluorescence resonance energy transfer (FRET) in a sandwich immunoassay.[69] FRET describes the energy transfer between two chromophores. A donor chromophore in its excited state can transfer energy to an acceptor chromophore, resulting in emission from the acceptor chromophore, opposed to the donor. FITC labelled TNT specific DNA aptamer was coated onto a poly-L-lysine microtitre plate allowing for capture of TNT followed by the introduction of a fluorescently labelled antibody specific for TNT. When TNT was present, FRET occurred between the labelled aptamer and the labelled antibody, resulting in a change in fluorescence emission compared to when TNT was absent. A limit of detection of 0.4 nM of TNT was obtained.

Mauro *et al.* have developed a fluorescence competitive binding immunoassay for the detection of TNT.[70] Antibodies specific for TNT were conjugated to a 96 well plate. Cyanine diaminopentane trinitrophenyl (Cy5-DAP-TNP) is a labelled analogue of TNT which was added, as it known to have a cross reactivity with the TNT specific antibody. Fluorescent spectroscopy was then performed on the well plate and an intense fluorescent emission spectrum was observed from the Cy5-DAP-TNP bound to the conjugated antibody. However, when TNT was present in the assay, Cy5-DAP-TNP was displaced due TNTs higher binding affinity to the antibody, resulting in a lower fluorescence emission intensity. Furthermore, the assay was found to be concentration dependant, the higher the concentration of TNT

present, the lower the fluorescence intensity observed. A limit of detection of 2.2 nM was obtained, however, this is a negative detection assay, resulting in a decrease in intensity as the concentration of TNT increases which is not ideal.

Mattoussi *et al.* reported the detection of TNT by functionalising quantum dots with a TNT specific antibody.[71] Quantum dots are semi conducting materials which range from 2-10 nm in diameter. Quantum dots, like nanoparticles, display unique electronic properties due to their high surface to volume ratio. In quantum dots, the most dominant feature is fluorescence. In the reported assay, a TNT antibody was conjugated to the fluorescent quantum dots. A dye labelled analogue of TNT, trinitrobenzene-1, 5-diaminopentane-black-holequencher 10 (TNB-DNP-BHQ-10), was then added to the assay. The analogue molecule will bind to the TNT specific antibody as it has a cross reactivity with it. In the presence of the analogue molecule, when fluorescence spectroscopy is performed, FRET occurs between the quantum dot and the labelled analogue, therefore quenching the photoluminescence of the quantum dot. When TNT is present, the labelled analogue is displaced and when fluorescence is subsequently measured, an emission spectrum of the quantum dots is observed. The intensity of the fluorescence emission from quantum dots was also quantitative as the more intense the emission of the quantum dot was recovered, the more TNT was present to displace the labelled analogue, preventing FRET. This overcame the issues with previous type of assay as the concentration of TNT increases the intensity is increased, a limit of detection of 30 mM was obtained for complex soil samples.

Whilst biomolecules have the potential to be specific and selective for the detection of explosives, fluorescence spectroscopy has the disadvantage that a broad spectrum is obtained, reducing the multiplexing capabilities i.e. the ability to detect multiple analytes simultaneously. Raman spectroscopy produces a unique 'fingerprint' spectrum in which the peaks are narrow and molecularly specific which has advantages for multiplexing. Moreover, surface enhanced Raman scattering (SERS) is a sensitive technique which can overcome the poor sensitivity of Raman scattering

whilst retaining the molecular specificity and it has been reported to be capable of detecting single molecules.[72]

1.6   Raman Scattering Spectroscopy

Current detection methods for trace explosive materials lack in specificity and sensitivity, therefore a method which can definitively identify not only a chemical group within an explosive molecule but can definitively identify trace volumes of an explosive molecule based on its whole molecular structure is required. Raman spectroscopy is highly molecular specific technique as a unique fingerprint spectrum is obtained for each molecule, therefore identifying a whole molecule, not just the presence of a nitro group.

1.6.1 Raman Scattering

The theory of inelastic scattering, known as Raman scattering, was first discovered by Smekal in 1923.[73] However, it wasn't until 1928 that this extraordinary hypothesis was demonstrated experimentally by Krishnan and Raman.[74] When light interacts with matter, photons can be scattered, absorbed or can pass through the material. If a photon has the exact energy, which coincides with the energy between the ground state and an excited state, the photon can be absorbed and the molecule is promoted to a high energy state shown in Figure 1.7. However, a photon which does not match the difference in energy between the energy levels can be scattered. Light distorts and polarises the cloud of electrons around the nuclei of the molecule to form a state known as a 'virtual state' which is very unstable and therefore short lived. Due to the instability of this excited state, energy is released rapidly in the form of elastic scattered light, known as Rayleigh scattering. Which has the same energy as the incident light and this is known as elastic scattering.
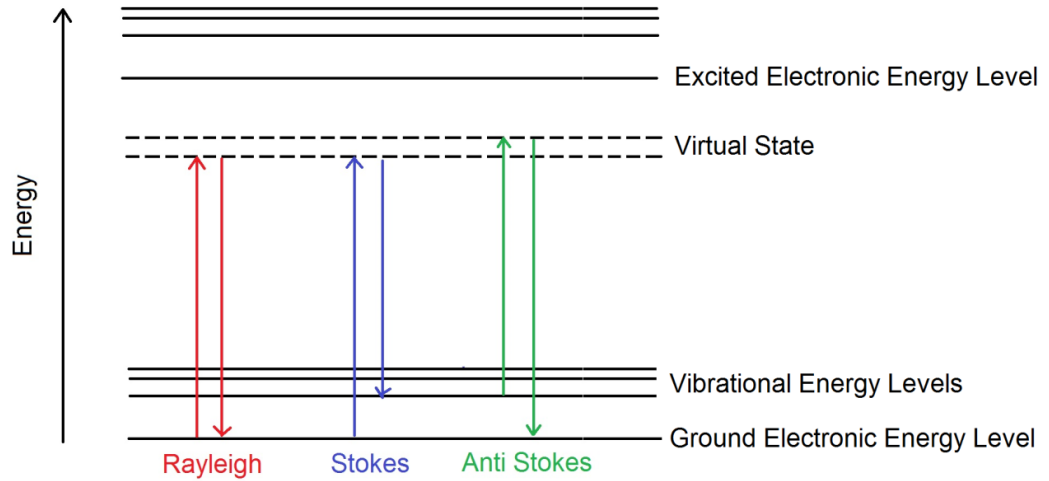
Figure 1.7: Jablonski diagram representing light scattering processes.

In addition to Rayleigh scattering, energy can be transferred during the scattering process by nuclear motion, known as inelastic scattering. This inelastic scattering is not dominant as only around one in every 10^6-10^8 photons are inelastically scattered, this is known as Raman scattering.[72] There are two different types of Raman scattering: Stokes and anti-Stokes. Stokes scattering involves excitement of a molecule by incident light from a ground state to a virtual state, which is defined by the energy of the incoming laser light, consequently resulting in the emission of a photon which is of a lower energy than that of the incident light, i.e. energy is transferred to the molecule, as shown in Figure 1.7. Anti-Stokes is the excitement of a molecule already in an excited state to a virtual state and back to the ground state upon emission of a photon, therefore energy is transferred from the molecule. The population of electrons in each state indicates the relative intensity each scattering process, hence anti-Stokes scattering is a much weaker process than Stokes scattering at room temperature as explained by Boltzmann distribution equation (1):

$$\frac{N_n}{N_m} = \frac{g_n}{g_m} \exp[\frac{-(E_n - E_m)}{kT}] \qquad (1)$$

Where: N_n is the number of molecules in an excited level (n), N_m is the number of molecules in the ground state (m), g is the degeneracy of the levels n and m, $E_n - E_m$ is the energy difference between the vibrational energy levels, k is

Boltzmanns constant and T is temperature. Therefore at room temperature, anti-Stokes scattering is weaker than Stokes scattering due to a lower number of molecules exsisting in an excited state at room temperature. However, as the temperature is increased, anti-Stokes scattering will be favoured as more molecules will be in an excited state.

The main disadvantage of Raman scattering is that most molecules, including explosive materials, have low Raman cross sections and therefore a weak Raman spectrum is obtained, therefore Raman is seldom used for the detection of low concentration analytes. Raman cross sections are discussed further in section 2.1.

1.6.1.1 Raman Scattering of Explosives

Although explosives are known to have a small Raman cross section, a Raman spectrum can be obtained from pure solid explosive samples. Nagli *et al.* reported the Raman spectroscopy of explosives, RDX, TATP PETN, TNT and urea nitrate using a 532 nm laser excitation frequency doubled pulse laser (20 mJ/pulse, 8 ns, 13 Hz).[75] Pulsed lasers are typically used to study the lifetime of short lived species, however it can be used to obtain the Raman spectrum of explosives. The first laser pump is used to photolyse the sample, and the second pulse is then used as a Raman probe. Repeating this technique several times improves the signal to noise ratio of the Raman spectrum, hence a Raman spectrum of explosives can be obtained. However, Nagli *et al.* required at least 1 mg of each sample to obtain a spectrum.

Asher *et al.* have also reported the Raman spectrum of the explosives TNT, RDX, PETN and HMX by using a near UV, 229 nm laser excitation wavelength.[76] By simply using a lower wavelength laser excitation, an enhancement of up to 200 times was observed in comparison to using a visable or near IR wavelength laser excitation. This can be explained by the fact that there is an increase in Raman scattering probability, as it is dependent on ω^4 of excitation laser, according to the Raman Intensity equation (2):[72]

$$I = K \, I_L \, \alpha^2 \, \omega^4 \quad (2)$$

Where, K is a constant, I is the Raman intensity, I_L is the power of the laser, α^2 is the polarisability of the molecule and ω^4 is the frequency of the laser excitation. However, an additional enhancement in signal can occur due to many explosives absorbing in the UV region of the electromagnetic spectrum, resulting in the enhancement in signal due to resonance Raman Scattering. [77]

Therefore using conventional Raman scattering spectroscopy, only a weak scattering spectrum of explosives can be obtained. Resonance Raman scattering has the potential to improve the sensitivity of the detection of explosives.

1.6.2 Resonance Raman Scattering

Resonance Raman scattering involves the excitation of a molecule by a laser frequency which is chosen such that it coincides with the frequency of the electronic absorption within the analyte molecule.[78] Resonance Raman scattering can be used to gain both vibrational and electronic information about a molecule, with enhancement of up to 10^4 being reported compared to conventional Raman scattering.[72]
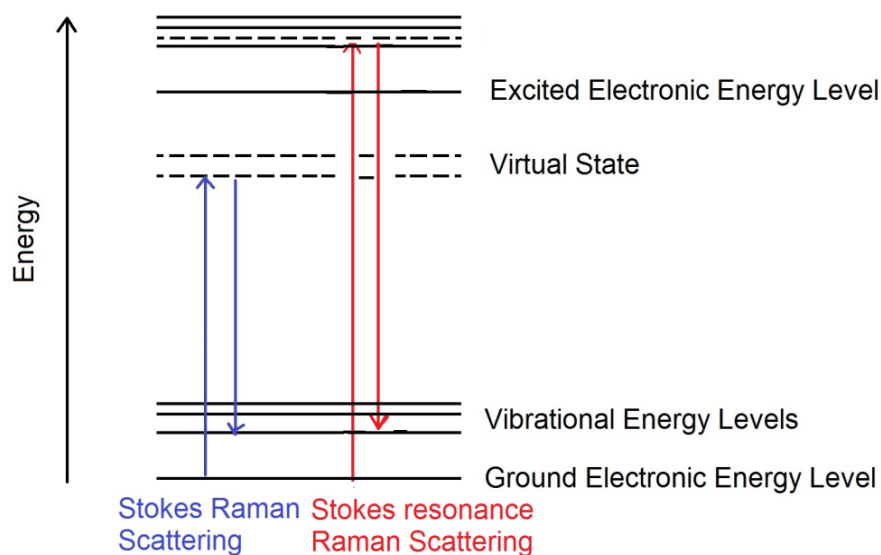
Figure 1.8: Jablonski diagram representing Stokes Raman scattering and Stokes resonance Raman scattering.

The degree of enhancement however, depends on the nature of the electronic states. If there are no symmetry selection rules, i.e. transitions between p and d orbitals are forbidden if the molecule has a asymmetrical vibration and a centre of symmetry, strong enhancements occur when a molecule is excited to a vibronic state, whereby Raman scattering is the excitement of a molecule to a virtual state, as shown in Figure 1.8. Therefore some bands are enhanced more than others in resonance Raman scattering. However, limitations arise due to the absorption process, as both absorption and scattering processes can occur. The time scales for these are different, scattering is considerably faster, however interference from the competing fluorescence emission process can also occur along with sample degradation.

1.6.2.1 *Resonance Raman Scattering of Explosives*

The enhancement of resonance Raman scattering over conventional Raman has allowed for the detection of explosives at lower concentrations. Previously, only a Raman spectrum of solid state explosives could be obtained due to explosive molecules having a low Raman cross section. However, it is known that explosives have an absorbance maximum in the UV region, therefore if a Raman excitation laser is selected such that is coincides with this absorption then a resonance Raman spectrum is obtained. TNT was reported to have an absorbance at 229 nm, RDX at 230 nm and PETN at 200 nm. Therefore, Asher *et al.* reported that by using a 299 nm laser excitation, a resonance Raman spectrum of TNT, RDX and PETN in solution was obtained.[76] Furthermore, they were able to obtain spectra for TNT at 2 mg/ml in acetonitrile, 1.33 mg/ml RDX in acetonitrile and finally 18.9 mg/ml PETN in acetonitrile.

However, these concentrations are relatively high, especially for PETN and therefore a technique which can detect lower limits with better sensitivity and selectivity is required.

1.6.3 Surface Enhanced Raman Scattering

A more sensitive technique is surface enhanced Raman scattering (SERS). This technique was first discovered in 1974 by Fleischmann *et al*, when a strong Raman scattering spectrum was reported from pyridine molecules adsorbed on to an electrochemically roughened silver electrode.[79] This enhancement was originally attributed to the increased surface area of the electrode, allowing for more pyridine molecules to be absorbed, however it was later found that the roughened metal surface facilitated this enhancement due to a surface enhanced effect.

Many theories have been reported on the mechanism of the enhancement of SERS, where the intensity has been reported to be enhanced by a factor of 10^6-10^7.[80] The enhancement is thought to be due to the contribution of two effects proposed by Van Duyne and Creighton.[81, 82] Charge transfer enhancement is proposed to involve the formation of a bond between the analyte and the roughened metallic surface, in which new electronic states arise, serving as a resonant intermediate for SERS. Enhancement arises due to the transfer of electrons from the metal to the analyte and back to the metal again.[83] Electromagnetic enhancement is thought to arise from the interaction between the adsorbed analyte and the oscillating surface plasmons on the roughened metallic surface. The analyte does not need to be bound directly to the surface for this enhancement. The adsorbed analyte experiences an increased localised electric field due to the surface plasmon electrons, creating a greater polarisation of the electrons around the analyte. This results in a significant enhancement of the Raman scattering field.[84] There is evidence for both these theories however, electromagnetic enhancement is generally more accepted to be the dominant contribution to SERS enhancement. Since the discovery of roughened surfaces enhancing Raman scattering, many different roughened metal surfaces can be prepared, such as: electrodes,[82] coated surfaces,[85] nanoparticles,[86] including a range of shapes, from spheres, rods to popcorn shaped.[87, 88] Many suitable metals have also been investigated for their SERS enhancement effects including: gold,[89] silver,[90] copper,[91] and platinum.[92] However, arguably the most common substrates are colloidal suspensions of gold and silver nanoparticles.[93]

A technique which utilises the enhancement from metal surfaces with the benefits of resonance Raman scattering was desired. This involves carrying out SERS on resonant chromophores, which then became known as surface enhanced resonance Raman spectroscopy (SERRS).

1.6.4 Surface Enhanced Resonance Raman Scattering

Surface enhanced resonance Raman scattering (SERRS) was first demonstrated by Van Duyne and Stacy.[84] They proposed that by adsorbing a resonant chromophore onto a roughened metallic surface a combination of the enhancement of resonance Raman and SERS scattering would be observed. In SERRS the excitation wavelength was chosen so that it coincides with the maximum absorption of the chromophore. This allows for a greater enhancement factor of the Raman signal and up to magnitudes of 10^{10} order has been reported and has enabled single molecule detection.[94]

Since the phenomenon of LSPR has been discovered many sensitive assays have been developed exploiting these optical properties. More specifically, the coupling of the optical advantages of nanoparticles and SERS with the high specificity and selectivity of biomolecules, has the potential to produce very sensitive SERS immunoassays for the detection of small molecules.

1.7   Introduction to Nanoparticles

Nanotechnology is the synthesis and study of discrete novel materials, which have at least one dimension in the range of 1-100 nm.[95] Nanoparticles are of great interest as they display unique characteristics such as electronic, optical, physical and magnetic properties, which the corresponding bulk material does not display.[96] Currently, uses of nanoparticles range from imaging, photothermal therapy,[97] biosensing,[98] DNA detection[99] as well as trace detection of explosives [100] amongst others. Nanoparticles are therefore, a very interesting and active area of research.

Nanoparticles were being unknowingly synthesised as far back as the 9th century.[101] Artists of the Renaissance period created a technique to use the unique colours of nanoparticles in their masterpieces. An extraordinary example is the Lycurgus cup.[102] The Lycurgus cup is dated to the 1600's, when the Romans fabricated a cup consisting of glass containing gold nanoparticles, resulting in the cup being ruby coloured in transmitted light, but green coloured in reflecting light as shown in Figure 1.9.

Figure 1.9: The Lycurgus Cup shown in reflected light and transmitted light, reproduced from [102] with permission.

However, the scientific study of colloidal solutions was first reported in 1857 by Michael Faraday.[103] Faraday introduced a method for synthesising gold nanoparticles and observed that they are more interesting optically than the corresponding bulk metal. The intrinsic properties of materials differ greatly when considering an individual atom, in comparison to the bulk material. This is due to the quantum

confinement.[104] Considering an individual atom at the nanoscale, significant property changes occur at the electron, proton and neutron levels. This occurs due to confinement of the electrons on the nanoscale dimensions, resulting in quantisation of energy and momentum, and reduced dimensionality of electronic states. Furthermore, the atoms are located at the surfaces or interface of the nanostructure, resulting in different mechanics, thermodynamics, electronic, magnetic, optical and chemical states, in comparison to the bulk material.[104] These materials display enhanced and useful radiative properties, such as Raman scattering,[105] absorption[106] and fluorescence[107] which is dependent on the material, particle shape and size.

The optical properties of nanoparticles can be attributed to the interaction of light, electromagnetic radiation, with nanoparticles inducing an oscillating cloud of electrons at the nanoparticles surface, which known as surface plasmon resonance (SPR) (Figure 1.10). A better understanding of light interaction with nanoparticles was proposed in 1908 by Mie.[108] He describes the plasmon band as being due to dipole oscillations of the free electrons in the conduction band occupying energy states immediately above the Fermi energy level. The excitation of the conductance band electrons results in strong absorption of the incident light and strongly scattered elastic light, hence the strong colours of noble metallic colloids. Furthermore, Mie's theory describes that the plasmon band can shift depending on a range of factors (Equation 3).
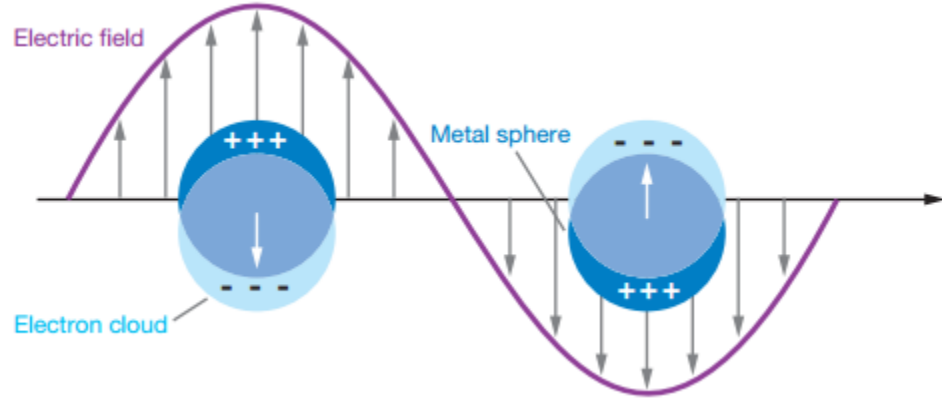
Figure 1.10: Effect of induced dipole on metallic nanoparticle from incident light.[109]

$$C_{ext} = \frac{24\pi^2 R^3 \varepsilon_m^{\frac{3}{2}}}{\lambda} \frac{\varepsilon_2}{(\varepsilon_1 + 2\varepsilon_m)^2 + \varepsilon_2^2} = C_{abs} + C_{sca} \quad (3)$$

Where, C_{ext} is the extinction coefficient, R is the radius of a nanosphere, ε_m is the dielectric constant of the surrounding medium, λ is the wavelength of the incident electromagnetic wave and $(\varepsilon_1 + 2\varepsilon_2)$ are the real and imaginary components of the dielectric function of the particle. The extinction coefficient is composed of two components: C_{abs} is the absorption coefficient and C_{sca} is the scattering coefficient. The main attributes to this equation therefore, are the dielectric constant of the surrounding media of the nanoparticle, the size and shape of the nanoparticle and the inter-particle distance of the nanoparticles. This theory can be applied only to small spheres less than 100 nm. Due to the spherical shape of the particle, symmetry dictates that nanospheres only have one plasmon resonance, hence tuning of LSPR is only possible by altering the type of metal, size of particle or by aggregation. By altering the type of metal the scattering to absorption ratio changes and hence a change in LSPR is observed, for example a 60 nm silver nanoparticle typically has an absorption maximum at ~410 nm, whereas a gold nanoparticle of 60 nm has an absorption maximum at ~525 nm.[110] By increasing the size of the nanoparticle there is a larger surface area on each nanoparticle, hence there is an increase in the maximum absorption in LSPR. For example, silver nanoparticles exhibit a red shift of the absorption peak at 409 nm, and a colour change can be observed from yellow/green to grey, upon increasing diameter of the nanoparticle.[111] Furthermore, when the nanoparticles interparticles distance is decreased, the plasmons can

combine, resulting in a red shift of the LSPR peak,[112] and the extent of the red shift is largely distance dependant; the shorter the distance, the more red shifted the LSPR peak.

1.7.1 Nanoparticle Synthesis

In 1857 Faraday developed the solution phase reduction of gold ions to gold atoms.[103] Since then a number of methods have been proposed for the synthesis of nanoparticles. The 'classic' Turkevich method developed in 1951 is the most commonly used method to synthesise spherical metallic nanoparticles.[113] Nanoparticles require a stabilising agent on their surface, to keep them dispersed in solution. Typically, silver or gold ions are added to a sodium citrate solution, which acts as a reducing agent and also as a stabilising agent. Citrate is a negatively charged ligand which forms a layer around each nanoparticle, therefore stabilising the nanoparticles as they are electrostatically repelled from each other. The proposed reaction for silver is:

$$4Ag^+ + C_6H_5O_7Na_3 + 2H_2O \rightarrow 4Ag^0 + C_6H_5O_7H_3 + 3Na^+ + H^+ + 2O_2$$

This method typically produces spherical monodispersed, yellow/green coloured silver nanoparticles in the size region of about 40 nm with an LSPR extinction band at approximately 410 nm.[114] This method has been shown to produce nanoparticles that are stable in solution over several months. However, in 1982, Lee and Meisel published a slightly modified version of this method utilising a different metal to citrate ratio, which is thought to reduce the silver nanoparticles faster and therefore requires heating for a reduced amount of time.[115]

Another common reduction method was developed by Creighton *et al.*[83] Mixing two solutions of silver nitrate and sodium borohydride and shaking vigorously, silver nanoparticles with improved monodispersity compared to the citrate reduction method were achieved. These nanoparticles were usually smaller, approximately 1-50 nm in size, and were not as stable as citrate reduced nanoparticles as they only

remain suspended in solution for a few weeks and typically have an LSPR extinction band at 400 nm.

In 1986, Schopfer *et al.* reported the reduction and capping of Ag with ethylenediaminetetraacetic acid (EDTA) ligand.[116] Silver nanoparticles were synthesised by adding silver salt to NaOH and EDTA. After boiling HCl was then added to the mixture and boiling was continued until a yellow/green colour was observed. An absorption band was typically observed at 404 nm. It was also reported that these nanoparticles were more stable than citrate reduced nanoparticles, there were however larger batch to batch variations.[117]

Recently, a more economical approach has been investigated by several research groups. Saifuddin and co-workers found a 'simple and green' novel method in which to synthesise silver nanoparticles using microwave irradiation.[118] Silver ions were treated with the bacterium *Bacillus subtilis* and put in a conventional microwave oven and the solution was subjected to short bursts of radiation, 15 s on and 15 s off for up to 15 cycles. *Bacillus subtilis* acts as a reducing agent and the addition of microwave irradiation provides uniform nucleation and growth of nanoparticles. The silver nanoparticles produced were in the range of 5-60 nm and an extinction peak 410 nm.

Nanoparticles have shown useful radiative and optical properties, however, these properties can be further advantageous with the coupling of a biomolecule. Functionalising a nanoparticle with a biomolecule can improve the sensitivity, selectivity and specificity of the detection of small target molecules.

1.8 SERS Based Detection Immunoassays

As previously discussed, the sensitive detection of solution based TNT, RDX and PETN by Raman and resonance Raman scattering is hard to achieve, as they are small molecules with low Raman cross sections. However, the Raman signal can be enhanced by adsorbing the explosives onto a roughened metallic surface and the SERS spectrum of explosives at nM concentrations has been reported. The direct adsorption of explosives onto nanoparticles to obtain a SERS spectrum is described in depth in section 2.1. However, nanoparticle surfaces also have the advantage that they are easily functionalised with biomolecules, which can be used for the detection of specific target molecules. Utilising the optical properties of nanoparticles coupled with SE(R)RS has shown promising results for the detection of explosives.

One approach makes use of a gold nano-popcorn and single wall carbon nanotubes (SWCNT) hybrid.[87] Gold nanopopcorn is synthesised using citrate reduction to form a popcorn shape rather than spherical nanoparticles. These gold nanopopcorns were subsequently decorated onto the surface of the SWCNT by oxidation and addition of glutathione. The nanopopcorn was then functionalised with *p*-aminothiophenol, which allows TNT to bind to the amine group, forming a Meisenheimer complex (Figure 1.11).
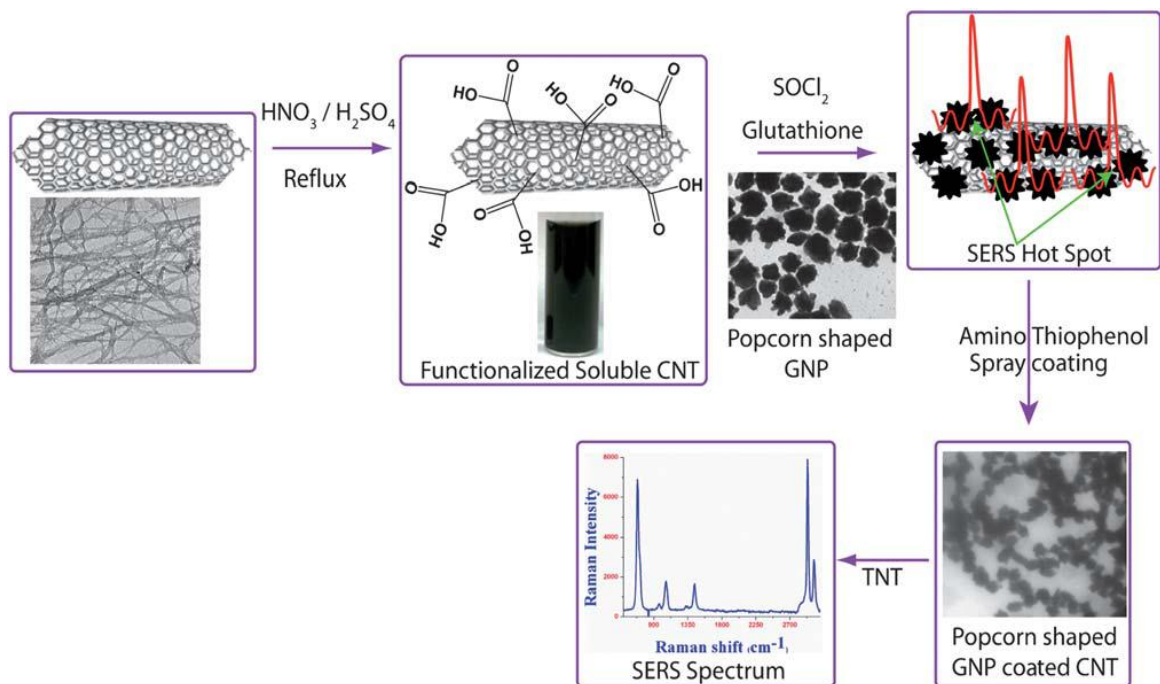
Figure 1.11: Schematic representation showing the synthetic procedure for the development of SWCNT- *p*-aminothiophenol-gold nanopopcorn substrates for the detection of TNT by SERS.

When TNT was present, it bound to the SWCNT- *p*-aminothiophenol-gold nanopopcorn via π donor and acceptor interactions. This allowed TNT to be detected by surface enhanced Raman scattering, in which the limit of detection was determined to be 100 fM.

TNT has also been detected directly by utilising molecular imprinted polymers (MIPs).[119] MIPs are made up of artificial recognition molecules to which target analytes of interest can bind specifically. In this case, the amine rich MIP was immobilised onto the commercially available gold SERS substrate, Klarite[TM]. The target TNT was subsequently captured and bound forming a Meisenheimer complex and resulting in a SERS spectrum of TNT specific peaks. This method was very powerful, highly specific and non-invasive, however the sensitivity of the assay was only in the μM range.

Previous research into SERS in combination with biomolecular capture of explosives includes a method developed by Singamaneni *et al*,[120] where gold nanorods were functionalised with a peptide. The peptide aptamer contained cysteine, which

allowed for the peptide to bind to gold nanorods. The peptide aptamer consisted of a specific sequence for the detection of TNT. The gold nanorod functionalised with the peptide aptamer was then transferred to filter paper, which was then exposed to TNT solutions, vapours and solids. TNT specifically bound to the filter paper which when analysed gave SERS spectra specific for TNT, in which the peak present at 1350 cm^{-1} was most intense and assigned to the NO_2 stretch. The limit of detection obtained from this method was ~100 pM.

The specific detection of TNT using nanoparticles and antibodies by SERS has not yet been reported without the addition of a SERS active label. Therefore a review of the literature was carried out to determine if any small molecules had been directly detected using a SERS based immunoassay. A SERS based immunoassay has been developed for the detection of cocaine, a small drug molecule, therefore this method could potentially be extended to other small molecules, such as explosives. The Chen group used a silver colloid film deposited on a gold disc which was functionalised with a mixed monolayer, consisting of 3-mercaptopropionic acid (MPA) and a thiolated DNA aptamer,[121] which was modified to contain a SERS active dye, tetramethylrhodamine (TMR), at the end of the aptamer sequence. When cocaine was not present the aptamers conformation was elongated so that the TMR molecule was located far away from the silver colloid film surface and hence, minimal SERS signals were obtained. However, when cocaine was present the aptamer folded and orientated itself so that the TMR was in close proximity to the silver film. The SERS spectra obtained when cocaine was present was 1.6 times more enhanced at a limit of detection of 1 μM cocaine than in the absence of cocaine.

A method was developed which utilises antibodies in the detection of, a metabolite of cocaine, benzoylecgonine (BCG). Sanles-Sobrido coated carbon nanotubes (CNT) with polyallylamine hydrochloride (PAH).[122] This allowed for the electrostatic attraction of silver nanoparticles to the CNT. An antibody specific for BCG was then conjugated to the silver nanoparticle-CNT by carbodiimide chemistry, using thiolglycolic acid. Aliquots of this suspension were then cast and dried on glass slides. In the presence of cocaine the SERS spectra showed enhancements of the

693 cm^{-1} band due to the out-of-plane CH bending in BCG. A limit of detection of 1 nM was obtained. This method was very powerful, highly specific and non-invasive, however CNTs are of high cost as well as having safety implications.

These examples suggest that small molecules can be detected by combining biomolecules specific to the target with metal nanoparticles and SERS. Nanoparticle surfaces have the advantage that they are easily functionalised with biomolecules, which can then be used for the detection of specific target molecules. Moreover, these biomolecules are selective and can detect trace amounts of the target from a complex matrix. Therefore, this has potential applications for explosives detection. For these reasons an assay which utilises the functionalisation of a biomolecule on to a nanoparticle surface would have promising results for the specific and selective detection of small target molecules such as TNT, with the use of SERS spectroscopy.

2. SERS of Explosive Materials

There are many materials which are commonly used as concealed explosives. These concealed explosives are typically found in trace amounts in landmines, aquatic environments and on the outside of suspicious containers holding explosives. As a result, a detection technique which can specifically and selectively detect low levels of these materials is required. In Section 1.6.2, the use of Raman spectroscopy for the detection of explosives was discussed. Raman spectroscopy produces sharp bands that are molecularly specific. This means that Raman has an advantage over other techniques since it can be used to easily discriminate between several analytes in a mixture. However, Raman scattering is an intrinsically weak process, therefore, one approach for the sensitive detection of explosives is to utilise the enhanced scattering properties of metallic nanoparticles, more specifically silver nanoparticles were used for the detection of explosive materials using surface enhanced Raman scattering (SERS). Here the use of SERS for the detection of TNT, RDX and PETN will be explored.

2.1   Aims

The aim of this chapter was to obtain an intrinsic SERS spectra of the explosives TNT, RDX and PETN in solution, in order to observe the explosives molecular specific peaks. Firstly, SERS active silver nanoparticles were synthesised using citrate reduction, the nanoparticles synthesised were then characterised by UV-vis, DLS and zeta potential. The silver nanoparticle surface allows for adsorption of the explosive materials, resulting in a unique SERS spectrum of each explosive material. A SERS spectrum of each explosive was achieved by adsorbing the explosive onto a silver nanoparticles surface, inducing aggregation and using 532 nm laser excitation for a 10 s accumulation time. Furthermore, a concentration study of each explosive molecule was explored, to determine the limit of detection by using this detection by direct adsorption approach. Moreover, this chapter allows for a reference SERS

spectra of each of the explosives and a control, acetonitrile in which the explosives were dissolved. This reference SERS spectrum of the explosive highlights specific SERS peaks, which can then be used to positively identify the presence of explosives in the assay developed later in Chapter 3.

2.2   Introduction to SERS of Explosives

Ever since the discovery of SERS by Fleischmann in 1974, many advances in terms of both instrumentation and the metal enhancing substrates have emerged to increase the capabilities of SERS for biochemical sensing.[79] However, the molecular identification of small molecules in solution, at trace concentrations by SERS still remains a challenge. Small molecules such as 2, 4, 6 - trinitrotoluene (TNT) and 1, 3, 5 – trinitroperhydro – 1, 3, 5 - triazine (RDX), have small Raman cross-sections. By definition, 'the term scattering cross-section is a constant of proportionality that relates the incident and scattered beam in a particular scattering process. In its simplest form it refers to scattering from one mode in phase space to another and has the dimensions of an area.[123] However the Raman cross-section applies to a single molecule, when in reality in any given experiment, multiple molecules will be interrogated. Furthermore, Raman cross-sections refer to detection of photons in all directions, when experimentally this is not the case, usually detection only occurs in the direction where the charge-coupled device (CCD) is. Therefore, a more rigorous definition is required.

The first important aspect of determining Raman cross-sections is the actual scattering process. This depends on the orientation of the molecules, and subsequently the active vibrational modes, in relation to the incident field polarisation. Other aspects that should be considered are: the wavelength of laser excitation, the refractive index of the molecule and the molecules environment. These aspects have the ability to significantly change the Raman cross-section of a molecule. Therefore, the absolute Raman cross-section is derived by a differential equation (4):

$$\frac{dP_R}{d\Omega}(90°) = \frac{d\sigma_R}{d\Omega}S_{Inc} \qquad (4)$$

Where $dP_R/d\Omega$ is the molecular orientation averaged Stokes Raman scattered power from the molecule, S_{Inc} is the power density of the laser and $d\sigma_R/d\Omega$ is the differential Raman cross-section of a given molecule.[124]

The Raman cross-section denotes the magnitude of Raman scattering for a given Raman active mode, however more information on the Raman mode can be extracted from equation (4). There are two possible electric field polarisations of the averaged Stokes Raman scattered light ($dP_R/d\Omega$): parallel and perpendicular. When taking these into account, the Raman depolarisation ratio can be defined (equation (5)). The Raman depolarisation ratio corresponds to the differential Raman cross-sections for parallel and perpendicular configurations of the averaged Stokes Raman scattered light.

$$\rho_{R=}\frac{d\sigma_{R\perp}/d\Omega}{d\sigma_{R\parallel}/d\Omega}S_{Inc} \qquad (5)$$

Where ρ_R is the depolarisation ratio and contains information on the symmetry of the molecule.[125] $d\sigma_{R\perp}/d\Omega$ and $d\sigma_{R\parallel}/d\Omega$ describe the differential Raman cross-sections for perpendicular and parallel polarised scattered light. This equation for the Raman cross-section is the standard equation used to calculate the differential Raman cross-section. There are, however, limitations to this equation, and these involve solution based detection. In solution, an extra refractive index is created as the incident light travels from the objective lens through the air and solution to focus on the sample. This could be overcome by using a liquid immersion lens, in which, the equation is notably more comparable to experimental Raman cross-section values. Therefore, a molecule with a high Raman cross-section should ideally be symmetrical, and have a

large depolarisation ratio, i.e. a molecular vibration perpendicular to the incident light, and have symmetrical vibrations.

With respect to 2, 4, 6 – trinitrotoluene (TNT), 1, 3, 5 – trinitroperhydro – 1, 3, 5 – triazine (RDX) and [3 – nitrooxy – 2, 2 – bis(nitrooxymethyl)propyl] nitrate (PETN), TNT is the larger Raman scatterer of the three molecules. This is mainly due to the aromaticity and symmetry of the molecule, as well as the presence of strong electron withdrawing groups. The strong electron withdrawing groups (NO_2) have the potential to make the TNT molecule more polarisable, and therefore a stronger scatterer. The first Raman spectrum of TNT was reported in 1994 by McNesby *et al.*[126] This was achieved by using Fourier transform (FT) Raman spectroscopy. FT Raman generally uses 1064 nm laser excitation and therefore has the advantage that it can overcome competing fluorescence by avoiding the absorption process as any materials do not fluorescence at higher excitation wavelengths.[127] In order to achieve a FT Raman spectrum of TNT, a powder sample was put into a glass capillary tube, and analysed by FT Raman. The laser excitation source was an Nd^{3+}: YAG excitation laser, with 1064 nm laser excitation, an acquisition time of 12 mins and a laser power of 300 mW was used. Strong spectral features were observed at 1500 and 1200 cm^{-1} due to the symmetrical NO_2 vibrations. However, due to the relatively low Raman cross sections of explosives, a Raman spectrum of dilute solutions of explosives has not been successful. However, by utilising the Raman enhancement from roughened metallic surfaces, SERS spectra of explosive materials in solution is possible.

Wackerbarth *et al.* reported a very weak SERS spectrum from the adsorption of TNT (1 mg/ml) on to a gold substrate.[128] The TNT was dissolved in acetonitrile, the solution was then spotted onto a gold substrate. The sample was then analysed by SERS using 785 nm laser excitation, with an operating power of 100 mW. However, only a SERS spectrum of acetonitrile could be obtained. In light of these results, the gold substrate was subjected to heat, 30 °C for 10 minutes, to evaporate the acetonitrile and concentrate the TNT. The gold substrate was analysed by SERS,

under the same conditions. However, only a weak spectrum of TNT was obtained. Wackerbarth then adsorbed the same TNT solution onto a different substrate, Klarite[TM]. Klarite[TM] is a gold coated substrate which consists of inverted pyramidal features, which has been shown to enhance Raman scattering. As before, TNT solution (1 mg/ml) was adsorbed onto the Klarite[TM] surface and subjected to heat, to evaporate the acetonitrile, and analysed by SERS. An enhancement in the SERS spectrum of TNT was observed on the Klarite[TM] surface in comparison the gold substrate. This demonstrates the challenges of detecting trace concentrations of small explosive molecules by SERS.

It has been reported by Steinfield *et al.* that by using a fibre optic probe, a SERS spectrum of TNT on silver nanoparticles can be achieved.[129] Fibre optics has the advantage of total internal light reflectance, this allows for increased and concentrated light at the sample, which allows for an enhanced Raman scattering spectrum in comparison to conventional Raman instrumentation. Furthermore, fibre optics also incorporates the light source with a beam splitter, allowing for the separation of excited and fluorescent light. Steinfield was able to successfully obtain a SERS spectrum of 100 nM of TNT adsorbed on silver nanoparticles. The sample was analysed with a 830 nm laser excitation wavelength, the laser operating power was 100 mW using an accumulation time of 40 s.

RDX is likely to be slightly less Raman active than TNT. This is due to the presence of the nitrogens in the cyclic ring, therefore there is no aromaticity in the ring which limits the depolarisation of the molecule. This is in agreement with the first Raman spectrum obtained from RDX, also reported by McNesby *et al.*[126] Under the same experimental conditions that were applied to TNT, a Raman spectrum of RDX could only be observed if the power of the excitation laser was increased from 300 to 400 mW, indicating that RDX is less Raman active than TNT.

However, Gu *et al.* have reported the solution based detection of RDX by SERS. RDX was directly adsorbed onto the surface of gold nanoparticles.[130] A range of

concentrations of RDX (1 mg/ml), dissolved in acetonitrile, was adsorbed onto gold nanoparticles with a diameter of 90 nm. This solution was then spotted onto a glass slide and left to dry. This allowed for the acetonitrile to evaporate, concentrating the RDX. Also, the nanoparticles were air dried on the glass slide resulting in clustering of nanoparticles. An enhancement in SERS can be observed for a molecule adsorbed between clusters of nanoparticles due to the coupling of LSPRs. The limit of detection of RDX was determined to be 1 μM using a 785 nm laser excitation, with 1 mW laser power and an interrogation time of 10 s.

PETN on the other hand is very difficult to detect by Raman spectroscopy as it is aliphatic, and therefore much less Raman active. Hence less been reported on the SERS of PETN by adsorption onto metallic surfaces. Again, McNesby reported the first Raman spectrum of PETN by interrogating a powdered sample in a glass capillary tube by FT Raman spectroscopy.[126] However, utilising the enhancement properties of Klarite[TM], PETN has been detected as low as 158 nM.[131] PETN (1 mg/ml) dissolved in ethanol, was spotted onto the Klarite[TM] surface. The low detection limit of PETN was further aided by allowing the PETN solution to evaporate, effectively concentrating PETN molecules onto the surface of Klarite[TM]. The sample was analysed with a laser power of 180 mW, using 785 nm laser excitation and an accumulation time of 10 s.

The detection of TNT, RDX and PETN by adsorbing the explosive materials onto metallic surfaces and analysing by SERS is not ideal. The examples reviewed required a high laser power and/or a long accumulation time in order to achieve a low limit of detection. These instrumental requirements may not be possible when using portable Raman instrumentation for rapid detection in the field, which is the aim of this project.

However, Graham *et al.* formed a Raman active stilbene from the CH_3 group on TNT.[132] A stilbene is a hydrocarbon with an ethene and a phenyl group substituted on the double bonded carbon. These TNT derivatives are easily synthesised by base

catalysed condensation of nitro toluenes with aromatic aldehydes. They were then added to a silver nanoparticle solution and controlled aggregation occurred by using poly-(L-lysine) as an aggregating agent. The TNT stilbene derivative nanoparticle aggregates were then analysed by SERS, using 514 nm laser excitation for an accumulation time of 10 s. Significant SERS spectra was obtained for stilbenes made from 5-methylthiopene and benzotriazole-5-carbahyde. The SERRS spectra obtained were individual and characteristic for each stilbene as each had different molecular vibrations present.

In spite of the high laser power and long accumulation times required to observe a SERS spectrum of explosives, low concentrations can be detected. However, instrumental and environmental factors can affect the SERS response for the same molecule. For example, Hernandez-Rivera *et al.* found that by simply changing the solvent the explosive material was dissolved in, resulted in a different Raman spectrum.[133] This is due to the solvents polarity. For example, it is well known that H_2O is not Raman active as the hydrogen bonds do not allow for a change in polarisability. However, ethanol has an increased polarisability compared to water, therefore a molecule in this solvent is more susceptible to polarisation. Therefore, a different SERS spectrum of the same molecule can be obtained in different solvents. Furthermore, there are numerous other factors which have the potential to change the Raman spectra: temperature, humidity, laser excitation wavelength, mirror positions in the instrument, concentration of the analyte, surface of the substrate and aggregation agent used. Therefore, the initial stage of this research is focussed on the direct SERS detection of TNT, RDX and PETN adsorbed on silver nanoparticle surfaces.

2.3   Results and Discussion

2.3.1 Nanoparticle Characterisation

The detection of TNT was initially investigated in this chapter by using silver nanoparticles and SERS. Silver nanoparticles were synthesised by using the citrate reduction method.[105] This method involves the reduction of silver ions to silver atoms, in the presence of citrate and heat. Furthermore, the citrate acts as a stabilising agent, encapsulating each nanoparticle with a negative layer, preventing self aggregation due to electrostatic repulsion. The silver nanoparticles prepared were measured to be 64 ± 4.26 nm in diameter using dynamic light scattering (DLS). The zeta potential of the nanoparticles was also measured, in order to determine the stability of the nanoparticles and surface charge. It has been established, that nanoparticles with a zeta potential that is greater than +/- 25 mV are stable in solution.[134] For the silver nanoparticles synthesised, the zeta potential was recorded to be -38.8 ± 11.1 mV. To further assess the stability of the nanoparticles, an extinction spectrum was obtained by UV-vis spectroscopy, Figure 2.1. As can be seen, the extinction spectrum has a LSPR with a λ_{max} at 410 nm, which is a typical value for this size of silver nanoparticle.[135] Furthermore, information on the monodispersity and size of the nanoparticles can be obtained by using the full width half maximum value (FWHM) of the LSPR peak.[136] The smaller the LSPR FWHM value is, the more monodispersed the nanoparticles. The nanoparticles synthesised in Figure 2.1 have a FWHM value of 83 nm, indicating a monodispersed colloidal solution. Furthermore, using the Beer-Lambert law, $(A = \varepsilon\, l\, c)$, the concentration of the colloidal solution can be determined. Where, A = absorbance maximum, ε = extinction co-efficient of silver nanoparticles (1.85×10^{10} M^{-1} cm^{-1}), l = path length of the cuvette and c = concentration. The concentration of the silver nanoparticles synthesised was determined to be 0.36 nM.
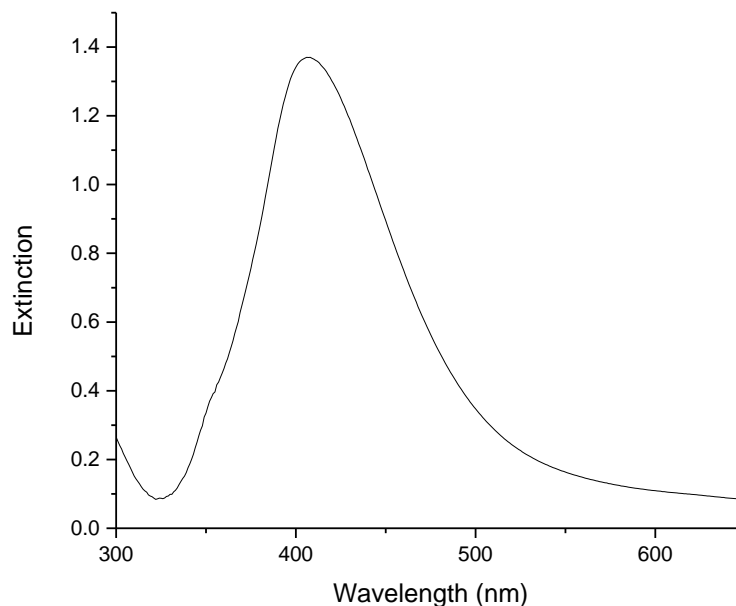
Figure 2.1: Extinction spectrum of silver nanoparticles.

In order to obtain a SERS spectrum of TNT, a range of concentrations from 50 nM – 3.5 μM of TNT, dissolved in acetonitrile, were added to a silver nanoparticle solution. The solution (150 μl) was then placed into a 96 well plate and was analysed using 532 nm laser excitation with a 10 s accumulation time. However, no spectrum of TNT was observed, as shown in Figure 2.2 (a), only peaks from the acetonitrile that the TNT was dissolved in could be observed. Therefore, an aggregating agent was added to the silver nanoparticles in order to aggregate the solution. Many aggregating agents have been previously reported,[137, 138] however salt solutions are the most commonly used. Upon addition of a salt solution, in this case NaCl, the protective citrate layer which encapsulates the silver nanoparticles becomes unstable, and subsequently large clusters of nanoparticles are formed. This is an advantage for use in SERS because, as the nanoparticles come into close proximity to each other, areas of high electron density are formed, known as 'hotspots'. These 'hotspots' enhance SERS intensities. Therefore, any analyte present in these 'hotspots' can exhibit an enhancement in the Raman scattering, as shown in Figure 2.2 (b).
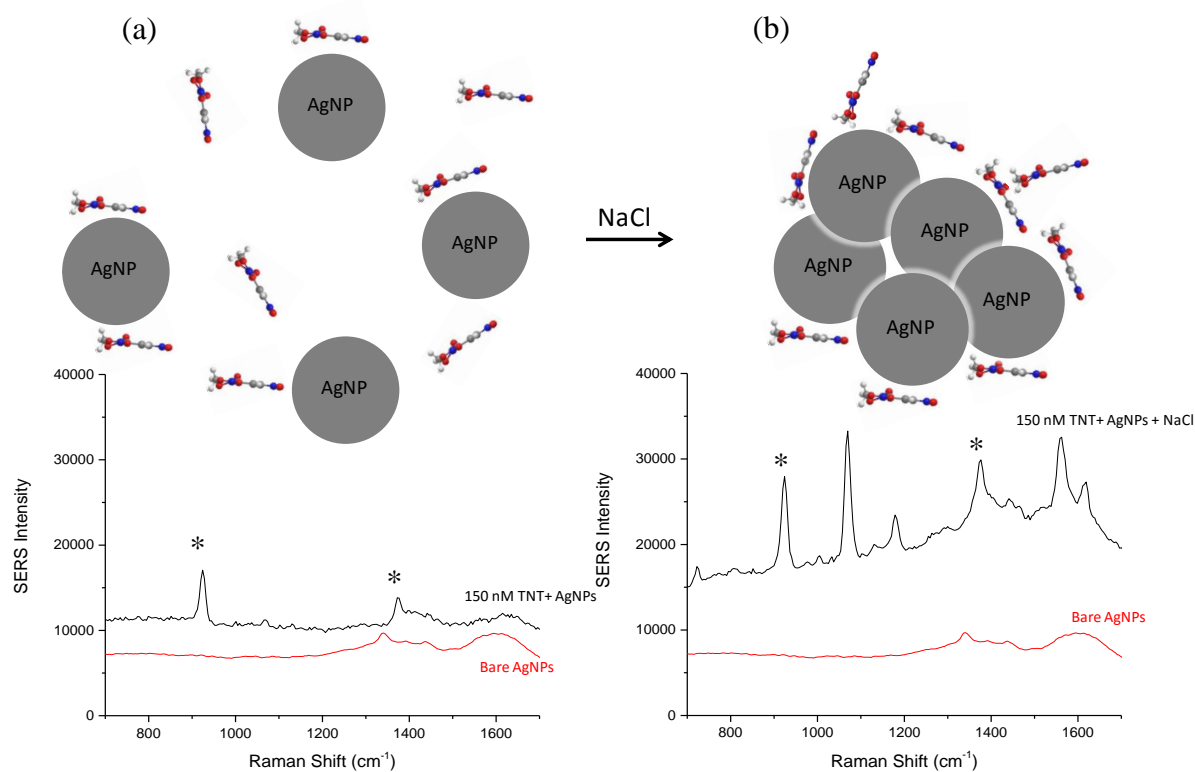
Figure 2.2: (a) Schematic representation of TNT adsorbed onto the surface of silver nanoparticles (AgNPs) and the SERS spectra of bare nanoparticles and TNT adsorbed onto the surface of silver nanoparticles, **(b)** schematic representation of salt (NaCl) induced aggregation of TNT adsorbed onto silver nanoparticles and the SERS spectra of bare nanoparticles and salt induced TNT adsorbed onto the surface of silver nanoparticles.

In Figure 2.2 (a), it can be seen in the red spectrum, when TNT is absent a SERS spectrum of citrate can be obtained. This is due to the stabilising citrate layer capping the nanoparticles. Citrate peaks can be observed at 1335 and 1600 cm^{-1} due to COO$^-$ stretching.[139] However, when TNT dissolved in acetonitrile is added to the nanoparticle solution, only a SERS spectrum of acetonitrile was observed (black (*) spectrum), there were no TNT specific peaks observed. However, upon the addition of NaCl (final concentration = 8.8 mM, Figure 2.2 (b)), 'hotspots' were formed, and therefore TNT specific peaks are observed.

2.3.2 SERS of Acetonitrile

The explosive materials, TNT, RDX and PETN were dissolved in acetonitrile, therefore it was necessary to obtain a control spectrum of acetonitrile adsorbed onto the surface of silver nanoparticles to eliminate acetonitrile specific peaks from the SERS spectra of the explosives. A SERS spectrum of acetonitrile was obtained by adding acetonitrile (100 μl) to the silver nanoparticles (150 μl, 0.326 nM) and NaCl (8.8 mM) was added to aggregate the nanoparticles. Immediately upon the addition of NaCl, a colour change was observed, from a yellow/green to a grey/black. This was due to the formation of large clusters of nanoparticles, resulting in a change in LSPR. Analysis by SERS was then performed by interrogating the sample, 532 nm laser excitation was used, with an accumulation time of 10 s (Figure 2.3).
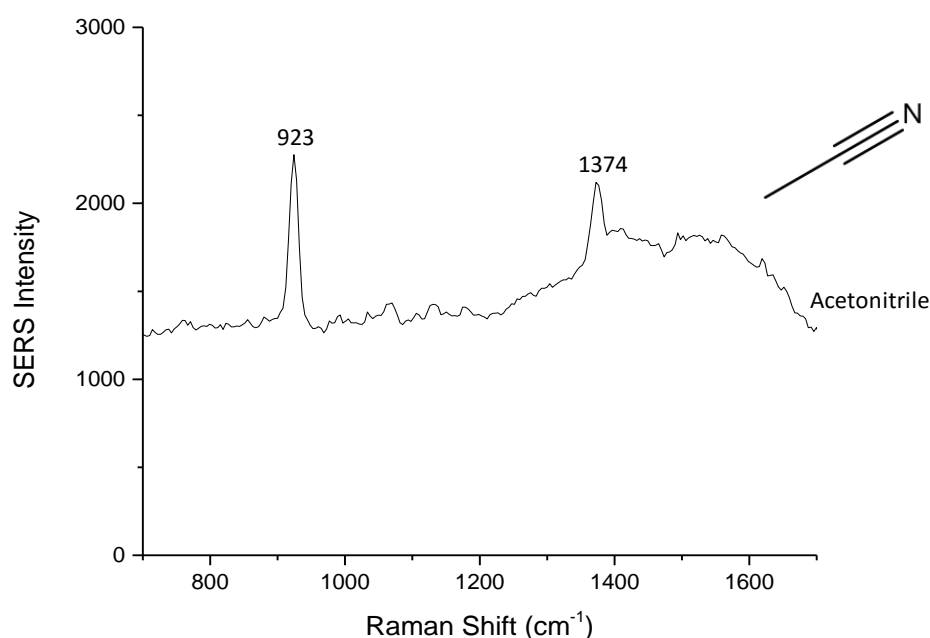
Figure 2.3: SERS spectra of acetonitrile (100 μl) adsorbed on silver nanoparticles (150 μl) with the addition of NaCl (8.8 mM) using a 532 nm laser excitation and a10 s accumulation time over 5 measurements for 3 samples.

In Figure 2.3, the spectrum denotes the SERS spectrum of acetonitrile. There were peaks present at 923 and 1374 cm^{-1}, due to C-C stretching and CH_3 deformation.[140]

2.3.3 SERS of TNT

A SERS spectrum of TNT was obtained by adding a range of concentrations of TNT to silver nanoparticles in the presence of an aggregation agent. A range of TNT concentrations (50 nM – 3.5 μM) were added to silver nanoparticles (0.326 nM) and NaCl (8.8 mM) was added to aggregate the nanoparticles. Analysis by SERS was then performed by interrogating the sample, 532 nm laser excitation was used, with an accumulation time of 10 s. Figure 2.4 demonstrates the SERS spectra of three different concentrations of TNT adsorbed onto silver nanoparticles. The black spectrum (Figure 2.4(a)) represents 80 nM of TNT adsorbed onto silver nanoparticles. Raman bands were observed at 923 and 1376 cm^{-1}, which are due to the presence of the acetonitrile in which the TNT was dissolved. No TNT specific peaks were observed at this low concentration. However, when the concentration of TNT was increased to 120 nM (red spectrum) a strong band at 1066 cm^{-1} was observed. This band was assigned to being due to the asymmetric staggering of the CH_3.[20] There were also peaks present at 1560 and 1618 cm^{-1}, which are due to the asymmetric NO_2 vibrations. The band present at 1178 cm^{-1} is due to the stretching of the phenyl ring of TNT. Furthermore, Clarkson *et al.* have previously performed DFT calculations on TNT, and the peaks present in the spectrum shown in Figure 2.4 are in agreement, within ± 5 cm^{-1}, to the theoretical values reported.[20]
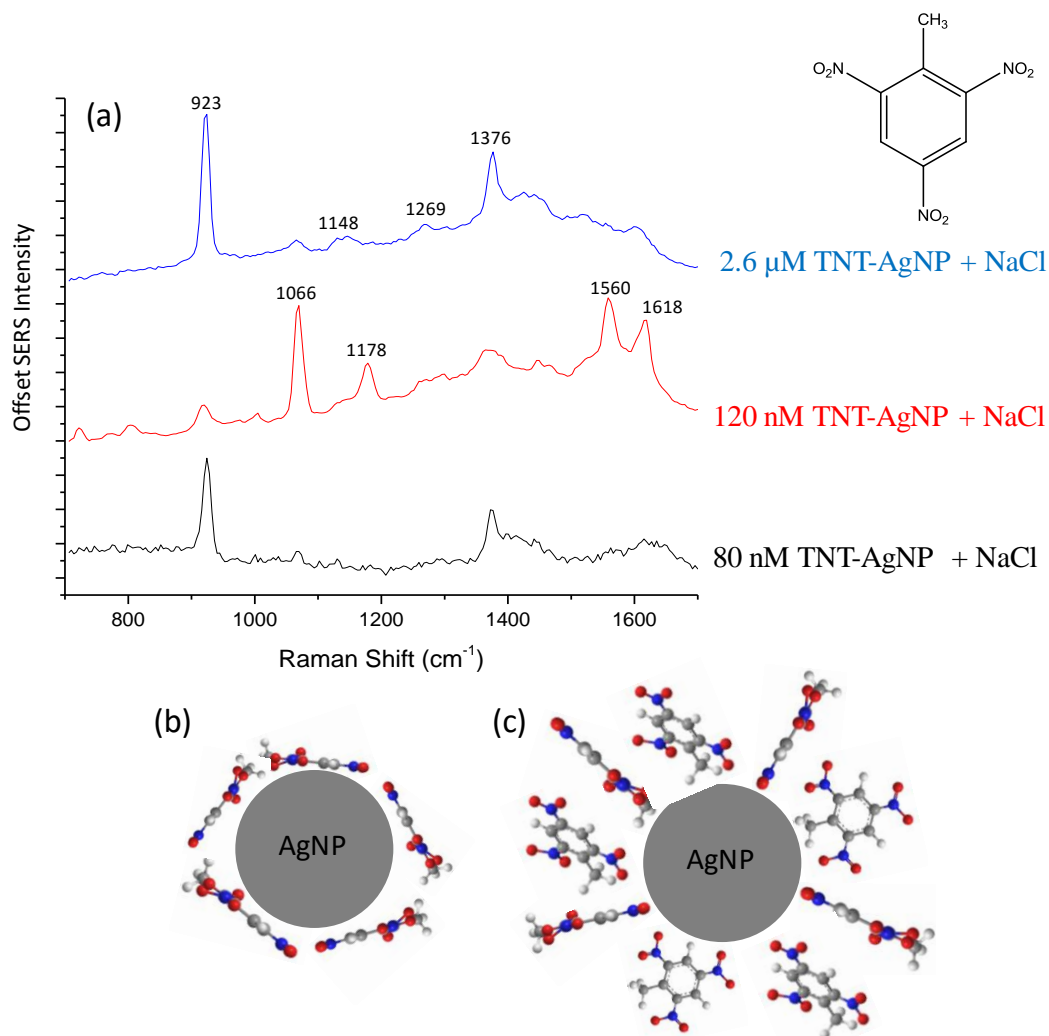
Figure 2.4: (a) SERS spectra of 80 nM (black), 120 nM (red) and 2.6 μM (blue, 250 μl) of TNT adsorbed onto silver nanoparticles (AgNPs) surface (250 μl) after the addition of NaCl (8.8 mM), 532 nm laser excitation was used with a of 10 s accumulation time for 5 measurements of 3 replicate samples. Spectra shown has been baseline corrected, scaled and offset for clarity, **(b)** schematic representation of low concentrations TNT on nanoparticles surface, **(c)** schematic representation of high concentrations of TNT on nanoparticles surface.

These peaks strongly suggested that the TNT molecules were laying flat on the surface of silver nanoparticles as shown in Figure 2.4 (b). This 'flat' orientation would result in a rotated out-of-plane nitro group, due to the internal rotation of the methyl group, orientating perpendicular to the nanoparticles surface. SERS selection rules dictate that molecular vibrations which are perpendicular to the nanoparticle surface are more enhanced than others. This orientation of TNT on the negatively charged nanoparticle surface, when at low concentrations, could be expected as TNT has strong electron withdrawing groups. The NO_2 groups of TNT are enhanced over

other molecular vibrations due to the SERS selection rules, the spectroscopic data suggests that the phenyl ring is parallel to the nanoparticle surface, as shown in Figure 2.4 (b). Therefore, at low concentrations it is proposed that TNT lies flat on the nanoparticle surface.

At 2.6 μM of TNT (Figure 2.4 (a), blue) there were peaks observed at 1148 and 1269 cm^{-1}, which were assigned to the symmetrical vibrations of CN and the 2- and 6- NO_2 groups. The change in the SERS spectrum, with increasing TNT concentrations suggests that the TNT is changing orientation, to allow for more molecules to be adsorbed onto the surface. It is suggested that the TNT molecules are change from a 'flat' orientation to a 'standing' orientation (Figure 2.4 (c)). This standing orientation would result in less SERS peaks, as the C-C stretches in benzene ring would now be perpendicular to the nanoparticle surface. These C-C stretches are not as Raman active as NO_2 vibrations as they are not as polarisable. Furthermore, it was found at higher concentrations of TNT, strong enhancements were also observed for acetonitrile. This was thought to be due to the 'upright' orientation of the TNT molecules. When the TNT coverage in this 'upright' orientation on the nanoparticle is below monolayer, there is space for acetonitrile to be adsorbed onto the surface, resulting in the enhancement of acetonitrile peaks. Figure 2.4 shows the three different concentrations of TNT adsorbed on the surface of silver nanoparticles, as the spectra obtained at these three concentrations emphasise this change in orientation of TNT with increasing concentration. The remainder of the SERS spectra, shown in Figure 2.5, represents the 'intermediates' of this change in orientation.
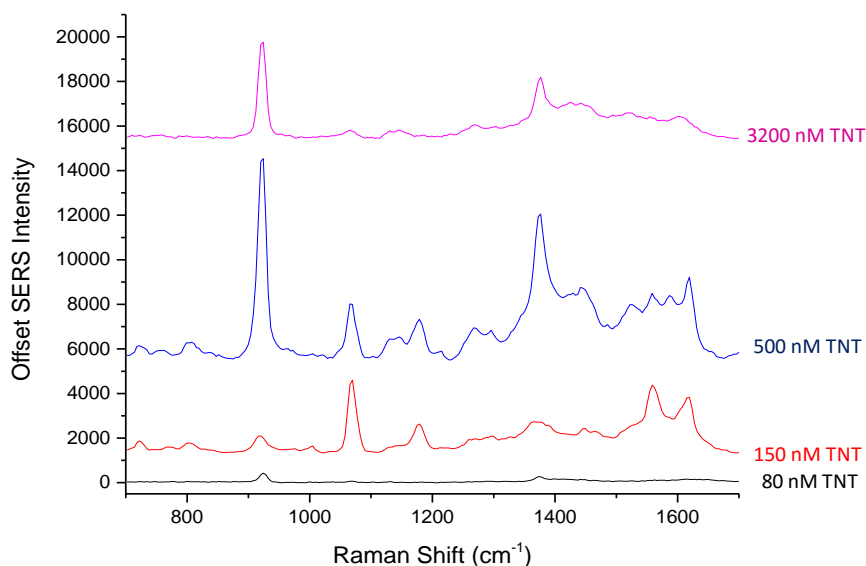
Figure 2.5: SERS spectra of 80 (black), 150 (red), 500 (blue) and 3200 (pink) nM of TNT adsorbed on silver nanoparticles with the addition of NaCl (8.8 mM). Spectra were obtained using 532 nm laser excitation with 10 s accumulations of for 5 measurements for 3 replicate samples. Spectra shown were baselined and offset for clarity.

In Figure 2.5, it is also demonstrated that as the concentration of TNT is increased to 500 nM, the bands at 1066, 1560 and 1618 cm^{-1} are enhanced due to the 'flat' orientation of TNT on the surface. Therefore, the out-of-plane CH_3 and the NO_2 vibrations are perpendicular to the nanoparticle surface. Furthermore, as the concentration of TNT is further increased to 3200 nM, the spectrum obtained is mainly of acetonitrile peaks, confirming a change in orientation. The peak assignments for TNT are summarised in Table 2.1.[20]

Using this method for direct adsorption of TNT to silver nanoparticles with NaCl aggregation of the nanoparticles and using a 10 s accumulation time, the lowest observed limit of detection of TNT was 120 nM. However, clearly this adsorption method is not very specific since the spectra of TNT changes significantly with increasing concentration. As a result, these spectral variations suggested it would be very challenging to selectively and quantitatively detect TNT in complex matrices using a direct SERS approach, therefore it was not deemed a suitable method for TNT detection.

Table 2.1: Summary of TNT peak assignments.

Wavenumber (cm^{-1})	Peak Assignment
1066	CH$_3$ asymmetrical staggering
1178	Phenyl ring
1560	NO$_2$ asymmetrical stretching
1596	C-C ring vibration
1618	NO$_2$ asymmetrical stretching

Furthermore, 2, 6- dinitrotoluene (DNT) was used as a control, it is commonly used a control in analytical experiments as it is structurally similar to TNT, containing only 2 nitro groups versus 3 for TNT. Hence, DNT is used regularly as a control molecule for nitro based explosive detection. The SERS spectrum of DNT is shown in Figure 2.6.
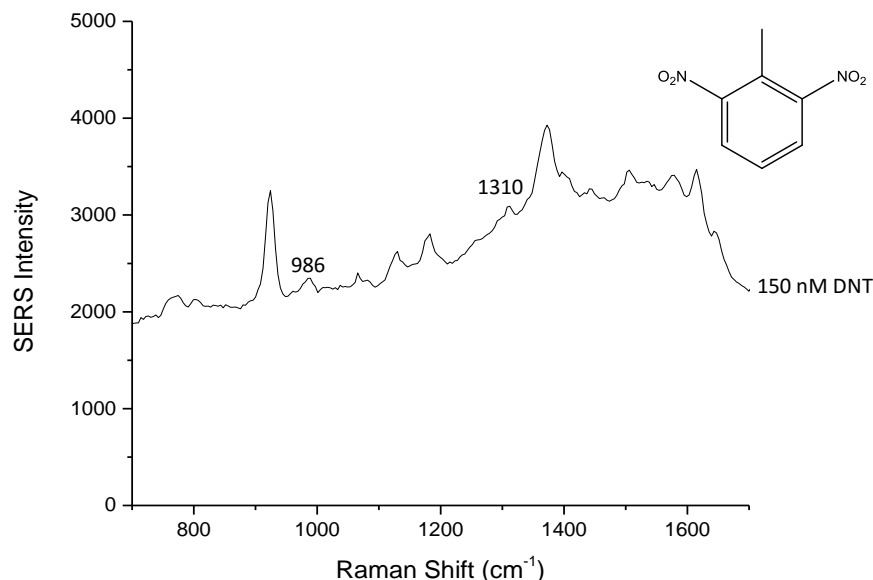
Figure 2.6: SERS spectra of DNT (150 nM) adsorbed on silver nanoparticles (150 μl) with the addition of NaCl (8.8 mM) using a 532 nm laser excitation for 10s over 5 measurements for 3 samples, in which the average is shown.

DNT was also dissolved in acetonitrile, therefore acetonitrile specific peaks at 923 and 1376 cm^{-1} were also present in the DNT spectrum. The main peaks associated with DNT, Figure 2.6, were 1310 cm^{-1} due to the NO_2 stretching and 986 cm^{-1} due to the aromatic ring.[141] Compared to TNT, DNT has two strong electron withdrawing groups rather than three, resulting in a different SERS spectrum. However, 2, 6 - DNT still has a rotated out of plane methyl group due to the steric hindrance of the two NO_2 groups.

2.3.4 SERS of RDX

Similar to TNT, RDX is also a high energy explosive material; chemically the structure of RDX is very different to TNT, it is not aromatic, it consists of a triazine ring with the nitro groups bound to the nitrogens in the hetrocyclic ring. A range of concentrations from 120 nM – 3.5 μM of RDX were added to silver nanoparticles (500 μl) in the presence of NaCl (8.8 mM) and analysed using 532 nm laser excitation with an accumulation time of 10 s. The RDX SERS spectra obtained are shown in Figure 2.7.
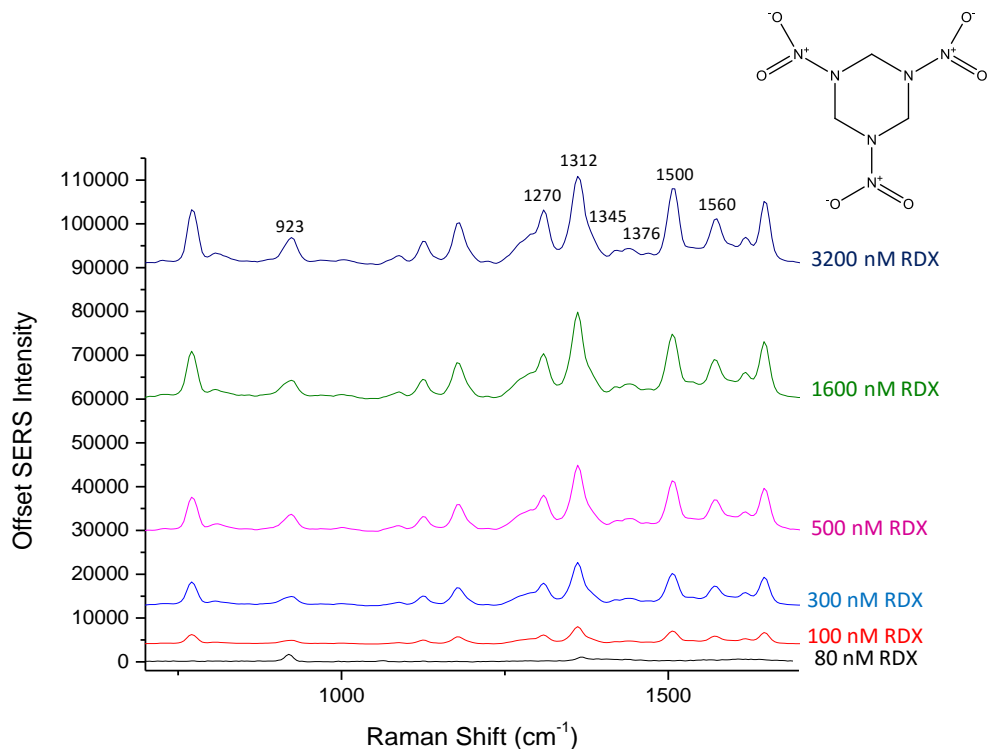
Figure 2.7: SERS spectra of a range of 80 (black), 100 (red), 300 (blue), 500 (pink), 1600 (green) and 3200 (navy) nM of RDX adsorbed onto surface of silver nanoparticles (250 µl) with the addition of NaCl (final concentration = 8.8 mM). Spectra were obtained using 532 nm laser excitation with an accumulation time of 10s. 5 measurements of 3 replicate samples were measured and the average spectrum is shown. Data set was baselined and offset for clarity.

As mentioned previously for TNT, RDX was dissolved in acetonitrile, therefore in the RDX spectra (Figure 2.7) peaks can be observed at 923 and 1376 cm^{-1} due to acetonitrile. The RDX spectra show that there are peaks observed at 1270, 1345 and 1500 cm^{-1}. These peaks have previously been assigned to N-N stretching and NO$_2$ stretching by Torres *et al.*[30] The peak present at 1312 cm^{-1} results from CH$_2$ wagging, and the peak at 1560 cm^{-1} is due to asymmetric NO$_2$ stretching.[130] Furthermore, it was found that as the concentration of RDX increased, the SERS spectra remained consistent at each concentration. A summary of the RDX specific peaks and their assignments are given in Table 2.2.

Table 2.2: Summary of RDX peak assignments.

Wavenumber (cm^{-1})	Peak Assignment
1270	N-N stretching
1345 and 1500	NO_2 stretching
1312	CH_2 wagging
1560	NO_2 asymmetrical stretching

Since the spectra obtained from RDX do not vary in terms of observed peak positions when the RDX concentration is varied, this suggests that RDX, unlike TNT, does not change orientation on the nanoparticle surface with increasing concentration. This is thought to be due to the lack of aromaticity in the ring, therefore the $N-NO_2$ group is not as electron withdrawing as the NO_2 in TNT. Therefore, the triazine ring will be less electropositive and there would be less attraction between the ring and the negatively charged nanoparticles. This could result in RDX orientating perpendicular to the nanoparticle surface. This is experimentally in agreement with the work of Baohua *et al.,* who used diamond shaped gold nanoparticles to directly adsorb RDX onto the surface in order to obtain a SERS spectrum. Baohua *et al.* indicate that RDX is most probably adsorbed 'upright' on the nanoparticle surface.[130] Furthermore, an observed detection limit of 100 nM of RDX was obtained. This was unexpected as TNT is thought to have a greater Raman cross-section, compared to RDX, however an observed limit of detection of 120 nM TNT was obtained. This may be due to the SERS limit of detection being dependent on how the molecule binds to the surface of the nanoparticles. Therefore, TNT has strong electron withdrawing groups, causing repulsion between the negatively charged nanoparticle and the electronegative NO_2 groups, therefore allowing less TNT molecules to be adsorbed onto the nanoparticles surface. As explained, RDX is less electron withdrawing, therefore more RDX

molecules could potentially be adsorbed onto the nanoparticles surface, resulting in a lower limit of detection.

2.3.5 SERS of PETN

The last explosive that was investigated was PETN. Similar to TNT and RDX, PETN also contains several nitro groups. However, unlike TNT, PETN is an aliphatic molecule. This makes PETN less Raman active and subsequently harder to detect by SERS at trace levels. In order to observe a SERS spectrum a range of concentrations of PETN (120 nM – 3.5 μM) were added to silver nanoparticles in the presence of NaCl (8.8 mM) and analysed using a 532 nm laser excitation and an accumulation time of 10 s (Figure 2.8).
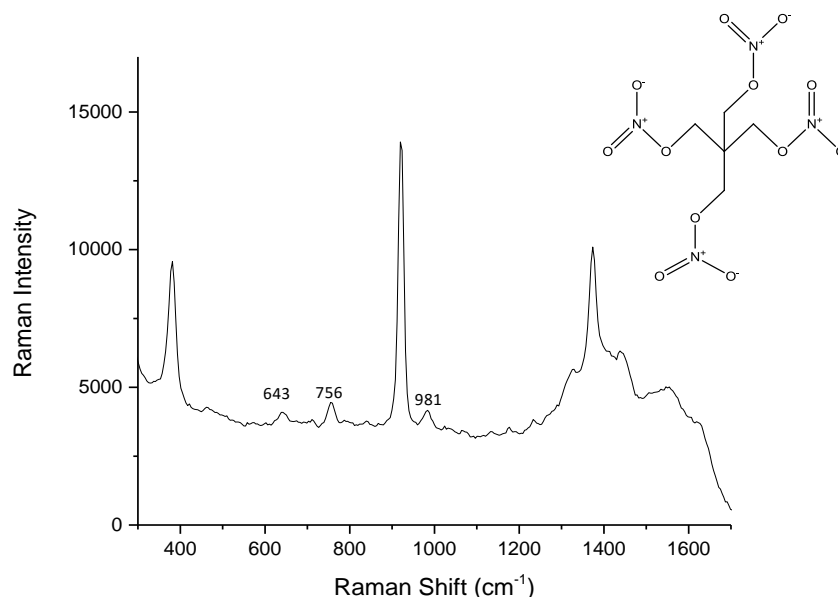
Figure 2.8: SERS spectra of 3.5 μM of PETN using silver nanoparticles (250 μl) with the addition of NaCl (8.8 mM) using 532 nm laser excitation with 10 s accumulation time. The spectrum shown is the average of 5 measurements of 3 replicate samples.

Due to the properties of PETN, a SERS spectrum (Figure 2.8) could only be obtained for the highest concentration of PETN available (3.5 μM). PETN was dissolved in acetonitrile, and it was observed that the acetonitrile peaks dominated the spectrum at 389, 923 and 1376 cm^{-1}.[140] However, small peaks assigned to PETN could be observed at 643, 756 and 981 cm^{-1}.[142] These peaks were present due to NO$_2$ rocking and stretching vibrations. As previously mentioned, PETN is an aliphatic

molecule hence it is a weak Raman scatterer. Therefore, the enhancement of the bands obtained from PETN, in comparison to TNT and RDX, was much weaker. In light of these observations, a technique which can positively identify this explosive material selectively and specifically at lower concentrations is highly desirable as detection was not achievable by using SERS combined with the direct absorption of PETN onto silver nanoparticles surface.

2.4   Conclusions

In conclusion, SERS was used, utilising silver nanoparticles as the enhancing surface, to acquire spectra for three explosive materials, in the presence of NaCl. All three target explosives TNT, RDX and PETN could be identified by SERS. TNT was identified due to the presence of the peak at 1066 cm^{-1} from the out-of-plane methyl group, 1178 cm^{-1} due to the phenyl ring, 1560 and 1618 cm^{-1} due to the NO$_2$ stretching. RDX was found to have two very intense peaks at 1270 and 1500 cm^{-1} from NO$_2$ vibrations. Finally, PETN was observed to have two weaker peaks associated with NO$_2$ vibrations at 643 and 756 cm^{-1}. The limit of detection of these explosives were found to be 120 nM for TNT, 100 nM for RDX and 3.5 μM for PETN, which was comparable to those previously reported in the literature.[129-131]

However, it was determined that the SERS response can be greatly influenced by an increase in TNT concentration which was postulated to be due to changes in orientation of the molecule on the nanoparticle surface. The data suggested that at low concentrations of TNT, the TNT orientating parallel to the nanoparticle surface. However, as the concentration of TNT increased, TNT orientated perpendicular to the nanoparticle surface, allowing for more molecules to be adsorbed. As a result, this technique would be challenging when attempting to quantify an unknown concentration of TNT, or when trying to distinguish multiplexed samples in a more complicated matrix due to change in spectra with TNT concentration. Furthermore, it was also determined that explosive molecules, especially those with strong electron withdrawing groups, do not have a high affinity for negatively charged silver nanoparticles, as it was observed that a lower limit of detection was obtained for RDX in comparison to TNT, despite TNT having a larger Raman cross-section. This

was again thought to be due to how the molecules orientate on the nanoparticle surface. The strong electron withdrawing groups on TNT makes TNT slightly more electronegative than RDX and hence will experience more repulsion with the negative silver nanoparticle, resulting in less TNT molecules being adsorbed on the nanoparticles surface, in comparison to RDX.

Furthermore, only a very weak SERS spectrum of PETN could be obtained at high μM concentration. It was for these reasons that it was determined that more sensitive assay would be required to allow selective and specific detection of explosives as the direct SERS approach was not sensitive or specific enough.

3. Molecular Identification of Explosives by a New Class of SERS Immunoassay

Metallic nanoparticles are an ideal surface for conjugation of biomolecules due to the ease of functionalisation. Biomolecule functionalised nanoparticles allow for the specific detection of a target using plasmon enhanced spectroscopies. Commonly used capture biomolecules which have been conjugated to nanoparticles include nucleic acids,[99] peptide aptamers,[143] and antibodies,[144] demonstrating very high selectivity and specificity. The previous chapter involved the detection of TNT, RDX and PETN by SERS. However, high concentrations of each material were required to obtain a SERS spectrum of the explosives. In the TNT spectra it was observed that as the concentration of TNT increased, the SERS spectra changed due to a change in orientation of TNT on the nanoparticles surface. This was not ideal for multiplex detection of several target analytes, therefore a method which allows for the detection of explosives at low concentrations, with no change in spectra as the concentration changes, was required. The use of SERS combined with biomolecule functionalised metallic nanoparticles for the detection of the small molecules has the potential to provide highly selective and sensitive detection.

3.1 Introduction

Antibodies are being increasingly used as detection elements in biosensors due to their high specificity and selectivity. However, the immobilisation of antibodies on a surface is of fundamental interest, yet still remains a key challenge.[145] Conventional strategies of antibody immobilisation usually involve three orientations: random, 'head on', and 'tail on'.[146] Whilst these immobilisation methods are of interest, no specific molecular spectrographic information from the target analyte has been obtained to date. Detection using these methods usually involves indirect detection aided by fluorescent or SERS labelling. Many immobilisation methods have been reported, for example, Johnson *et al.* used protein G encapsulated nanoparticles for

subsequent antibody binding.[147] Protein G has a high binding affinity for metallic surfaces due to the aspartic acid content, it also has a high affinity for the fragment, antigen binding (Fab) region and for the fragment crystallisable (Fc) region of an antibody, due to its more thermodynamically stable tertiary structure when the antibody is bound. Whilst this method provides a high affinity for an antibody to subsequently bind to the nanoparticle, it is not ideal as there is a possibility that the binding site for the analyte on the antibody is not free, as it could be bound to the protein G. El Sayed *et al.* reported the conjugation of an antibody directly onto the surface of gold nanoparticles surface by using a pH correction method. In this method, the free positive amine groups present in the amino acid chain electrostatically adsorb onto the negative citrate capped nanoparticles.[144] This method allows for a random immobilisation approach, in which some antibodies are orientated 'tail on', 'head on' and some antibodies are orientated 'flat' on the gold nanoparticles surface. This is not ideal as not all binding sites of the antibody will be accessible to the target. However, it is likely that the binding sites that are available will result in the antibody being orientated on the nanoparticles surface such that the target molecules will be held several nm away from the metal surface. This orientation is not ideal for target detection by SERS as the response obtained is dependent on the distance between the analyte and the metal surface, therefore labelling or tagging is usually required.[72]

3.2   Overview of Aims

The aim of this research was to design a novel SERS assay for the detection of explosives using silver nanoparticles conjugated to a fluorescently labelled highly specific monoclonal antibody, as shown in Figure 3.1. An antibody which has a high affinity for an analyte is an attractive capture probe as it will specifically bind to the analyte, even within a complex matrix.[148] It can therefore be used to bring the analyte molecule close to the nanoparticles surface in order to obtain a specific spectrum of the analyte, even when low analyte concentrations are present. The fluorescently labelled antibody was immobilised on the nanoparticle surface, allowing for the target molecule to come in close proximity to the metal surface,

allowing for the direct detection of the target specifically by SERS, as shown in Figure 3.1.
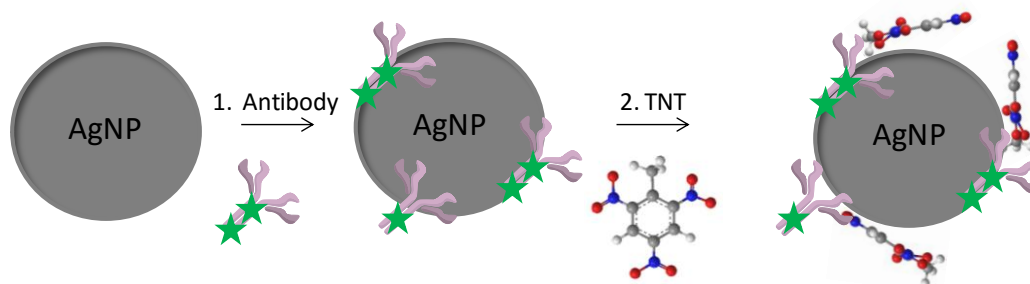
Figure 3.1: Schematic representation of the conjugation of fluorescently labelled antibodies to the surface of silver nanoparticles following the capture of the target, in this case TNT.

An assay was designed using silver nanoparticles which were functionalised with antibodies highly specific for explosives. These antibodies were specifically orientated on the nanoparticle surface to reduce the distance between the metal surface and the analyte, in order to obtain the intrinsic SERS response from the analyte molecule. A commercially available antibody was used in this assay that has a fluorophore modification which acts as an anchoring group, subsequently allowing for the antibody to bind to the metal surface. The fluorophore, fluorescein isothiocyanate (FITC), was stated as being bound to the antibody in such a way, that the ITC group was free to allow for nanoparticle binding, allowing the terminal sulfur to bind to the silver nanoparticle. Furthermore, it was stated that there were approximately 4 FITC molecules conjugated to a single antibody, thus suggesting that the FITC molecules allow for the antibody to be immobilised parallel or 'flat' to the nanoparticles surface, as opposed to the random or 'tail on' orientation previously reported.

Shown in Figure 3.2, is a schematic representation of a 'tail on' orientated antibody, and a 'flat' orientated antibody on a metallic surface. As shown by the red arrows (Figure 3.2) this 'flat' orientation should significantly decrease the distance (approximately 10.5 nm) between the nanoparticle and the target analyte, therefore resulting in the target being detected by SERS directly. To demonstrate the specificity of this assay, the analytes 2, 4, 6-trinitrotoluene (TNT) and hexahydro-1,

3, 5-trinitro-1, 3, 5-triazine (RDX) and a non explosive example 2-aminomethyl-1, 4-benzodioxane (dioxane) were selected.
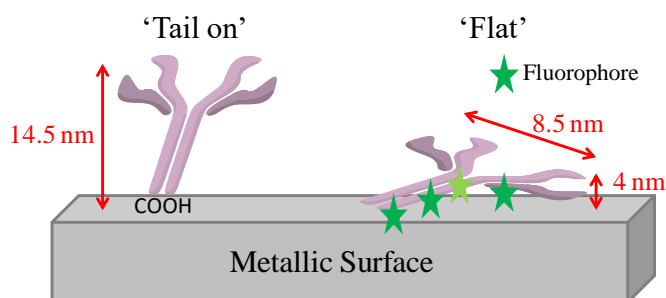
Figure 3.2: Schematic representation of antibody immobilisation on a metallic surface.

3.3 Results and Discussion

3.3.1 Antibody Conjugated Nanoparticles

A fluorophore modified antibody was used in this assay, allowing for the antibody to bind to the silver nanoparticle surface in a novel orientation. Usually antibodies are immobilised on a surface via the free COOH group, a free amine group or by using a linker molecule.[144, 147] Thus, the antibody is orientated in such a way that the analyte molecule is held several nm away from the nanoparticle surface due to the antibody being orientated randomly on the surface. This is not ideal since all the binding sites on the antibody may not be available for target binding, or 'tail on'. 'Tail on' orientation results in the target analyte being distal to the nanoparticle surface, therefore direct detection of the analyte by SERS cannot be achieved, as SERS is a distance dependence technique.[72] Therefore, the antibody used in this assay was purchased with a fluorophore, fluorescein isothiocyanate (FITC), conjugated to the antibody, the structure of FITC is given in Figure 3.3.
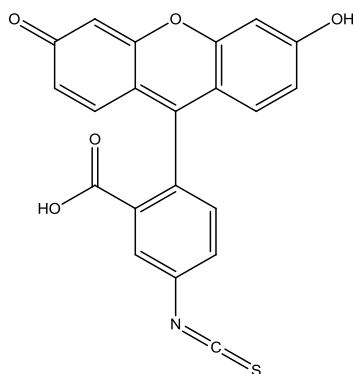
Figure 3.3: Structure of FITC.

FITC was stated as being coupled to the antibody such that the ITC group was available for further conjugation and therefore free to bind to the surface of silver nanoparticles. This strong thiol-metal bond results in the antibody binding on the nanoparticles surface, allowing for controlled orientation on the nanoparticle surface, in which the target analyte can bind to, thus allowing for the detection of the target by SERS.

The monoclonal TNT specific FITC modified antibody (2 mg/ml) was added dropwise, in a range of volumes (10 – 50 µl), to silver nanoparticles (500 µl, 0.34 nM). After 3 h, the sample was centrifuged, in order to remove any free antibody from the solution. Characterisation and optimisation of the silver nanoparticles was carried out using UV-Vis spectrophotometry, fluorescence spectroscopy and NanoSight tracking video analysis, as shown in Figure 3.4.
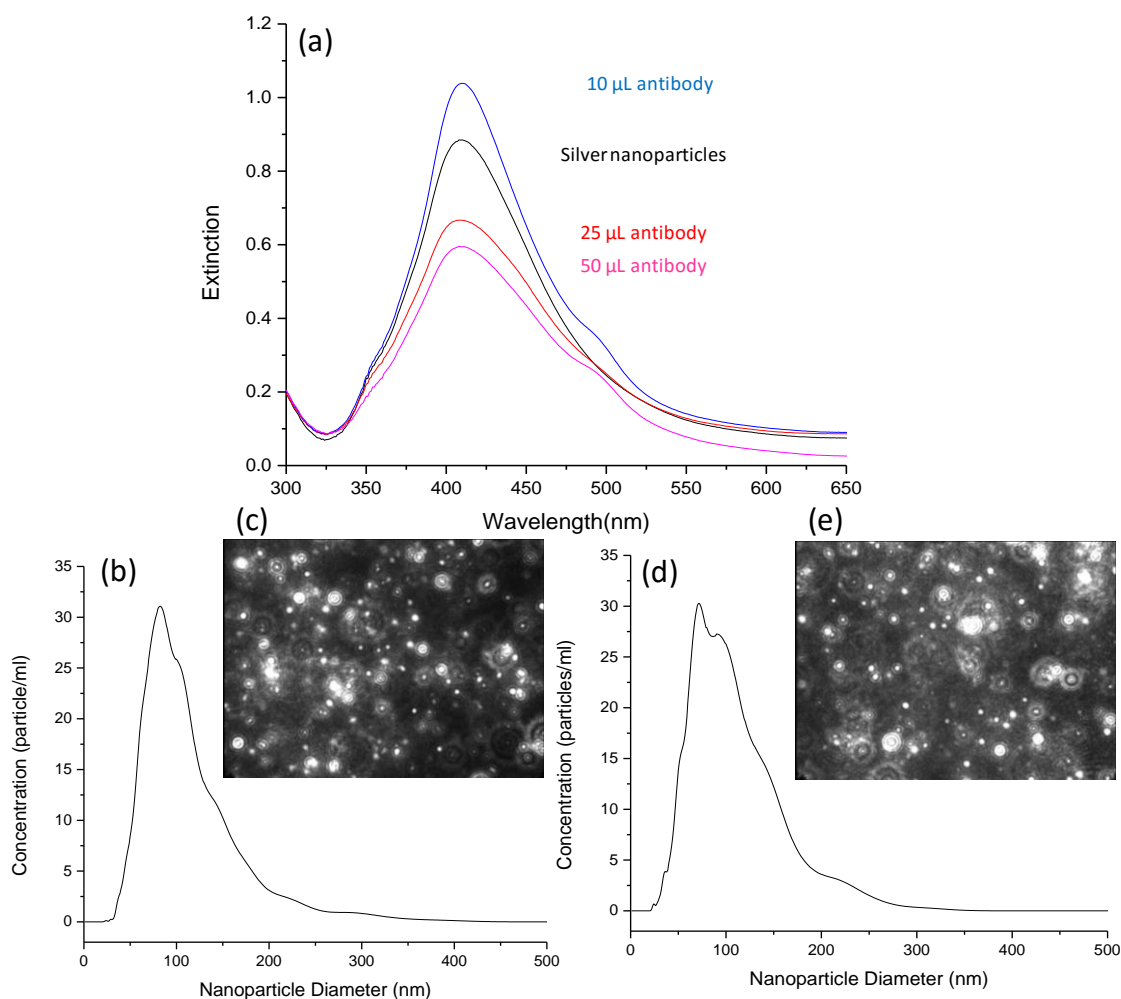
Figure 3.4: (a) The extinction spectrum of bare nanoparticles (black) and antibody (10 µl (blue), 25 µl (red) and 50 µl (pink) 2 mg/ml) conjugated nanoparticles, in which the spectrum shown is the average of three replicate samples. **(b)** Linear histogram chart representing size distribution of bare silver nanoparticles and **(c)** A frame from the NanoSight video tracking analysis showing bare nanoparticles (0.36 nM). **(d)** Antibody conjugated nanoparticles size distribution,, and **(e)** A frame from the NanoSight video tracking analysis showing antibody (10 µl, 2 mg/ml) conjugated nanoparticles (0.36 nM).

As shown in Figure 3.4 (a), bare citrate reduced silver nanoparticles (black spectrum) showed an extinction maximum at 409 nm. Upon the addition of antibody (10 µl, 2 mg/ml) to the nanoparticles, there was a slight red shift of 2 nm, from 409 to 411 nm in the extinction peak (blue), the peak has also broadened very slightly in size indicating the conjugation of an antibody to the silver nanoparticles surface. Furthermore, a small shoulder at 495 nm can be observed in the spectrum due to the presence of the FITC modification on the conjugated antibody, which has an

extinction maximum at 495 nm. This highly suggests that the antibody is on the surface of the silver nanoparticles. Figure 3.4 (a) also demonstrates that as the volume of the antibody added to the nanoparticles was increased from 10 µl to 50 µl there was a blue shift in the extinction peak of 5 nm. There was also considerable dampening of the maximum extinction, indicating slight aggregation had occurred probably due to formation of small aggregates of nanoparticle dimer and trimers. Therefore, a concentration of 10 µl (2 mg/ml) antibody per 500 µl silver nanoparticles (0.36 nM) was used throughout the rest of this study. Furthermore, NanoSight video tracking analysis was performed as shown in Figure 3.4 (b-e). The NanoSight system uses similar principles to a DLS instrument, whereby a laser beam is passed through the sample resulting in the nanoparticles scattering the light. This can then be visualised using a video camera on the NanoSight instrument. The hydrodynamic radius of the nanoparticle was determined by capturing a video of the nanoparticles under Brownian motion. The tracking software can track numerous individual nanoparticles to provide information such as particle size, concentration and aggregation state. Figure 3.4 (b-c) demonstrated that the bare nanoparticle solution was monodisperse, and the histogram showed the average hydrodynamic diameter of the nanoparticles was 71 nm. Similarly, Figures (d-e) demonstrate that when the antibody was conjugated to the silver nanoparticle surface, the solution was still monodispersed and the average hydrodynamic diameter of the nanoparticles was determined to be 81 nm. This demonstrates that the nanoparticle suspension is stable and the nanoparticles have increased in size as expected after successful conjugation of the modified antibody.

3.3.2 Fluorescence Spectroscopy

Due to the presence of the FITC modification on the antibody, fluorescence spectroscopy was used to determine how many FITC molecules were present to estimate how many antibodies were bound on the nanoparticle surface. After the antibodies were successfully conjugated to the surface of the nanoparticles, a strong reducing agent, dithiothreitol (DTT) was used to displace the antibody from the nanoparticle surface. After being left at 55 $^{\circ}$C for 16 hours, the sample was then centrifuged and the free antibodies were collected in the supernatant. A calibration

graph of FITC was obtained by measuring the fluorescence emission from solution of FITC concentrations of 3, 4, 5, 6, and 7 x10^{-10} M. The number of antibodies present on the nanoparticle surface was then determined by measuring the fluorescence emission from the supernatant, as shown in Figure 3.5.
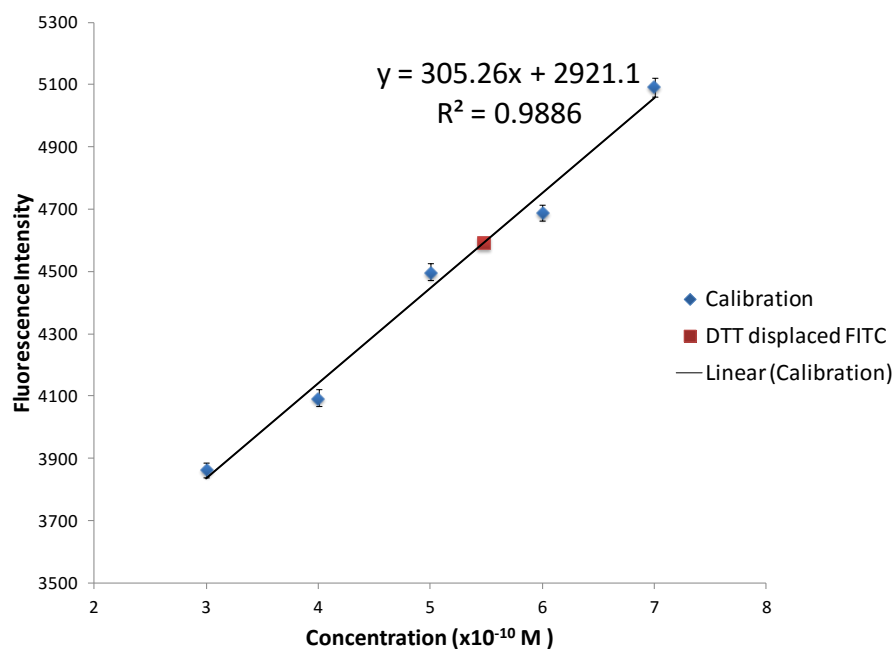
Figure 3.5: Fluorescence calibration graph of varying concentration of FITC. The red square is the fluorescence emission obtained from the FITC antibody supernatant. Samples were excited at 492 nm for 20 s and the fluorescence emission was observed at 515 nm. Fluorescence intensity plotted was from the average of 5 replicate samples, in which the error bars represent the standard deviation of the replicate samples. ($R^2 = 0.9886$)

In Figure 3.5 (blue dots) the calibration graph obtained for 3, 4, 5, 6 and 7 x10^{-10} M of FITC is shown. An excitation wavelength of 492 nm was used for 20 s and the emission was measured at 515 nm and the average fluorescence emission from five replicate samples was obtained. The error bars represent the standard deviation of the five replicate samples. In Figure 3.5, it was observed that as the concentration of FITC increased, the fluorescence emission intensity also increased as expected in a linear fashion with a linear regression of 0.9886 being obtained.

The DTT displaced FITC antibody supernatant was then measured using the same experimental conditions used for the FITC calibration graph. In Figure 3.5, the red

square represented the fluorescence emission intensity of the displaced conjugated antibody, which was determined to have a concentration of 5.45 x10^{-10} M. From this, it was determined using Avogadro's number and the fact there was approximately 4.5 fluorophores per antibody, that for every single nanoparticle, 74 antibodies were conjugated. Theoretically, assuming an antibody has a footprint of 14.5 x 8.5 nm in dimension,[149] and every antibody aligns perfectly 'flat' on the nanoparticle surface, a maximum of 114.89 antibodies can fit onto the surface of a 64 nm nanoparticle. Therefore 74 antibodies conjugated on the silver nanoparticle surface seems a reasonable approximation.[150] Based on this, the antibody conjugation was deemed to be successful and the number of antibodies per nanoparticle was approximated to be 74.

3.3.3 Detecting TNT With Antibody Conjugated Silver Nanoparticles

Since the antibody was determined to have been successfully conjugated to the surface of the silver nanoparticles, the specific detection of TNT by SERS could be explored as shown in Figure 3.1. The antibody (clone A.1.1.1) was shown to have a high binding affinity, a measure of the strength of a receptor-ligand interaction, of 1.5 x 10^{-13} M, indicating a promising methodology for the detection of low concentrations of TNT.[68] The detection of TNT was achieved by adding antibody conjugated silver nanoparticles (150 μl) to a 96 well plate. A range of concentrations of TNT (0-150 nM) were then added and the SERS spectrum was obtained immediately, using 532 nm laser excitation and a 0.5 s accumulation time. Since the TNT was dissolved in acetonitrile, a control sample of acetonitrile added to the antibody functionalised silver nanoparticles was also performed in order to obtain a background spectrum, shown in Figure 3.6.
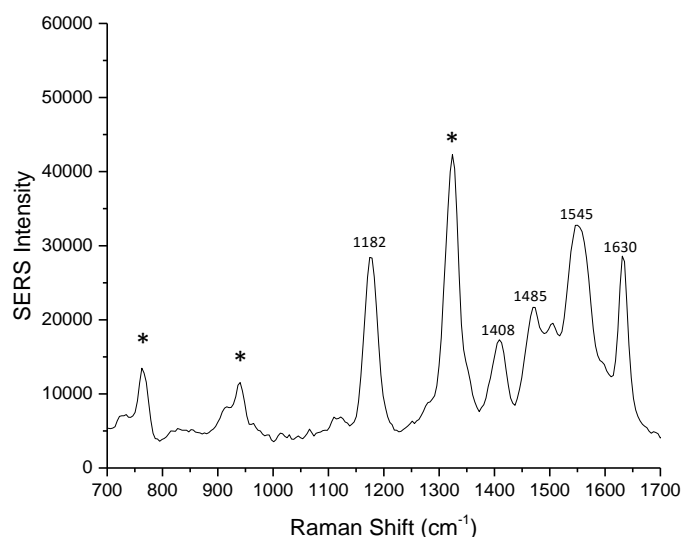
Figure 3.6: Control SERS spectrum of acetonitrile (*) added to antibody conjugated silver nanoparticles obtained using 532 nm laser excitation for 0.5 s accumulations. The spectrum shown is the average of 5 measurements of 3 replicate samples, and has been baseline subtracted.

The control SERS spectrum in Figure 3.6 was obtained by adding acetonitrile (150 μl) to the functionalised silver nanoparticle (150 μl). The SERS peaks obtained were assigned to be from FITC. This is due to the FITC modified antibody being immobilised onto the nanoparticles surface through the ITC. FITC peaks were observed at 1182 cm^{-1} due to the C-OH stretch,[151] 1408 cm^{-1} due to CH_2 stretching,[152] 1485 and 1545 cm^{-1} due to C-C ring formation and finally 1630 cm^{-1} due to C=N, table 3.1 summarises the FITC peak assignments.

Table 3.1: Summary of FITC peak assignments.

Wavenumber (cm^{-1})	Peak Assignment
1182	C-OH stretch
1408	CH_2 stretch
1485, 1545	C-C ring formation
1630	C=N stretch

In an hypothetical assay format, the antibody would be attached to the nanoparticle using a linker that did not give a SERS response as the background from the FITC modification is not ideal. Preferably, little or no background should be obtained so that when the target is added, a spectrum of the target alone can be clearly observed. However, since these FITC modified antibodies were commercially available they were used as a starting point. The subtraction of the FITC spectrum is relatively straightforward and therefore, TNT was then introduced into the assay at a range of concentrations from (1 nM – 150 nM). The solution was analysed by SERS using 532 nm laser excitation with a 0.5 s accumulation time, immediately after addition of TNT to the assay. The data set shown in Figure 3.7 has been baseline corrected using the polynomial least square method in Matlab. The data was then subjected to scaling, in which every spectrum was scaled by subtracting the original data from the mean of the data divided by the standard deviation of the data set. In this case, the data set mean is due to the FITC modification, and the standard deviations are due to the SERS response from the target analytes. The data set was then offset by an arbitrary number for clarity. [153, 154]
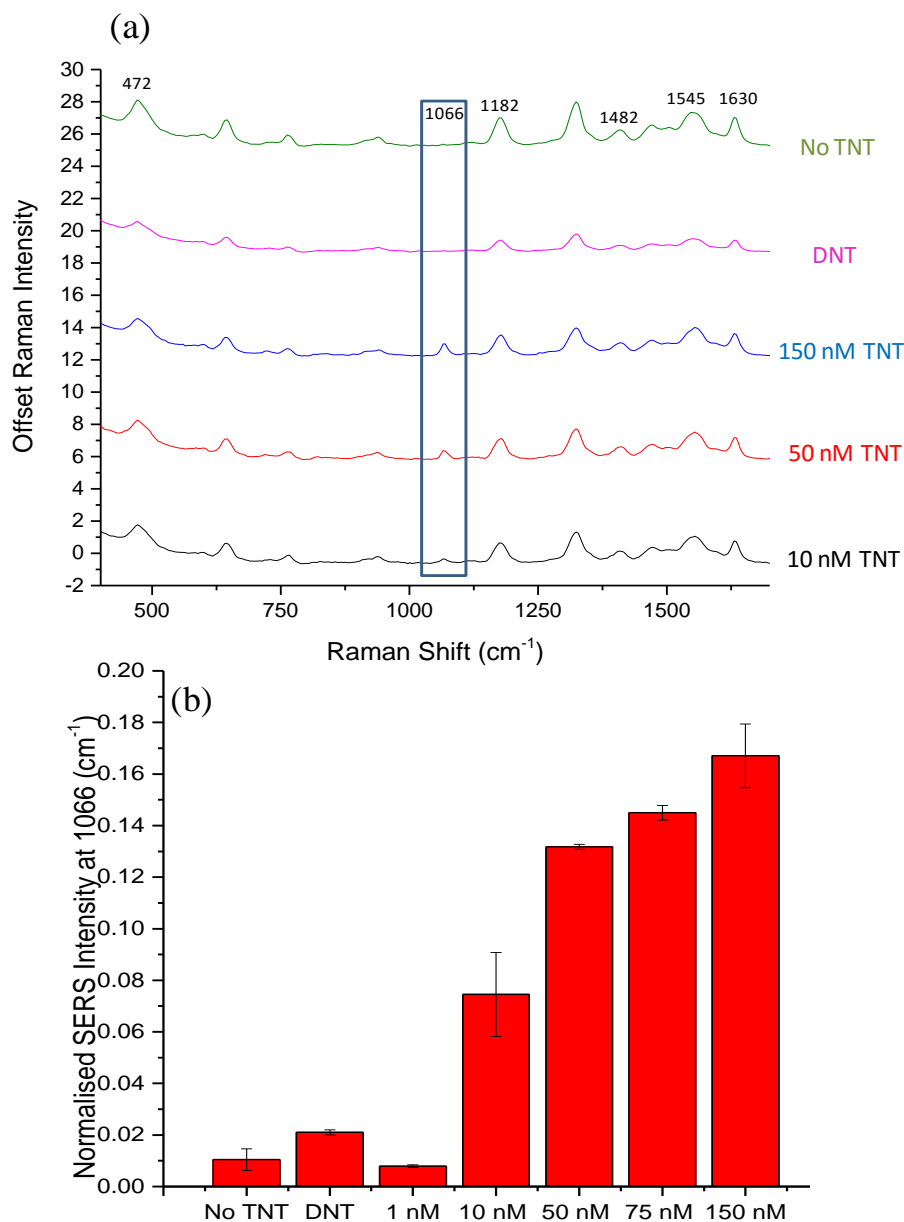
Figure 3.7: SERS spectra of 0 (green), 10 (black), 50 (red) and 150 (blue) nM of TNT binding to antibody conjugated nanoparticles, 150 nM of DNT (pink) was used as a control. SERS spectra were obtained by using 532 nm laser excitation with a 0.5 s accumulation, spectra shown are the average of 5 measurements of 3 replicate samples. Data set was baseline subtracted, scaled and offset for clarity. **(b)** Bar chart of the SERS intensity of the TNT peak present at 1066 cm^{-1} for TNT concentrations of 1, 10, 50, 75 and 150 nM in the assay and the control samples acetonitrile (no TNT) and DNT. The error bars represent the standard deviation of 5 measurements of 3 replicate samples.

As shown in Figure 3.7, when no TNT was present, a background spectrum from the FITC modification on the antibody was observed. However, when three different concentrations of TNT were present in the assay, shown in Figure 3.7 (a) (10, 50 and 150 nM TNT) an enhancement in the peak at 1066 cm^{-1} was observed. Interestingly,

as the concentration of TNT was increased in Figure 3.7, from 0 to 150 nM of TNT, the peak counts at 1066 cm^{-1} also increased. This was further demonstrated in the bar chart in Figure 3.7 (b), in which the peak intensity at 1066 cm^{-1} was plotted against concentration. As the concentration of TNT was increased in Figure 3.7 (b), the peak present at 1066 cm^{-1} was also enhanced. Surprisingly, this peak at 1066 cm^{-1} was attributed to TNT, assigned to the asymmetric staggering of CH_3 which can be observed in the spectrum of TNT alone (Figure 2.2).[155] This highly suggests, that the antibody orientation on the nanoparticle surface is allowing for TNT to come into close proximity to the nanoparticle surface, resulting in the direct detection of TNT by SERS.

Furthermore, DNT was used as a control as it is chemically very similar to TNT and hence, can be used to prove the specificity of the assay towards TNT. DNT was added into the assay at the same concentration as the highest concentration of TNT measured (150 nM). In Figure 3.7 (a), pink, it can be seen that the only peaks present are those which represent FITC. However, in the bar graph in Figure 3.7 (b) it can be seen that DNT (150 nM) did have a small enhancement at 1066 cm^{-1}. This could be due to the antibody having a slight cross reactivity with DNT.[68] Furthermore, by using 2, 6 – DNT as a control over 2, 4 – DNT, 2, 6 – DNT has a rotated out of plane methyl group due to the steric hindrance of the two NO_2 groups which the peak at 1066 cm^{-1} was attributed to. However, this enhancement is miniscule in comparison to the 10 nM TNT enhancement. More specifically, at 10 nM TNT there was over a 7 times enhancement in signal in comparison to no TNT present. Furthermore, at 150 nM of TNT there was a large enhancement of over 17 times in comparison to no TNT present.

To further investigate whether the TNT spectrum could be observed in the overall spectrum, the FITC background spectrum was subtracted. The spectra obtained from the 10, 50 and 150 nM of TNT in the assay had the FITC background spectrum subtracted (Figure 3.8).
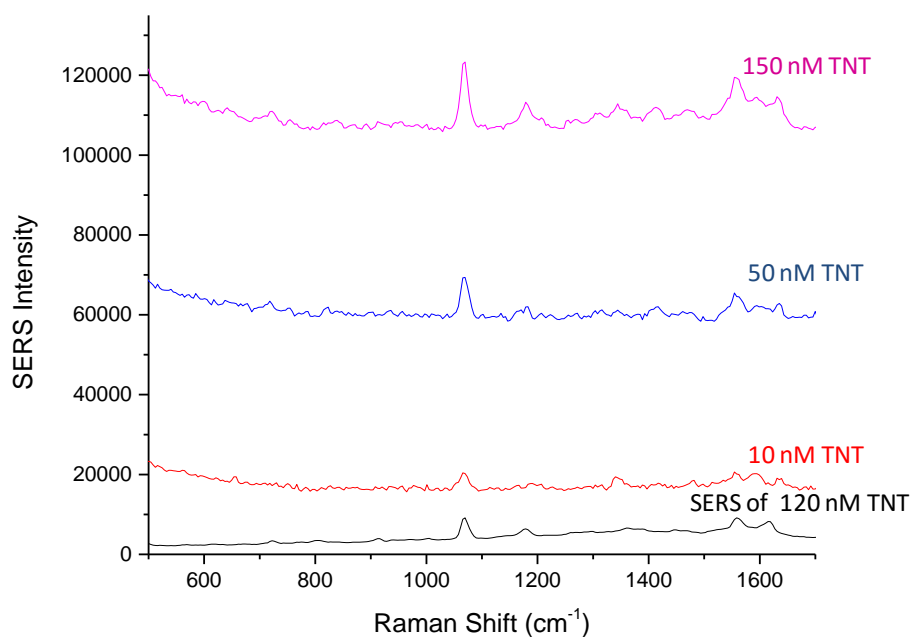
Figure 3.8: SERS spectrum of 10 (red), 50 (blue) and 150 (pink) nM of TNT in the assay, FITC background subtracted and SERS of 120 nM TNT (black) adsorbed onto silver nanoparticles with NaCl (8.8 mM) in the absence of antibodies.

This was achieved by directly subtracting the control acetonitrile spectrum, in Figure 3.6, from the spectra shown in Figure 3.7, as each had been scaled to the background FITC spectra. Interestingly, in Figure 3.8, the same peaks were present at 720, 1066, 1179 and 1558 cm^{-1}, which were assigned to be from TNT in Table 2.1, thus, indicating the spectrum of TNT can be clearly observed within the background spectrum from FITC. This result is highly significant as the molecular SERS vibrations from the TNT target could be clearly observed, opposed to being masked by the strong SERS peaks from the fluorescent modification on the antibody.

This suggests that the use of the ITC group on the antibody plays an essential role as it allows for the antibody to be conjugated to the surface of the nanoparticles in an unusual orientation. It is suggested that the antibody was immobilised on the nanoparticle in a 'flat' orientation, allowing for the target molecule to come in close proximity (approximately 4.5 nm)[156] to the nanoparticles surface and crucially, that the binding of the target to the antibody conjugated silver nanoparticles resulted in a SERS spectrum being obtained specifically for the target analyte. If the antibody was immobilised to the nanoparticle by the Fc chain, in the 'standing' position, the TNT

69

would be orientated too far (approximately 14.5 nm)[156] from the metal surface for a spectrum of TNT itself to be obtained.

The spectra observed in Figure 3.7 and 3.8 were taken immediately after addition of the target to the assay, as the ultimate aim for this project was to develop an assay which can be used for in field detection, which requires rapid detection. However, the optimum time required for TNT to conjugate to the antibody was explored.

3.3.4 *Enhancement of SERS assay over time*

To optimise the binding of TNT to the antibody functionalised silver nanoparticles and the subsequent detection of TNT by SERS, the samples were analysed over time (every 10 min for 100 min) to observe the optimum time required for maximum TNT binding. Concentrations ranging from 0-150 nM of TNT were added to the antibody conjugated silver nanoparticles (150 μl). The samples were analysed at time intervals of 10 min over a 100 min period using 532 nm laser excitation and a 0.5 s accumulation time, as shown in Figure 3.9.
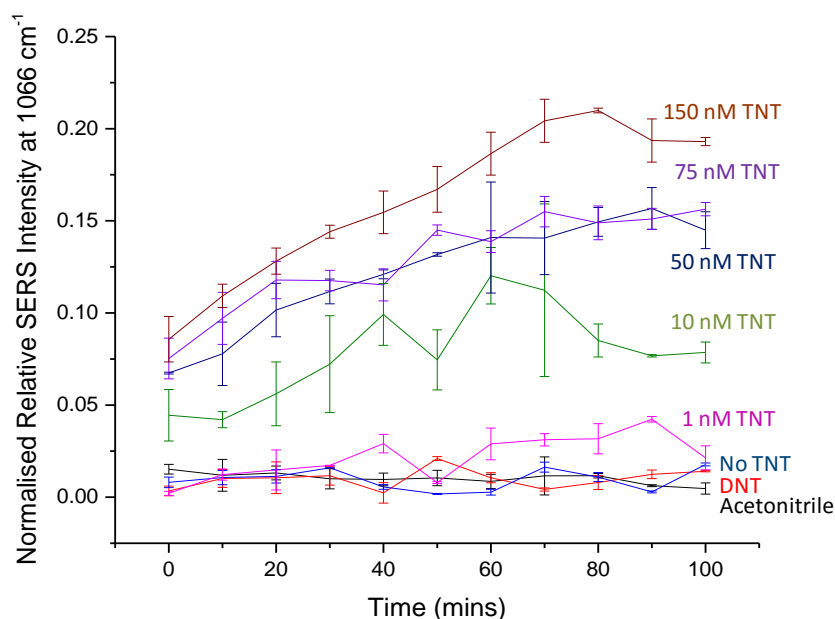
Figure 3.9: SERS peak intensity observed at 1066 cm^{-1} over time for control samples acetonitrile (black), DNT (red), and no TNT (blue). Increasing concentrations of TNT (1 nM (pink), 10 nM (green), 50 nM (navy), 75 nM (purple) and 150 nM (brown)) was added to antibody conjugated silver nanoparticles and SERS spectrum was obtained using 532 nm laser excitation and a 0.5 s accumulation time was used. The error bars represent the standard deviation of 5 measurements of 3 replicate samples. Data set was baseline subtracted and scaled.

70

Figure 3.9 shows a line graph of the SERS intensity observed due to the peak at 1066 cm^{-1} over 100 min. Control samples were also analysed which consisted of: antibody conjugated silver nanoparticles alone with no TNT present, (blue, Figure 3.9), acetonitrile which was added to the antibody conjugated silver nanoparticles (black, Figure 3.9) and DNT (red, Figure 3.9). The results clearly show that the control samples showed no peak at 1066 cm^{-1} over the time period of the measurement as expected. However, when 1 nM of TNT (pink) was added, a small peak at 1066 cm^{-1} appeared at around 60 min after addition of TNT. Interestingly, at 10 nM TNT (green), there was an increased in signal observed immediately after the addition of TNT, which steadily increases until approximately 70 mins after which it no longer increases. Concentrations higher than 10 nM of TNT demonstrate a similar trend; there is an increased in intensity observed immediately after addition of TNT into the assay, and the intensity is greatest after about 70 mins. However, for in field explosive detection, rapid detection is required; therefore all the results shown in this thesis are taken immediately after addition of TNT to the assay. This was justified by the fact that an immediate increase in the signal was observed for all the concentrations above 1 nM. However, if the application of this assay required longer analysis times, then the optimum time to allow for the TNT molecule to bind to the antibody and achieve maximum SERS response would be 70 min.

3.4   Summary of TNT Assay

In Chapter 2, it was shown that by directly adsorbing the target analyte, TNT, onto the silver nanoparticle a SERS spectrum could not be observed at concentrations lower than 120 nM. Also, to obtain a spectrum of TNT, aggregation was required using NaCl together with an increased accumulation time (10 s) and laser power (10 mW).

In the approach reported in this chapter, TNT has been successfully detected using a novel antibody immobilisation approach. It has been proposed that the antibody has a modification which allows the antibody to bind 'flat' on the surface, which subsequently allows for the target molecule to come in close proximity to the nanoparticle surface. This assay allows for the intrinsic SERS spectrum of the target

molecule, TNT to be directly observed. An observed limit of detection of 10 nM of TNT was obtained when the SERS measurement was carried out immediately after TNT addition. This detection limit could possibly be reduced if longer incubation times were used, as 1 nM TNT could be observed after 70 mins, however this is beyond the scope of this work.

3.5 Investigation of Antibody Orientation on Nanoparticle Surface

To investigate the role of the FITC modification on the binding and the subsequent orientation of the antibody on the metal surface some controls were carried out. To investigate the antibody orientation on the nanoparticle surface the dimensions of an antibody was considered. It has been reported that an IgG antibody is approximately 14.5 x 8.5 x 4 nm.[149,156,157] Therefore if the novel FITC modified antibody was lying flat on the surface it should have a height profile of approximately 4 nm. A comparison to the FITC modified antibody was to investigate an unlabelled antibody. Therefore this involved conjugating the same TNT specific antibody (clone A.1.1.1) which did not have the FITC modification to silver nanoparticles, which should adsorb on the nanoparticles surface in non-specific, random orientations. This would prove that the ITC group is necessary for orientating the antibody specifically on the nanoparticles' surface for the detection of a target analyte directly. Thus, by conjugating an unlabelled antibody with no ITC group present, and obtaining the SERS spectrum after addition of the target TNT analyte, if the antibody is not in a 'flat' orientation there should be no TNT specific peaks observed as the TNT will be located too far from the metal surface. This would be a result of the antibody binding with a random orientation, in which the antibody height profile will consist of a mixture of 14.5, 8.5 and 4 nm height profiles, due to the antibody dimensions. In this random orientation the analyte may not be able to bind to the antibody as the binding site is blocked by the nanoparticle or when the analyte does bind it is too far from the nanoparticle surface to obtain a SERS spectrum of the analyte specifically.

3.6   Unlabelled Antibody Conjugation

The antibody without the ITC group was bound to the nanoparticle through the free amine groups on the antibody by altering the pH to 7.4 with HEPES buffer, previously reported by El-Sayed *et al*.[144] Characterisation of the silver nanoparticles and the unlabelled antibody conjugated silver nanoparticles was carried out using UV-Vis spectroscopy and gel electrophoresis, to ensure that the antibody was bound to the surface of the nanoparticles. As described by El-Sayed *et al.* the silver nanoparticles were diluted in HEPES buffer (10 mM, pH 7.4) to allow for the antibodies to bind electrostatically via the positive amine groups to the negative nanoparticle surface, as amine groups have a pKa of approximately 9. Therefore below this pH the amine group will be positively charged. Antibody (20 µl, 1 mg/ml) was then added to the silver nanoparticles (500 µl, 0.34 nM) and left for 16 h to conjugate. The sample was then centrifuged to remove any antibody which was free in solution and the sample was analysed by UV-Vis spectroscopy, Figure 3.10.
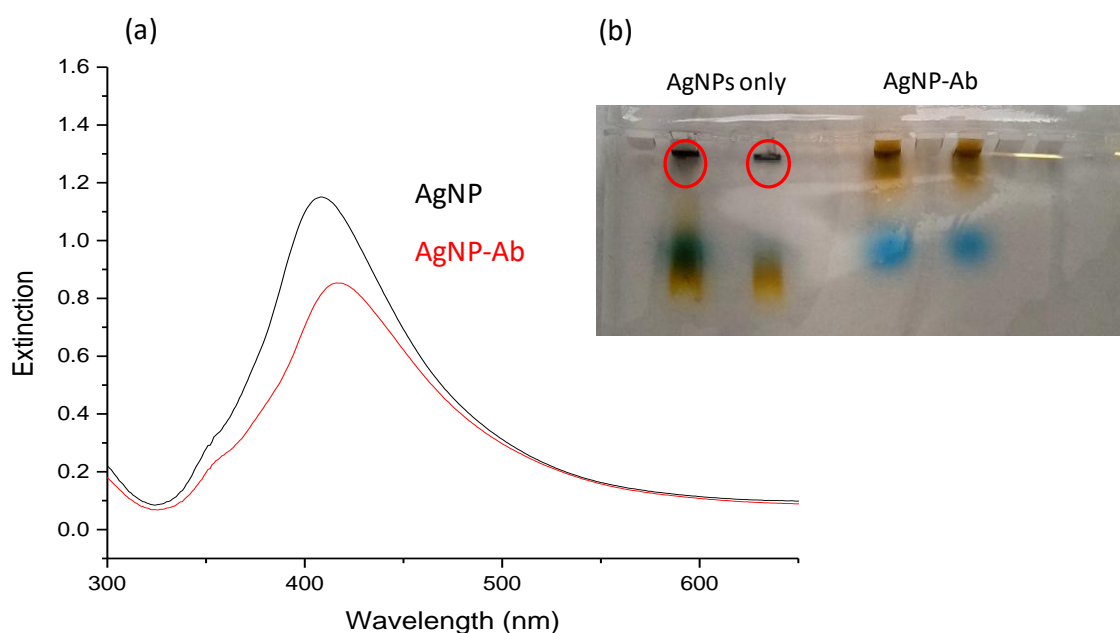
Figure 3.10: (a) The extinction spectra of bare silver nanoparticles (black) and unlabelled antibody conjugated nanoparticle (red), the spectrum shown is the average of 3 replicate samples. **(b)** Image of gel electrophoresis of silver nanoparticles (well 1&2) and antibody conjugated nanoparticles (well 3&4).

The extinction spectrum shown in Figure 3.10 demonstrates bare silver nanoparticles (black) have an absorbance maximum at 409 nm. The red spectrum shows the

extinction spectrum of unlabelled antibody conjugated silver nanoparticles, which shows an extinction band present at 417 nm. Therefore, this demonstrates that there is an 8 nm shift in the extinction maximum due to the antibody binding to the nanoparticle. The peak has also very slightly broadened indicating an increase in size, suggesting successful conjugation of antibody to the silver nanoparticles surface. Furthermore, the bare nanoparticles and antibody conjugated nanoparticles were also analysed by gel electrophoresis (Figure 3.10 (b)).

Gel electrophoresis involves the movement of charged particles through an electric field based on mass to charge ratio. As the electric field is applied, larger molecules are expected to move through the pores of the gel more slowly and smaller molecules faster, producing distinct bands on the gel. Therefore antibody conjugated silver nanoparticles should travel a shorter distance down the gel in comparison to silver nanoparticles only as they will be larger than bare nanoparticles. Furthermore, the antibody consists of several reactive groups and therefore will have a different charge to the bare nanoparticles. The bare and antibody conjugated nanoparticles were both centrifuged prior to gel electrophoresis analysis in order to concentrate the sample. The nanoparticle pellet (15 μl) was then added to a coloured loading buffer in order to observe the bands on the gel. SYBR green was used as the loading buffer (1 μl) , which was then added to the nanoparticle pellets and placed in the gel chamber, which was immersed in tris-borate-EDTA buffer. In Figure 3.10 (b) it can be observed that the bare nanoparticles were unstable in the loading buffer, subsequently precipitating out of solution, as shown by the black aggregates in the well. This is expected as the surface of the nanoparticles are unprotected and addition of the buffer salts results in nanoparticle aggregation. The yellow band shown further down the well was thought to be from the citrate, which capped the nanoparticles. In contrast however it can be observed that the antibody conjugated nanoparticles appeared to have travelled down the well without aggregating. This suggests that the antibody is on the surface of the nanoparticles and is stabilising the nanoparticle and protecting them from aggregation by the buffer. A control blue band was present in all well lanes due to the SYBR green loading buffer, to ensure both lanes had travelled the same distance. The extinction spectra and gel

electrophoresis both suggest the antibody was successfully bound to the nanoparticles, therefore, TNT was added to the assay and SERS was performed to determine if the conjugated unmodified antibody allowed for direct detection of the target analyte.

3.6.1   SERS of TNT Bound Unlabelled Antibody

TNT was added to the unlabelled antibody functionalised silver nanoparticles as previously described for the labelled antibody functionalised nanoparticles. A range of concentrations (10-100 nM) of TNT were added to the unlabelled antibody conjugated silver nanoparticles (150 μl, 0.34 nM) and the SERS spectra were obtained. In Figure 3.11, the black spectrum represents only the unlabelled antibody bound silver nanoparticles with no TNT added. The peaks present at 1100 and 1128 cm^{-1} were thought to be from the presence of the antibody, which could be due to C-C aliphatic stretching.[72]
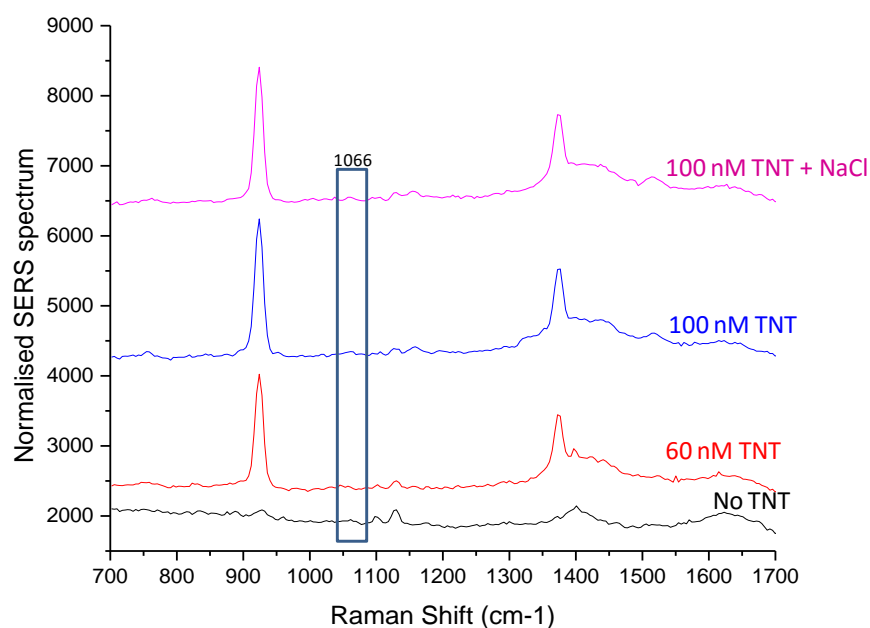
Figure 3.11: SERS spectra of unlabelled antibody conjugated to silver nanoparticles with 0 (black), 60 (red) and 100 (blue) nM of TNT, and 100 nM TNT (pink) in the presence of NaCl (8.8 mM). Spectra were obtained using 532 nm laser excitation with a 0.5 s accumulation time for 5 measurements of 3 replicate samples, in which the spectra shown is the average. Data set was baseline subtracted, scaled and offset for clarity.

However, when TNT was added at a concentration of 60 and 100 nM (red and blue) there were no TNT peaks observed, only peaks attributed to acetonitrile. This could be due to the non-specific, random orientation of the antibodies on the nanoparticle surface, resulting in TNT being held too far from the metallic surface to allow for a SERS spectrum of TNT itself to be observed. Another possibility is that the random orientated antibodies could be immobilised 'head on' on the nanoparticle surface, resulting in the antibody binding to the nanoparticle by the Fab region resulting in the paratopes not being available to bind to the TNT. Therefore, the binding site on the antibody will not be available for TNT, and hence no detection of TNT will be observed. Conversely, upon the addition of NaCl solution to the assay, the nanoparticles aggregated and a shoulder could be observed at 1066 cm^{-1}, which has been assigned to the out of plane methyl stretching of TNT. This could be due to the nanoparticle coming in close proximity to each other and forming 'hotspots'. These 'hotspots' can then enhance molecular vibrations, hence a small shoulder at 1066 cm^{-1}.

This suggests that the antibody was successfully conjugated to the surface of the nanoparticles in a random orientation. However, no SERS spectrum of TNT was obtained using this adsorption method resulting in the random orientation of the antibody on the surface. These results demonstrate that the ITC group is essential for direct detection of small molecules by SERS as the ITC group allows for the antibody to orientate 'flat' on the surface of silver nanoparticles so that the target molecule is in closer proximity and hence, a surface enhanced Raman spectrum of the target can be observed. In spite of this, further investigation was required to obtain physical evidence of the antibody orientation on the surface.

3.6.2   Atomic Force Microscopy

To further support the conclusions drawn from the spectroscopic data, atomic force microscopy (AFM) was used to study the orientation of the antibody upon binding to a metal surface. AFM is a technique in which a sharp cantilever tip is scanned across a surface. A constant force is applied to the tip, however, when the tip is in contact with a surface the cantilever is deflected. These deflections are monitored by a focussed laser beam, which is then reflected to the photodiode detector, as shown in Figure 3.12. This allows for an image of the sample topography to be obtained with precision, usually in the sub-nanometer range.[158]
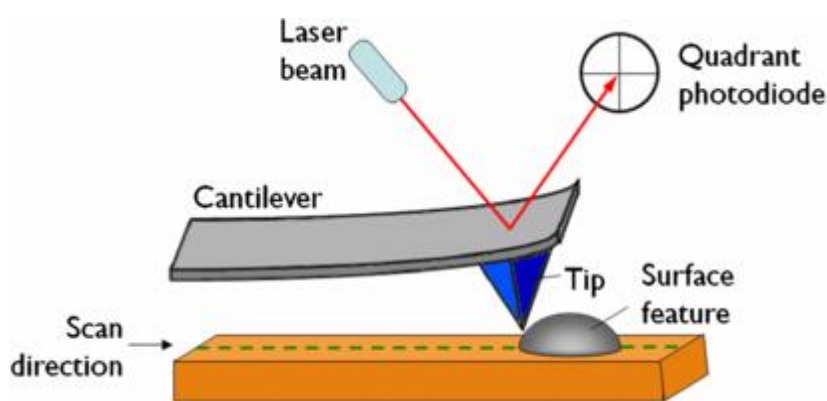
Figure 3.12: Schematic representation of an AFM set-up.[159]

Two antibodies were conjugated with fluorescein (F). One antibody had an ITC group specific for TNT, used in the previous FITC antibody experiments, and the other, the control antibody, did not have an ITC group present. Both were immobilised onto an addressable gold surface and analysed by AFM. The control antibody with no ITC was modified with fluorescein (F) to ensure the orientation of the antibody was specific to the presence of the ITC group on the flat gold surface. A flat gold surface was selected as it was envisaged that this would be the most suitable comparison of the antibodies binding to the metal silver nanoparticle in the SERS detection assay. Silver nanoparticles are not an ideal surface for AFM measurements, as it is difficult to achieve a single monolayer of nanoparticles on a surface. Furthermore the nanoparticles have curvature, and it could therefore prove difficult to discriminate between the presence of an antibody and the curvature of the

nanoparticles. Based on this, the antibodies were immobilised on a flat gold surface. The antibodies with the FITC group were expected to bind to the surface in a 'flat' orientation due to the ITC group, as previously discussed. The dimensions of an antibody are approximately 14.5 x 8.5 x 4 nm as shown in Figure 3.13.[149] Therefore the FITC bound antibody was expected to be around 4 nm in height on the gold surface, when 'flat' on the surface. The antibody with just the F group, no ITC, was expected to bind randomly on the gold surface, which would result in a mixture of antibody dimensions.
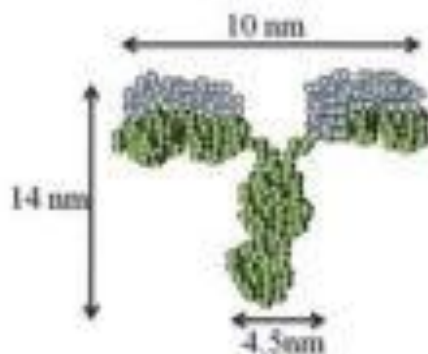
Figure 3.13: Schematic representation of an antibodies dimensions analysed by AFM.[160]

For the antibodies to bind to the gold surface, the surface was treated was HEPES buffer (pH 7.8) to ensure the amine groups were positively charged so the antibody will electrostatically bind to the gold surface. After 30 mins the solution was removed and the antibodies were spotted and dried. The gold surface was then washed with H_2O three times to remove any unconjugated antibodies. AFM imaging and processing was performed by Dr Stacey Laing, on a DPN 5000™ nanofabrication system using ACT silicon probes with a spring constant of 37 N/m and a resonance frequency of 300 kHz. All images were collected in close-contact (or tapping) mode under ambient conditions. Figure 3.14 (a) represents an example of the images which were obtained from the FITC modified antibodies conjugated to the gold surface.
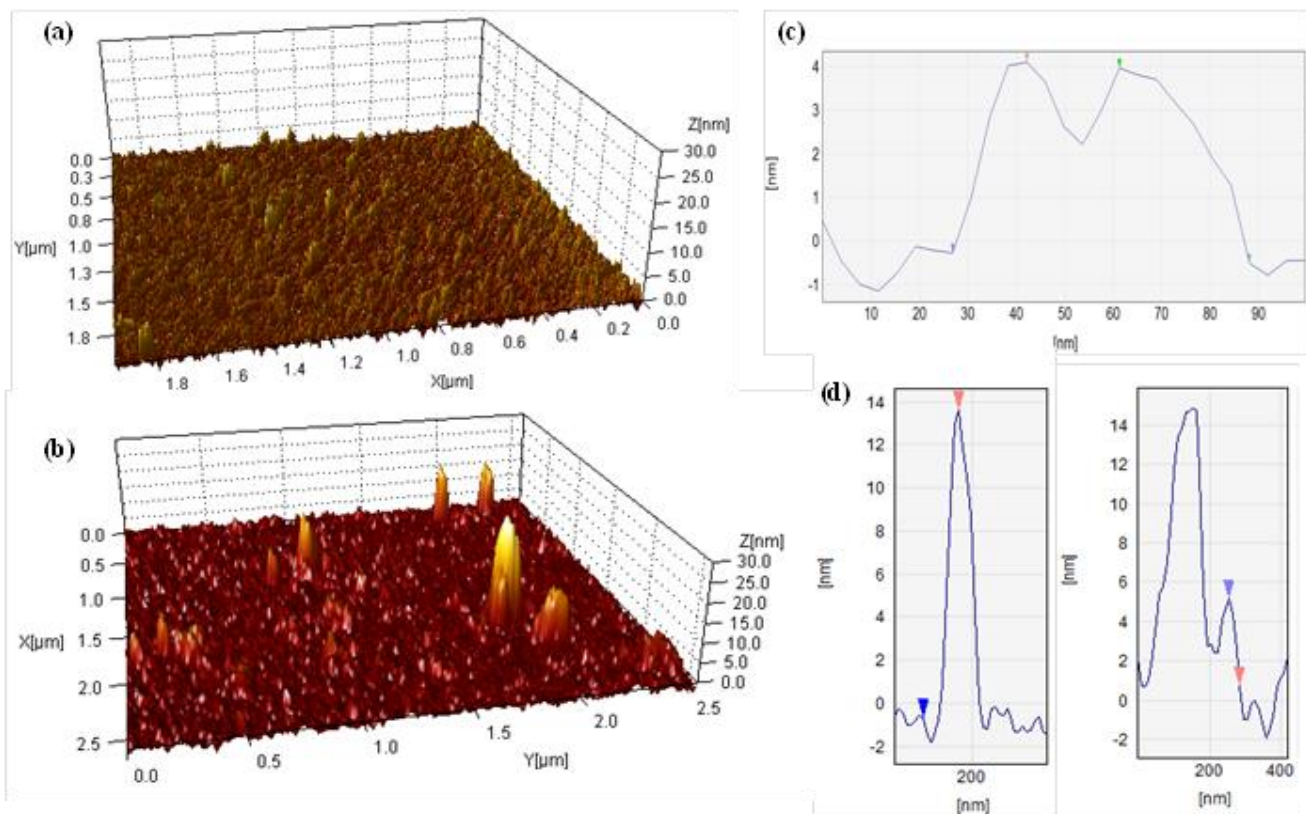
Figure 3.14: 3D AFM images of a gold surface with **(a)** FITC modified antibody and **(b)** F modified antibody. **(c)** and **(d)** are examples of line profiles across a feature on **(a)** and **(b)**, respectively. AFM images were obtained in air at room temperature using tapping mode AFM.

In Figure 3.14 (a) an AFM image was obtained from FITC modified antibodies. Numerous small features can be observed which have an average height of 4.73 ± 1.14 nm. This average height was taken from the height profiles (Figure 3.14(c)) of 36 features across the area where the FITC labelled antibody had been spotted. Considering the dimensions of an antibody (14.5 nm x 8.5 nm x 4.0 nm), this 4.73 nm height strongly indicates that the antibody is orientated 'flat' on the surface. This orientation is consistent with the SERS data, as a target TNT spectrum would only be observed if upon binding to the antibody, the TNT was brought into close proximity to the metallic surface. Figure 3.14 (b) demonstrates the AFM image of the F antibody, with no ITC modification. Several features were observed around 14.06 ± 1.80 nm in height, (Figure 3.14 (d)) which is close to the estimated height of an antibody in the 'tail on' or 'head on' orientation. However, there are also smaller features present, at around 4 nm, and a larger feature around 28 nm, which is indicative that the antibodies are randomly orientated on the metal surface. The

average height calculated was taken from 12 features across the area where the antibody had been spotted. It should be noted that significantly less F antibodies were observed to be bound to the gold surface when using the pH correction method compared to the FITC modified antibodies. This is because the pH method will result in weaker binding to gold surface than the formation of the ITC-metal bond and therefore more antibodies will be removed during the wash steps. This is because the pH method resulted in electrostatic binding to the gold surface and is much weaker than the formation of a thiol-metal bond. This resulted in more antibodies being bound to the surface in a specific orientation when the ITC group was used. To prove that the features observed in the AFM images were exclusively present in the area where the antibody had been spotted, images were also obtained from areas outside the area where the antibodies were spot.
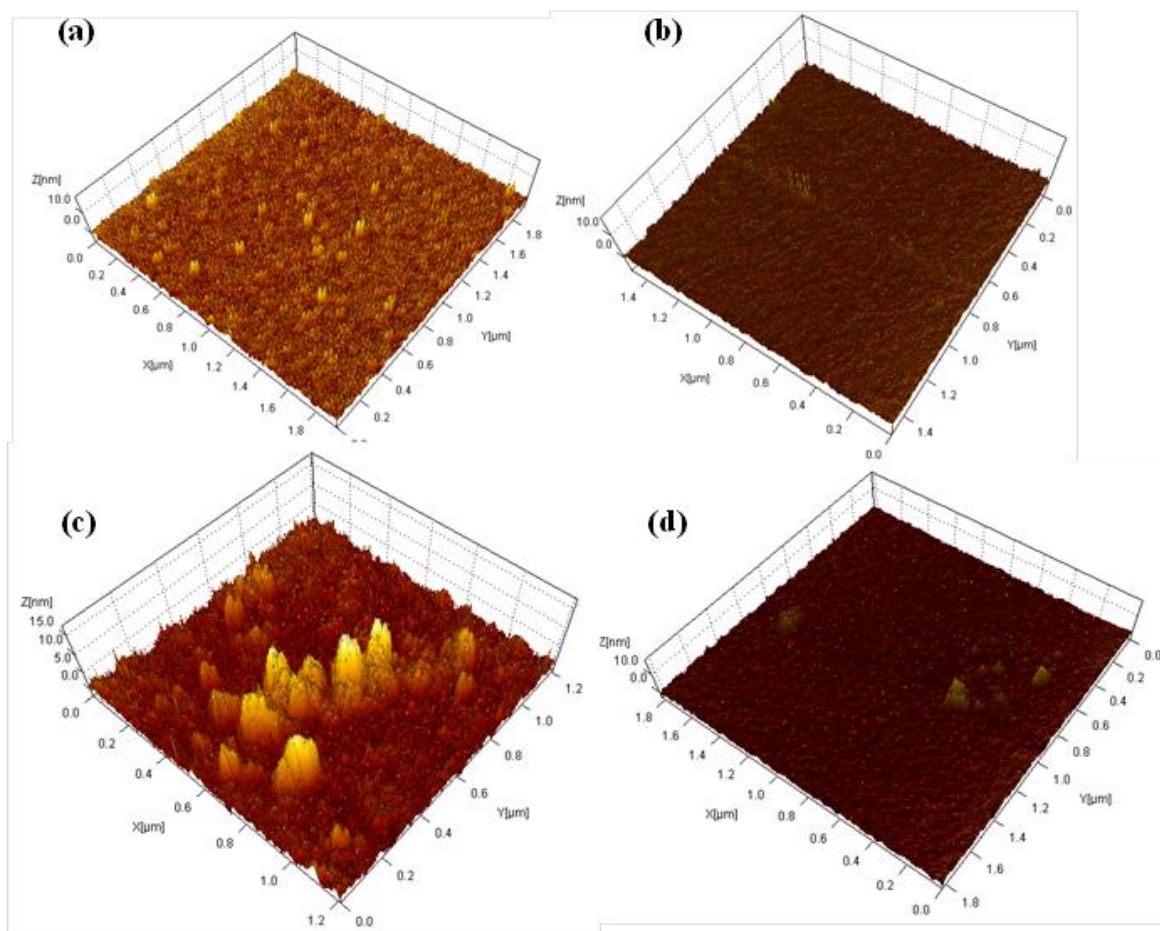
Figure 3.15: 3D AFM images from the gold surface where FITC labelled antibody was spotted, **(a)**, the spot of F antibody with no ITC group, **(c)**, and areas outside the antibody spots, **(b)** and **(d)**. Images were obtained using tapping mode AFM in air at room temperature.

It can be observed in Figure 3.15, that the images obtained off the spot (b) and (d) have no features present with sizes corresponding to antibodies in either 'flat', 'tail on' or 'head on' orientation, as expected. However, the on-spot images for the FITC labelled antibody (a) had several features around 4 nm. The F antibody with no ITC group (c) had several features around 4 nm and 14 nm, which supports the suggestion that the antibodies are randomly orientated. In contrast, there are no features around 14 nm in height on the surface with the FITC labelled antibody, indicating that no antibodies are conjugated in the 'tail on' or 'head on' orientation. Furthermore, to ensure representative data was obtained, AFM images were collected from various points within the area where the antibody was spotted, as shown in Figure 3.16.
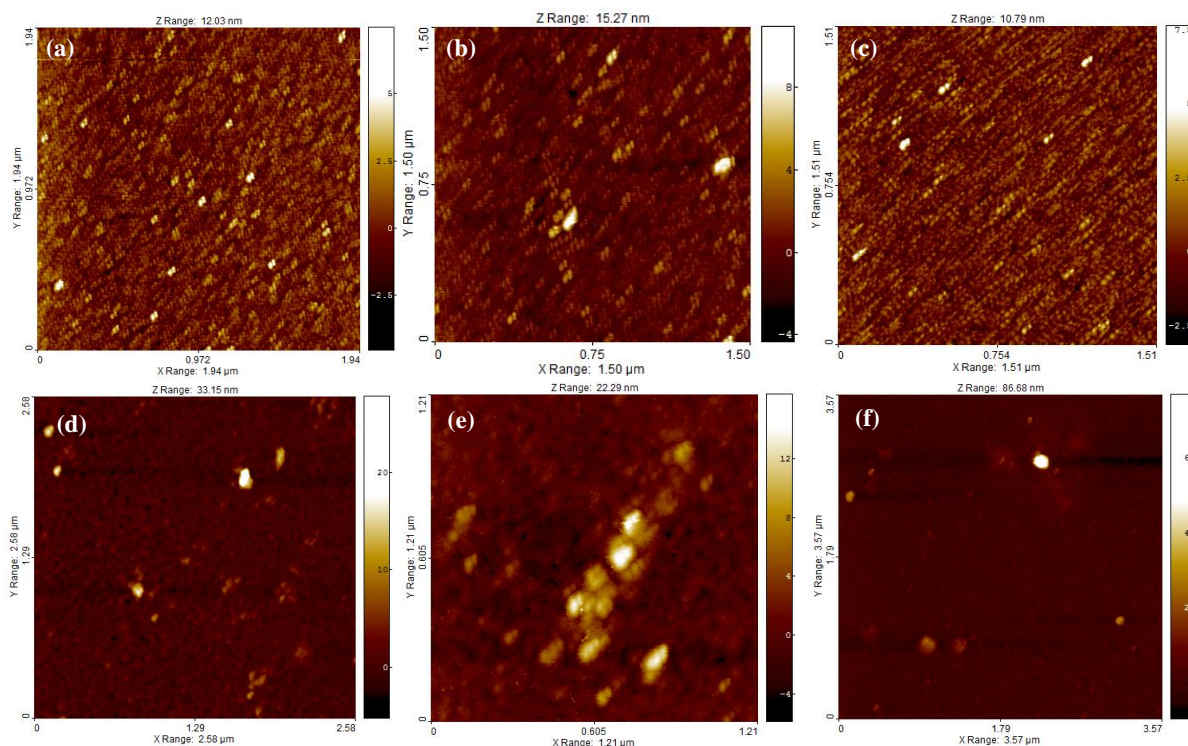
Figure 3.16: Tapping mode AFM images from the spot of FITC labelled antibodies **(a)**, **(b)** and **(c)** and the F antibody without ITC group **(d)**, **(e)** and **(f)** on a smooth gold surface. Images were collected using tapping mode AFM in air at room temperature.

Figure 3.16 shows three images from the FITC labelled antibody spot (a), (b) and (c) and three images from the spot of F antibody where no ITC group was present (d), (e) and (f). Average feature heights for the FITC labelled antibody were calculated from the average height profile of 12 features from each of the three images. It should also be noted that, although there are a few slightly larger features present, there are no features with a height as large as 14 nm. It can therefore be concluded that the FITC labelled antibody is not conjugated in the 'tail' or 'head' on orientation but instead appears to be in a 'flat' orientation, which is consistent with the spectroscopic results obtained in the SERS detection assay. In the AFM images collected from the spot of the F antibody with no ITC group present, Figure 3.14 (d), (e) and (f), it can be observed that there are less features overall and that the features were more varied in size. This is consistent with the suggestion that the ITC group provides more efficient binding to the metal substrate. Many features were present with a height of around 14 nm which could be a result of the antibody binding in a 'tail' or 'head' on orientation and some features around 4 nm were also observed, indicating that in some instances the antibody may be lying 'flat' on the surface. Some larger features were also present which may be indicative of the antibodies being adsorbed on top of one another in small clusters. This suggests that the antibodies were randomly orientated on the surface.

To conclude, AFM was used to successfully identify the orientation of antibodies on a flat gold surface. It was found that an ITC group was essential for specifically orientating the antibody in a 'flat' orientation, in which a height profile of 4.73 nm was obtained. This 'flat' orientation on a surface allows for the target molecule to come in close proximity to the surface, resulting in an intrinsic SERS spectrum of the target molecule. However, in the absence of this ITC group, it was found that the F antibody immobilised randomly on the surface resulting in height profiles of 14.06, 4 and 28 nm. Therefore the antibody was orientated 'head', 'tail' and 'flat' on the surface, this is not ideal as not all the paratopes are available to bind to the target. Furthermore, when the target can bind, it is far (>10 nm) from the metallic surface and a SERS spectra of the target cannot be obtained.

To demonstrate that the assay can be employed for other explosives the detection of RDX was of investigated. As previously mentioned RDX is also an explosive material of high interest, therefore the specific detection of RDX was also desired.

3.7   RDX Assay

The assay developed for TNT was slightly modified for the direct detection of RDX. In this case, silver nanoparticles were functionalised with a FITC modified antibody specific for RDX detection. This modified antibody was also commercially available in the same way as the TNT FITC modified antibody. In Section 2.2.2, a reference SERS spectrum of RDX was previously obtained which demonstrated that the two main peaks observed from RDX were at 1271 and 1500 cm^{-1}. Therefore, the presence of RDX in the assay should have Raman bands present at 1271 and 1500 cm^{-1} if the RDX is bound to the FITC modified antibody which is orientated 'flat' on the nanoparticles surface, allowing RDX to specifically bind to the antibody in close proximity to the nanoparticle.

Silver nanoparticles were functionalised with the RDX antibody labelled with FITC in the same way as before for TNT, and in this case RDX was then captured. Concentrations of 0.15, 0.3, 0.6, 0.9, 1.2, 1.5 and 3 nM of RDX were added to silver nanoparticles conjugated with FITC labelled RDX antibody and the sample was analysed by SERS using 532 nm laser excitation. As previously mentioned for TNT spectra, the data presented in Figure 3.17 has been processed; the data set was baseline corrected using the polynomial least square method in Matlab. The data was then subjected to scaling, the data was also offset for clarity.[153, 154]
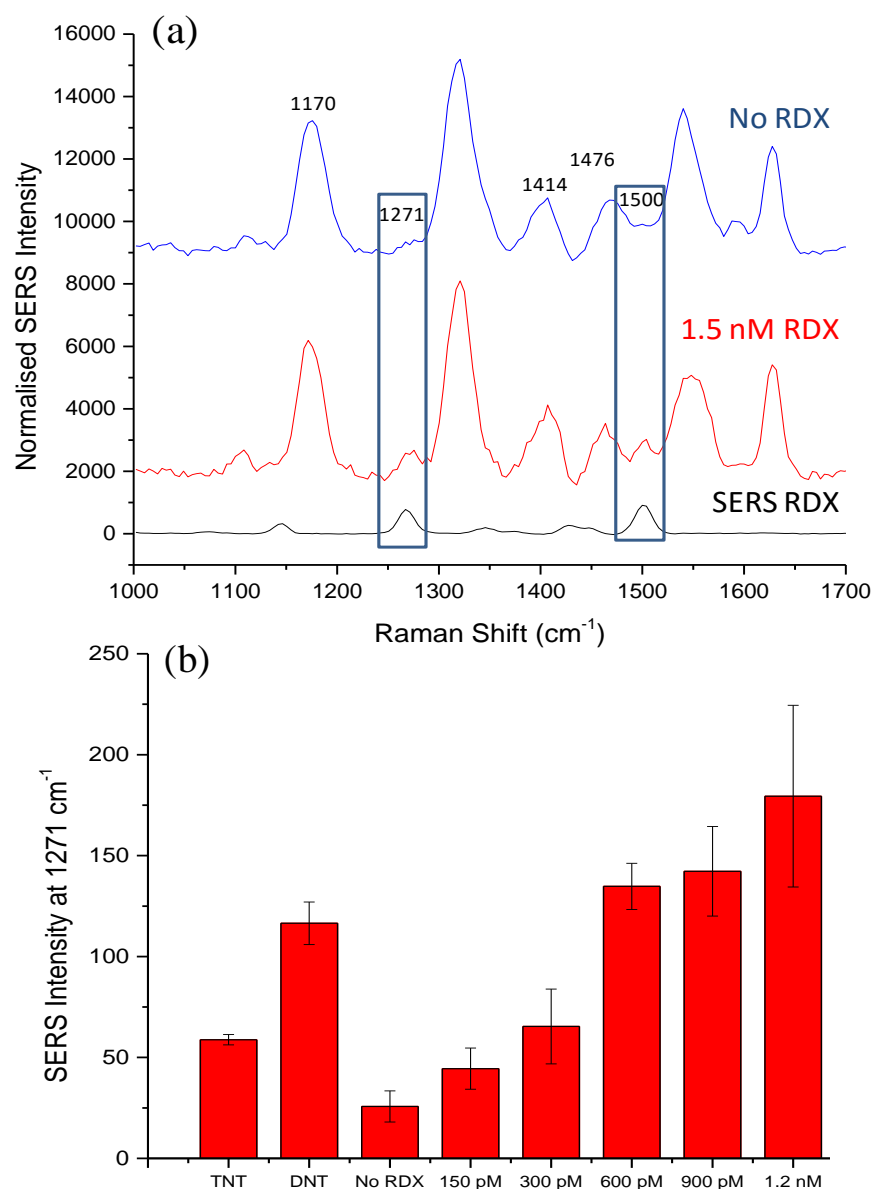
Figure 3.17: (a) SERS spectra of 500 nM RDX (black), silver nanoparticles conjugated to antibodies with no RDX present (blue) and silver nanoparticles conjugated to antibodies with 1.5 nM RDX present (red). SERS spectra shown were obtained using 532 nm laser excitation with a 0.5 s accumulation, spectra shown are the average of 5 measurements of 3 replicate samples. Data set was baseline subtracted, scaled and offset for clarity. **(b)** Bar chart of peak intensity at 1271 cm^{-1} for no RDX, 30, 150, 300, 600, 900, 1200, 1500 and 3000 pM RDX and control samples TNT and RDX.

Figure 3.17 (a) shows that there were FITC peaks present in the SERS spectrum at 1170 cm^{-1} due to the C-OH stretch,[151] 1414 cm^{-1} due to CH$_2$ stretching,[152] 1476 and 1555 cm^{-1} due to C-C ring deformation and finally 1640 cm^{-1} due to C=N, which was to be expected due to the FITC on the antibody. When RDX was added to the functionalised nanoparticles peaks were observed at 1271 and 1500 cm^{-1} (Figure 3.17

(a), blue box) which were not present when RDX was absent. These bands were assigned to the N-O stretching of RDX.[30] Furthermore, the bar chart in Figure 3.17 demonstrated the SERS intensity observed at 1271 cm^{-1} for increasing concentrations (0 – 1.2 nM) of RDX. As the concentration of RDX was increased in the assay, the peak intensity at 1271 cm^{-1} also increased.

TNT and DNT were added (150 nM) to the RDX specific antibody conjugated silver nanoparticles as controls and a SERS peak at 1271 cm^{-1} was observed. It is shown in Figure 3.17 (b) that DNT had a high cross reactivity, as did TNT for the antibody designed specifically to detect RDX, as a peak at 1271 cm^{-1} was observed in both cases. The RDX antibody was reported to have up to a 12 % cross reactivity with other explosive materials, with TNT and DNT displaying 3.7 % of cross reactivity (assuming RDX binds 100 %).[161] This was thought to be from the fact that the explosive molecules are structurally similar. The peak at 1271 cm^{-1} is due to the NO_2 groups that both TNT and DNT possess. Therefore if some cross reactivity with TNT and DNT was exhibited and binding occurred, then the peak at 1271 cm^{-1} would be expected. This is not ideal, however the antibody was more selective towards RDX, as a higher SERS signal for RDX was observed versus the same concentration of TNT and DNT. Therefore, the antibody was still preferentially binding to RDX over the other explosives, however analysis of more than one peak should be performed in order to distinguish between different targets as a more selective antibody was not available. Despite this cross reactivity, this result strongly agrees with the results for TNT, as the signal from RDX can be detected directly using this method.

This suggests that RDX was binding to the antibody and being held close to the nanoparticles surface, allowing for detection by SERS due to the orientation of the antibody. An observed limit of detection of 600 pM RDX was obtained which produced a SERS response of 5 times greater than when RDX was absent. This result is very exciting as it demonstrates that both the small molecule targets bound in a similar manner to the FITC labelled antibody and could be detected at very low concentrations.

3.8   Summary of RDX Assay

In Section 3.3 it was shown that by using a FITC modified antibody, the antibody was orientated onto the surface of silver nanoparticles in such a way that the TNT was selectively brought into close proximity to the nanoparticle surface, and hence TNT was directly detected by SERS. This method was then repeated for the detection of RDX and it was found that RDX could also be successfully detected using the same novel antibody orientation on silver nanoparticles. An observed limit of detection of 600 pM was obtained using this approach. Similarly to TNT, the accumulation time was significantly reduced from 10 s for the direct adsorption approach to 0.5 s, again suggesting that the spectra observed in this assay was specifically from the RDX binding to the antibody nanoparticle conjugate rather than RDX adsorbing to the surface of the nanoparticle directly.

3.9   Multiplexing Capabilities

Multiple explosive materials are usually used in an explosive device. An unstable explosive is usually used to detonate a higher energy explosive material, and therefore a method which can detect multiple explosive materials simultaneously and specifically is required. The specificity of this assay was investigated by adding TNT and RDX specific antibody conjugated silver nanoparticles together (500 µl, 0.36 nM), in order to determine if each explosive could be uniquely detected and differentiated in the presence of both antibody conjugates. RDX and TNT specific antibody functionalised nanoparticles were synthesised separately. TNT specific antibody conjugates were then added to RDX specific antibody conjugates. Each target (1 nM) was then introduced into the multiplex solution individually, and SERS spectra were obtained by using 532 nm laser excitation with a 0.5 s accumulation time. As before, RDX was detected through the presence of the peaks at 1271 and 1500 cm^{-1}. TNT was also detected by positive identification of the peaks present at 1066 cm^{-1}. The data was then subjected to baseline subtraction using polynomial least squares method in Matlab. The data set was also scaled, principal component analysis (PCA) was then performed by selecting 10 principle components coefficients. PCA assesses the variations of a data set by reducing its dimensionality, therefore making it easier to identify spectrally similar data.[153, 154] The observed limit

of detection for RDX was 600 pM therefore, 1 nM of RDX in the multiplex assay should be successfully identified. The observed limit of detection of TNT was found to be 10 nM, however over time a SERS enhancement of 1 nM of TNT was observed, therefore it was thought that by using PCA and reducing the dimensionalities of the data set, each target could be identified at low concentrations in the multiplex assay.
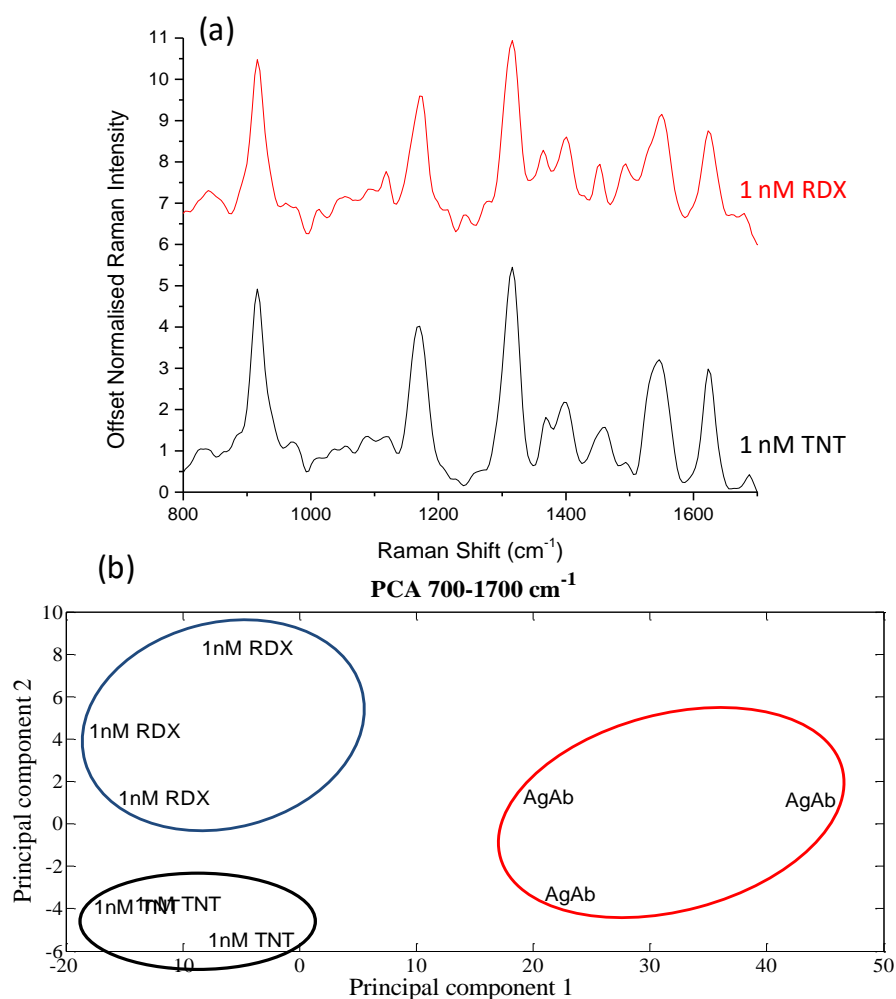
Figure 3.18: (a) Multiplex spectra of TNT (black) and RDX (red). The spectra shown are the average of 5 measurements of 3 replicate samples using 532 nm laser excitation and a 0.5 s accumulation time. Data set was baseline subtracted, scaled and offset for clarity. **(b)** PCA plot on control (no target, red), TNT (black) and RDX (blue) samples, in which the labels shown in the plot is the average of 5 accumulations for each of the three samples.

In Figure 3.18 (a) the red spectrum denotes 1 nM of RDX being added to the mixture of TNT and RDX antibody functionalised nanoparticles and the black spectrum represents 1 nM of TNT added. It can be seen that there are slight differences in the Raman shifts and in the peak intensities observed. In the red spectrum in Figure 3.18 (a), there were RDX specific peaks at 1271 cm^{-1}. There are also slight differences in peak ratios at 1500 cm^{-1}, however it was difficult to definitely identify each targets presence by eye. Therefore multivariate analysis was performed on the multiplex data in the form of PCA, Figure 3.18 (a) to aid differentiation of the spectra. In Figure 3.18 (b) the PCA scores plot shows that each target sample was grouped separately emphasising the clear discrimination between no target (red), RDX capture (blue) and TNT capture (black).
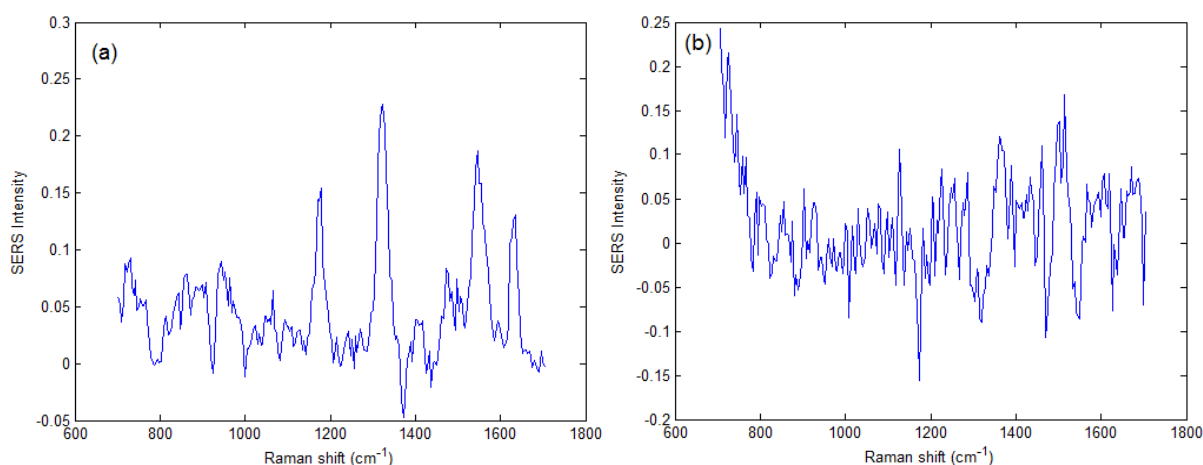
Figure 3.19: (a) Loading plot for principal component 1 from PCA plot in Figure 3.18, **(b)** Loading plot for principal component 2 from PCA plot in Figure 3.18.

The loading plots (Figure 3.19) showed the spectral variations responsible for the separation of the target analytes, which were due to the presence of 1066 and 1271 cm^{-1}. The loading plot for principal component 1 (Figure 3.19 (a)) represented 89.65% of the covariance in the data set, indicating mainly FITC peaks contribute to the separation. However, principal component 2 loading plot represents 3.23% of the covariance which was very slightly anti-correlated demonstrating the presence of the target peaks in the score plots at 1066 and 1271 cm^{-1}. In conclusion PCA is capable of discriminating between controls and 1 nM of each target analyte in a multiplex system.

This assay has been successful for the detection of TNT and RDX at concentrations as low nM and pM respectively, and furthermore, by using multivariate analysis. TNT and RDX could be identified as low as 1 nM in a multiplexed solution. To determine if the assay was only specific to explosive detection or could be used for other small molecule targets, the detection of a non explosive was explored to show the diversity of this assay.

3.10 Non Explosive Example: Dioxane

This detection approach has been successfully demonstrated for the explosives TNT and RDX, therefore a non explosive example was also explored to demonstrate that this assay could potentially be employed for detection of any small molecule, not just explosives. 2-Aminomethyl-1, 4-benzodioxane (dioxane) is very toxic to the environment and is formed in many manufacturing processes, structure shown in Figure 3.20, therefore the assay was also investigated for the specific detection of this non explosive example.
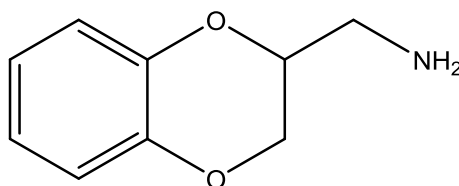
Figure 3.20: Structure of 2-Aminomethyl-1, 4-benzodioxane (dioxane).

Similarly to the previous examples, a reference SERS spectrum of dioxane was firstly obtained by adsorbing dioxane (170 nM) onto silver nanoparticles (150 μl, 0.34 nM) and inducing aggregation by adding NaCl (8.8 mM). The SERS spectrum of dioxane was obtained using 532 nm laser excitation using a 10 s accumulation time (Figure 3.21, black).
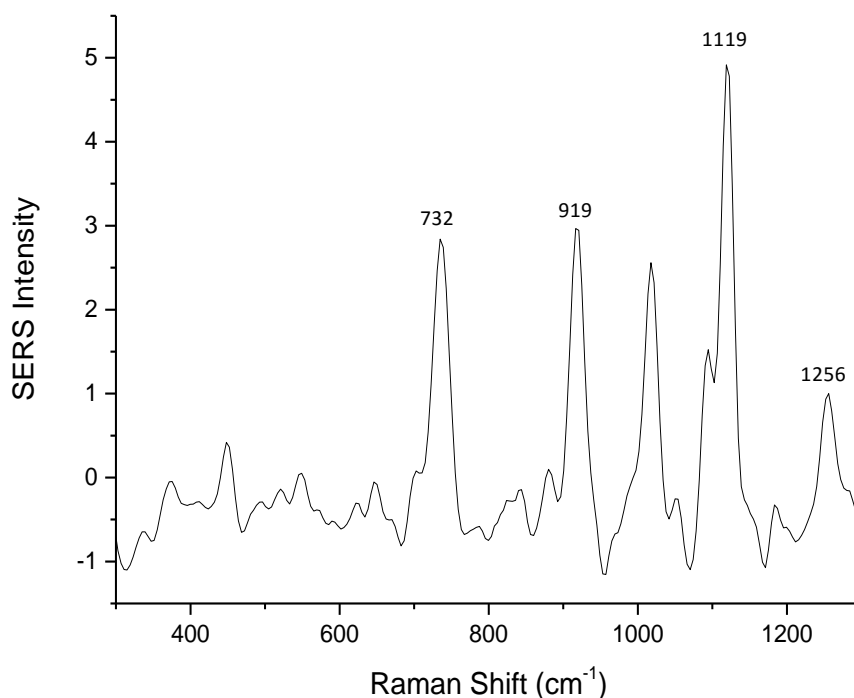
Figure 3.21: SERS spectra of 170 nM of dioxane (black) adsorbed on silver nanoparticles (150 μl) with the addition of NaCl (8.8 mM) using a 532 nm laser excitation for 10s over 5 measurements for 3 samples. Data set was baseline subtracted and scaled.

The SERS of dioxane shown in Figure 3.21, shows peaks are present at 732 cm^{-1} which can be assigned to C-C-C deformation, 879 cm^{-1} due to ring bending, 1119 cm^{-1} from C-C stretching and 1256 cm^{-1} assigned to C-H bending.[162] The peak assignments for dioxane are summarised in table 3.2.

Table 3.2: Summary of dioxane peak assignment.

Wavenumber (cm^{-1})	Peak Assignment
732	C-C-C deformation
879	Ring bending
1119	C-C stretching
1256	C-H bending
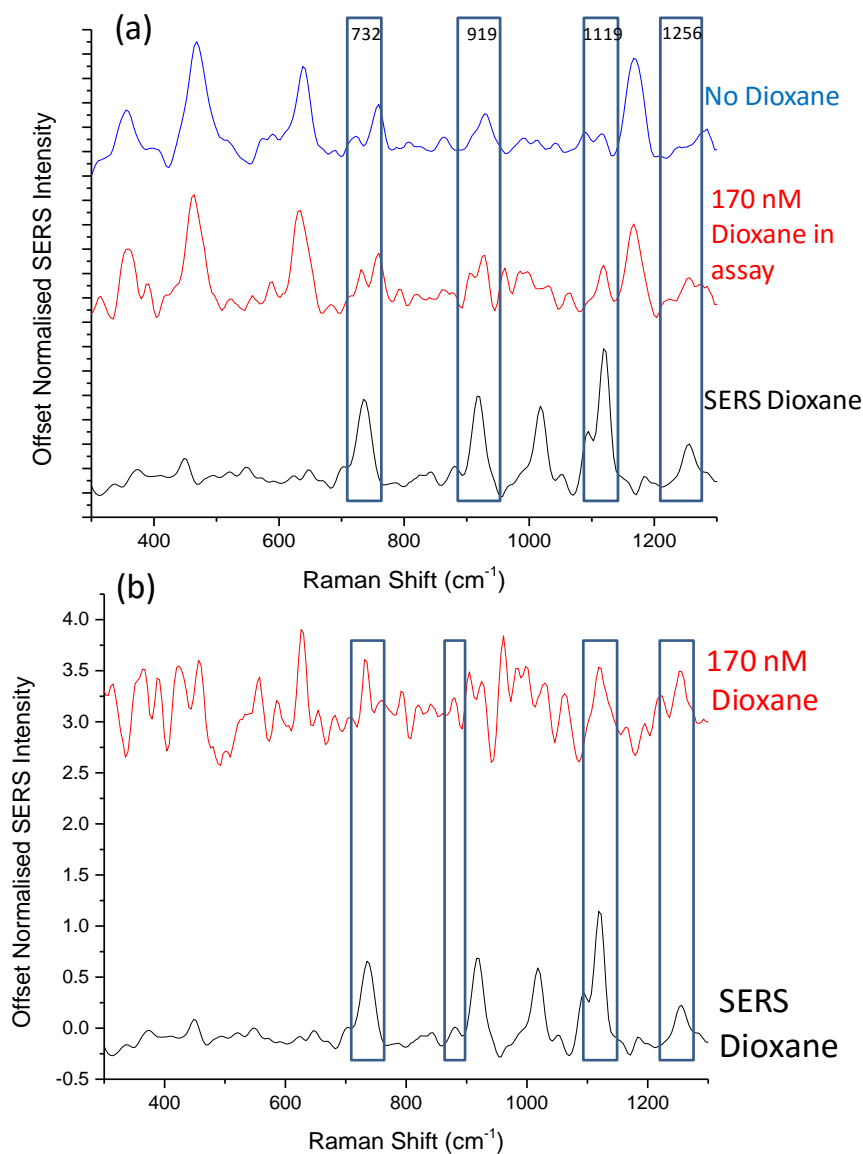
Figure 3.22: **(a)** shows SERS spectra of 170 nM of dioxane (black), silver nanoparticle conjugated to antibody with no dioxane present (blue) and 170 nM dioxane present in assay (red). Spectra shown was obtained using 532 nm laser excitation and a 0.5 s accumulation time, spectra shown is the average of 5 measurements of 3 replicate samples. Data set was baseline subtracted, scaled and offset for clarity. **(b)** SERS spectrum of 170 nM dioxane (black) adsorbed onto silver nanoparticles and SERS spectrum of 150 nM RDX bound to antibody conjugated silver nanoparticles with the FITC spectrum subtracted (red).

The blue spectrum in Figure 3.22 (a), shows the antibody functionalised silver nanoparticles with no target, dioxane. As described previously, only FITC peaks are expected to be observed due to the modification on the antibody and the FITC peak

assignments can be found in Table 3.1. However, when 170 nM of dioxane was added to the antibody functionalised silver nanoparticles peaks were observed at 732, 879, 1119 and 1256 cm^{-1} which can be assigned to dioxane. Furthermore, Figure 3.22 (b) shows that when the FITC background was subtracted from 170 nM dioxane in the assay, dioxane specific peaks were clearly present (blue box).

Therefore, the assay developed showed that the ITC group modification on the antibody is essential for allowing the target molecule to selectively come in close proximity to the nanoparticles surface. Furthermore, this assay has now been shown to work for three small molecule examples, supporting that with changing the specific antibody, this assay can potentially be used for the detection of many different small target analytes.

3.11 'Dirty' Samples

Whilst this assay has achieved high sensitivity and selectivity dissolved in solvent with no other components present, this is not representative of what an explosive samples collected in the field would consist of. Therefore, more complex matrices were investigated to ascertain if the explosive could still be detected in complex matrices. The complex matrix consisted of using a cotton swab to obtain a 'dirty' sample from both a commercially available synthetic dirt sample and a natural dirt sample obtained from a garden. The 'dirty' samples were then extracted using different solvents and spiked with the explosive material. This sample was then introduced into the assay and analysed by as previously described.

'Dirt' consists of many components such as organo-phosphorus, chlorinated pesticides, volatile organics and chlorinated herbicides and a full certificate of analysis for the synthetic dirt can be found in appendix. The aim was to carry out an extraction using a solvent which allowed for the least amount of the dirt components to be dissolved, but would still allow for TNT to be extracted.

A solvent's polarity can determine what can be dissolved in the matrix; the more polar an unknown is, the more likely it is to dissolve in a more polar solvent. The

Log P value describes the polarity, or more specifically the partition coefficient, i.e. the ratio of a compound in a mixture of two immiscible phases at equilibrium. This coefficient measures the difference in solubility in these two phases. The higher the log P value is, the more hydrophobic the phase is. Therefore, it was determined that a more hydrophobic solvent would be of benefit, as less of the 'dirt' would be dissolved. Table 3.3 shows the solvents investigated throughout this section and their hydrophobicity values. Acetonitrile was the most polar solvent explored, with ethyl acetate being the most hydrophobic.

Table 3.3: Solvents and their log P value.

Solvent	Log P Value
Acetonitrile	-0.33
Acetone	-0.04
1, 4 - Dioxane	0.03
THF	0.59
Ethyl Acetate	0.9

3.12 SERS of TNT in Increasing Hydrophobic Solvents

Hernandez-Rivera *et al*. have previously shown that by simply changing the solvent the explosive material was dissolved in, a different Raman spectrum of the explosive can be obtained.[133] This is due to the solvents polarity, which can influence the polarity of the explosive, resulting in changes in the SERS spectra. For this reason, the SERS of TNT in each of the solvents given in Table 3.3 was explored.

TNT (3000 nM) in acetonitrile was further diluted, to 300 nM, in each of the solvents in Table 3.3. This TNT solution (150 µl) was then added to silver nanoparticles (150 µl, 0.34 nM) and was aggregated with NaCl (8.8 mM). SERS analysis was performed using a 96 well plate and 532 nm laser excitation with an accumulation time of 10 s. The SERS spectrum of TNT in different solvents is shown in Figure 3.23.
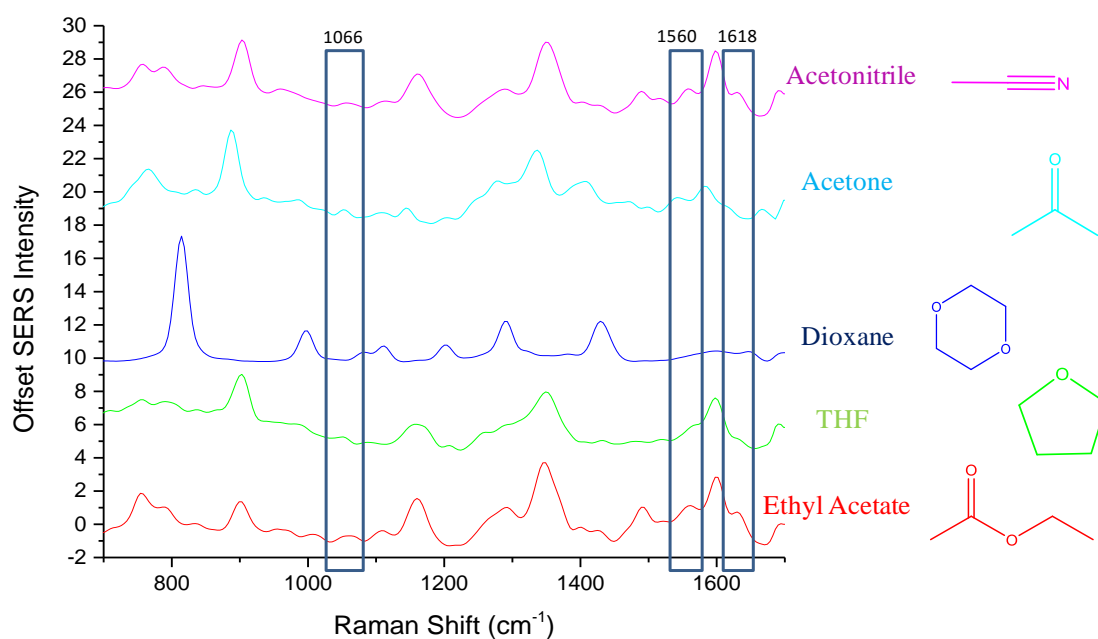
Figure 3.23: SERS spectra of 150 nM TNT in: ethyl acetate (red), THF (green), dioxane (dark blue), acetone (light blue) and acetonitrile (pink) with silver nanoparticles (0.34 nM, 150 µl) and NaCl (8.8 mM) obtained using 532 nm laser excitation with an accumulation time of 10 s. Data set was baseline subtracted, scaled and offset for clarity.

In Figure 3.23, TNT specific peaks are highlighted (blue box) at 1066, 1560 and 1618 cm^{-1}. These peak assignments can be found in Table 2.1. It was observed in Figure 3.23, that when acetonitrile was used as the solvent, all three TNT bands could be observed. This was to be expected as this was the solvent used in the reference spectra that were obtained in Chapter 2. Acetonitrile specific peaks were observed at 923 and 1374 cm^{-1} due to C-C stretching and CH$_3$ deformation.[140] When acetone was used as a solvent (light blue spectrum) it was observed that acetone specific bands were present at 914 and 1364 cm^{-1}, assigned to be from C-C stretching and CH$_3$ deformation.[163] The TNT specific peak at 1066 cm^{-1} was still present, however, the TNT peaks at 1560 and 1618 cm^{-1} appeared to have shifted to 1537 and 1602 cm^{-1}. This could be due to the increase in hydrophobicity exhibited for acetone in comparison to acetonitrile. When dioxane was used to dilute TNT (dark blue spectrum), no TNT specific peaks were observed and only dioxane specific peaks were seen. Dioxane specific peaks were present at 824 and 1005 cm^{-1} due to ring stretching, 1120 cm^{-1} was denoted to CH$_3$ wagging and 1441 cm^{-1} due to CH deformation.[164] It was thought that TNT specific peaks were not observed when dissolved in dioxane due to the presence of a lone electron pair on both the oxygen atoms in the ring system of dioxane, which have a high affinity for the nanoparticle surface. Therefore, the dioxane may preferentially be adsorbed onto the nanoparticles surface over TNT and hence explain why no spectrum of TNT was obtained. Therefore, dioxane was deemed an unsuitable solvent. THF was the second most hydrophobic solvent explored (green spectrum). THF specific peaks were observed at 890 cm^{-1} due to C-O-C stretches, and 906 cm^{-1} due to the ring breathing mode.[165] TNT peaks were also observed in THF, at 1066 and 1560 cm^{-1}. Ethyl acetate was the most hydrophobic solvent explored (red spectrum). However, it was so hydrophobic that it formed two layers, the aqueous layer consisted of silver nanoparticles and the organic layer likely consisted of ethyl acetate and TNT. This would be of no use for explosive detection, as a base would be required to phase transfer the explosive from the organic layer to the aqueous layer. It is known that adding a base to TNT results in the formation of a pink/red complex known as a Meisenheimer complex, and no phase transfer occurs.[53] A small peak from ethyl acetate could be observed at 937 cm^{-1} due to C-C stretching.[166] Interestingly, TNT

specific peaks could also be observed in the ethyl acetate sample, despite the two phase mixture. In summary, the TNT specific peak present at 1066 cm^{-1} was present in all solvent spectra, apart from 1, 4 –dioxane. Therefore, it was decided to test all of these solvents with the 'dirty' TNT solutions. Table 3.4 summarises all SERS spectra peak assignments from the solvents.

Table 3.4: Solvents and their SERS peak assignments.

Solvent	Raman Shift (cm^{-1})	Peak Assignments
Acetonitrile	932, 1374	C-C stretching, CH$_3$ deformation
Acetone	914, 1364	C-C stretching, CH$_3$ deformation
1, 4 - Dioxane	824/1005, 1120, 1441	Ring stretching, CH$_3$ wagging, CH deformation
THF	890, 906	C-O-C stretch, ring breathing
Ethyl Acetate	937	C-C stretching

3.12.1 Synthetic Dirt

The current explosive matrix consists of an ideal and clean solution, which does not represent a real life explosive matrix. Based on this, explosives were analysed in 'dirt'. The SERS spectrum of TNT in different solvents in the presence of silver nanoparticles was obtained in order to identify TNT specific peaks. It was determined that all the solvents in Table 3.3 had the TNT specific peak present at 1066 cm^{-1}, apart from dioxane. Therefore, the SERS of synthetic dirt was explored in these solvents, to determine which solvent allowed for more dirt components to be dissolved.

A commercially available synthetic dirt (clean clay sediment No.2), was chosen to mimic Afghan dirt as the aim of this project was to develop an assay that can be used

for in the field explosive detection. The synthetic dirt (5 mg) was dissolved in each of the solvents: acetonitrile, acetone, THF and ethyl acetate (5 ml). 100 µl of the synthetic dirt solution was then added to silver nanoparticles (150 µl) and aggregation was induced with NaCl (8.8 mM). The SERS spectrum of the dirt was then obtained using 532 nm laser excitation and a 10 s accumulation time. The data set obtained was subjected to baseline correction using polynomial least squares, the
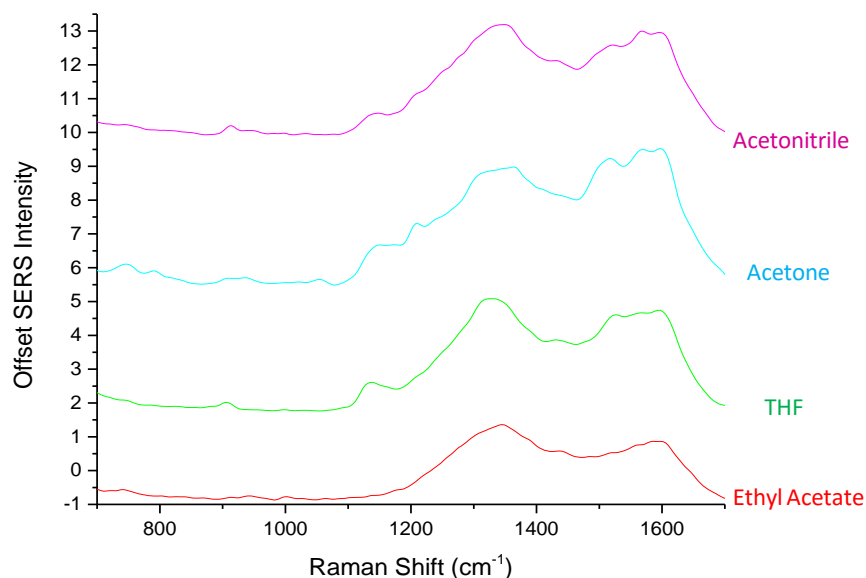
data set was then offset by an arbitrary number for clarity, as shown in Figure 3.24.

Figure 3.24: Shows SERS spectra of 100 µl of synthetic dirt in: ethyl acetate (red), THF (green), dioxane (dark blue), acetone (light blue) and acetonitrile (pink) with silver nanoparticles (0.34 nM, 150 µl) and NaCl (8.8 mM) using a 532 nm laser excitation for 10 s. Data set was baseline subtracted, scaled and offset for clarity.

In Figure 3.24, it can be seen that similar SERS spectra of dirt were obtained with each of the solvents. The pink spectrum represents acetonitrile dissolved dirt. An acetonitrile specific peak was observed at 923 cm^{-1}. Therefore, dirt peaks were observed at 1145, a very broad peak at 1330 and 1600 cm^{-1}. The peak present at 1145 cm^{-1} could be due to sulphonic acid stretches or C=S vibrations or C-C aliphatic chains, all of these groups are likely to be present due to the chemical composition of the synthetic dirt.[72] The peak present at 1330 cm^{-1} is most likely due to nitro species, and the peak at 1600 cm^{-1} could be due to the presence of nitro groups or aliphatic azos in the dirt.[72] Interestingly, all synthetic dirt spectra have

these peaks present, indicating that the same components of the dirt were extracted and dissolved in the solvent, despite using different solvents. In the acetone dissolved dirt (light blue spectrum) there is a weak band, associated with the C-C stretching of acetone. In the THF dissolved dirt, a THF specific peak was present at 906 cm^{-1}. Lastly in the ethyl acetate sample (red spectrum) only dirt specific peaks could be observed. This could be due to the fact that two separate phases were produced due the hydrophobicity of ethyl acetate.

The solvent used also has a large effect on the reactivity of the antibody in the assay. Biomolecules are sensitive to minor changes, hence the antibody may not have the same biological activity in a different solvent, i.e. high specificty and selectivity in a different solvent. With regards to the activity of the antibody in organic solvents, Klibanov *et al*. discovered that a target binds specifically and selectively to its antibody not only in water based solutions, but also in anhydrous organic solvents.[167] More specifically they demonstrated that the strength of the target-antibody interaction was related to the hydrophobicity of the organic solvent. In their studies they used a 30-40% solution of 5 organic solvents ranging in hydrophobicity, it was found as hydrophobicity increased, the activity of the antibody decreased. In this example large concentrations (>30 %) of solvent were used; conversely in this experiment, the solvent concentration did not exceed 10% when the antibody was present. Nevertheless, the antibody biological activity has to be taken into consideration when selecting an appropriate solvent, however this is beyond the scope of this thesis, and the biological activity of the antibody was crudely determined by the ability to detect the target analyte.

In Figure 3.24, all the solvents appeared to dissolve the same dirt components, since the same SERS response was observed. Therefore, the dissolved synthetic dirt in each solvent (15 µl) was spiked with TNT (150 nM) and was added it to the antibody functionalised nanoparticle assay (150 µl). The samples were analysed by SERS using 532 nm laser excitation and a 0.5 s accumulation time. The data set obtained was subjected to baseline correction using polynomial least squares, the data set was then scaled in Matlab and offset by an arbitrary number for clarity, as shown in Figure 3.25.
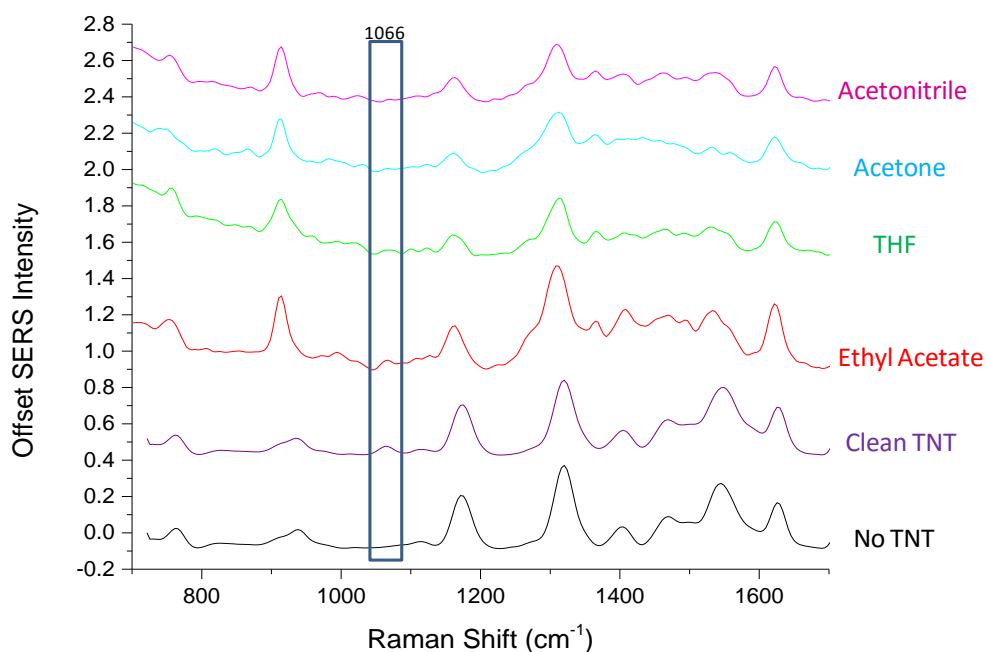
Figure 3.25 SERS spectra of antibody conjugated silver nanoparticles with 150 nM TNT in spiked 'dirt' samples with the following solvents: No TNT, just water (black), TNT in no dirt in water (purple), ethyl acetate (red), THF (green), acetone (light blue) and acetonitrile (pink) with NaCl (8.8 mM) using a 532 nm laser excitation and a 0.5 s accumulation time. Data set was baseline subtracted, scaled and offset for clarity.

Figure 3.25 demonstrates that when no TNT is present, just water (black spectrum), a FITC spectrum is obtained due to the modification on the antibody. Table 3.1 highlights the FITC bands and assignments. The clean TNT sample in water (purple spectrum) represents the presence of TNT in the assay, in the absence of dirt. TNT specific peaks were observed at 1066 cm^{-1}. The ethyl acetate dissolved 'dirt' was spiked with TNT (red) shows FITC bands, indicating that the FITC modified

antibody was on the surface of the nanoparticles. Furthermore, a weak peak at 1066 cm^{-1} could be observed, from the binding of TNT to the antibody. This indicates the TNT can still bind to the antibody in the presence of ethyl acetate, however further analysis would need to be performed to determine if the biological activity of an antibody, in a 10 % (v/v) ethyl acetate solution, is reduced. The solvent THF was also used to dissolve the dirt, however this solvent is less hydrophobic and therefore theoretically, more components of the dirt will be dissolved compared to ethyl acetate. However according to Klibanov *et al*., the biological activity of the antibody should be increased.[167] It was observed in the THF spectrum (green), that there was a weak peak at 1066 cm^{-1}, due to the presence of TNT. However, the more hydrophilic solvents acetone and acetonitrile, displayed no peaks at 1066 cm^{-1}, indicating that TNT could not be identified in the complex matrix. This could be due to the solvents dissolving more of the dirt components, hence complicating the matrix even further than that for the hydrophobic solvents. Therefore, TNT could not be detected by SERS using acetonitrile or acetone.

The purchased synthetic dirt samples were chosen to mimic Afghan dirt and as a result consisted mainly of sand which was very easily dissolved. Therefore, it was also of interest to test the assay on natural dirt, to compare the results.

3.12.2 Soil Samples

It was shown that TNT could be extracted from synthetic 'dirt' samples with acetone, acetonitrile, THF and ethyl acetate. It was of interest to investigate if the same results could be obtained for a different 'dirt' samples. This was achieved by swabbing 'dirt' from a local flower bed. The solvents, shown in Table 3.3, (500 μl) were then added to the swab of dirt and mixed for 10 min. 100 μl of the dissolved dirt was added to silver nanoparticles (150 μl) and NaCl (8.8 mM).

A SERS spectrum of the dirt dissolved in each solvent was obtained and mentioned in Table 3.3. The SERS of the dirt was obtained using 532 nm laser excitation for 10 s accumulation time, as shown in Figure 3.26.
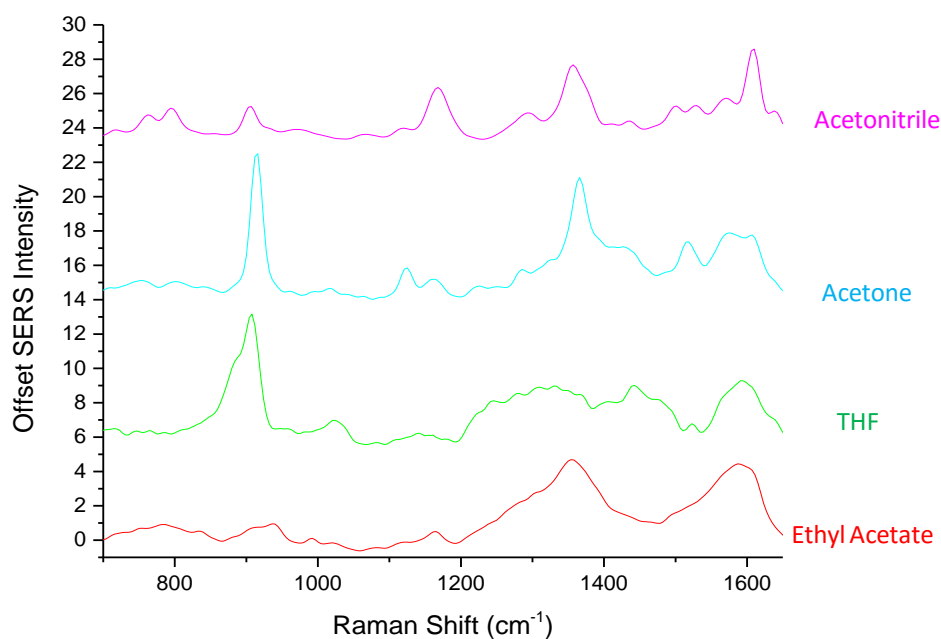
Figure 3.26: Shows SERS spectra of 100 μl of natural dirt in: ethyl acetate (red), THF (green), dioxane (dark blue), acetone(light blue) and acetonitrile (pink) with silver nanoparticles (0.34 nM, 150 μl) and NaCl (8.8 mM) using 532 nm laser excitation and an accumulation time of 10 s. Data set was baseline subtracted, scaled and offset for clarity.

It can be seen in Figure 3.26 that each solvent produced a slightly different SERS spectrum of the natural dirt. The ethyl acetate 'dirt' spectrum is very weak due to the dirt being present in a different phase, due to the hydrophobicity of the solvent. 'Dirt' peaks were observed at 1357 and 1600 cm^{-1}. These could be assigned to the presence of nitro groups in the soil components.[72] The SERS spectrum of 'dirt' dissolved in THF (Figure 3.26, green) shows dirt peaks at 1023 cm^{-1} which could be due to aromatic ring vibrations, sulphonic acid or C-C stretching which are all components commonly found in dirt. There was also a Raman band present at 1439 cm^{-1}, which could be assigned to carboxylate salt or the presence of nitro stretching in a molecule. Finally, a broad peak was observed at 1593 cm^{-1}, which could be assigned to nitro based stretching or aliphatic azos. Acetone (Figure 3.26, light blue) was the second most hydrophilic solvent explored, therefore it was expected that it would dissolve many of the components in 'dirt'. Dirt peaks were observed at: 1122 cm^{-1} due to sulphonic acid or C-C aliphatic stretching, 1160 cm^{-1} due to C=S or C-C stretching, 1286 cm^{-1} due to sulphonic acid and 1517 cm^{-1} due to aromatic ring vibrations. Acetonitrile (Figure 3.26, pink) was the most hydrophilic solvent

explored, and hence should be the solvent to dissolve most components of 'dirt'. Dirt SERS bands were present at: 763 and 795 cm^{-1} due to C-Cl or C-S vibrations, 1168 cm^{-1} assigned to the stretching of C=S or C-C, 1296 cm^{-1} due to sulphonic acid, 1357 cm^{-1} due to carboxylate salts or nitro compounds, 1500 and 1529 cm^{-1} assigned to aromatic ring vibrations, 1570 cm^{-1} due to nitro or aliphatic azos and 1609 cm^{-1} due to the presence of amides.

A solvent which dissolved the least amount of dirt and produced the least SERS bands would be the most desirable as it would give rise to a less complicated matrix, meaning TNT could be detected within the background signal. The difference in the hydrophobicity of the solvents used to dissolve the natural dirt, in comparison to the synthetic dirt, allowed for different components of the dirt to be dissolved. This was of great interest as TNT was spiked into each of these 'dirt' solutions and added to the antibody conjugated assay.

The swabbed 'dirt' (5 mg) was dissolved in each of the solvents (5 ml), and spiked with TNT (50 nM). This solution (15 µl) was then added to the antibody conjugated nanoparticles (150 µl) as previously described for the synthetic dirt spiked TNT samples. This sample was then added to a 96 well plate and was analysed by SERS using 532 nm laser excitation for a 0.5 s accumulation time. The data set underwent baseline correction, using polynomial least squares, and the dataset was scaled as for the synthetic dirt samples. Finally, the data set was offset for clarity, as shown in Figure 3.27.
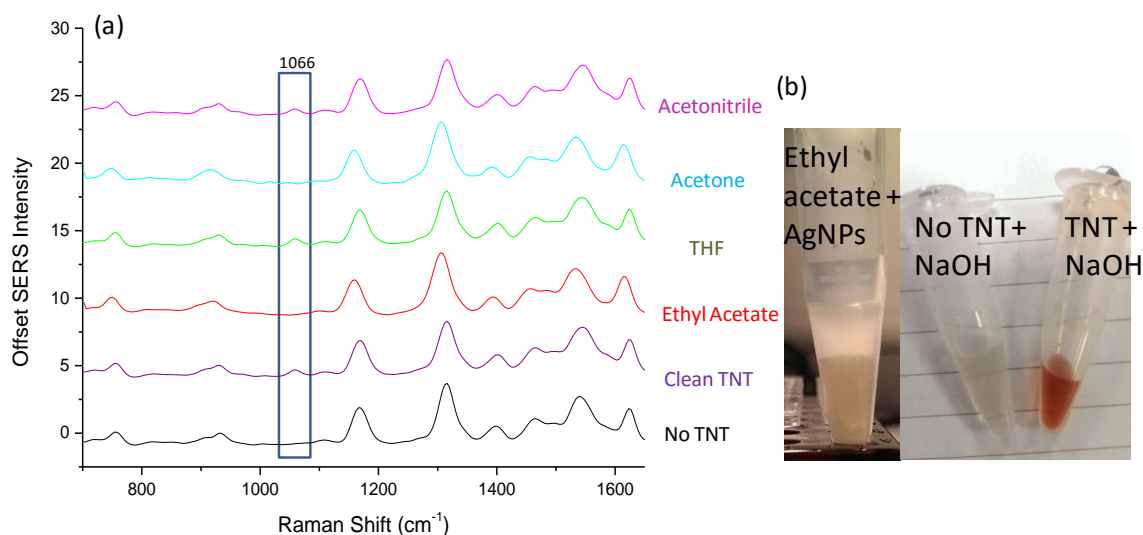
Figure 3.27: (a) SERS spectra of antibody conjugated silver nanoparticles with 150 nM TNT in spiked 'dirt' samples with the following solvents: No TNT (black), TNT in clean sample (purple), dirt sample in ethyl acetate (red), THF (green), acetone (light blue) and acetonitrile (pink) with NaCl (8.8 mM) using 532 nm laser excitation for a 0.5 s accumulation time. Spectra shown is the average of 5 measurements of 3 replicate samples. Data set was baseline subtracted, scaled and offset for clarity. **(b)** Image of 'dirty' TNT sample in ethyl acetate with silver nanoparticles, the sample with NaOH added to phase transfer TNT, showing the formation of the red Meisenheimer complex.

Figure 3.27 represents 'dirty' spiked TNT samples in the novel antibody conjugated silver nanoparticle assay. When TNT was absent (black), a spectrum of FITC was observed. This is due to the FITC modification on the antibody which is discussed in section 3.3.3. The purple spectrum in Figure 3.27 demonstrates the 'clean' TNT sample dissolved in acetonitrile, in the absence of dirt. Again, the FITC spectrum was observed, however there was a peak present at 1066 cm^{-1}, which was determined to be from the out-of-plane CH$_3$ group on TNT. Ethyl acetate dissolved spiked 'dirt' sample (red), resulted in a slight shift in the SERS FITC specific peaks from 1182 to 1177 cm^{-1}, 1485 to 1479 cm^{-1} and 1630 to 1622 cm^{-1}. Perhaps due to the effects of the hydrophobic solvent, or indicating that the antibodies activity has been compromised. Furthermore, no TNT specific peaks were observed at 1066 cm^{-1}, however this was to be expected as ethyl acetate formed a two phase mixture, and it was hypothesised that TNT was in the organic phase. As previously mentioned, a base is required to phase transfer TNT, however upon adding a base to TNT, a complex known as the Meisenheimer complex is formed, as shown in Figure 3.27

(b) (Meisenheimer complexes are described fully in chapter 5).[53] Therefore it was concluded that ethyl acetate was not a good solvent to extract TNT from the complex matrix.

THF was the most hydrophobic solvent used which did not generate two phases when added to nanoparticles. In Figure 3.27 ((a), green), there was a peak present at 1066 cm^{-1} indicating that TNT had been detected successfully, despite the more complex matrix. With acetonitrile sample (pink) a small shoulder at 1066 cm^{-1} was observed, but for acetone, no TNT specific peaks were observed. This is probably due to the fact that these solvents were able to dissolve more 'dirt' components and hence the matrix was much more complicated. Thus, only THF was successful in detecting TNT specifically using a 'dirty' matrix in this assay. In Figure 3.25 and Figure 3.27, a 10% 'dirt' solution was used, therefore it was of interest to increase the dirt content of the matrix and ascertain if TNT could still be successfully detected. THF was selected as the solvent due to it being the most hydrophobic solvent which allowed for successful TNT detection in the 10% dirt assay.

3.12.3 Dirt Concentration Study

The synthetic dirt (5 mg) was dissolved in THF (5 ml). These 'dirt' samples were then spiked with TNT (150 nM). A range of 'dirt' concentrations (0-100% v/v) were then added to antibody conjugated silver nanoparticles (150 µl) in a 96 well plate, as shown in Table 3.5.

Table 3.5: Summarises the concentration of 'dirt' added to antibody functionalised silver nanoparticles form a complex matrix in the presence of 150 nM of TNT.

Sample Name (% dirt)	Volume of TNT spiked 'dirt' (5 mg/ 5 ml) added to assay (µl)	Volume of THF added to assay (µl)	Volume of antibody functionalised nanoparticles (µl)	Total Volume (µl)
No TNT	0	150	150	300
Clean TNT (0% dirt)	0	150	150	300
2 % dirt	3	147	150	300
5 % dirt	7.5	142.5	150	300
10 % dirt	15	135	150	300
20 % dirt	30	120	150	300
30 % dirt	45	105	150	300
50 % dirt	75	75	150	300
80 % dirt	120	30	150	300
100 % dirt	150	0	150	300

Table 3.5 demonstrates that the percentage of 'dirt' in each sample arises from the volume of dirt which was added to the volume of the antibody conjugated silver nanoparticles, i.e. the 100% dirt sample contains 150 µl of TNT spiked 'dirt' which is 100% of the volume of the antibody conjugated silver nanoparticles in the assay. The SERS spectrum was then obtained by using 532 nm laser excitation and 0.5 s accumulation time, as shown in Figure 3.28.
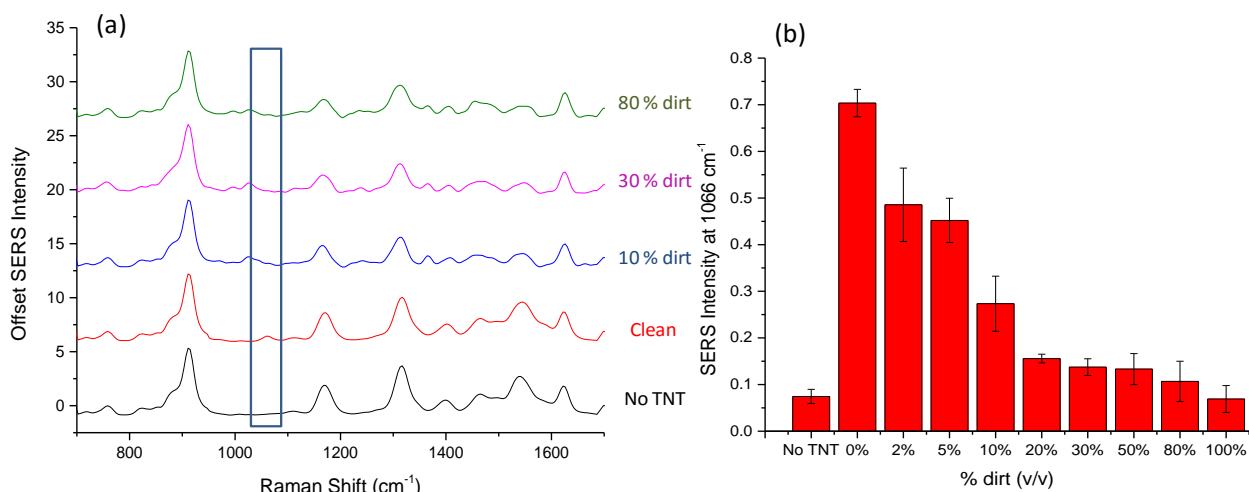
Figure 3.28: (a) Demonstrates SERS spectra of antibody conjugated silver nanoparticles with: no TNT in 0% dirt (black), 150 nM TNT in 0% dirt (red), 10% spiked 'dirt' (blue), 30 (pink) and 80 % spiked 'dirt' (green), using 532 nm laser excitation with a 0.5 s accumulation time for 5 measurements of 3 replicate samples, **(b)** Demonstrates a bar graph showing the SERS intensity of the peak at 1066 cm^{-1} for no TNT and concentrations of dirt from 0-100% (v/v), error bars arise from the standard deviation of the 5 measurements of 3 replicate samples. Data set was baseline subtracted, scaled and offset for clarity.

Figure 3.28 demonstrates the SERS response observed as increasing concentrations of synthetic dirt was added to the assay. The black spectrum represents no TNT and no dirt in the sample. Therefore, SERS bands were observed solely from the FITC modification on the antibody. In Figure 3.28, the red spectrum represents no dirt in the assay, just TNT and antibody conjugated nanoparticles. Hence a TNT band can be observed at 1066 cm^{-1}. However, when 'dirt' is introduced into the assay, the peak at 1066 cm^{-1} is no longer present. This is shown in the 10, 30 and 80 % dirt spectra in Figure 3.28. It can be seen in Figure 3.28 (b), that as the concentration of dirt is increased, the peak present at 1066 cm^{-1} exponentially decreases. These preliminary studies on this type of dirt suggest that this assay is not able to be used out in the field when this type of dirt is present.

A dirt concentration study of the local soil sample was also investigated. The natural dirt swab was added to THF (500 µl), the swab was left mixing for 10 minutes. Any dirt components that were dissolved were then spiked with TNT (50 nM). A range of 'dirt' concentrations (0-100% v/v) were then added to antibody conjugated silver

nanoparticles (150 µl) in a 96 well plate, similarly as described in table 3.5. The SERS spectra were then obtained using 532 nm laser excitation and a 0.5 s accumulation time, as shown in Figure 3.29.
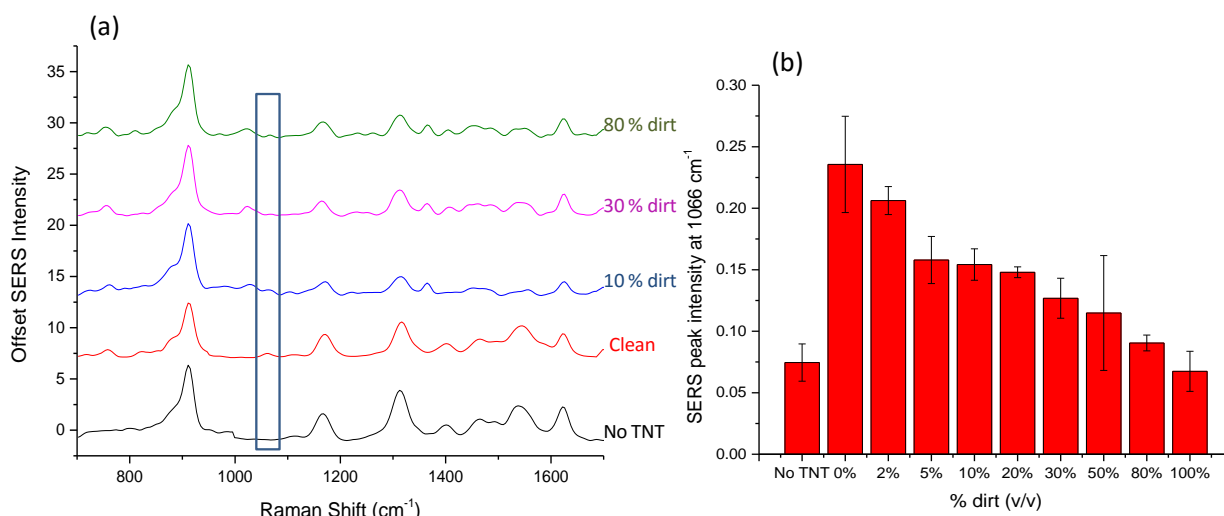
Figure 3.29: (a) SERS spectra of antibody conjugated silver nanoparticles with: no TNT (black), 50 nM TNT (red), 10% spiked 'dirt' (blue), 30 (pink) and 80 % spiked 'dirt' (green), using a 532 nm laser excitation for 0.5 s accumulation time for 5 measurements of 3 replicate samples, **(b)** Shows bar graph showing the SERS intensity of the peak at 1066 cm^{-1} for no TNT and concentrations of dirt from 0-100% (v/v), error bars arise from the standard deviation of 5 measurements of 3 replicate samples. Data set was baseline subtracted, scaled and offset for clarity.

Figure 3.29 demonstrates a natural dirt concentration study of spiked TNT samples. The black spectrum represents no TNT in the sample. Therefore only FITC bands could be observed. The red spectrum shows TNT present in the assay, however, no dirt was present. A peak at 1066 cm^{-1} was observed from the out-of-plane methyl group of TNT. The blue spectrum comprises of 10% dirt in the spike TNT assay. In this case, the TNT peak at 1066 cm^{-1} was still present. As the concentration of dirt was increased the TNT peak steadily decreased. Furthermore, above 80% dirt (green), no TNT peaks could be observed. This is further demonstrated in the bar chart in Figure 3.29 (b), as the concentration of dirt is increased the SERS peak present at 1066 cm^{-1} is decreased. This demonstrates that the assay is suitable in natural dirt at dilutions less than 80% v/v.

Synthetic dirt is available in over 200 different forms from LGC standards, therefore in order to state with confidence in which environments the assay can successfully detect TNT, much more research is required. Furthermore, only one concentration of TNT was investigated in these two soil examples, therefore further research into TNT concentrations with different soils would be of great interest. Finally, the detection of TNT was only investigated here, however several explosive materials may be present in any given sample, therefore further investigation into RDX and other explosive materials in different soils would also be of interest for simultaneous detection.

3.13 Conclusions

In conclusion, antibodies have major selective advantages which, when bound to nanoparticles, offer direct detection of specific target analytes without labeling. We have developed a direct SERS detection assay which offers quantitative results, is fast, simple, highly specific and selective towards targeting small molecules. The use of the ITC group plays an essential role in direct detection of target molecules as it allows for the antibody to conjugate to the nanoparticles surface in a flat orientation. This orientation allows for the target molecule to come in close proximity to the nanoparticles surface, allowing an intrinsic SERS signal of the target molecule to be obtained. Quantitative detection of the explosives, TNT and RDX, was achieved, with nM sensitivity for TNT and pM sensitivity demonstrated for RDX. In addition, PCA was used to allow multiplexed analysis based on unique Raman bands for the two different explosives which could be clearly identified in the SERS spectra. Furthermore, this assay has been demonstrated to work for a non explosive example to demonstrate the diversity of the assay when the specific antibody is changed to suit the target. This was possible due to the unique design of the assay. This approach demonstrates fast, sensitive and selective detection of TNT and RDX and provides distinct spectral analysis of the explosives for the first time at these concentrations.

Moreover, it was demonstrated that TNT could be detected in a more complex matrix. TNT was added to two different types of dirt, natural and synthetic dirt in

order to mimic a more realistic matrix in which TNT would be found in the field. Different solvents were explored in order to obtain a solvent which would dissolve the minimum amount of the dirt components, in order for TNT detection. It was found that THF was the best solvent. It was shown that TNT could be detected up to 80% natural dirt, however, only 10% synthetic dirt. These result demonstrate that the assay was not consistent for both complex matrices however only one TNT concentration (50 nM) was investigated, meaning much more research is needed before this assay can be used for in the field detection.

The aim of this project was to develop an assay which can be used for in field detection. However, due to time constraints, this assay was not performed on a portable device. However, it has been shown that a portable 532 nm laser excitation device could offer better detection due to the rastering function opposed to the static measurement approach present in the plate reader used for this project. Therefore, a portable Raman instrument should provide promising results in the future.

4. Modification of Antibodies for Detection of Explosive Materials

In chapter 3, the successful development of a solution based SERS assay using modified antibodies conjugated to silver nanoparticles for the detection of multiple explosives was demonstrated. However, the commercially modified antibody was available for the detection of TNT, RDX and dioxane. Therefore, it was required to develop a method to functionalise an antibody with a free ITC group, for the detection of pentaerythritol tetranitrate (PETN). The fluorophore used in the commercial antibody, fluorescein isothiocyanate (FITC), can potentially be conjugated to an antibody by three different routes (Figure 4.1).

There remains a challenge in functionalising surfaces with antibodies, as biomolecules usually carry several reactive groups. Methods of successful functionalisation have been described in section 2.1, including protein A/G and utilising PEG linkers. Whilst these allow for the antibody to be successfully bound to a surface, they are bound in such a way that the target is several nm away from the metallic surface. This is not ideal for SERS analysis since SERS is a distance dependant technique.[72] Therefore, a functionalisation step which is relatively simple and allows for successful conjugation, whilst maintaining biological activity of the antibody, is required.
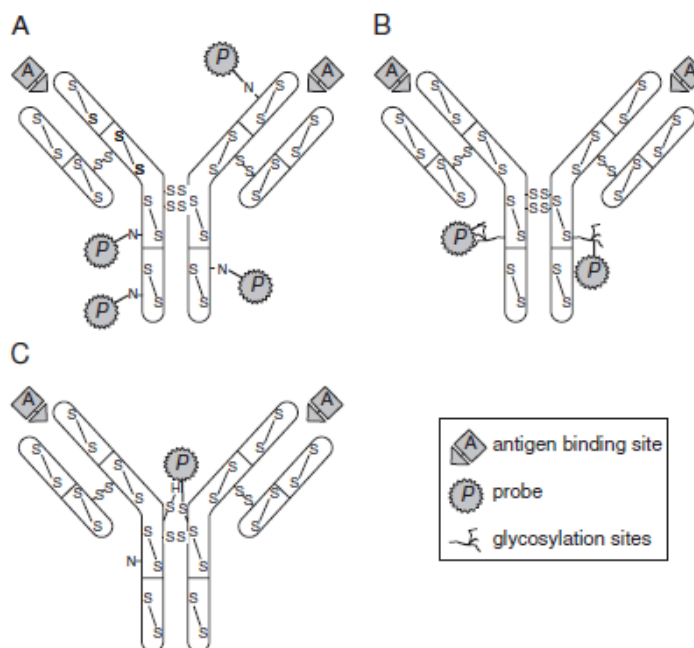
Figure 4.1: Schematic representation of available conjugation sites on antibodies, **(a)** via the free amine groups on the antibody, **(b)** Conjugation through the carbohydrate groups on the antibody, and **(c)** at the disulphide bridge in the hinge region of the antibody.[168]

A probe such as FITC, can be conjugated to an antibody via the free amine groups as shown in Figure 4.1 (a). The most conventional method to conjugate FITC to an antibody is to utilise the ITC group on FITC to form a thiourea with the free amine groups on the antibody. However, this method does not leave the ITC groups available for binding to a metallic surface, as demonstrated in the commercially available modified antibodies. Thus, the antibody may not immobilise 'flat' on the nanoparticle surface as discussed in chapter 3, hence a intrinsic SERS spectra of the target analyte will not be obtained. The free ITC was essential for the immobilisation of the antibody on the nanoparticle surface for subsequent SERS detection of the target analyte. This can be achieved by coupling the COOH group on FITC to the free amines in the amino acid sequence of the antibody by carbodiimide chemistry. This would result in the ITC group of the FITC being available for binding to a metallic surface. This immobilisation method allowed for the target molecule to come in close proximity to the metallic surface allowing a SERS spectrum of the target molecule itself to be observed. Figure 4.1 (b) demonstrates the binding of a probe through the glycosylation sites found on an antibody. Glycosylation involves a

carbohydrate molecule binding to a functional group such as a hydroxyl group via a covalent bond by a condensation reaction.[169] However, the glycosylation sites on an antibody depend on the interaction between the protein moiety and the oligosaccharide moiety. It has been reported that <10% of the total IgG molecule has beneficial properties for glycosylation, and therefore conjugation via this method was not considered further.[170] The final method for conjugation of a probe to an antibody is demonstrated in Figure 4.1 (c), attachment at the thiol group in the hinge region of the antibody. Reduction of the disulphide bridges in the antibody will form thiol groups, which can bind to FITC. However, this reduction method is hard to control due to the presence of disulphide bridges at various locations in the antibody. Mixtures of reduced disulphide bridges and antibody fragments have been reported using this method.[171] Therefore, the antibody functionalisation using carbodiimide chemistry shown in Figure 4.1 (a) was investigated.

4.1 Antibody Thiolation

It has been well reported that Au/Ag-thiol bonds are very strong and therefore would be ideal for immobilisation of antibodies on a metallic nanoparticles.[172] It is for this reason that antibodies for the detection of explosives are desired to be thiolated. Tang *et al.* reported the thiolation of antibodies using a cyclic compound, 2 – iminothiolane, known as Traut's reagent.[173] EDTA was added to Traut's reagent and was mixed with the antibody. This resulted in free amine groups on the antibody reacting with the sulfhydryl groups from Traut's reagent, allowing for the thiol to freely bind to Au-nanorods. A fluorescently labelled secondary antibody was used to determine the sensitivity of the assay. Using fluorescence spectroscopy the fluorescent emission from the secondary antibody could be obtained if the antibody was bound, such that the binding sites on the primary antibody were available for the secondary antibody to bind, therefore suggesting the thiol had immobilised the antibody in a 'tail on' orientation on the surface. The sensitivity of the assay was shown to be improved using this antibody immobilisation method.[174]

Collins and group have reduced the disulphide bridges which are present on an antibody to orientate an antibody on an Au electrode for the detection of *staphylococcal enterotoxin B*.[89] It was reported that by using a strong reducing agent, dithiothreitol (DTT), cleavage of the hinge of the disulphide bridge occurred, resulting in formation of a thiol and antibody was subsequently incubated with an Au electrode. Another antibody was then introduced after the addition of the target, to form a sandwich assay. This antibody had a biocatalytic tag, which when the whole assay was assembled, a non electroactive substance was converted to an electroactive product, producing an on/off detection method.

The most common route to thiolate an antibody is to use a polyethylene glycol (PEG) linker molecule which has a terminal thiol group at one end and a terminal amine group or carboxyl group on the other. Therefore, the thiol will bind to the nanoparticle and if terminated with an amine group, it can be coupled to the COOH group on an antibody, or if COOH terminated, it can be coupled to the amine groups on the antibody by carbodiimide chemistry. 1-ethyl-3- (3-dimethylaminopropyl) carbodiimide hydrochloride (EDC) is a cross-linker molecule which activates carboxyl groups for the addition of a primary amine. This occurs when EDC is added to a COOH group resulting in the formation of an unstable urea compound. N-hydroxysulfosuccinimide (sNHS) can then be added to form a more stable ester intermediate, which is amine reactive. Therefore, an amide bond is then formed from the addition of a primary amine to the solution, as shown in Figure 4.2.[175]
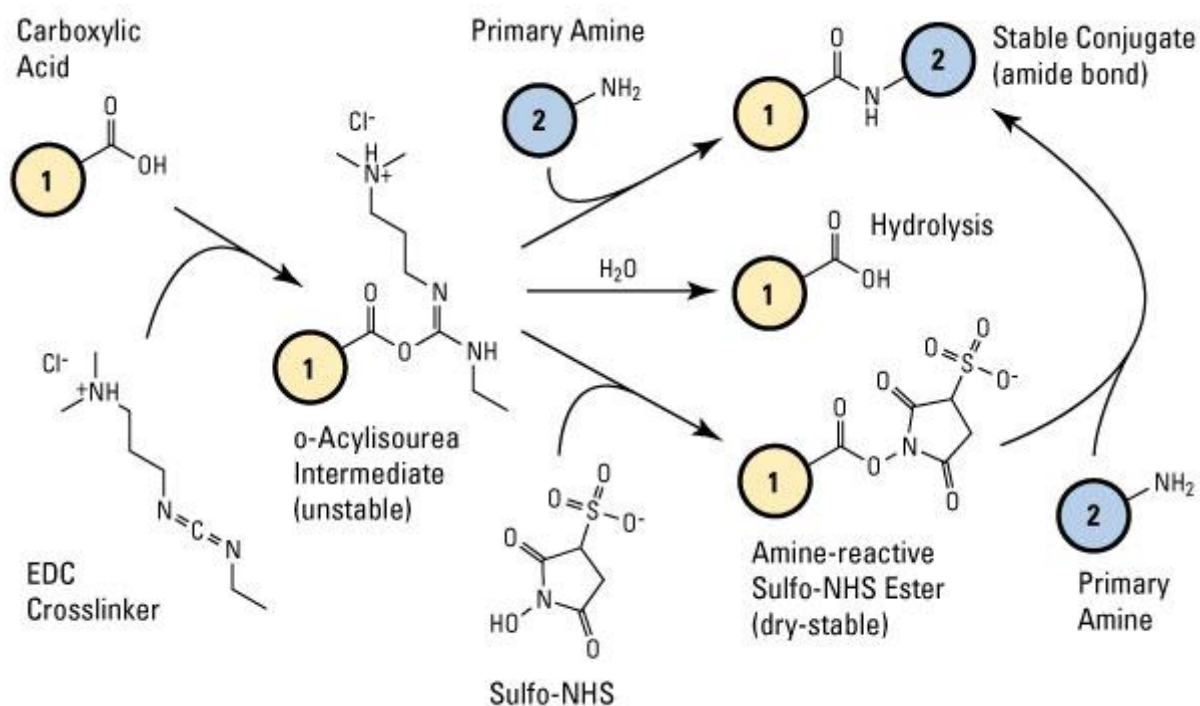
Figure 4.2: Schematic representation of carbodiimide chemistry.[176]

Covalently conjugating antibodies via a thiol group has been proven to be more effective in terms of the number of antibodies available on the surface of a metallic nanoparticle,[146] however these methods do not address the distance between the target analyte and the surface for SERS detection. This can be achieved, as mentioned in the previous chapter, by utilising a commercially available FITC modified antibody. The FITC molecule has an ITC group which is available for binding to the silver nanoparticle surface. It was therefore proposed thought that the antibody was conjugated to the FITC via the carboxylic acid of the FITC molecule and the free amine groups on the antibody. This could be achieved by using carbodiimide chemistry as mentioned in Figure 4.2.

Whilst, the FITC modification on the antibody was an almost ideal label, in that it allowed for the antibody to bind to the nanoparticle surface in a flat orientation, it was not ideal in the fact that it produced a strong background SERS spectrum from the fluorescein. Therefore, it was thought that using a molecule which had the same functional groups as FITC i.e. a COOH and ITC group but without the fluorophore, would conjugate to the antibody resulting in the antibody orientating flat on the

silver nanoparticles surface. However, the conjugation of FITC onto an antibody was first investigated to determine if the coupling could be achieved to allow for a comparison to the commercial labelled antibodies.

4.2 Results and Discussion

4.2.1 Isothiocyanate Protection

Conventional methods of conjugating FITC to an antibody utilises the ITC group to form a thiourea bond with the free amine groups on the antibody. Thus, when considering the antibody conjugation with FITC by carbodiimide chemistry, it was necessary to protect the isothiocyanate (ITC) group in order to reduce any cross reactivity between the ITC and primary amine, which can occur via acylation and/or alkylation forming the thiourea bond, as shown Figure 4.3.
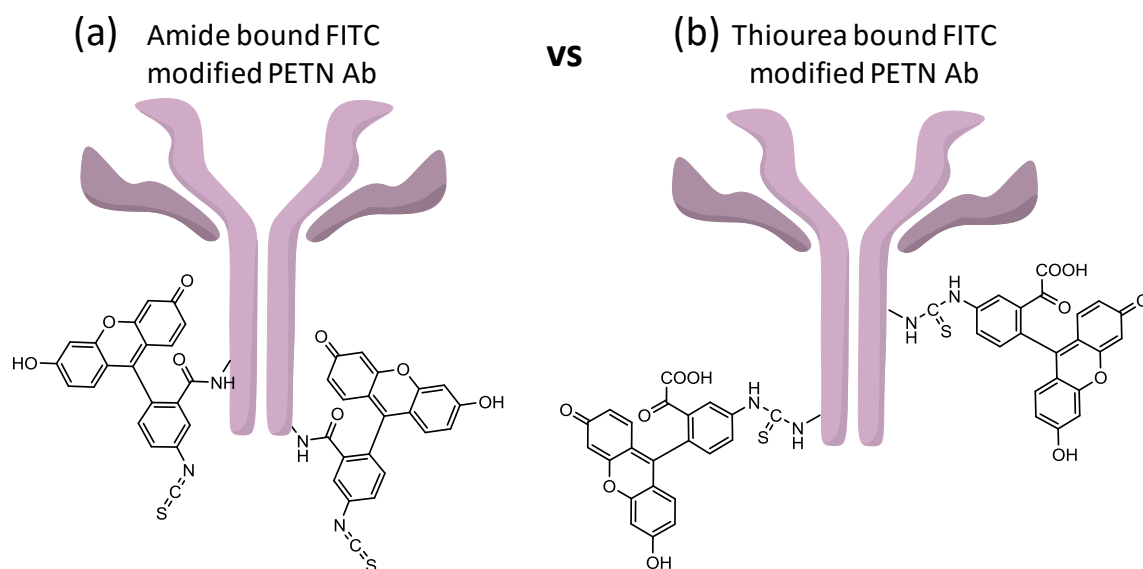
Figure 4.3: Schematic representation of FITC modified PETN antibody by **(a)** carbodiimide chemistry, forming an amide bond between the free amine groups on the antibody and the COOH on FITC, **(b)** forming a thiourea bond by the free amine group on the antibody and the isothiocyanate group.

Possible thiol protecting groups had to be stable, but could be easily removed when required. Pastuszak *et al.* reported the protection of the thiol group on cysteine for peptide synthesis using a *tert*-butyl.[177] The thiol was refluxed with a mixture of HCl and *tert*-butyl alcohol, resulting in the *tert*-butyl protecting the thiol group on the cysteine, as shown in Figure 4.4. Furthermore, the *tert*-butyl group can subsequently

be removed by using 2 equivalents of (2-nitrophenyl)sulfenyl chloride (NpsCl). One equivalent of the NpsCl bound to *tert*-butyl forming *tert*-butyl-Nps. This was easily removed by gel chromatography. The second equivalent of NpsCl bound to the thiol on the cysteine group. The thiol-Nps bond was easily converted back to the thiol by reduction with $NaBH_4$.
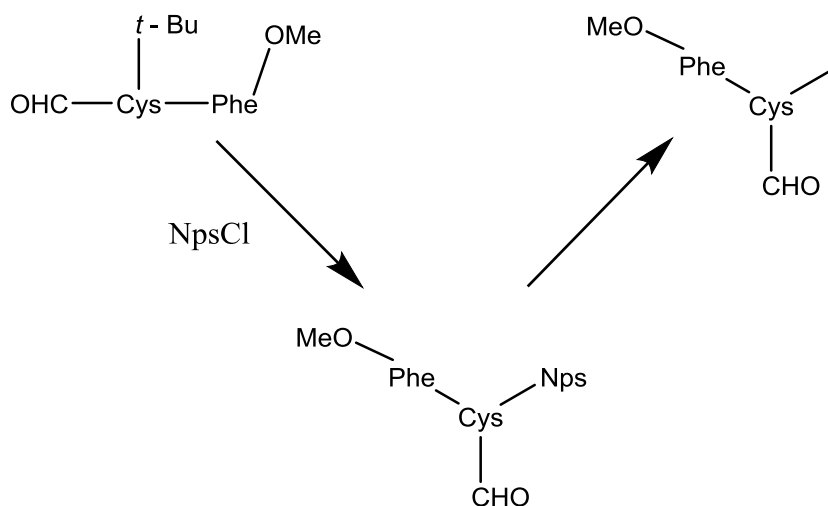
Figure 4.4: Schematic representation of *tert*-butyl protecting a thiol group in cysteine.[177]

Another method for the reversible protection of a thiol on a natural protein is using acetamidomethyl (product II, Figure 4.5).[178] Under acidic conditions, the protection of the thiol group on cysteine was obtained by forming acetamidomethyl – L - cysteine, product III, Figure 4.5. This acetamidomethyl protected thiol was easily removed with mercuric ions and gel filtration, in the presence of mercaptoethanol. However, this reaction only yielded 50% of the protected thiol derivative, as under anhydrous conditions, the acetamidomethyl is in equilibrium, as shown in Figure 4.5.
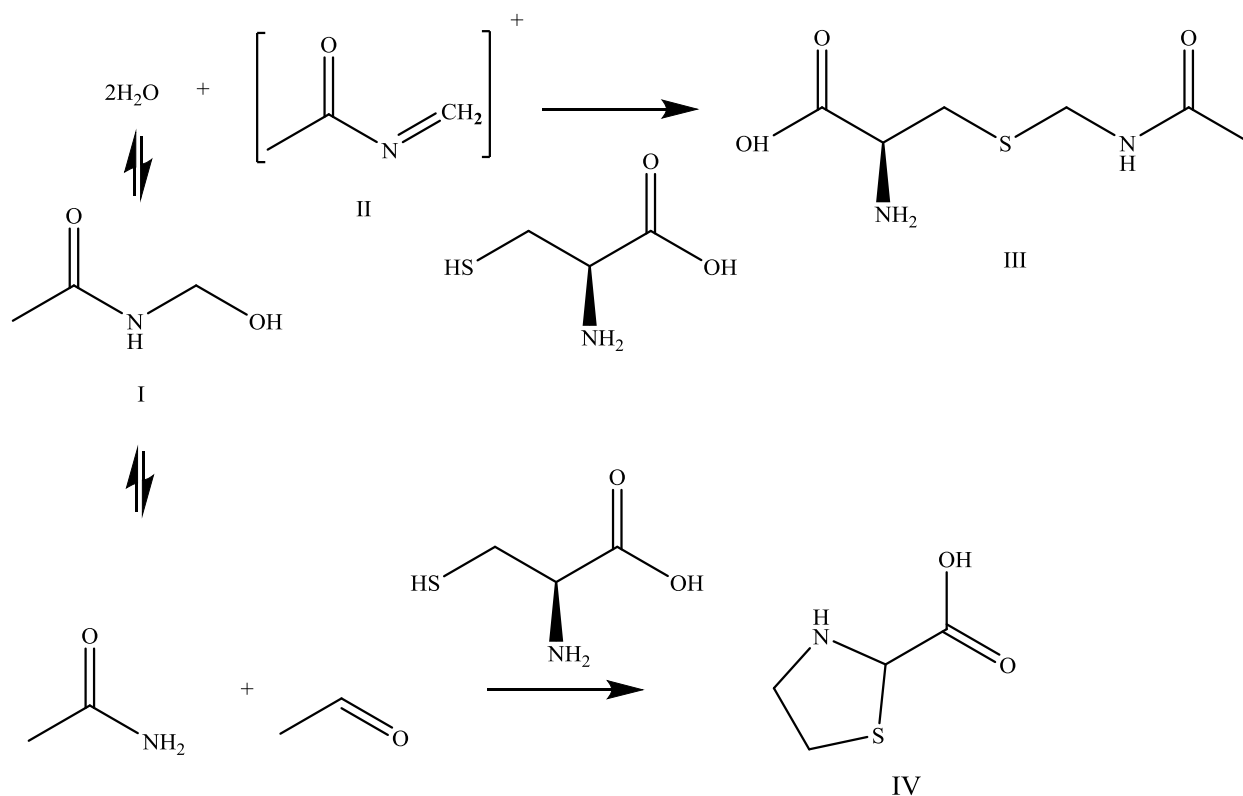
Figure 4.5: Schematic representation of acetamidomethyl protection of thiol in cysteine, where product I is acetamidomethyl under anhydrous conditions, II is acetamidomethyl, III acetamidomethyl – L – cysteine and IV is thiazolidine-2-carboxylic acid.

Under anhydrous conditions the equilibrium favours product I (Figure 4.5), therefore when cysteine is added, the side product is formed, thiazolidine-2-carboxylic acid (product IV, Figure 4.5).

Whilst both of these methods provide reversible protection of thiol groups on proteins they are not yield efficienct. Therefore, it was decided to determine how much of the antibody yielded the free ITC product and how much yielded the thiourea product, shown in Figure 4.3, if thiol protection was not used. It was decided that using a lower pH (<9) the EDC/sNHS coupling would selectively activate COOH, favouring the ITC free product, without using a protecting group, therefore this option was explored first.

4.2.2 Concentration Ratios

It has previously been reported that the optimum concentration of COOH: EDC: sNHS: NH_2 is approximately 1: 1.5: 2: 4.[175] Increasing concentrations of FITC (2, 6, 10 and 20 μM) and EDC (1.12, 5.6, 11.2 and 19.8 μM) were added dropwise to the sNHS (10.86 μM) and PETN specific antibody (2 mg/ml, 20 μl) solution in HEPES buffer (pH 7.2). The solution was left to mix for 4 hours before purifying via cartridge centrifugation. A 10 kDa cartridge was selected, molecules smaller than 10 kDa, i.e. unconjugated FITC, should flow through the cartridge and be discarded in the supernatant. The cartridge was then reversed centrifuged in order to obtain conjugates over 10 kDa, i.e. unconjugated antibody and FITC conjugated antibody. Further seperation of the FITC conjugated antibody from the unconjugated antibody could be obtained by reverse phase high performance liquid chromatography (RP-HPLC).

4.2.3 Fluorescent Spectroscopy

Fluorescent spectroscopy was performed in order to determine the concentration ratio of antibody to FITC. This can be quantified by exciting the antibody FITC conjugate at 280 nm and observing the emission wavelength from 300 to 360 nm. Excitation at 280 nm was investigated due to biomolecules typically absorbing at 280 nm due to specific aromtaic amino acids, such as tryptophan, absorbing in the UV region of the electromagnetic spectrum.[179] The concentration of FITC of the antibody can be determined by exciting at 492 nm which is the maximum absorbance of FITC and observing the fluorescence emission from 500 – 560 nm. The commercially available FITC conjugated antibodies specific for TNT and dioxane, were also analysed in order to compare the number of FITC molecules conjugated to the commercial antibody versus the in-house functionalised antibody. 10, 30, 50 and 100 μl of FITC (200 μM) was conjugated to 20 μl of antibody (2 mg/ml) by EDC/sNHS coupling. After cartridge centrifugation, the FITC conjugated antibodies were analysed by fluorescence spectroscopy in order to determine the concentration of FITC actually conjugated to the antibody. The samples were excited using 280 nm excitation, to observe any antibody fluorescence emission at 300 – 360

nm. The samples were also excited using 492 nm, to observe the FITC fluorescence emission at 500 – 560 nm. The commercially available TNT and dioxane antibodies were also analysed by fluorescence spectroscopy to determine the FITC to antibody concentration, as shown in Figure 4.6.
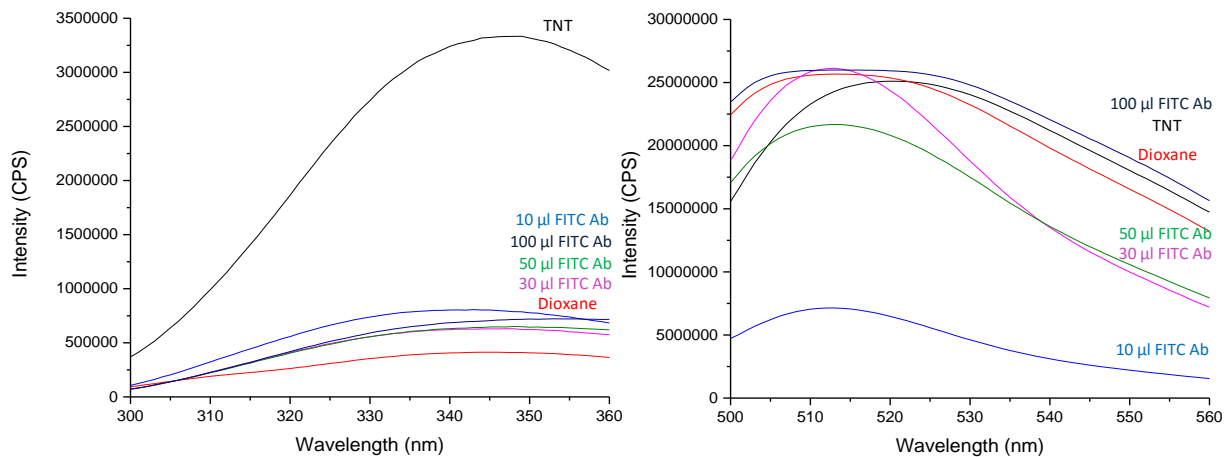
Figure 4.6: Fluorescence emission spectra of commercially available FITC modified TNT (black) and dioxane (red) antibody (FITC Ab), modified in-house FITC antibody after conjugation of a range of FITC concentrations: 10 μl (light blue), 30 μl (pink), 50 μl (green) and 100 μl (dark blue). **(a)** Fluorescence emission observed from 300 – 360 nm after 280 nm laser excitation for 10 s, **(b)** the fluorescence emission observed from 500 – 560 nm after 495 nm excitation for 10 s.

Figure 4.6 (a) represents the fluorescence emission from excitation at 280 nm for the commercially available TNT and dioxane FITC modified antibody and after coupling of a range of FITC concentrations (10, 30, 50, 100 μl of 200 μM) conjugated to the PETN antibody (20 μl, 2 mg/ml). The fluorescence emission from the antibody itself after excitation at 280 nm was used to quantify the concentration of antibody in each sample. It can be seen in Figure 4.5 that TNT had the highest fluorescence emission intensity and dioxane had the lowest emission intensity, suggesting that the TNT antibody contained a higher aromatic amino acid content or a higher concentration of antibody was present, despite both antibodies purchased at 2 mg/ml concentration. The in-house modification antibodies appeared to have similar emissions to each other, which was to be expected. However, despite all antibody concentrations being kept constant as per manufacturer (2 mg/ml), the fluorescence demonstrates that TNT contained more aromatic amino acids, such as

tryptophan, or TNT was higher in the concentration in comparison to the other antibodies investigated. Figure 4.6 (b) represents the fluorescence emission observed after laser excitation at 495 nm. It was expected that any FITC conjugated to the antibody would fluoresce and as a result be quantified. It was demonstrated that as the concentration of FITC conjugated to the antibody increased, the fluorescence intensity also increased. It was also observed that TNT and dioxane had similar fluorescence emission intensities, which was also similar to the 100 µl FITC (200 µM) sample. The ratio of antibody to FITC was then determined by equation (5):

$$\left(\frac{A_{FITC}}{\varepsilon^m_{FITC}}\right) \div \left[\frac{(A_{280} - A_{FITC} \times CF)}{\varepsilon^m A_{280}}\right] \quad (5)$$

Where, A_{FITC} is the emission intensity of the FITC at maximum peak wavelength, ε^m_{FITC} is the approximate molar extinction co-efficient of the FITC (68000 cm^{-1} M^{-1}), A_{280} is the emission intensity of the antibody at maximum peak wavelength (280 nm), CF is the correction factor equal to A_{280} for dye/ A_{FITC} (0.3) and $\varepsilon^m A_{280}$ is the approximate molar extinction co-efficient of the antibody (203000 cm^{-1} M^{-1}). Therefore, the dye to antibody ratio was calculated as shown in Table 4.1.

Table 4.1: Summary of the dye: antibody concentration according to equation (5).

Sample	Dye : Antibody (mol of dye/ mol of antibody)
TNT	0.77
Dioxane	7.56
10 FITC Ab	0.922
30 FITC Ab	4.64
50 FITC Ab	3.69
100 FITC Ab	4.02

As shown in the table above, the concentrations of FITC in the commercialised antibodies are not similar, and are not equal to the 4.5 which was quoted by the manufacturers, Fitzgerald, USA. Therefore this analysis can only conclude that FITC was successfully conjugated to the antibody as fluorescence emission was observed from both 280 and 495 nm excitation. Furthermore, as the concentration of FITC conjugated to the PETN antibody was increased, the fluorescence emission observed after 495 nm excitation also increased. However, the concentration ratio of FITC conjugated to antibody could not be obtained by this technique, thus another analytical method for quantification was required.

4.2.4 Protein BCA Quantification Kit

It was shown that fluorescence spectroscopy was not able to quantify the ratio of FITC to antibody, therefore another method was required. This can be achieved by using a protein bicinchoninic acid (BCA) quantification kit. This quantification kit is primarily used to determine the concentration of a protein in a sample by using the Biuret reaction. More specifically, the reaction measures the amount of amide bonds present in the protein, as amides in an alkaline environment reduce Cu^{2+} ions to Cu^{1+} ions forming a blue coloured chelate, as shown in Figure 4.7. The Cu^{1+} ions then form a purple complex with BCA, in which the intensity of the purple colour is proportional to the number of amide bonds.
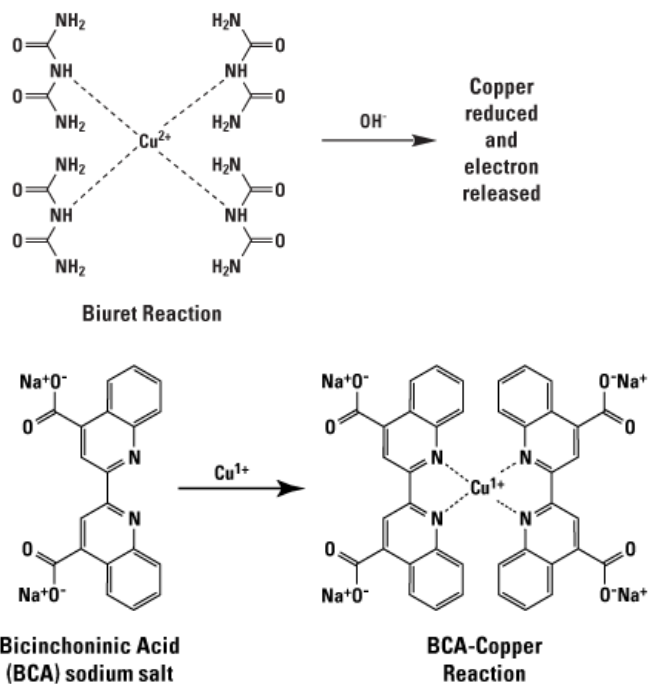
Figure 4.7: Demonstrates the reaction of bicinchoninic acid (BCA) quantification kit for the presence of amide bonds.[63]

Therefore, it was proposed that the FITC conjugated onto the antibody by carbodiimide chemistry, forming an amide bond, would produce a more intense purple complex than the unmodified antibody when analysed by UV-vis spectroscopy. Firstly, a calibration graph of known concentrations of a protein, bovine serum albumin (BSA), were analysed to ensure that increasing the concentration of BSA resulted in an increase in the concentration of purple complex formed. Analysis of the purple complex was performed by observing the absorbance intensity of the complex at 562 nm, the absorbance intensity was then plotted against concentration as shown in Figure 4.8.
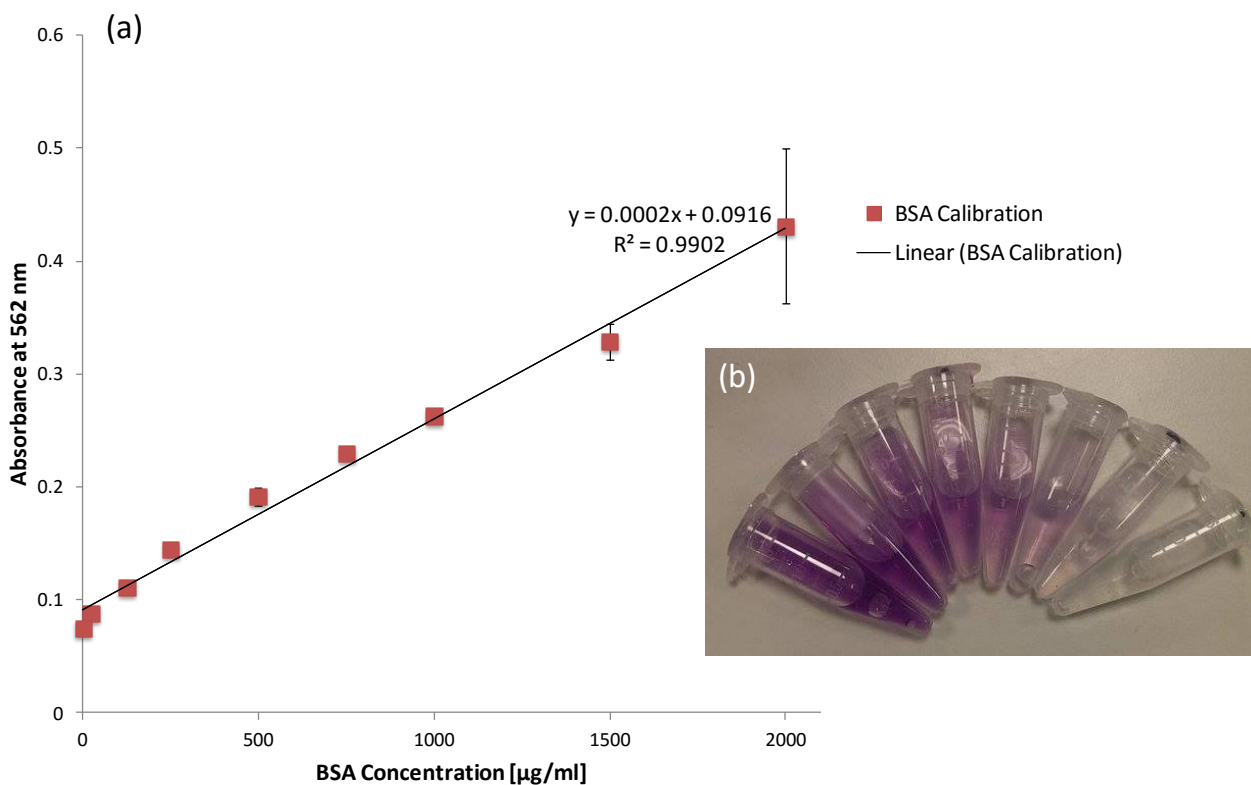
Figure 4.8:(a) Calibration graph of absorbance at 562 nm of increasing concentrations of BSA, error bars arise from the standard deviation of 3 measurements of 3 replicate samples, R^2= 0.9902 **(b)** Image demonstrating the colour intensity of the purple complex increasing as the concentration of BSA increases.

A calibration graph demonstrating the BCA quantification kit is shown in Figure 4.8. It was demonstrated that as the concentration of BSA increased, the number of amide bonds increased, increasing the intensity of the purple complex formed as a result. Therefore, the in-house FITC modified antibodies were analysed, to determine if amide bonds had been formed due to the coupling. The commercially available dioxane FITC modified antibody, and a range of FITC concentrations (10, 30, 50, 100 μl of 200 μM) conjugated to the PETN antibody (20 μl, 2 mg/ml) were analysed by UV-vis. Control samples consisting of 50 μl FITC (200 μM) only, PETN antibody (20 μl, 2 mg/ml) only, FITC (50 μl, 200 μM) labelled PETN antibody (no EDC/sNHS was added during the modification to determine if any thiourea bonds were made) and 50 μl fluorescein, FAM (200 μM, no ITC group) was explored to observe the intensity of amide bonds in the absence of ITC. Prior to the copper ions being added to the solutions, the samples were first analysed by UV-vis to ensure the antibody concentration was the same, therefore ensuring any differences in the intensity of the purple complex were due to the increase in amide bonds, formed by

the FITC modification. Figure 4.9 demonstrates the absorbance of the purple complex obtained after the Buiret reaction for each of the samples superimposed on the BSA calibration previously obtained in Figure 4.8.

Figure 4.9:(a) Calibration graph of absorbance at 562 nm of increasing concentrations of BSA, error
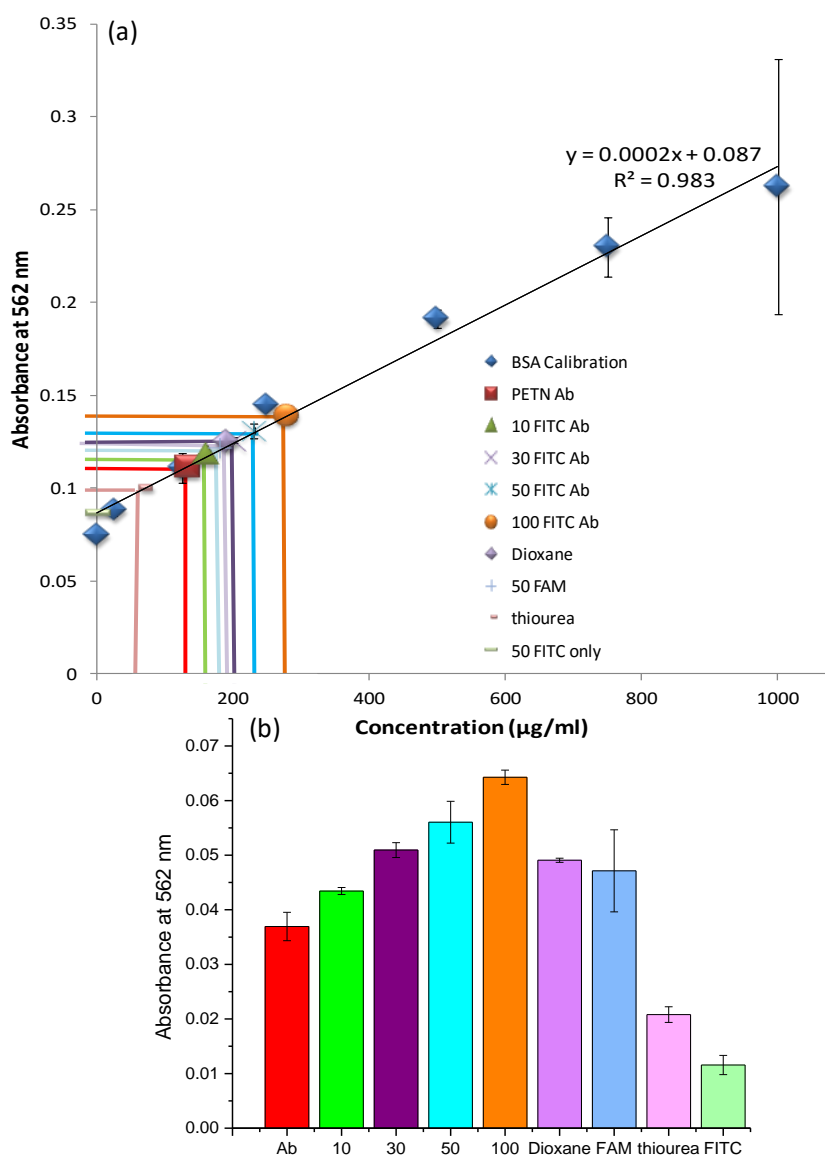
bars arise from 3 measurements of the standard deviation of 3 replicate samples, $R^2 = 0.983$. The absorbance intensity of PETN antibody (red), antibody conjuagted to 10 (green), 30 (purple), 50 (blue) and 100 (orange) μl of FITC (200 μM), the commerically available FITC modified dioxane antibody (light purple), fluroscein (FAM, with no ITC group) conjugated to PETN antibody (light blue), FITC conjugated to antibody with no EDC/sNHS coupling, demonstrating the possibility of thiourea bonds (pink), and FITC only (50 μl, 200 μM, light green). **(b)** Bar chart demonstrating the absorbance oat 562 nm as the concentration of FITC conjugated to the antibody is increased and the controls, intensity has had the blank subtracted.

In the presence of amide bonds, under alkaline conditions, Cu^{2+} is reduced to Cu^{1+}. This reduced copper ion can form a complex with BCA resulting in a purple colour, in which the intensity of the purple complex is proportional to the amount of amide bonds present. It was observed in Figure 4.9 (a) that the antibody only sample had an absorbance of 0.112. This was to be expected as the antibody is a protein, therefore it should have amide bonds present. However, when FITC (10 μl, 200 μM, green) was conjugated to the antibody (20 μl, 2 mg/ml) an increase in absorbance to 0.118 was observed. This suggests that successful amide bonds were formed between the COOH of the FITC and the amine groups on the antibody by carbodiimide chemistry, as the concentration of FITC conjugated to the antibody was increased (30, 50 and 100 μl, 200 μM, purple, blue and orange), it was observed that the absorbance also increased (0.126, 0.131 and 0.139). This is in agreement that as more FITC molecules were conjugated, more amide bonds were formed, hence more Cu^{2+} ions were reduced and a more intense purple coloured complex was formed. The commerically available FITC modified dioxane antibody was also analysed by the BCA quantification kit to observe how the absorbance intensity compares to the in-house modification. An absorbance of 0.125 was obtained. This is simular to the in-house 30-50 μl of FITC (200μM) conjugated to antibody absorbance intensity. However, this control can not be used for a direct comparison between the two different antibodies as the dioxane antibody may simply have more or less amino acids, and therefore a different number of amide bonds.

A control sample of fluoroscein (FAM) with no ITC group (50 μl, 200 μM) was conjugated via carbodiimide chemistry to the antibody to determine the absorbance intensity of the purple complex formed from the direct amide bond, with no possibility of a thiourea bond forming. It was observed (Figure 4.9 (a), light blue) that an absorbance of 0.122, this indicates that in the absence of the ITC group, an amide bond was made between the COOH group and the free amine groups on an antibody. A further control was performed which involved the addition of FITC to the antibody, in the absence of EDC/sNHS, therefore if there was competition between the amide and thiourea bound FITC PETN antibody, then this control would determine the concentration of thiourea product formed. Figure 4.9 (a) demonstrates

that the thiourea product had an absorbance of 0.103. This was lower than that of the absorbance of the antibody on its own. Interestingly, this could be due to thiourea being an unstable product, therefore a decrease in absorbance was observed.

Finally, a FITC only control was explored to ensure no purple complex was formed as there are no amide or thiourea bonds present. An absorbance of 0.08 was observed, indicating background absorbance. Furthermore, Figure 4.9 (b) demonstrates a bar chart of the absorbance concentrations with the blank subtracted, in which the blank sample was PBS buffer in which the antibody was dissolved. It was observed that as the concentration of FITC conjugated to the antibody increased, the absorbance at 562 nm increased, suggesting more amide bonds were formed due to carbodiimide coupling. Since the concentration of FITC to antibody could not be determined it was necessary to further purify and isolate the FITC conjugated antibody. This could be achieved by size exclusion chromatography.

4.2.6 *Size Exclusion High Performance Liquid Chromatography*

High performance liquid chromatography (HPLC) is a separation technique where the analyte is passed through a column containing a stationary phase for which the components of the analyte have an affinity.[180] Separation is achieved by the strength of the interaction between the analyte and the stationary phase. The HPLC was coupled with UV-vis spectroscopy to detect the desired molecule after separation and isolation.

Size exclusion HPLC (SE-HPLC) separates due to differences in size. The stationary phase consists of small polymeric beads which only allow small molecules to penetrate the pores, whilst larger molecules flow straight through the column, unretarded. The mobile phase consisted of distilled H_2O at a flow rate of 1 ml/min. Therefore, larger molecules elute first, small molecules elute last. Therefore, it was expected that the labelled antibody will elute first, followed by unconjugated antibody. The samples (10, 30, 50, 100 µl) of FITC (200 µM) conjugated antibody (2 mg/ml), FITC only, antibody with no modification and PBS were injected into the HPLC, and the elution was followed using UV-vis spectroscopy at 280 nm, as shown

in Figure 4.10. The absorbance was monitored at 280 nm as both FITC and antibody absorb at this wavelength.
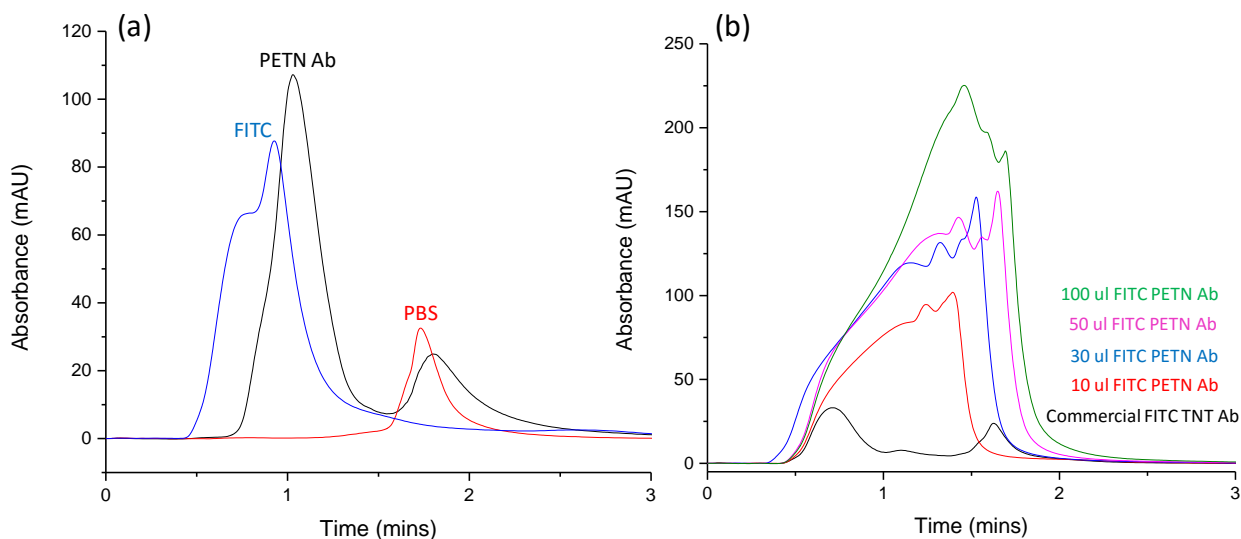
Figure 4.10: (a) SE-HPLC of FITC (blue), PETN antibody (black) and PBS (red), **(b)** SE-HPLC of commercially available FITC modified TNT antibody (black), 10 (red), 30 (blue), 50 (pink) and 100 (green) µl of FITC (200 µM) conjugated antibody monitored at 280 nm.

In Figure 4.9 (a) the components of the PETN antibody modification were monitored by SE-HPLC. A sample of FITC only (blue) had a retention time of 0.93 mins, indicating that the molecule is large and hence passed through the column unretarded. The unmodified PETN antibody was observed to have a retention time of 1.03 mins, again suggesting that the molecule was large and passed through the column. PBS buffer was also analysed by SE-HPLC since the antibody was dissolved in PBS, Figure 4.10 ((a), red) showed that PBS consists of smaller molecules and hence penetrated the pores, resulting in a longer retention time of 1.74 mins.

Figure 4.10 (b) demonstrates the analysis of the modified antibodies by SE-HPLC. The commercially available FITC modified TNT antibody (black) demonstrates an elution peak at 0.713 mins. This is due to the FITC modification on the antibody, making the molecule even larger and hence will elute from the column first. There is a small shoulder observed at 1.11 mins which could be due to the presence of unmodified antibody in the sample. A PBS peak was also observed at 1.632 mins,

which was expected as the commercially available antibody was dissolved in this buffer. The red spectrum in Figure 4.10 (b) is from the conjugation of FITC (10 μl, 200 μM) to the antibody. Elution peaks were observed at 1.20 and 1.39 mins. The peaks at 1.20 mins is proposed to be due to successful FITC conjugation to the antibody and the peak at 1.39 mins may be due to the unmodified antibody as it is slightly smaller and hence will be retained longer. Due to FITC modified antibodies and unmodified antibodies eluting at similar times it is difficult to interpret the peaks, hence another analytical method was required to determine successful conjugation. However, the blue sample in Figure 4.10 (b) represents a higher concentration of FITC (30 μl, 200 μM) conjugated to the antibody. It was observed that there were peaks present at 1.32 and 1.53 mins, there was also a small shoulder present at 1.45 mins. A higher absorbance in comparison to the FITC (10 μl, 200 μM) suggests that more FITC molecules were successfully conjugated to the antibody. It was thought that the two peaks and the shoulder may arise due to FITC modified antibody in both the amide and thiourea product and from the unmodified antibody. Since the unmodified antibody was smaller in size it should elute last at 1.53 mins. However, the peak at 1.32 mins and the shoulder present at 1.45 mins were difficult to assign as both the amide and thiourea product will have similar sizes. As the concentration of FITC was further increased to 30 and 50 μl of 200 μM FITC conjugated to the antibody (pink and green), three elution peaks were observed as well as an increase in absorbance, suggesting successful FITC conjugation. Interestingly, the FITC conjugated antibody peak showed increasing retention times of 1.42 and 1.46 mins and a small shoulder was observed, at 1.55 and 1.59 mins, suggesting both thiourea and amide products were present. The unmodified antibody peak was thought to be observed at 1.65 and 1.69 mins.

Whilst SE-HPLC was able to suggest the FITC conjugation to the antibody, the elution times of the conjugated and unconjugated antibody were very similar, hence isolation of each product was difficult. Therefore, another HPLC method, with higher resolution, which can determine the difference between FITC conjugated antibodies via an amide bond and FITC conjugation via the thiourea bond was required. This could be achieved by using reverse phase (RP)-HPLC.

4.2.7   Reverse Phase High Performance Liquid Chromatography

Reverse phase (RP)-HPLC seperates proteins, and other biomolecules, due to differences in hydrophobicity.[181] The stationary phase is non-polar, usually consisting of silica functionalised with long chain alkyl groups, in this case, C_4 (buytl silane). Since biomolecules are hydrophobic they are strongly retained in the column, however, using an Accucore C4 HPLC column, the pore size has been optimised to reduce hydrophobic retention. Furthermore, the mobile phase usually consists of a water miscible solvent, such as acetonitrile, and is usually gradient eluded. This increasing organic gradient in the mobile phase resolves the analytes in a minimal amount of time. It was observed that the binding of the FITC to the antibody results in an amide bond or a thiourea bond formation. In the case of the formation of an amide bond, the xanthene ring with the isothiocyanate group is free for binding, the log P (described in section 3.11) value of this is 2.23. However, when a thiourea bond is formed, the xanthene ring and the carboxylic acid group are free for binding, the log P value for this is 1.55. Therefore, since the thiourea product is more hydrophillic than the amide bonded product, the thiourea should elute from the column earlier. The FITC (30, 50 and 100 μl, 200 μM) conjugated PETN antibodies (2 mg/ml) were injected into the HPLC and the elution was monitored at 214 nm, as shown in Figure 4.11. An absorbance of 214 nm was selected as the column 'Accucore C4 HPLC column' had specifically been optimised for monoclonal antibodies, a sharp absorbance peak in the chromatogram was observed at 214 nm.[182]
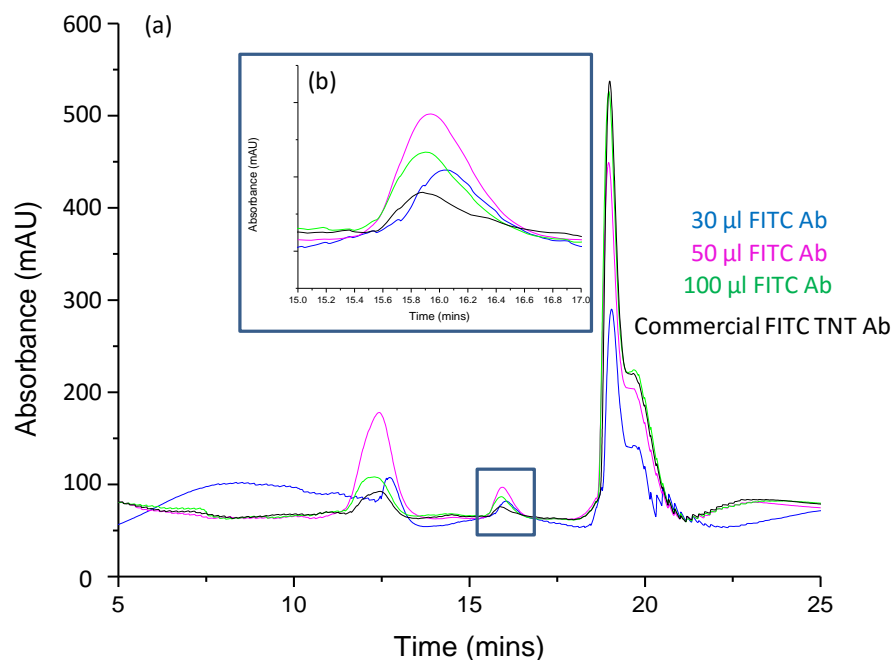
Figure 4.11: (a) RP-HPLC of commercially available FITC modified TNT antibody (black), 30 (blue), 50 (pink) and 100 (green) μl of FITC (200 μM) conjugated to PETN antibody monitored at 214 nm, **(b)** RP-HPLC of the amide product peak.

Figure 4.11 represents the RP-HPLC anaysis of the FITC modified antibodies. The commericialised FITC conjugated antibody (black) had three eluted peaks present at 12.47, 15.86, 18.99 and a small shoulder at 19.79 mins. The peak at 12.47 mins may be due to the thiourea product, due to the molecule being more hydrophilic than the amide product. The peak present at 15.86 mins may be due to amide product of the FITC conjugated antibody. The peak and small shoulder at 18.99 and 19.79 mins are possibly due to the unmodified antibody. The ratio of amide to thiourea product was determined to be 1: 2.13. Increasing the concentration of FITC conjugated to the antibody produced similar results to the commerically available FITC modified TNT antibody, in that a thiourea product peak was observed at 12 mins, an amide product peak was observed at 16 mins and unmodified antibody were obtained at 19 mins. Figure 4.11 (b) is focussed on the amide product peak and the peak ratios were obtained. For 30 μl of FITC (200 μM) modified antibody the ratio of amide to thiourea product was determined to be 1: 1.89. It was observed that for 50 μl of FITC (200μM) modified antibody that the ratio of amide to thiourea product was

1: 3.3. For the highest concentration of FITC (100 µl, 200 µM) conjugated to the antibody the ratio of thiourea to amide product was observed to be 1: 1.94.

Each product was collected and was analysed by UV-vis spectroscopy and fluoresence spectroscopy to confirm the presence of the antibody and the FITC in each RP-HPLC fraction. Antibodies absorb at 280 nm, therefore UV-vis spectroscopy will be able to identify any antibody present from the RP-HPLC collected fractions. Similarly, FITC can be detected by fluoresence spectroscopy by exciting the sample at 492 nm and observing the fluoresence emission at 515 nm. The 30 µl of FITC (200 µM) conjugated to the antibody (2 mg/ml) was analysed, shown in Figure 4.12.
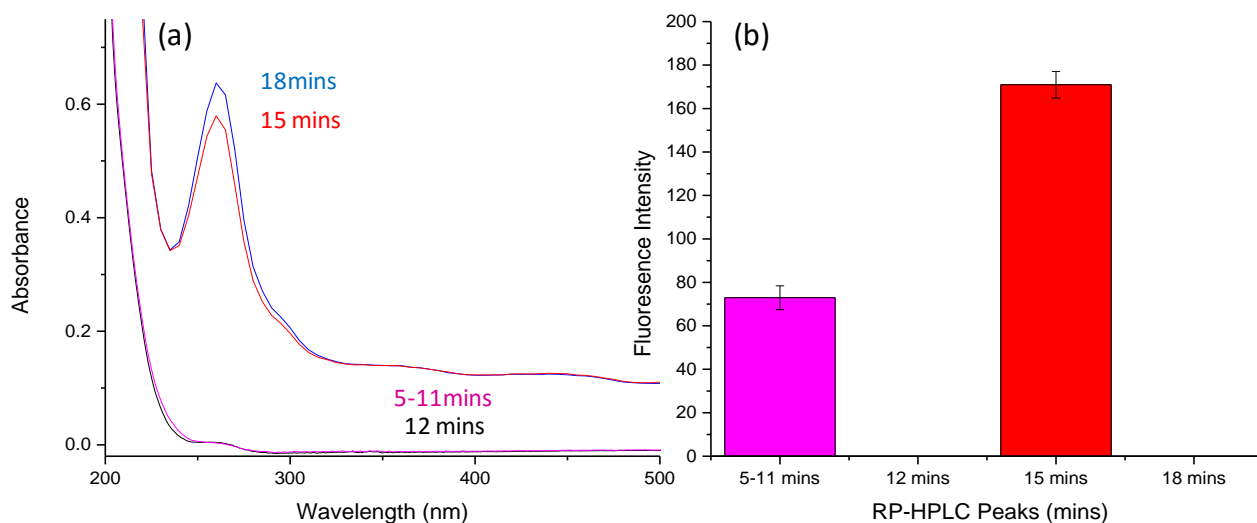
Figure 4.12: (a) UV-vis spectrum of the FITC (30 µl, 200µM) conjugated antibody product collected from RP-HPLC between 5-11 mins (pink), 12 mins (black), 15 mins (red) and 18 mins (blue) **(b)** Fluorescence spectroscopy of the samples excited at 495 nm for 20s and fluorescence emission observed at 525 nm. Error bars arise from the standard deviation of 3 replicate samples.

Figure 4.12 represents the UV-vis spectrum and fluoresence intensity of the products which were purified using a cartridge centrifuge to remove any unconjugated FITC. The products were then separated by RP-HPLC and the fractions were collected and analysed by UV-vis spectroscopy, as shown in Figure 4.12 (a). It was observed that at 15 and 18 mins, there was antibody present in the products which is in agreement with the RP-HPLC data, 12 mins was deduced to represent the thiourea bound FITC antibody which should elute first however, no antibody peaks were observed on the

UV spectrum, this could be due to the low concentration of the antibody in the collected fraction. The peak at 15 mins was thought to be from the amide product of the FITC conjugated antibody, in which there were antibody absorption peaks present in Figure 4.12. There was no absorbance peaks observed between 5-11 mins as expected as no antibody should be present. At 18 mins there was an antibody peak suggesting the unmodified antibody was present. Furthermore, Figure 4.12 (b) demonstrates analysis of the products by fluorescence spectroscopy. Interestingly, it was observed in the fraction collected between 5-11 mins that there was fluorescence products present. However, due to the cartridge centrifugation, no free FITC should be present in the sample therefore, the presence of fluorescent products in 5-11 mins fraction was unexpected. However it was possible that due to the negative charge on FITC that it was attracted to a positive charge on the antibody, thus not passing through the cartridge, resulting in a small fluorescence background. Increasing the concentration of FITC (50 μl, 200 μM) conjugated to the PETN antibody by carbodiimide chemistry was also analysed by RP-HPLC (Figure 4.12, pink) and the fractions were collected and analysed by UV-vis and fluoresence spectroscopy, as shown in Figure 4.13.
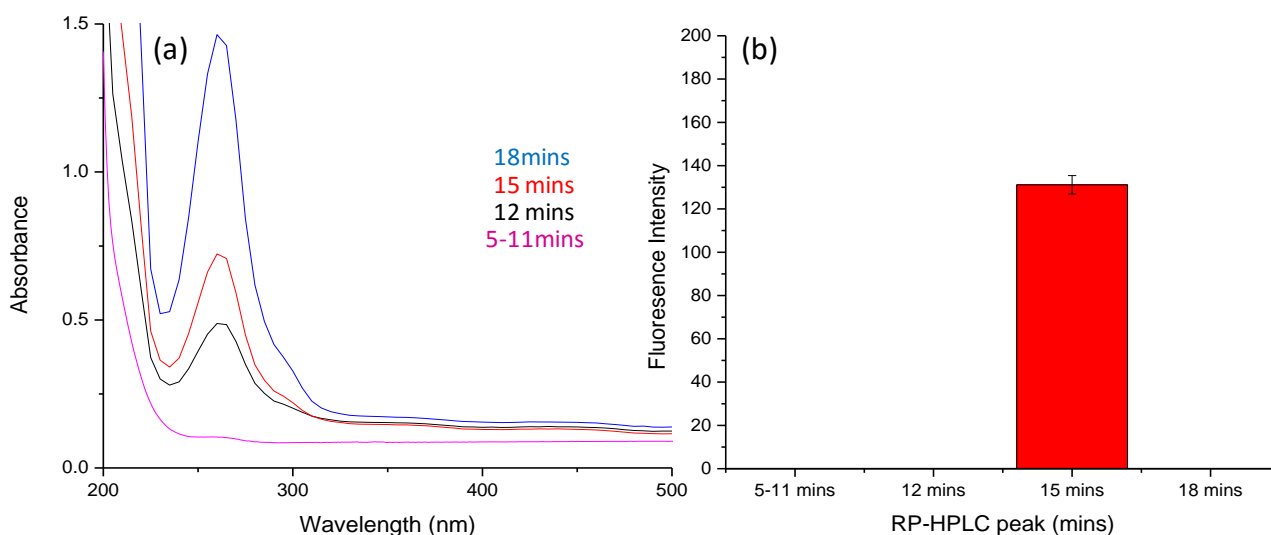
Figure 4.13: (a) UV-vis spectrum of the FITC (50 μl, 200μM) conjugated antibody product fractions collected from RP-HPLC between 5-11 mins (pink), 12 mins (black), 15 mins (red) and 18 mins (blue) **(b)** Fluorescence spectroscopy of the samples excited at 495 nm for 20s and fluorescence emission observed at 525 nm. Error bars arise from the standard deviation of 3 replicate samples.

Figure 4.13 (a) represents the UV-vis analysis of FITC (50 µl, 200 µM) conjugated to antibody (2 mg/ml) after RP-HPLC collection. It was observed that at 12, 15 and 18 mins there was antibody present in the products which is in agreement with the previous RP-HPLC data, 18 mins was thought to represent the thiourea bound FITC antibody and the 15 mins was thought to be from the amide bound FITC antibody. There was no absorption peaks observed between 5-11 mins, suggesting that no antibody products were present. Furthermore, Figure 4.13 (b) demonstrates analysis of the products by fluorescence spectroscopy. Interestingly, only fluorescence emission was observed at 15 mins, thought to be the amide product suggesting successful FITC conjugation to the antibody, however whilst the chromatogram suggests successful conjugation further analysis is required to differentiate between the thiourea and the amide bound FITC antibodies. No fluorescence was observed between 5-11 mins indicating successful isolation and purification of the FITC modified antibody. Interesting it was found that by increasing the concentration of FITC (100 µl, 200 µM) conjugated to the antibody, which was also analysed by UV-vis and fluoresence spectroscopy, as shown in Figure 4.14, resulted in a simular trend: antibody was present in the 12, 15 and 18 mins fractions, with the 15 min fraction fluorescing. Interestingly, it was observed at 5-11 mins there was fluorescence products present as for the 30 µl, 200 µM sample, suggesting the purification of the antibody was not ideal, as some free FITC was not filtered, resulting in fluorescence emission.
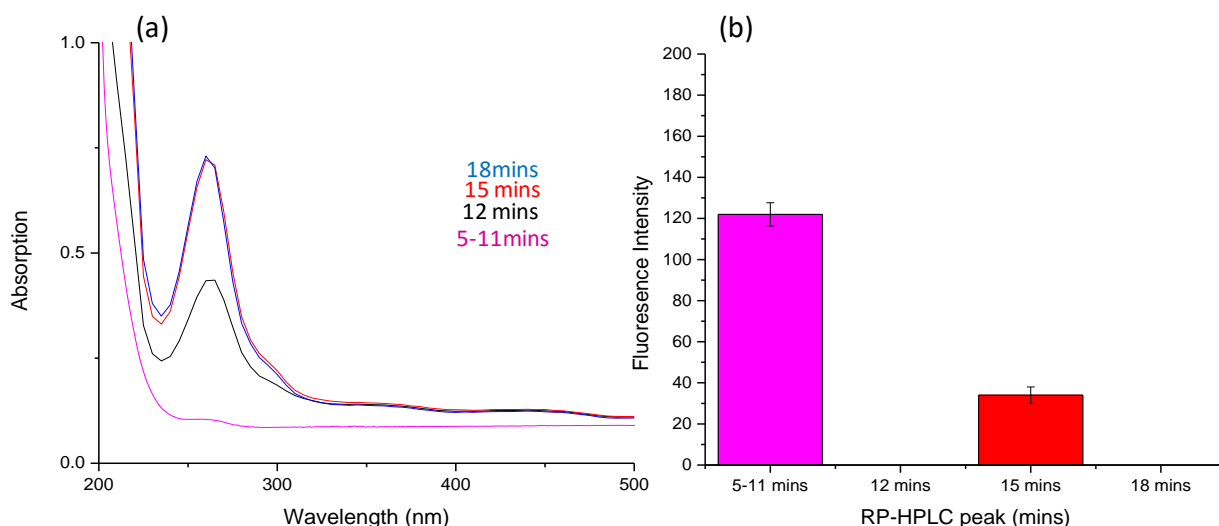
Figure 4.14: (a) UV-vis spectrum of the FITC (100 μl, 200μM) conjugated antibody product collected from RP-HPLC at 5-11 mins (pink), 12 mins (black), 15 mins (red) and 18 mins (blue) **(b)** Fluorescence spectroscopy of the samples excited at 495 nm for 20 s and fluorescence emission observed at 525 nm. Error bars arise from the standard deviation of 3 replicate samples.

It was observed that two different products from the FITC conjugated antibody were obtained and RP-HPLC was able to isolate the products. However, no definitive confirmation of the products or the amount of FITC conjugated to each antibody was obtained. Therefore, another method was required such as mass spectrometry to be able to differentiate between the thiourea and the amide product definitively. Unfortunately, due to the size of the antibody (>150 kDa) we do not have the facilities to perform mass spectroscopy, therefore a more direct approach was taken and the mixture of products, amide and thiourea FITC conjugated PETN antibody, from the cartridge centrifugation step were added to silver nanoparticles to use SERS to determine if the FITC modified PETN antibody would orientate 'flat' on the nanoparticles surface.

4.2.8   PETN Assay

The assay developed for TNT and RDX in chapter 2 utilised a modified antibody on the surface of silver nanoparticles. The modification on the antibody allowed for the antibody to bind 'flat' on the surface of the nanoparticle, hence detection of the target analyte was obtained by SERS. However, the antibody with this modification was only available for the explosives TNT and RDX, therefore to extend the assay to

the detection of PETN, PETN was modified in-house using the approach described in the preceding sections. It was observed that two products were obtained; the thiourea bound FITC and the amide bound FITC antibody. Therefore, by adding these to silver nanoparticles the amide bound FITC product will preferentially bind to the silver nanoparticle over the thiourea due to the strong metal-thiol bond.

Silver nanoparticles were functionalised with the in-house modified antibody for the specific detection of PETN. It was hoped that the antibody was modified with FITC in the same way as the TNT antibody, resulting in a 'flat' orientation of the antibody on the nanoparticle, subsequently allowing for the detection of PETN by SERS. The modified antibody (10 µl) was conjugated to silver nanoparticles (0.36 nM, 500 µl). The sample was then centrifuged (6000 rpm, 20 mins) to remove unbound FITC labelled antibody from solution. The samples were then analysed by SERS (Figure 4.15) to observe if the FITC modification on the antibody was present and could be detected by SERS, as for the TNT and RDX assays in Figure 3.7 and 3.15.
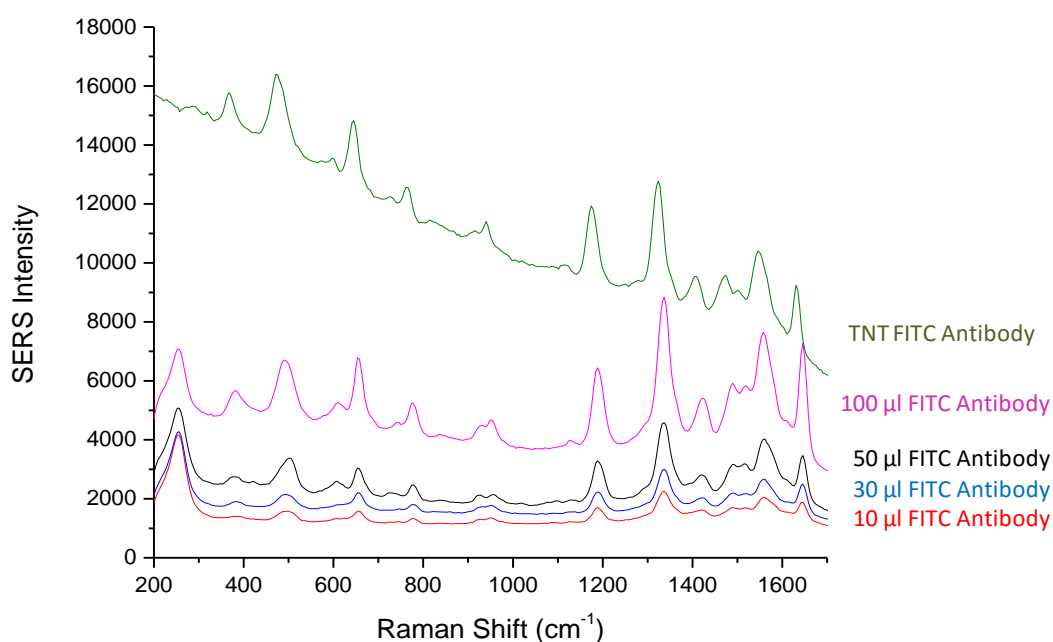
Figure 4.15: SERS spectrum of the commercial TNT FITC antibody (green), the in-house modified FITC PETN antibody with 10 (red), 30 (blue), 50 (black) and 100 (pink) µl of FITC (200 µM) conjugated to PETN antibody (2 mg/ml, 10 µl) functionalised silver nanoparticles (0.36 nM, 500 µl). SERS spectra was obtained using 532 nm laser excitation and a 0.5 s accumulation time. Spectra shown are the average of 5 measurements of 3 replicate samples.

Figure 4.15, green spectrum, demonstrates the SERS spectrum of the commercially available TNT FITC modified antibody (10 µl, 2 mg/ml), in which FITC only peaks were observed. This was due to the FITC modification on the antibody being in close proximity to the metallic surface and hence, a SERS spectrum was observed. FITC peaks were observed at 1182, 1408, 1485, 1545 and 1630 cm^{-1}, the peak assignments were previously given in Table 3.1. In Figure 4.14, red spectrum shows the SERS spectrum of the in-house FITC (10 µl, 200 µM) modification on PETN antibody (2 mg/ml, 10 µl) functionalised silver nanoparticles (0.36 nM, 500 µl). It was observed that there FITC peaks present at 1187, 1421, 1557 and 1648 cm^{-1}, in which there is a slight shift of approx 12 cm^{-1} of the FITC peaks in comparison to the TNT sample. This could be due to a different isomer of FITC being used for the conjugation as there are five possible isomer confirmations of FITC.[183] Upon increasing the concentration of FITC conjugated to the PETN antibody in the presence of silver nanoparticles, the same SERS spectrum was obtained (blue, black and pink spectrum). However the signal was more intense to more FITC molecules being bound to the antibody and hence silver nanoparticle surface. Furthermore, the peak present at 477 cm^{-1} in the TNT spectrum, 491 cm^{-1} in the PETN spectra, is due to S-metal vibrations, indicating that ITC group of the FITC is bound to the silver surface. Therefore, PETN was added to the PETN antibody functionalised nanoaprticles to observe if any PETN specific peaks could be observed.

In Section 2.2.2, a reference SERS spectrum of PETN was obtained which demonstrated three main peaks associated with RDX at 643, 756 and 981 cm^{-1}, due to NO_2 rocking and stretching. Therefore, the binding of PETN to the PETN antibody functionalised nanoparticles should result in Raman bands being present at 643, 756 and 981 cm^{-1} due to the antibody specifically binding to PETN and bringing it into close proximity to the nanoparticle surface. The modified antibody (10 µl) was conjugated to silver nanoparticles (0.36 nM, 500 µl). The sample was then centrifuged (6000 rpm, 20 mins) to remove antibody which was free in solution. PETN was then added to the assay and the samples were then analysed by SERS (Figure 4.16).
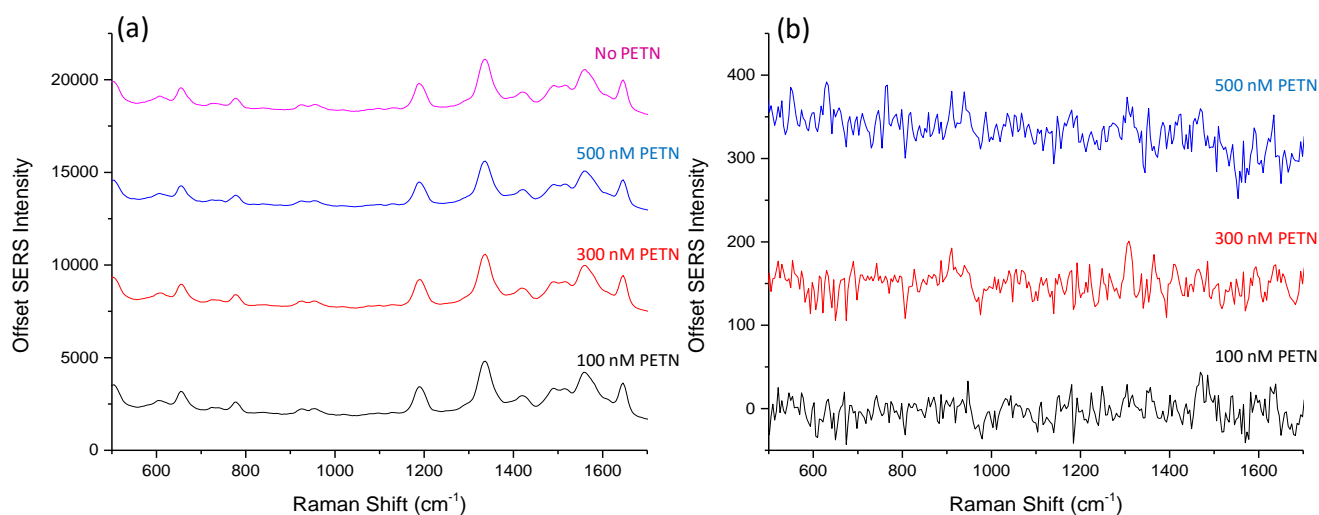
Figure 4.16: (a) SERS spectra of 0 (pink), 500 (blue), 300 (red) and 100 (black) nM of PETN conjugated to the FITC (10 μl, 200 μM) modified PETN specific antibody conjugated nanoparticles. SERS spectra were obtained using 532 nm laser excitation and a 0.5 s accumulation time, **(b)** SERS spectrum of 500 (blue), 300 (red) and 100 (black) nM of PETN in the assay with the FITC background subtracted. Spectra shown are the average of 5 measurements of 3 replicate samples, which have been baseline subtracted, scaled and offset for clarity.

In Figure 4.16, FITC peaks were observed in the SERS spectra at 1182 cm^{-1} due to the C-OH stretch,[151] 1408 cm^{-1} due to CH$_2$ stretching,[152] 1485 and 1545 cm^{-1} due to C-C ring formation and finally 1630 cm^{-1} due to C=N , these are due to the FITC modification on the antibody. However, upon the addition of PETN, (blue, red and black spectrum) no Raman specific peaks of PETN were obtained. Furthermore, Figure 4.16 (b) demonstrates the subtraction of the FITC background from the spectrum and no PETN peaks were observed. This suggests that there was FITC conjugated to the nanoparticle, however there may not be any antibody, therefore no specific detection of TNT was obtained. Another possibility is that the location of the FITC modification on the antibody does not orientate the antibody flat on the nanoparticles surface, thus PETN is not in close proximity to the silver surface and a SERS spectrum of PETN will not be obtained. A final possibility could be due to the fact that PETN is a poor Raman scatterer, due to having a low Raman cross-section, therefore a weak or no SERS spectrum of PETN would be obtained. Therefore increasing the number of FITC molecules (30 μl, 200 μM) conjugated on to the PETN antibody (2 mg/ml, 10 μl) functionalised silver nanoparticles (0.36 nM, 500 μl), in hope that more FITC molecules would allow for the antibody to lie in a flat

orientation on the nanoparticles surface, allowing for the PETN to come in close proximity to the nanoparticle and an intrinsic SERS spectrum of PETN to be obtained.

A higher concentration of FITC was conjugated on to the PETN antibody Increasing concentrations of PETN (0 - 500 nM) were added to the assay and analysed by SERS using 532 nm laser excitation for 0.5 s accumulation time, as shown in Figure 4.17.
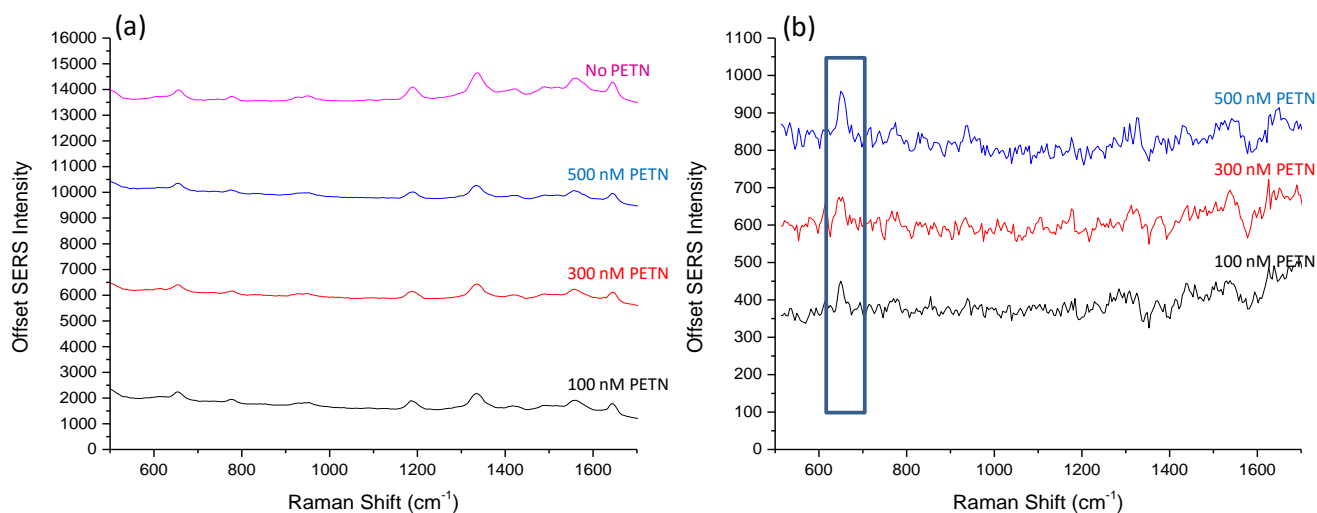
Figure 4.17: (a) SERS spectra of 0 (pink), 500 (blue), 300 (red) and 100 (black) nM of PETN conjugated to the FITC (30 μl, 200 μM) modified PETN specific antibody conjugated nanoparticles. SERS spectra were obtained by using 532 nm laser excitation and a 0.5 s accumulation time, **(b)** SERS spectrum of 500 (blue), 300 (red) and 100 (black) nM of PETN in the assay, FITC background subtracted. Spectra shown is the average of 5 measurements of 3 replicate samples, which have been baseline subtracted, scaled and offset for clarity.

Figure 4.17 (a) demonstrates the SERS spectra of a higher concentration of FITC conjugated to the PETN antibody. As expected, FITC peaks were observed in SERS spectra. However, upon the addition of PETN, (blue, red and black spectrum) no PETN specific peaks could be observed. Figure 4.17 (b) shows the SERS spectra of PETN assay, with the FITC background subtracted in order to see if any PETN bands can be observed. A peak at 643 cm^{-1} can be observed, which was increasing in intensity as the concentration of PETN increased. Although there is a FITC peak present at this position, after subtracting the FITC background, it was determined that if the FITC spectrum was still present, the most intense peak at 1316 cm^{-1}

should be observed. Furthermore, the fact this band increases with increasing PETN concentration, suggests a PETN peak. The band at 643 cm^{-1} was assigned to be from the NO$_2$ rocking of PETN. This suggests that FITC was orientating the antibody such that the target analyte could come in close proximity to the nanoparticle surface. However, PETN peaks at 756 and 981 cm^{-1} were not observed. This could be due to PETN binding to the antibody in different orientation compared to the direct adsorption of PETN on silver nanoparticles, in Figure 2.8. Therefore, different Raman bands will be enhanced due to the change in orientation. Another possibility is that the antibody is not 'flat' on the surface of the silver nanoparticles due to the lack of FITC molecules conjugated to the antibody, therefore increasing the FITC concentration conjugated to the antibody was explored.

An antibody with a higher concentration of FITC conjugated (50 μl, 200 μM) on to the PETN antibody (2 mg/ml, 10 μl) functionalised silver nanoparticles (0.36 nM, 500 μl) was explored for the detection of PETN (0 - 500 nM) by using 532 nm laser excitation for 0.5 s accumulation time, as shown in Figure 4.18.
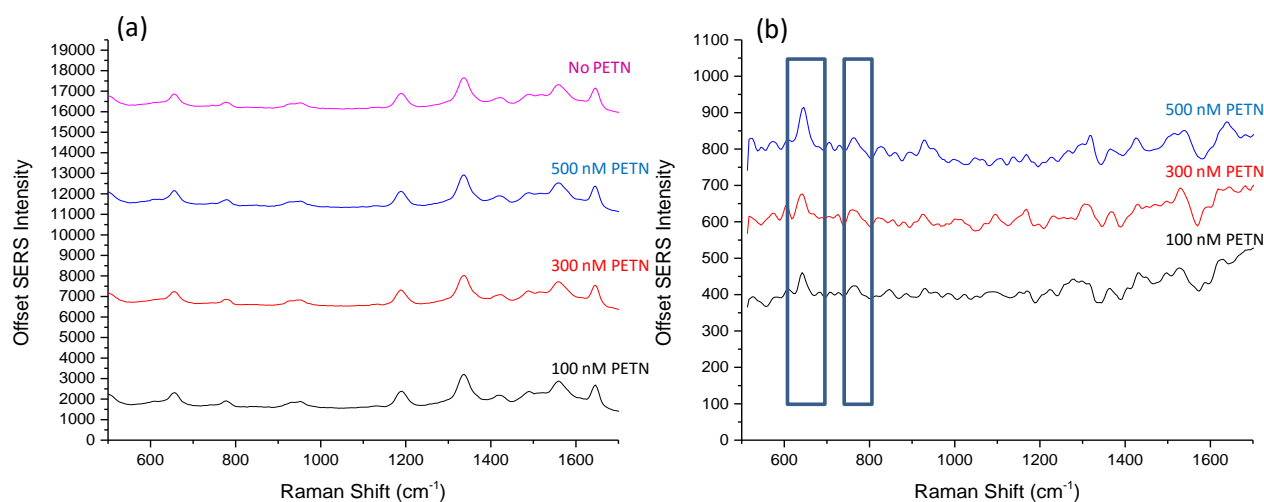
Figure 4.18: (a) SERS spectra of 0 (pink), 500 (blue), 300 (red) and 100 (black) nM of PETN conjugated to the FITC (50 μl, 200 μM) modified PETN specific antibody conjugated nanoparticles. SERS spectra were obtained by using 532 nm laser excitation and a 0.5 s accumulation time, **(b)** SERS spectrum of 500 (blue), 300 (red) and 100 (black) nM of PETN in the assay, FITC background subtracted. Spectra shown is the average of 5 measurements of 3 replicate samples, which have been baseline subtracted, scaled and offset for clarity.

In Figure 4.18 (a) the SERS spectra of PETN added to silver nanoparticles functionalised with FITC (50 µl, 200 µM) was obtained. As before, FITC peaks were observed in SERS spectra. Upon the addition of PETN, (blue, red and black spectrum) no PETN specific peaks could be observed in the background of FITC. However upon subtraction of the FITC background, peaks were observed at 643 cm^{-1} and 756 cm^{-1} and intensity increased as the concentration of PETN was increased. The bands at 643 and 756 cm^{-1} were assigned to be from the NO_2 rocking and stretching of PETN. This suggests that using this higher concentration of FITC conjugated to the antibody was orientating the antibody similarly to the commercial antibody, such that the target analyte could come in close proximity to the nanoparticle surface. The concentration of FITC bound to the antibody was again increased to observe if the antibody binding to the silver nanoparticles was more efficient.

A final concentration of FITC (100 µl, 200 µM) was conjugated on to the PETN antibody (2 mg/ml, 10 µl) functionalised silver nanoparticles (0.36 nM, 500 µl). Increasing concentrations of PETN (0 - 500 nM) was added to the assay and analysed by SERS using 532 nm laser excitation for 0.5 s accumulation time, as shown in Figure 4.19.
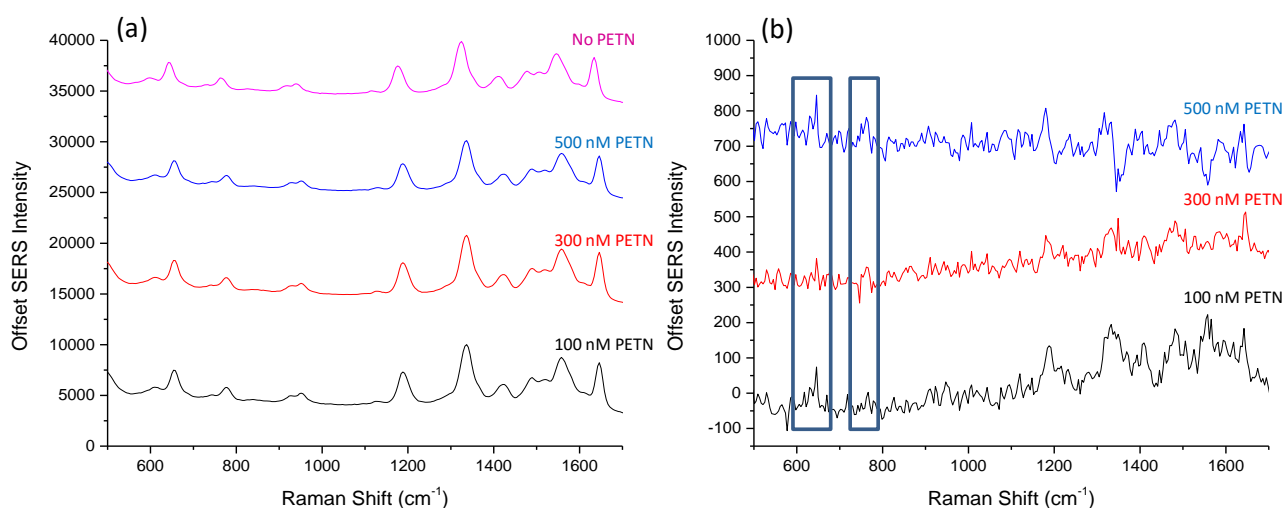
Figure 4.19: (a) SERS spectra of 0 (pink), 500 (blue), 300 (red) and 100 (black) nM of PETN conjugated to the FITC (100 µl, 200 µM) modified PETN specific antibody conjugated nanoparticles. SERS spectra were obtained by using 532 nm laser excitation and a 0.5 s accumulation time, **(b)** SERS spectrum of 500 (blue), 300 (red) and 100 (black) nM of PETN in the assay, FITC background subtracted. Spectra shown is the average of 5 measurements of 3 replicate samples, which have been baseline subtracted, scaled and offset for clarity.

In Figure 4.19 (a) the SERS spectra of FITC (100 µl, 200 µM) conjugated to the PETN antibody was obtained. As before, FITC peaks were observed in SERS spectra and upon the addition of PETN (blue, red and black spectrum) no PETN specific peaks could be observed. Figure 4.18 (b) is the SERS spectra of PETN assay, however the FITC background has been subtracted. Interestingly, the peaks that were previously present at 643 cm^{-1} and 756 cm^{-1} have diminished. This suggests that FITC is in excess of the PETN antibody during the conjugation and has bound to the antigen binding site on the antibody, therefore PETN could not bind to the antibody and PETN could not be detected by SERS.

From the protein quantification assay, it was determined that between 30-50 µl of FITC (200 µM) conjugated to the antibody was most similar to the commercial dioxane FITC modified antibody. The SERS spectra shown in this chapter, is in agreement with this, it was found that the FITC (50 µl, 200 µM) conjugated to the antibody was the optimum for detection of PETN, and therefore was used for the rest of these studies. However, in order to observe the PETN spectra the background FITC spectrum needed to be subtracted. PCA was performed to determine if any

141

variations in the spectrum, without subtracting the FITC background, the results are shown in Figure 4.20.
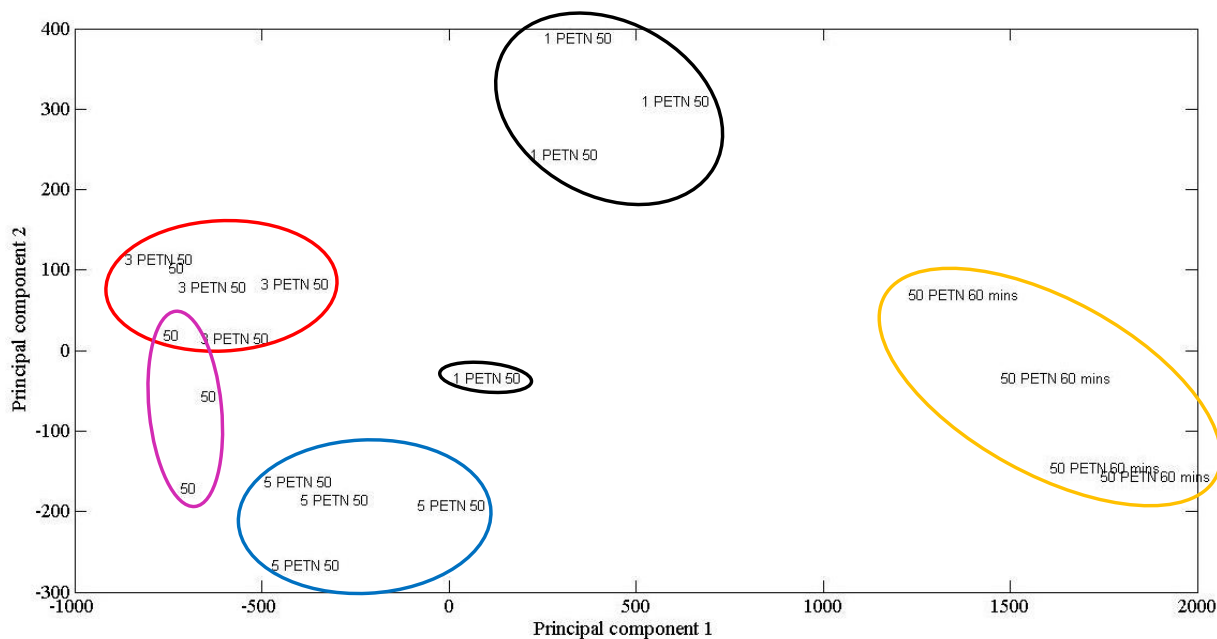
Figure 4.20: PCA plot of control '50' representing 50 µl of 200 µM of FITC conjugated PETN antibody with no target (pink), '1 PETN 50' representing 100 nM of PETN bound to 50 µl of 200 µM FITC conjugated PETN antibody (black), '3 PETN 50' represents 300 nM of PETN bound to 50 µl of 200 µM FITC conjugated PETN antibody (red), '5 PETN 50' represents 500 nM of PETN bound to 50 µl of 200 µM FITC conjugated PETN antibody (blue) and '50 PETN 60 mins' represents 500 nM PETN bound to 50 µl of 200 µM FITC conjugated PETN antibody for 60 mins (yellow). The labels shown in the plot is the average of 3 accumulations for each of the 4 replicate samples.

In Figure 4.20, PCA analysis was performed on the data set shown in Figure 4.18 (a), in which principal component 1 was plotted against principal component 2. The PCA scores plot shows that each different concentration of PETN was grouped separately from the control, showing clear discrimination between no target (pink), 100 nM of PETN (black), 300 nM of PETN (red) and 500 nM of PETN detection (blue). The yellow label demonstrates the detection of 500 nM PETN and analysis after 60 mins incubation. The loading plots showed the spectral variations responsible for the separation of the target analytes, which were due to the presence of the band at 643 cm^{-1}. In conclusion PCA is capable of discriminating between controls and increasing concentrations of the PETN target analyte in the assay.

The 50 μl of 200 μM FITC in-house modified PETN antibody appears to be orientating on the surface of silver nanoparticles in a similar manner to the commercial FITC modified antibodies. Therefore, it was of interest to carry out a multiplex using the commercial TNT, RDX and the in-house modified PETN antibodies for the detection of multiple targets.

4.2.9   Multiplex Assay

The aim of this project was to design an assay which can detect several explosive materials in a mixture simultaneously by SERS. In section 3.3.3, an assay was designed for the specific detection of TNT by utilising a modified antibody. This assay was shown to also be adaptable for the successful detection RDX (chapter 3.7). Furthermore, a multiplex assay of these two targets was able to detect down to 1 nM of each target as shown in section 3.9. Therefore, it was of interest if a triplex could be used to successfully detect TNT, RDX and PETN in 'one pot'.

Each explosive specific antibody nanoparticle conjugate was synthesised separately. TNT specific antibody conjugates, RDX specific antibody conjugates and PETN antibody conjugates were added together. Each target was then introduced into the multiplex solution individually, and then all three targets were added at once. The SERS spectra were obtained by using 532 nm laser excitation with a 0.5 s accumulation time, Figure 4.21. As before, RDX was detected through the presence of the peaks at 1271 and 1500 cm^{-1}. TNT was also detected by positive identification of the peaks present at 1066 cm^{-1} and 1558 cm^{-1}, PETN was identified by the peaks present at 643, 756 and 981 cm^{-1}.
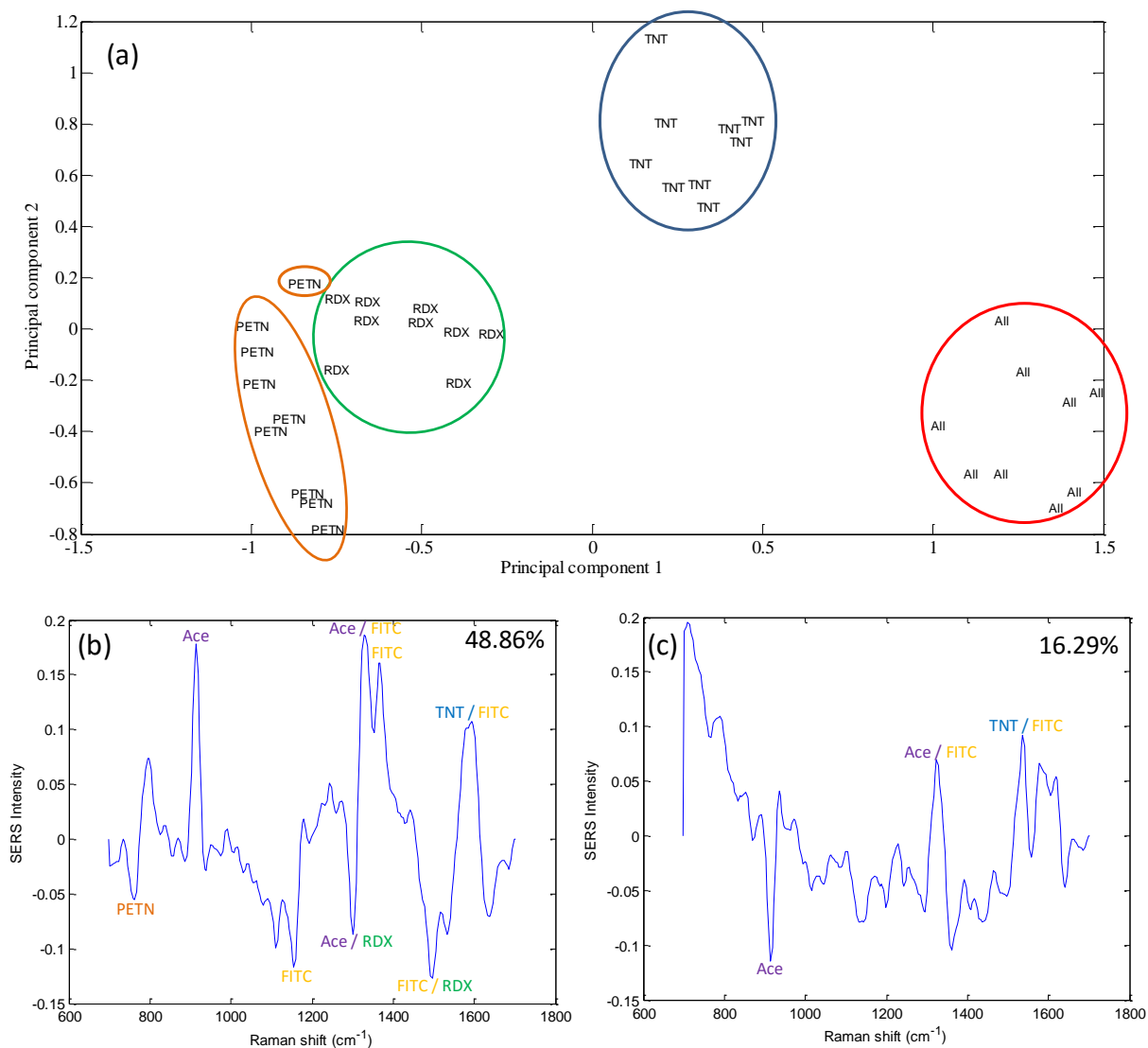
Figure 4.21: (a) PCA plot of PETN capture (150 nM, yellow), RDX capture (50 nM, green), TNT capture (blue) and all three target analytes captured. The labels shown in the plot is average of 3 measurements for each of the 3 replicate samples.

In Figure 4.21 (a), PCA analysis was performed on the multiplex data set in which principal component 1 was plotted against principal component 2. The PCA scores plot shows that each target sample was grouped separately, emphasising the clear discrimination between PETN capture (150 nM, yellow), RDX capture (50 nM, green), TNT capture (50 nM, blue) and all targets present (red). Figure 4.21 (b) represents the loading plots, which show the spectral variations responsible for the separation across principal component 1, which were due to the presence of the TNT band at 1596 cm^{-1}, the PETN band at 756 cm^{-1} and the RDX bands at 1270 and 1500 cm^{-1}. Furthermore, the sample where all three explosive targets were separated

mainly due to the FITC peaks. In conclusion PCA is capable of discriminating between the three different targets in a matrix.

4.3 Conclusions

This chapter contains preliminary results on the development of a method for the conjugation of FITC onto antibodies with a free ITC group to allow functionalisation to metal nanoparticles. This was achieved by using carbodiimide chemistry, however, more research and analysis of the products such as mass spectroscopy is required to determine the absolute yield of thiourea to amide product.

Detection of PETN using the in-house FITC modification on the PETN antibody was found to be successful for a concentration of 50 µl of 200 µM FITC conjugated to the antibody. PETN was detected at concentrations as low as 100 nM, compared to the direct absorption of PETN onto the silver nanoparticle, shown in section 2.2.2 which only achieved an observed limit of detection of 3.6 µM of PETN. Furthermore, with the use of multivariate analysis, we can also detect and distinguish all three explosive targets, TNT, RDX and PETN from within a complex matrix i.e. when three antibody conjugated nanoparticle solutions are present.

5.Magnetic Immunoassay for the Detection of 2, 4, 6-Trinitrotoluene

In section 3.11, the detection of TNT in the presence of a 'dirty' matrix was explored. Different solvents were investigated to determine which solvent would result in the least amount of the 'dirt' components being dissolved. However, it was found that detection of TNT was not successful above 5% (v/v) in synthetic dirt. Therefore an assay was developed using magnetic nanoparticles and an external magnetic field that would allow removal of the target from the 'dirty' matrix as well as concentrating the sample onto a magnetic plug, resulting in an increase in SERS.

5.1 Introduction

Magnetic nanoparticles have gained considerable interest in recent years due to their applicability in a wide range of fields including magnetic resonance imaging,[184] labelling and manipulating biomolecules,[185] data storage,[186] site-specific drug delivery,[187] hyperthermia therapy and environmental remediation.[188] Success of these applications relies on the properties of magnetic nanoparticles which include high field irreversibility, superparamagnetism and ease of surface functionalisation.[189-191] The particles are optimum when below a critical size; this is dependent on the material, but typically 10-20 nm.

At this finite size magnetic nanoparticles display single domain[192] or superparamagnetic boundaries.[193] Single domain is a region within a magnetic material in which the magnetisation is in a uniform direction. Whereas, superparamagnetism is a form of magnetism which can change direction randomly under the influence of temperature. Magnetic ordering can be classified as ordered and disordered. Ferro-, ferri- and antiferromagnetism are examples of ordered magnetism. In ferromagnetism the spins are aligned parallel to each other, examples of ferromagnetic materials are iron, nickel and cobalt.[194] Ferrimagnetism involves the spins being anti-parallel to each other, examples of materials are usually oxides, such as manganese oxide.[195] In antiferromagnetism adjacent ions can behave as

small magnets which spontaneously align themselves.[196] At low temperatures, they align anti-parallel, however this spontaneous anti-parallel alignment is disrupted by heating and disappears above a certain temperature, known as the Nèel temperature, which is unique for each magnetic material.[197]

Disordered magnetism includes paramagnetic and diamagnetic.[198] Paramagnetic is characteristic of materials weakly attracted to a strong magnet, exhibited by most elements. Diamagnetism is when the materials align at right angles to a non-uniform magnetic field, examples are usually substances with symmetric electronic structure such as ionic crystals. However, magnetic nanoparticles usually exhibit superparamagnetism. Superparamagnetism is exhibited by compounds containing iron, palladium and rare earth elements. These compounds have incomplete inner electron shells, the unpaired electrons orbit the shell, making the atom a permanent magnet, which aligns and strengthens an applied magnetic field.

In terms of biofunctional magnetic nanoparticles, magnetite (Fe_3O_4) and maghemite (γ-Fe_2O_3) are most utilised compared to other magnetic nanoparticles due to their biocompatibility and chemical stability.[185] Magnetite and maghemite can be synthesised by co-precipitation,[199] thermal decomposition[200] and hydrothermal synthesis.[201]

The co-precipitation method is most simplistic and can form magnetite from aqueous Fe^{2+} and Fe^{3+} salt solutions by addition of a base.[191] The size, shape and composition of the magnetic nanoparticles depend on the salt used, the iron ions ratio, the reaction temperature and the pH of the solution. Magnetite nanoparticles are not very stable under ambient conditions as they are easily oxidised, therefore by adding an acidic medium, magnetite is oxidised to a more stable maghemite nanoparticle. A co-precipitation method was developed by Kumar et $al.$ using $FeCl_2.4H_2O$ and $FeCl_3.6H_2O$ in the presence of sodium hydroxide (NaOH).[199] Magnetite nanoparticles were then formed and oxidised by nitric acid (HNO_3) as shown:

$$Fe^{2+} + 2Fe^{3+} \xrightarrow{NaOH} Fe_3O_4 \xrightarrow{HNO_3} \gamma - Fe_2O_3$$
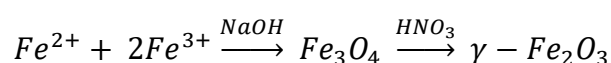
Iron is very sensitive to air, although many significant developments in the synthesis maintain the stability of the nanoparticles for long periods of time. The addition of a protective shell however, can offer even greater stability, such as metals and polymers.

Metals can be deposited on magnetic nanoparticles to protect the core against oxidation. Furthermore, the use of metal encapsulation provides a SERS active surface, which can be easily functionalised. Gold and silver coated magnetic nanoparticles can be prepared by using a glucose reduction method developed by Mandal *et al.*[199] A mild reducing agent was essential for the reduction of gold and silver salts in the presence of the magnetic nanoparticles to prevent surface poisoning. In this method, Au^{3+} or Ag^+ ions are adsorbed on the nanoparticles surface. The ions are reduced by glucose and encapsulate the magnetic nanoparticle. Upon collection of the gold/silver coated magnetic nanoparticles in a magnetic plug, the supernatant was clear, indicating that no non-magnetic metal nanoparticles were formed.

Maghemite nanoparticles (MNP) have been used in assays for DNA detection, for delivery of anticancer agents and for the detection of explosives.[185, 202, 203] In the assay developed here, magnetic nanoparticles were used to form a Meisenheimer complex with 2, 4, 6 – trinitrotoluene (TNT). A Meisenheimer complex is formed due to nucleophilic aromatic substitution. The aromatic π system is disrupted by the attack of a nucleophile on the aromatic ring. The negative charge on the carbanion is delocalised. It is distributed among the five remaining, formally sp^2 hybridised ring carbons. If the nucleophile is a poor leaving group and the nitro groups are in the ortho and para positions, the intermediate carbanion of the nucleophilic aromatic substitution is stable enough to be isolated.

Jiang *et al.* have utilised cysteamine functionalised gold nanoparticles for the detection of TNT.[204] Gold nanoparticles were synthesised using the citrate reduction method and were then functionalised with cysteamine. In the presence of TNT the

terminal amine group on the cysteamine functionalised nanoparticles forms a Meisenheimer complex with TNT, resulting in aggregation of the gold nanoparticles. Detection of TNT was then determined colourmetrically since upon aggregation of the gold nanoparticles, a colour change was observed from red to blue. Furthermore, the amount of aggregation was correlated to the concentration of TNT, therefore the detection assay was able to quantify the amount of TNT with pM sensitivity.

Qian *et al.* used poly (2 – aminothiophenol) functionalised SHINER (shell-isolated nanoparticle-enhanced Raman spectroscopy) nanoparticles.[205] SHINER nanoparticles are gold nanoparticles which are encapsulated with an ultrathin silica layer in which the Raman signal is amplified. The poly (2 – aminothiophenol) functionalised SHINER nanoparticles form a Meisenheimer complex with TNT resulting in aggregation of the SHINER nanoparticles and detection by SERS. The formation of the Meisenheimer complex produces a Raman band at 2955 cm^{-1} due to the NH_2^+ symmetric stretch however a high limit of detection of 10 μM was achieved.

Dasary *et al.* used cysteine functionalised gold nanoparticles which formed a Meisenheimer complex with TNT,[206] however, after the formation of the Meisenheimer complex, hydrogen bonding was thought to occur between the cysteine molecules resulting in further aggregation of the nanoparticles, as shown in Figure 5.1.
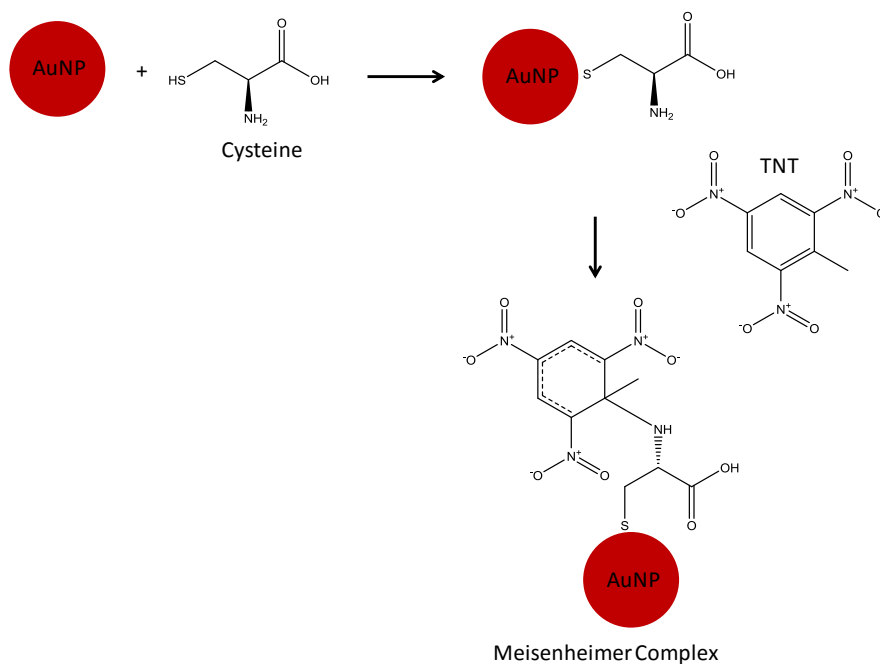
Figure 5.1: (a) Schematic representation of the formation of Meisenheimer complex between cysteine modified gold nanoparticle and TNT.[206]

Detection of the Meisenheimer complex was achieved by SERS with an NH_2^+ peak observed at 2900 cm^{-1} using a 670 nm laser excitation. The additional effect of the hydrogen bonding as a cross-linker enabled a limit of detection of 2 pM to be obtained.

Therefore the formation of a Meisenheimer complex, in the presence of TNT, using a nanoparticle assembly has shown promising results. However, here it is proposed that utilising the magnetic properties of silver coated magnetic nanoparticles would allow for the Meisenheimer complex to be pulled out of the surrounding matrix and concentrated on an external magnet, resulting in a lower limit of detection.

5.2 Aims

The aim of this chapter was to design a novel SERS immunoassay for the detection of explosives using a combination of silver coated magnetic nanoparticles conjugated to a molecule with a terminal amine group and a FITC modified antibody functionalised silver nanoparticles, as shown in Figure 5.2.
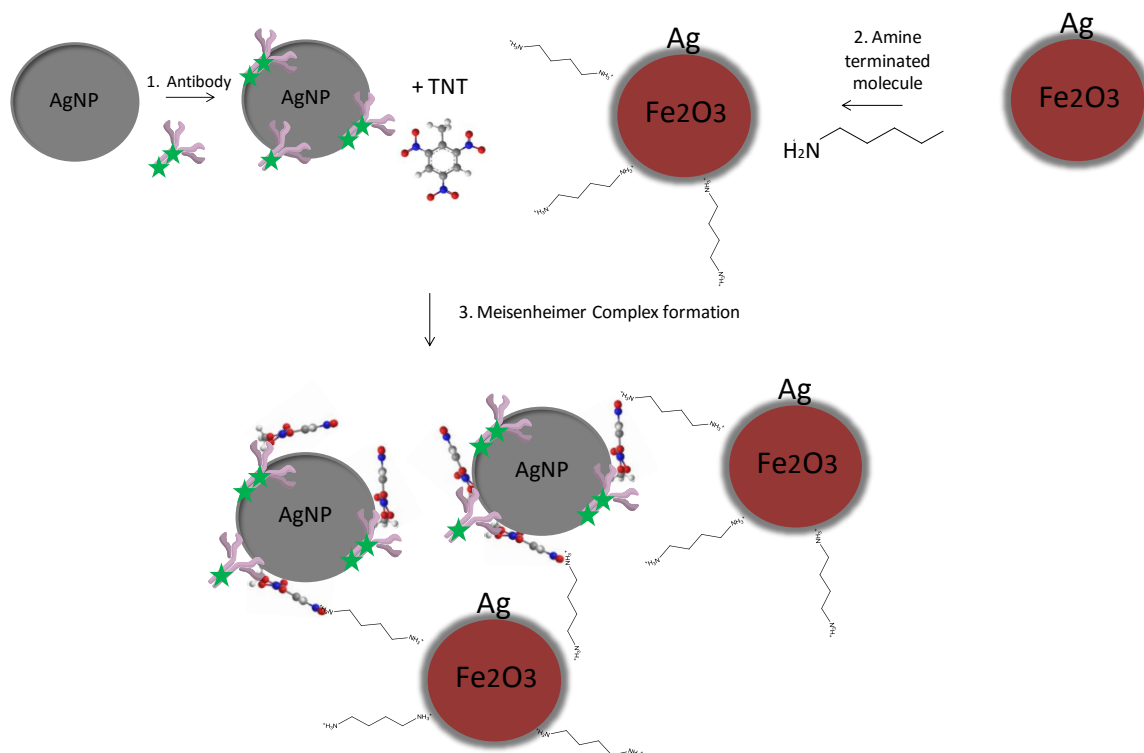
Figure 5.2: Schematic representation of the conjugation of FITC labelled antibodies to the surface of silver nanoparticles (1), silver coated iron oxide magnetic nanoparticles functionalised with a molecules with a terminal amine group (2). Upon the addition of TNT both nanoparticles will bind to TNT and a Meisenheimer complex is formed (3).

Figure 5.2 represents the schematic representation of the proposed assay. FITC modified antibodies were conjugated to silver nanoparticles, a process which was previously described in section 3.1. The second part of this assay utilised silver coated magnetic nanoparticles which were functionalised with a molecule containing a terminal amine group. An amine and a thiol terminated PEG (HS-PEG-NH$_2$) and hexamethylenediamine (HMD) were investigated for the functionalisation of the silver coated magnetic nanoparticles. In the presence of TNT, the antibody conjugated silver nanoparticle should bind to the TNT and the aminated silver

encapsulated magnetic nanoparticle should also bind to the TNT forming a Meisenheimer complex. After the formation of the Meisenheimer complex, a magnetic plug was used to pull the nanoparticle assembly out of the matrix, concentrating the sample, as shown in Figure 5.3.
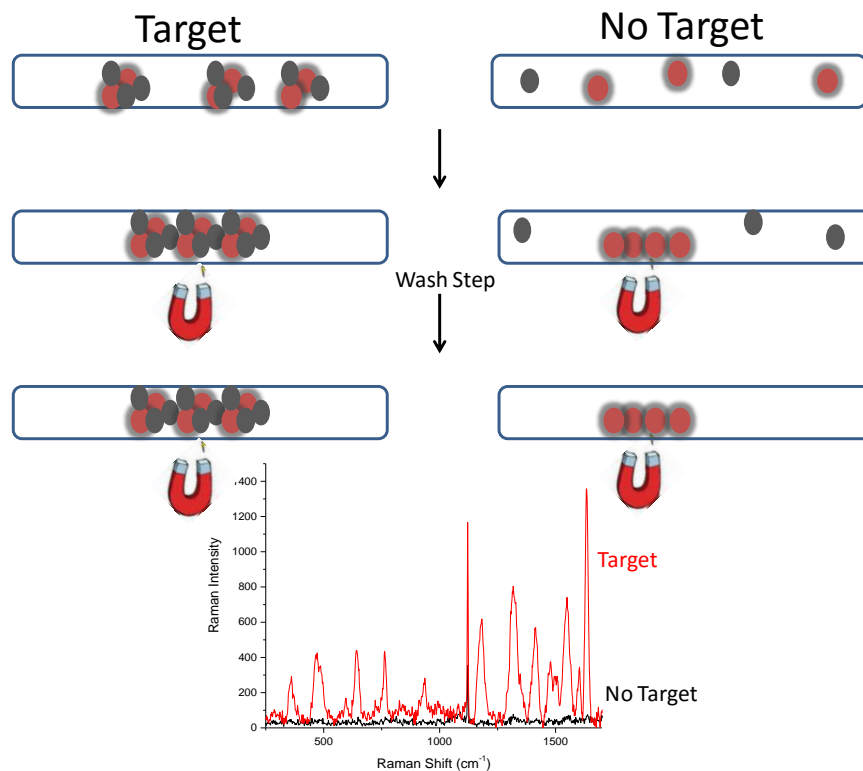
Figure 5.3: Schematic representation of the Meisenheimer complex formed in the presence of TNT and the nanoparticles free in solution, when TNT is absent. A magnet was used to pull down the nanoparticle assembly, concentrating the sample. After a wash step, if the target was present the full assembly will be present resulting in a SERS response. In the absence of TNT, the FITC modified antibody conjugated nanoparticles are washed away, therefore no SERS spectra was obtained.

Figure 5.3 represents the assay format using magnetic separation and SERS to monitor the formation of the Meisenheimer complex in the presence of TNT. After addition of TNT, a magnetic plug was used to remove the nanoparticle assembly from the surrounding matrix and concentrate it into a plug. A wash step was then used to remove any unbound FITC conjugated silver nanoparticles. Therefore in the presence of TNT, the nanoparticle assembly should not be removed by the wash step due to the antibody binding to the TNT and formation of the Meisenheimer complex and a SERS response should be observed. When TNT is absent, the SERS active

silver nanoparticles will remain free in solution. When the magnetic plug is present, the SERS active silver nanoparticles should be removed in the wash step, resulting in no SERS spectrum.

5.3 Results and Discussion

5.3.1 Meisenheimer Complex

The first part of the assay involved the conjugation of FITC modified antibodies to silver nanoparticles. This conjugation was optimised in section 3.1. It was found that 10 µl of FITC modified TNT antibody (2 mg/ml) added to silver nanoparticles (0.36 nM, 500 µl) was optimum for TNT detection. Prior to the optimisation of the silver coated magnetic nanoparticle with a terminal amine group, a molecule aminated at each end (HMD) was added to FITC antibody conjugated silver nanoparticles and TNT, as shown in the schematic (Figure 5.4), to ensure the Meisenheimer complex would form between TNT and the amine, cross-linking the nanoparticles resulting in aggregation and an enhancement in SERS.
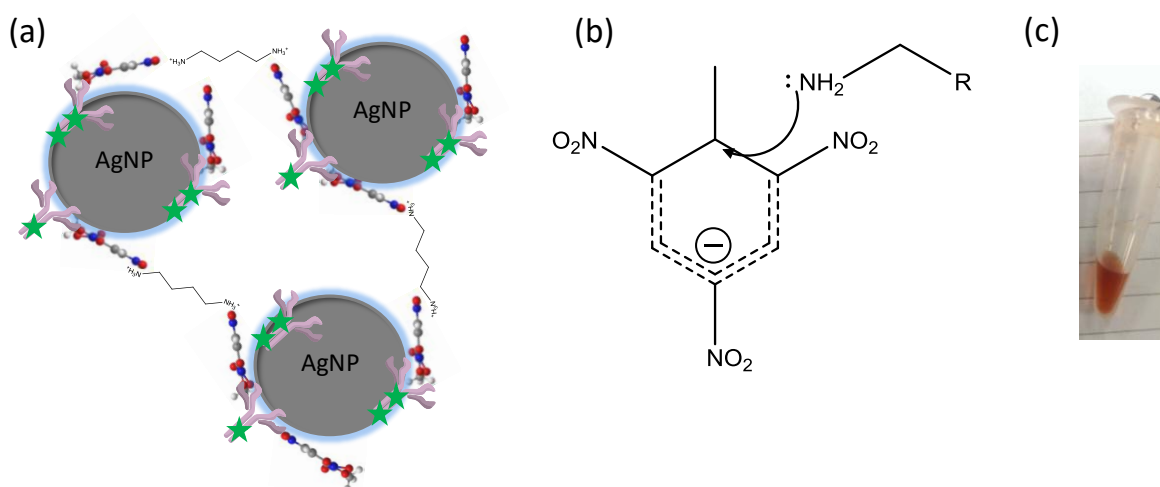
Figure 5.4: (a) Schematic representation of FITC modified antibody conjugated silver nanoparticles specific for the detection of TNT. Upon the addition of HMD, in the presence of TNT, a Meisenheimer complex is formed causing controlled aggregation of the silver nanoparticles, **(b)** Schematic representation of nucleophilic attack of TNT by an amine forming a Meisenheimer complex, **(c)** Image of Meisenheimer complex.

Figure 5.4 demonstrates the functionalisation of FITC modified TNT antibody onto silver nanoparticles. TNT is then bound to the antibodies, and in the presence of

HMD formation of the Meisenheimer complex is observed due to the lone pair from the terminated amine on HMD with TNT, in which the mechanism is shown in (b). Upon the formation of the Meisenheimer complex, cross-linking occurs between the nanoparticles causing aggregation. HMD was added to TNT to demonstrate the colour change observed upon the formation of the Meisenheimer complex from colourless to red/brown was observed as shown in Figure 5.4 (c).

Therefore, when the HMD (20 μM) was added to the assay in the presence of TNT (50 nM), it should bind to TNT to form the Meisenheimer complex. Analysis of the specific aggregation of the nanoparticles from the formation of the Meisenheimer complex was observed using UV-vis spectroscopy as shown in Figure 5.5.
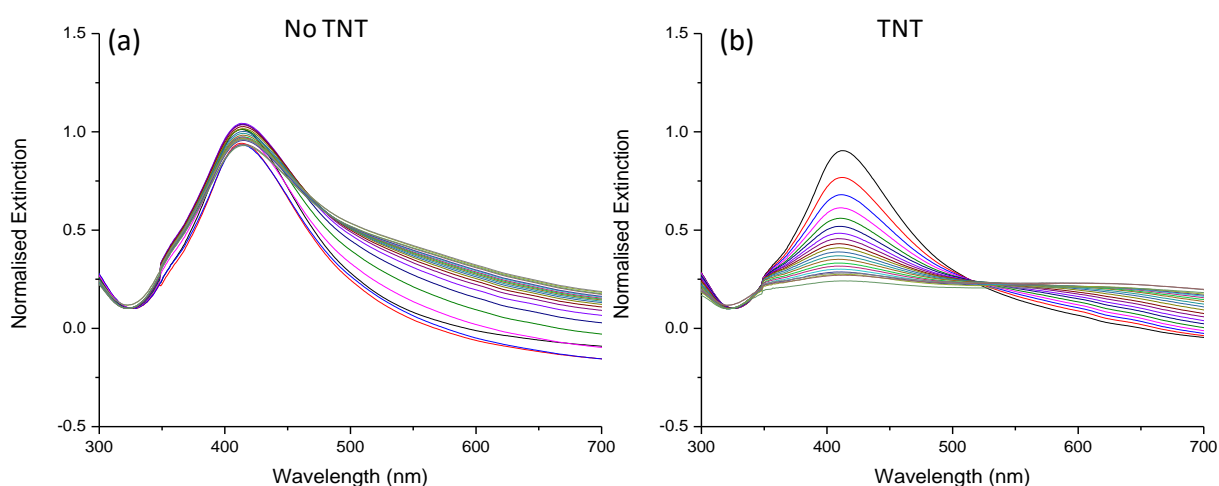
Figure 5.5: (a) Extinction spectrum of antibody conjugated silver nanoparticles in the presence of HMD (20 μM) every 40 mins over 14 hrs, **(b)** antibody conjugated silver nanoparticles in the presence of HMD every 40 mins over 14 hrs after addition of 50 nM of TNT.

Figure 5.5 (a) demonstrates the extinction spectrum of antibody conjugated silver nanoparticles with HMD in the absence of TNT over time, every 40 mins for 14 hrs. It was expected that no aggregation should occur since the Meisenheimer complex should not form, however, it can be seen in Figure 5.5 (a) aggregation was observed over time as the LSPR peak has broadened and dampened. This indicates that non-specific binding had occurred. This was thought to be due to electrostatic attraction from the positive amine on the HMD molecule and the negatively charged citrate silver nanoparticles. Therefore a non-specific binding agent or a small molecule

should be added to the silver nanoparticles after antibody conjugation to occupy any free binding sites available on the nanoparticles surface. However, in the presence of TNT, Figure 5.4 (b) rapid and extensive aggregation was observed, indicating the formation of the Meisenheimer complex, hence the nanoparticles were in close proximity to each other, which dampened the LSPR peak and ultimately resulted in the coupling of the nanoparticles plasmons and a new peak appearing at approximately 700 nm, therefore demonstrating that the Meisenheimer complex had formed. However, to overcome the non-specific binding observed in the absence of TNT absent extinction, protein A was investigated to bind the antibody to silver nanoparticle and to prevent non-specific binding, as protein A encapsulates the silver nanoparticle and hence prevent non-specific aggregation in the absence of TNT.

Protein A is a single polymer chain which is a cell wall component of the bacterium S*taphylococcus aureus*.[207] This bivalent protein binds to the Fc face of an antibody and has a very high affinity for colloidal suspensions of nanoparticles due to its aspartic acid content. The Fc orientation of antibody is optimum for detection as it orientates the antibody such that both paratopes are available to bind to the target. Encapsulating the nanoparticles with protein A should eliminate any non-specific binding that was observed in Figure 5.5, and allow for the antibody to bind to the protein A on the nanoparticles surface. The IgG binding domain of protein A consists of three anti-parallel α-helicies, the third of which is disrupted when the protein is complexed with an antibody. Therefore, optimisation of the concentration of protein A to be added to the nanoparticle surface was performed, to ensure monolayer coverage of the protein on the nanoparticles surface and subsequently determine the functionalised nanoparticles stability using salt addition. This method was previously described by Horisberger *et al.* and involved adding NaCl (0.17 M, 200 μl) to the nanoparticle suspension, which causes the nanoparticles to aggregate.[208] Increasing concentrations of protein A (8 – 300 μM) were added to the silver nanoparticles (500 μl, 0.36 nM), if protein A forms a complete monolayer on the surface of the nanoparticles, then the nanoparticles should remain stable upon the addition of salt (8.8 mM), therefore the addition of salt should not allow aggregation

to occur. Figure 5.6 demonstrates the extinction spectra of the nanoparticle suspension functionalised with protein A after the addition of NaCl.

Figure 5.6: (a) Extinction spectrum of bare silver nanoparticles (violet), silver nanoparticles and
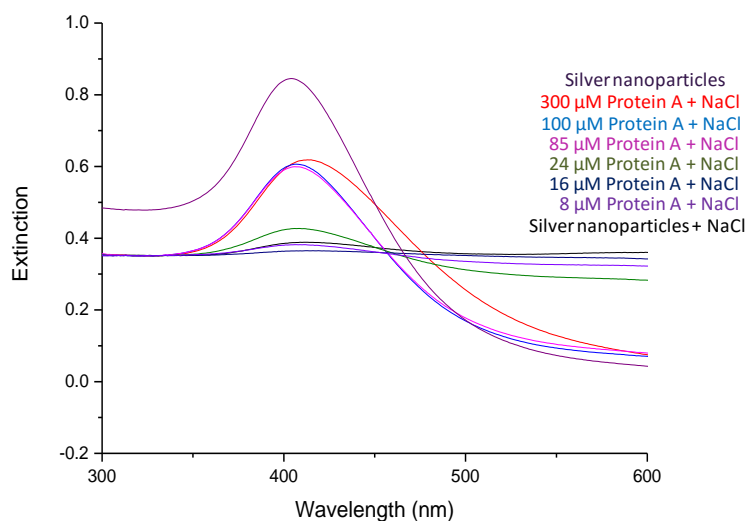
NaCl (8.8 mM, black), increasing concentrations of protein A: 8 µM (purple), 16 µM (navy), 24 µM (green), 85 µM (pink), 100 µM (blue) and 300 µM (red) functionalised silver nanoparticles.

Figure 5.6 illustrates that at higher concentrations of protein A conjugated on the surface of silver nanoparticles, the more stabilised the nanoparticles remained after the addition of salt. It was found that 100 µM of protein A (blue) was the optimum concentration to allow optimal monolayer of coverage of the nanoparticles surface, resulting in nanoparticles which were stable to the addition of salt. After addition of 8.8 mM of salt to silver nanoparticles functionalised with 100 µM of protein A (violet), a slight red shift of 3 nm from 411 to 414 nm was observed. However, after salt addition to the nanoparticles functionalised with 300 µM of protein A (red), a red shift of 8 nm was observed and the peak appears to have broadened, which can indicate aggregation due to higher protein concentrations. This could be a result of the protein forming more than one layer around the nanoparticle, consequently resulting in the nanoparticle suspension becoming unstable and forming precipitates. However, at 24 µM and concentrations below this, the salt also caused the nanoparticles to aggregate, as can be seen by the dampening and broadening of the LSPR peak, which suggests that protein A has not fully

encapsulated the entire surface of the nanoparticle. Therefore a concentration of 100 µM of protein A was used for the rest of this study.

The previously optimised FITC modified TNT antibody (10 µl, 2 mg / ml) was added to the protein A funtionalised silver nanoparticles (500 µl, 0.36 nM). HMD (20 µM) was then added to the assay, in which it was hoped that the protein A would prevent non-specific binding. However when TNT was present and HMD was added, the Meisenheimer complex should form, causing aggregation of the nanoparticles, as shown in Figure 5.7.
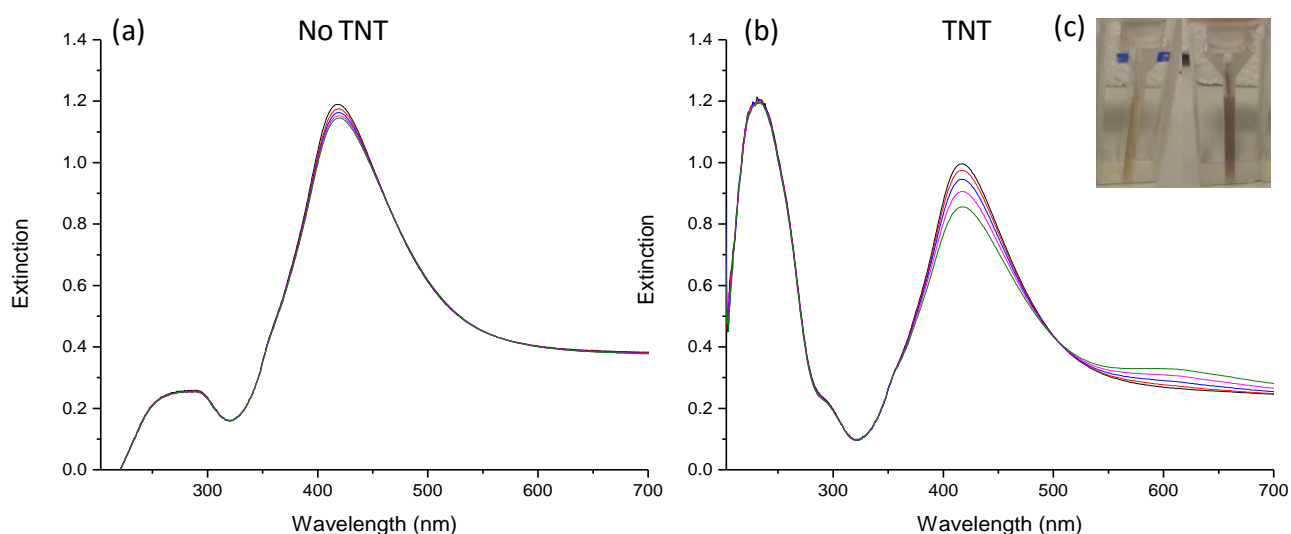
Figure 5.7: (a) Extinction spectrum of protein A and antibody conjugated silver nanoparticles with HMD in the absence of TNT, spectra were measured every 40 mins over 14 hrs, **(b)** antibody and protein A conjugated silver nanoparticles with HMD and 50 nM TNT added, over 14 hrs, **(c)** Image of the colour change of the nanoparticle solution upon the addition of TNT to the sample.

In the absence of TNT, the protein A and antibody conjugated silver nanoparticles in the presence of HMD should not form a Meisenheimer complex, and should be stable in solution, as demonstrated in Figure 5.7 (a). In the absence of TNT in the assay, no aggregation was observed. This suggests that the protein A was stabilising the nanoparticles in comparison to Figure 5.6. However, upon the addition of TNT (Figure 5.7 (b)) the LSPR peak broadened, dampened and a LSPR peak appeared at approximately 600 nm. This aggregation was due to the formation of the Meisenheimer complex, resulting in the nanoparticles controllably aggregating. The formation of the peak at 270 nm is likely to be due to the Meisenheimer complex.

It was investigated that protein A was a suitable ligand to encapsulate the silver nanoparticles surface, which ultimately prevented non-specifc binding between the aminated silver coated magnetic nanoparticles and the negatively charged silver nanoparticles. Furthermore, it was shown that upon addition of TNT to the amine terminated silver coated magnetic nanoparticles and the FITC modified TNT antibody functionalised silver nanoparticles, a Meisenheimer complex was formed, resulting in specific aggregation of the nanoparticles. Therefore, the assay was analysed by SERS, in the hope that the aggregation should result in an intense spectra in the presence of TNT.

5.3.2 SERS of Magnetic Immunoassay

The formation of the Meisenheimer complex in the magnetic immunoassay was successfully analysed by UV-vis, therefore the assay was analysed using SERS to determine if the controlled aggregation of the nanoparticles, due to the Meisenheimer complex, resulted in an enhancement in the SERS spectrum. Increasing concentrations of TNT (0 - 100 nM) were added to protein A and antibody functionalised silver nanoparticles, in the presence of HMD (20 μM), the samples were analysed by SERS using 532 nm laser excitation and a 3 s accumulation time, as shown in Figure 5.8. The data set shown has been baseline corrected using the polynomial least square method in Matlab. The data set was then offset by an arbitrary number for clarity. [153, 154]

A control sample of 2, 6 –dinitrotoluene (DNT) was explored to demonstrate the specificity of the assay, as DNT is chemically very similar to TNT. However, DNT should not form a Meisenheimer complex with the amines from HMD as the three electron-withdrawing nitro groups in TNT enables the ring to be electron-poor, so that TNT forms the red-colour Meisenheimer complex, whereas DNT does not.
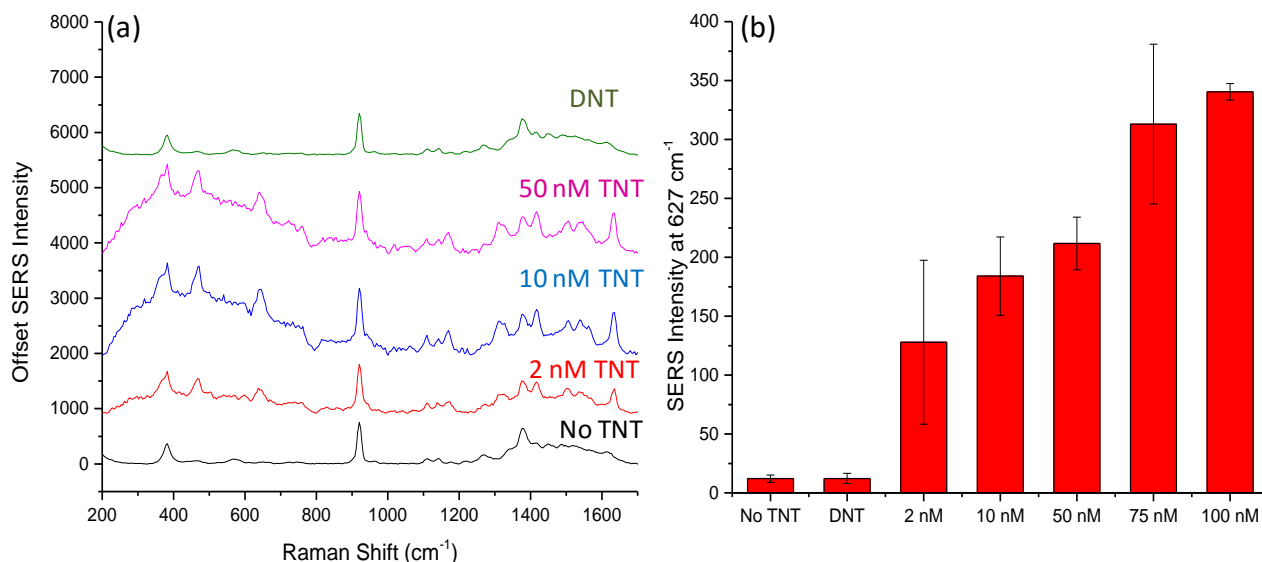
Figure 5.8: (a) SERS spectra of protein A and FITC antibody conjugated silver nanoparticles in the presence of HMD (20 μM), with no TNT present (black), 2 nM (red), 10 nM (blue), 50 nM (pink) of TNT present and a negative control of DNT (100 nM, green). Spectra were obtained using a 532 nm laser excitation for 3 s accumulation time, the spectra shown were the average of 5 measurements of 3 replicate samples, the data set was baseline corrected and offset for clarity. **(b)** Bar chart of SERS intensity at 627 cm^{-1} for DNT and 0, 2, 10, 50, 75 and 100 nM TNT in the assay in which the error arises from the standard deviation of the replicate samples.

Figure 5.8 (a) demonstrates the SERS spectra obtained from the specific interaction of TNT with the protein A and FITC antibody bound silver nanoparticle after addition of HMD, forming a Meisenheimer complex. In absence of TNT (black), low intensity peaks were observed from the FITC labelled antibody. The spectrum observed was from acetonitrile with peaks at 390 and 873 cm^{-1}, in which the TNT was dissolved, the spectrum of acetonitrile is shown in Figure 2.3. Similarly, the control DNT sample (green) also showed a low FITC signal, suggesting that no aggregation had occurred in these samples as the Meisenheimer complex was not formed, again the spectrum observed was from acetonitrile, which DNT was also dissolved. However, upon addition of 2 nM TNT (red) shows an increase in the SERS spectrum of FITC was observed, due to the controlled aggregation caused by the formation of the Meisenheimer complex. The enhanced peaks present were due to the FITC modification on the antibody. Furthermore, as the concentration of TNT is increased, the signal intensity also increased as seen in Figure 5.8 (b). An

observable limit of detection of 2 nM TNT was achieved for this indirect detection assay.

The addition of HMD to the FITC modified silver nanoparticles and the aminated silver coated magnetic nanoparticles demonstrated that non-specific binding occurred between the positive amine and the negative nanoparticles, therefore protein A was used to encapsulate the silver nanoparticle to avoid non-specific binding. The next step was to conjugate the HMD molecule to silver encapsulated magnetic nanoparticles electrostatically, and using an external magnetic force to concentrate the sample resulting in a lower observed limit of detection.

5.3.2 Magnetic Nanoparticles

The synthesis of magnetic γ-Fe_2O_3 nanoparticles (MNPs) involved using the co-precipitation method,[199] in which iron salts are added to a base to form Fe_3O_4. Fe_3O_4 was then further oxidised to form MNPs. MNPs are not SERS active and are prone to further oxidation, therefore metal encapsulation can provide a SERS active surface aswell as stabilising the magnetic nanoparticles. The MNPs were encapsulated with silver ions, which were reduced using glucose to form a silver shell around the MNPs (Ag@MNPs). The Ag@MNPs were analysed using UV-vis spectroscopy and DLS, as shown in Figure 5.9.
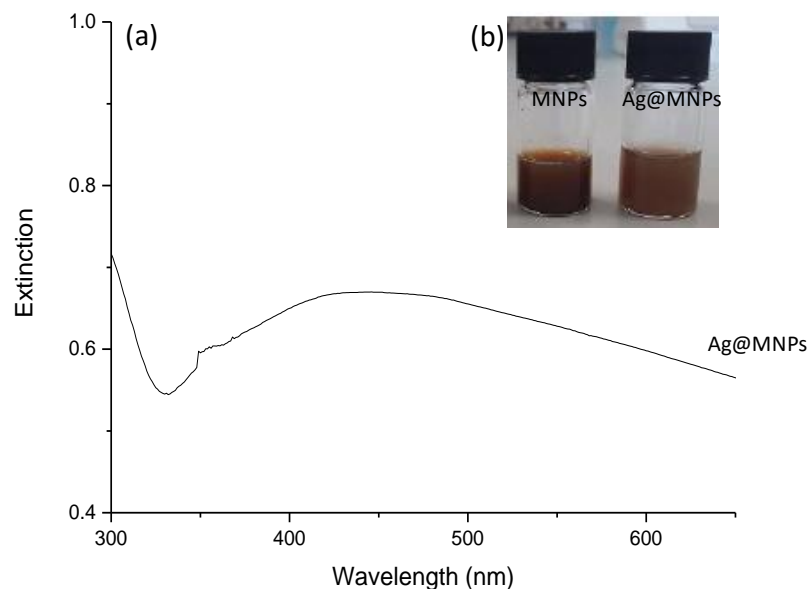
Figure 5.9: (a) Extinction spectrum of silver coated magnetic nanoparticles (Ag@MNPs), **(b)** Image of magnetic nanoparticles and silver coated magnetic nanoparticles.

Figure 5.9 (a) shows the extinction spectrum of Ag@MNPs with an LSPR at 443 nm, which is typical for Ag@MNPs.[185] The LSPR peak is broad in comparison to silver only nanoparticles (Figure 2.1), due to the size of the silver coating on the nanoparticle, as shown in Figure 5.3 (b). The size of the Ag@MNPs was determined to be 345 ± 13 nm in diameter by DLS. The nanoparticle diameter was much larger than expected, however, it is thought as the nanoparticles are so small (<20 nm) they appear in large clusters, in which the DLS measures the hydrodynamic radius of the clusters.[185] The Ag@MNP solution was then placed on a magnetic rack, the presence of a clear supernatant confirmed that the MNPs were fully encapsulated and no silver only nanoparticles were synthesised. The Ag@MNPs were then functionalised with increasing concentrations of HMD (0 – 40 μM) through the amine, leaving the other terminal amine group available to form a Meisenheimer complex with TNT. The HMD functionalised silver magnetic nanoparticles were analysed using UV-vis and DLS, as shown in Figure 5.10.
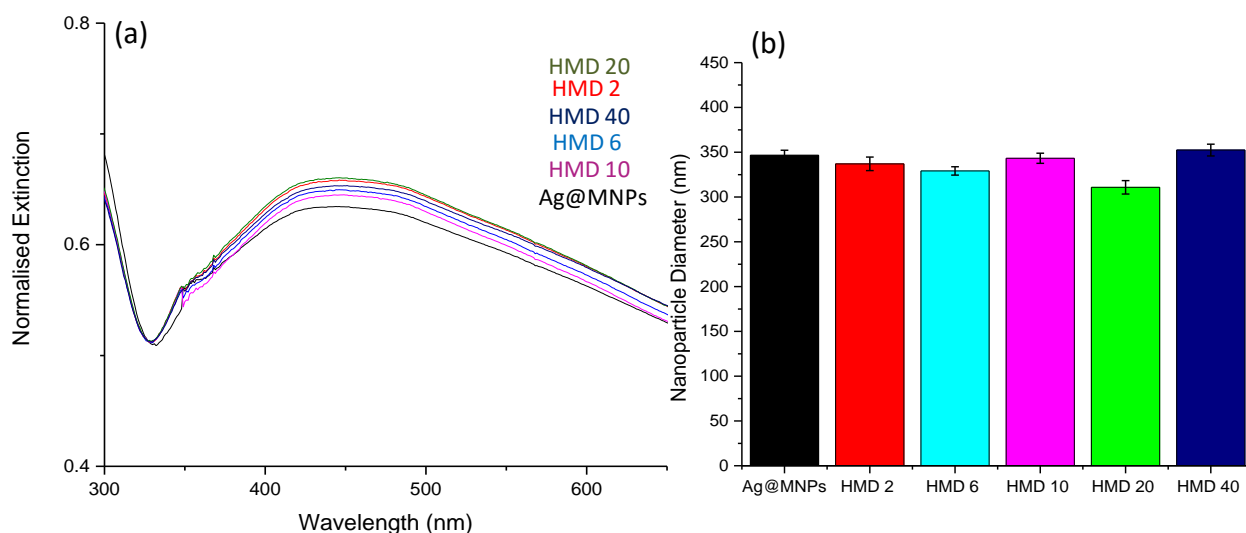
Figure 5.10: (a) Extinction spectrum of bare Ag@MNPs (black) and increasing concentrations of HMD, 2 (red), 6 (light blue), 10 (pink), 20 (green) and 40 (navy) μM conjugated to Ag@MNPs, **(b)** Nanoparticle diameter with increasing concentrations of HMD, 2 (red), 6 (light blue), 10 (pink), 20 (green) and 40 (navy) μM conjugated to Ag@MNPs analysed by DLS. Data shown is the average of three replicates samples in which the error is the standard deviation of the replicate samples.

Figure 5.10 (a) shows the extinction spectra obtained from increasing the concentration of HMD conjugated to Ag@MNPs. It was observed that upon the addition of HMD, the LSPR band broadened, indicating the dispersity of nanoparticle sizes was increasing. The optimum concentration of HMD was considered to be the highest concentration of HMD on the nanoparticle which would not aggregate the nanoparticles. It was observed that a concentration of 20 μM of HMD was optimum as the LSPR peak indicated the nanoparticles were stable in solution. At a higher concentration of HMD (40 μM) a dampening in the LSPR peak was observed, indicating slight aggregation. Furthermore, the hydrodynamic radius of the nanoparticles were measured. It was observed that upon addition of HMD no significant size changes were observed, therefore, a concentration of 20 μM of HMD was used for the rest of these studies, due to the UV-vis data.

5.3.3 Meisenheimer Complex Assay

The optimisation of both types of nanoparticles for the formation of a Meisenheimer complex sandwich immunoassay in the presence of TNT was carried out in sections 3.2 and 5.3.2. Therefore, TNT was added to the assay in an attempt to induce aggregation between the nanoparticles due to the formation of a Meisenheimer complex in the presence of TNT. The protein A and FITC labelled antibody functionalised silver nanoparticles were added in a 1:1 (v/v) ratio to HMD functionalised Ag@MNPs. TNT (50 nM) was then added to the assay and the UV-vis spectrum was obtained every 30 mins for 14 hrs, as shown in Figure 5.11.
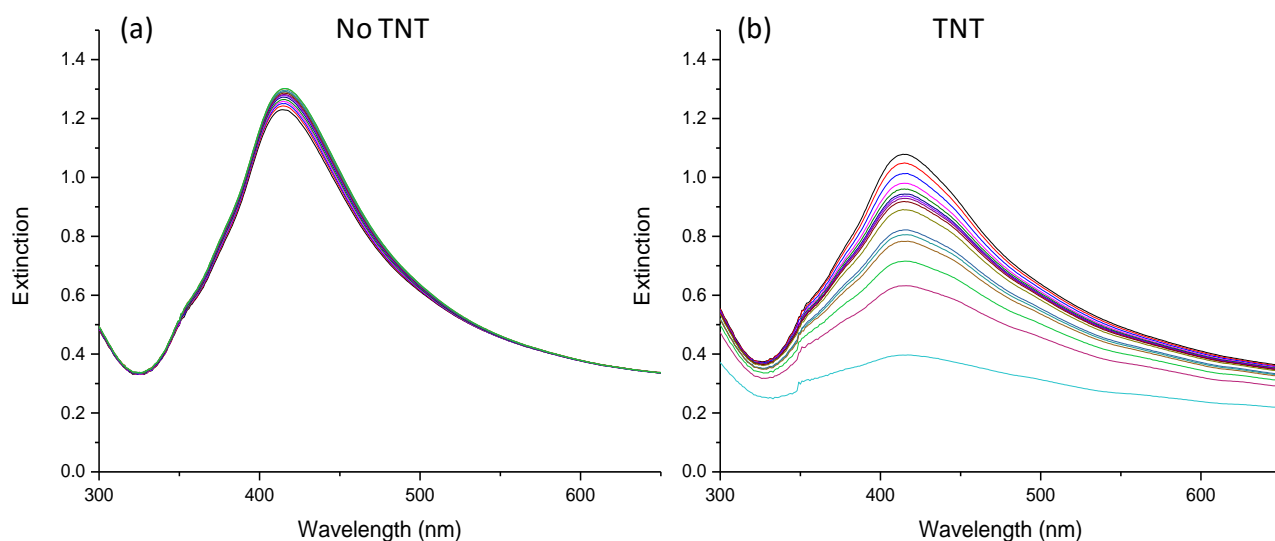
Figure 5.11: (a) Extinction spectrum of protein A and antibody conjugated silver nanoparticles with HMD functionalised Ag@MNPS in the absence of TNT over 14 hrs, **(b)** antibody and protein A conjugated silver nanoparticles with HMD functionalised Ag@MNPs after addition of 50 nM TNT, every 40 mins over 14 hrs. Spectra shown was the average of three replicate samples.

Figure 5.11 shows the extinction spectra obtained from protein A and FITC antibody conjugated silver nanoparticles in the presence of HMD functionalised Ag@MNPs, the assay in the absence of TNT should not form a Meisenheimer complex, and should be stable in solution. No aggregation was observed, indicating the assay was stable and little or no non-specific binding occurred. However, in Figure 5.11 (b) it was demonstrated that upon the addition of TNT, the LSPR peak broadened and dampened due to the formation of the Meisenheimer complex, resulting in the nanoparticles aggregating. Therefore, the assay was analysed using SERS to determine if the formation of the Meisenheimer complex resulted in an

enhancement in the SERS spectrum. The samples were magnetically separated by an external rare-earth magnet and any unbound nanoparticles were washed away, the concentrated magnetic collection was then analysed by SERS using 532 nm laser excitation and a 3 s accumulation time, the results are shown in Figure 5.12.
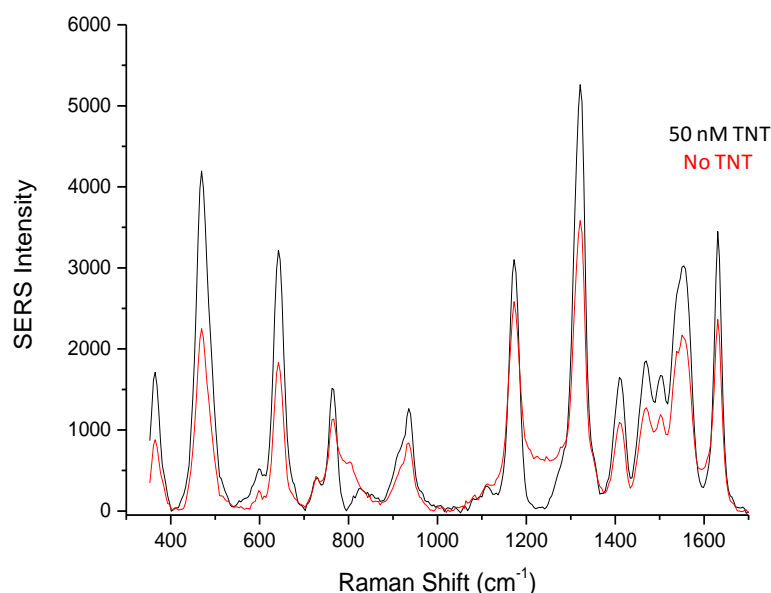
Figure 5.12: (a) SERS spectra of protein A and FITC labelled antibody conjugated silver nanoparticles in the presence of HMD functionalised Ag@MNPs, with no TNT present (black) and with 50 nM TNT present (red) collected on a magnet. Spectra shown were the average of 5 measurements of 3 replicate samples obtained using a 532 nm laser excitation and a 3 s accumulation time. Data shown has been baseline corrected.

Figure 5.12 (black) demonstrates the SERS spectrum obtained from the protein A and FITC antibody bound silver nanoparticle HMD functionalised Ag@MNPs, without TNT present. When TNT is absent (black) the peaks from the FITC conjugated antibody should not be enhanced, however in the red spectrum it was observed that there was a SERS spectrum of FITC observed. This could be due to non-specific trapping of the FITC antibody functionalised nanoparticles, which when magnetically pulled down, the sample is aggregated due to the close proximity of the nanoparticles, hence a large background was observed in comparison to Figure 5.7, when no magnetic separation was performed. However, when TNT (50 nM) was added to the assay, an increase in signal was observed. The increase in the intensity of the SERS spectrum was expected to be larger than that observed after addition of

TNT. This is could be due to the protein A adding an extra layer to the nanoparticle surface, therefore the Raman active molecule is further from the nanoparticle surface, as SERS is a distance dependent technique.[72] Protein A in this case, was observed to not prevent non-specific binding. Therefore, bovine serum albumin (BSA) was explored as a non-specific binding agent after the conjugation of the antibody to the silver nanoparticles surface.

5.3.4 Non-specific Binding Agents

Non-specific binding agents saturate unoccupied binding sites on a nanoparticle, without taking an active part in the specific assay reaction. Blocking agents which have been previously been used include include Tween 20, BSA, PEG and polymers such as polyvinylpyrrolidene (PVP).[209] BSA (1-5 %) is widely used in enzyme linked immunosorbant assays (ELISA) as a non-specific binding agent as it is an inexpensive agent and it is known to reduce background signals, improving the signal to noise ratio.[210]

Therefore, after the conjugation of FITC antibody to the silver nanoparticles, BSA (5 %, 10 μl) was added to prevent any non-specific binding, the samples were centrifuged removing any BSA that was free in solution. The FITC antibody functionalised silver nanoparticle solution (150 μl) with BSA was then added to the HMD conjugated Ag@MNPs (150 μl) and TNT was added. The assay was analysed using UV-vis over 15 hours, the results are shown in Figure 5.13.
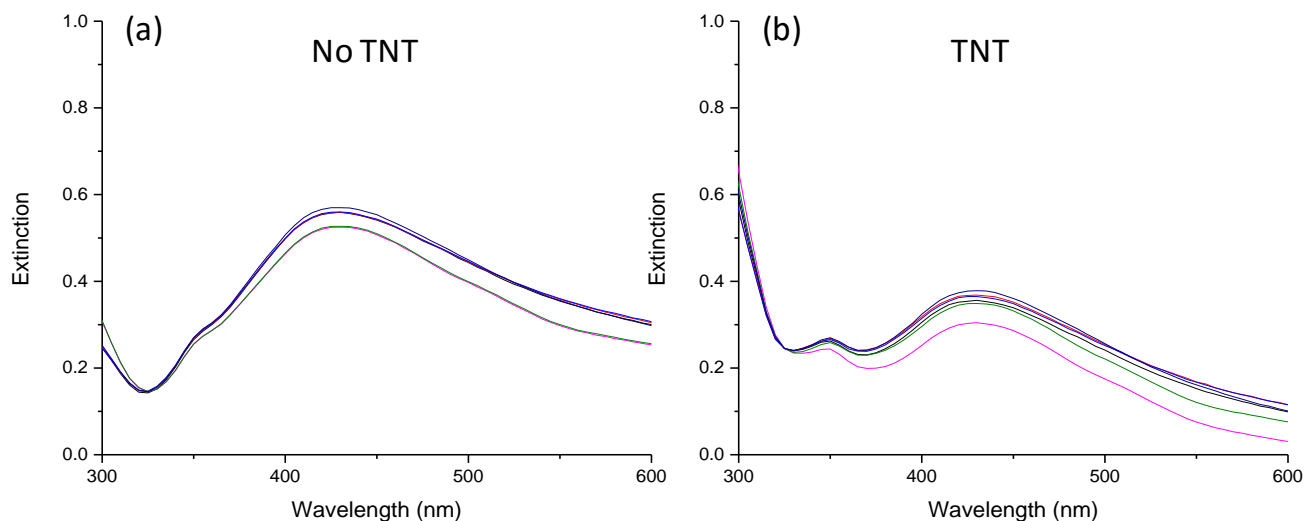
Figure 5.13: (a) Extinction spectrum of FITC antibody conjugated silver nanoparticles blocked with BSA in combination with HMD functionalised Ag@MNPS in the absence of TNT, recorded every 1 hr over 15 hrs, **(b)** FITC antibody functionalised silver nanoparticles blocked with BSA in combination with HMD functionalised Ag@MNPs with the addition of 75 nM TNT, forming a Meisenheimer complex over 15 hrs.

Figure 5.13 shows the UV-vis spectra of antibody conjugated silver nanoparticles, blocked BSA, to occupy any free binding sites on the silver nanoparticle, added to HMD functionalised Ag@MNPs, in the absence of TNT. In Figure 5.13 (a) it was observed when TNT was absent in the assay, very slight aggregation was observed as the LSPR peak broadened and dampened slightly, indicating some non-specific binding may have occurred. However, in Figure 5.13 (b) it was demonstrated that upon the addition of TNT the LSPR peak broadened and dampened due to the formation of the Meisenheimer complex, resulting in the nanoparticles aggregating. Upon increasing the concentration of TNT, from 50 nM to 75 nM, more TNT anions are formed, thus a more intense coloured Meisenheimer adduct is formed, inducing a shift in the UV-vis from 270 nm as seen in Figure 5.7 to 350 nm. Therefore, the assay was analysed using SERS to determine if the controlled aggregation of the nanoparticles, due to the formation of a Meisenheimer complex, resulted in an increase in the SERS spectrum (Figure 5.14). The samples were analysed after magnetic separation by an external rare-earth magnet therefore any unbound nanoparticles were washed away, the concentrated magnetic plug was then analysed by SERS using 532 nm laser excitation and a 3 s accumulation time.
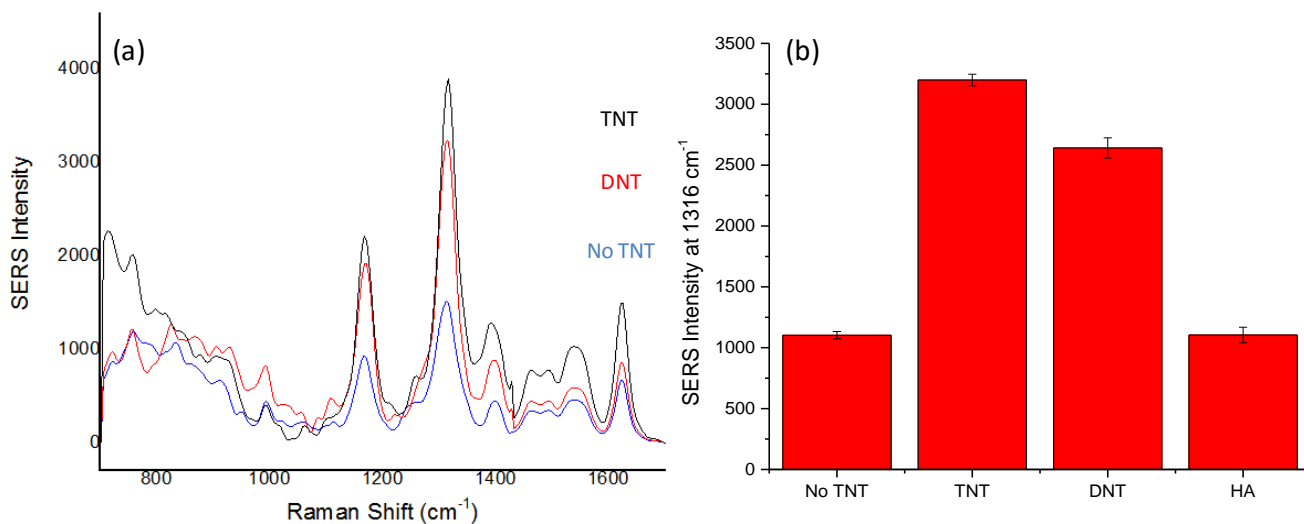
Figure 5.14: (a) SERS spectrum of FITC labelled antibody conjugated silver nanoparticles in the presence of HMD functionalised Ag@MNPs, with no TNT present (blue), 75 nM DNT (red) and 75 nM TNT (black) collected on a magnet. Spectra shown were the average of 5 measurements of 3 replicate samples obtained using a 532 nm laser excitation and a 3 s accumulation time, data set has been baseline corrected. **(b)** Bar chart demonstrating the SERS intensity observed at 1316 cm^{-1} for No TNT, TNT, DNT and a single amine terminated silver magnetic nanoparticle (HA). Error arises from the standard deviation of the replicate samples.

Figure 5.14 demonstrates the SERS spectra obtained from magnetically separated Meisenheimer complexed nanoparticles, the SERS active nanoparticle should be removed in the wash step when TNT is absent as no Meisenheimer complex should form, and therefore no SERS spectrum should be observed. Figure 5.14 (a) shows that when TNT was absent (blue) a spectrum of FITC was observed suggesting non-specific binding between the FITC labelled antibody functionalised silver nanoparticles and the HMD functionalised Ag@MNPs had occurred, which is in agreement with the UV-vis spectrum. Upon the addition of TNT (black), an increase in the FITC spectrum was observed indicating the Meisenheimer complex had formed and aggregation had occurred. DNT was added as a negative control to demonstrate the specificity of the assay as DNT should not form a Meisenheimer complex. However in Figure 5.14 (a) when DNT was added (red) an enhancement in the SERS spectra was also observed, indicating that DNT was causing aggregation of the assay. This was further demonstrated in Figure 5.14 (b), a bar chart of the SERS intensity at 1316 cm^{-1} was plotted. Interestingly, an increase in signal of 2 times was observed when TNT (75 nM) was present in the assay, however, from the previous results a greater increase in intensity was expected.

This was may be due to the HMD molecule having a weak electrostatic bond to the magnetic nanoparticles, therefore when the complex was pulled down onto the magnet, some of the complex may have been removed during the washing step.

An additional control to ensure the specific interaction of the terminal amine on the Ag@MNPs with the TNT was forming the Meisenheimer complex, a single terminated amine was bound to Ag@MNPs. In this case, the amine terminus should bind the Ag@MNPs and the methyl terminus would be free. Therefore, when TNT and the antibody functionalised silver nanoparticles were added to the assay, no aggregation should be observed and no increase in SERS as no Meisenheimer complex should be formed. This is shown in Figure 5.14 (b) that when the single terminated amine (HA) was added instead of the HMD molecule, no increase in the SERS was observed, indicating no formation of the Meisenheimer complex.

To overcome the weak electrostatic interaction of the HMD functionalised Ag@MNPs, a PEG molecule which had an amine and thiol terminus was investigated, since a covalent thiol-metal bond is much stronger. The Ag@MNPs were functionalised with increasing concentrations of HS-PEG-NH$_2$ (0 – 40 μM), leaving a terminal amine group available to form a Meisenheimer complex with TNT, and prior to being analysed using UV-vis and DLS the PEG functionalised Agg@MNPs were centrifuged (6000 rpm, 20 mins), as shown in Figure 5.15.
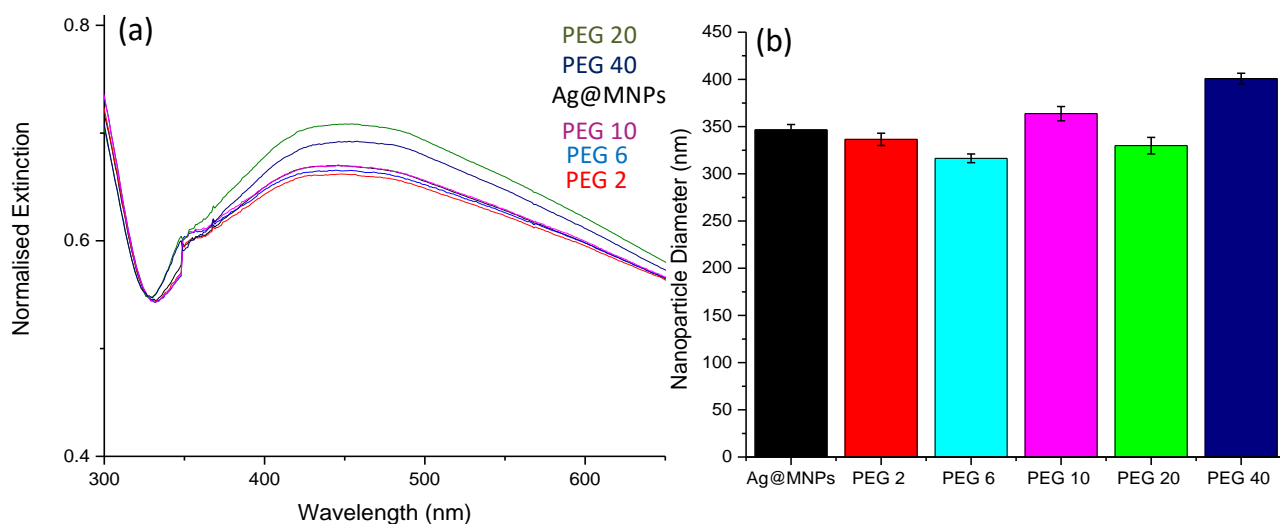
Figure 5.15: (a) Extinction spectrum of bare Ag@MNPs (black) and increasing concentrations of HS-PEG-NH$_2$, 2 (red), 6 (light blue), 10 (pink), 20 (green) and 40 (navy) µM conjugated to Ag@MNPs, **(b)** Nanoparticle diameter of increasing concentrations of HS-PEG-NH$_2$, 2 (red), 6 (light blue), 10 (pink), 20 (green) and 40 (navy) µM conjugated to Ag@MNPs analysed by DLS.

In Figure 5.15 (a) it was observed that the extinction spectrum, with the addition of HS-PEG-NH$_2$ to Ag@MNPs, showed similar results to that of the conjugation of HMD to Ag@MNPs. It was observed that a concentration of 20 µM HS-PEG-NH$_2$ was optimum as was previously observed with HMD conjugated nanoparticles. The DLS data in Figure 5.15 (b) also demonstrated that upon addition of low concentrations of PEG (2 and 6 µM), a decrease in the size was observed and a slight increase in size was observed for the 10 µM of PEG sample. At 20 µM of PEG full monolayer coverage was observed and the nanoparticles were stabilised. Therefore a concentration of 20 µM of PEG was used for the rest of these studies. TNT was then added to the FITC antibody functionalised silver nanoparticles in combination with the PEG functionalised Ag@MNPs. The FITC labelled antibody functionalised silver nanoparticles were added in a 1:1 (v/v) ratio to PEG functionalised Ag@MNPs. TNT (75 nM) was then added to the assay and a UV-vis spectrum was obtained every 30 mins for 15 hrs, as shown in Figure 5.16.
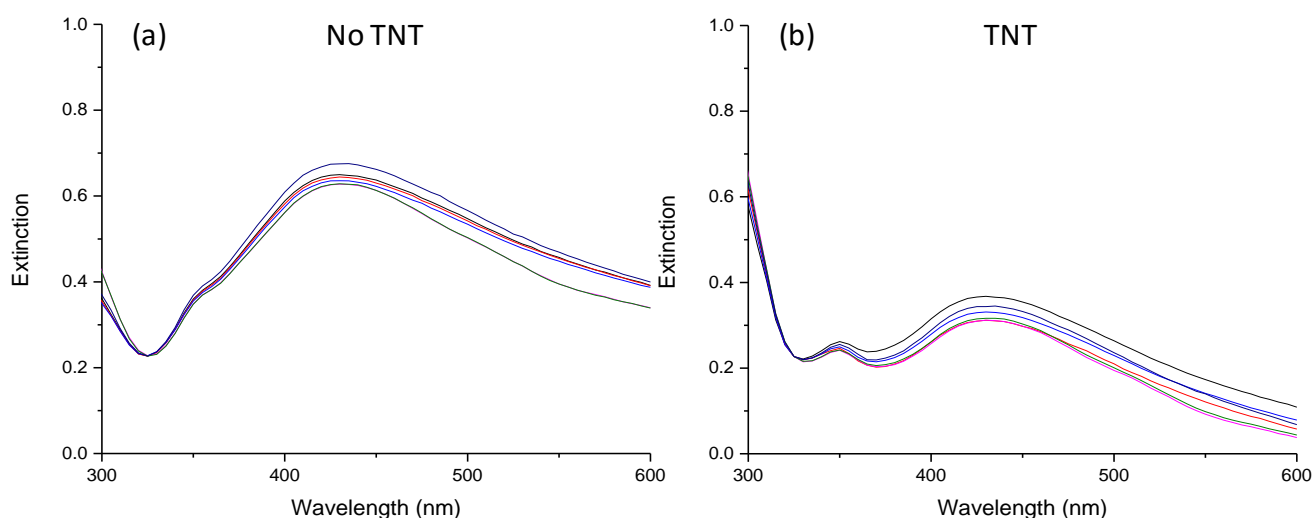
Figure 5.16: (a) Extinction spectrum of antibody conjugated silver nanoparticles with HS-PEG-NH$_2$ functionalised Ag@MNPS in the absence of TNT over 15 hrs, **(b)** antibody functionalised silver nanoparticles with HS-PEG-NH$_2$ functionalised Ag@MNPs in the presence of 100 nM TNT.

In Figure 5.16 (a) it was observed when TNT was absent in the assay, very slight aggregation was observed as the LSPR peak broadens and dampens, indicating that non-specific binding occurred between the FITC labelled antibody functionalised silver nanoparticles and the PEG functionalised Ag@MNPs, similarly to the HMD sample. However, in Figure 5.16 (b) it was demonstrated that upon the addition of TNT the LSPR peak broadened and dampened due to the formation of a Meisenheimer complex, resulting in the nanoparticles controllably aggregating. Therefore, the assay was analysed using SERS to determine if the controlled aggregation of the nanoparticles, resulted in an increase in the SERS spectrum. The samples were analysed after magnetic separation by an external rare-earth magnet therefore any unbound nanoparticles were washed away, the concentrated magnetic collection was then analysed by SERS using 532 nm laser excitation and a 3 s accumulation time, as shown in Figure 5.17.
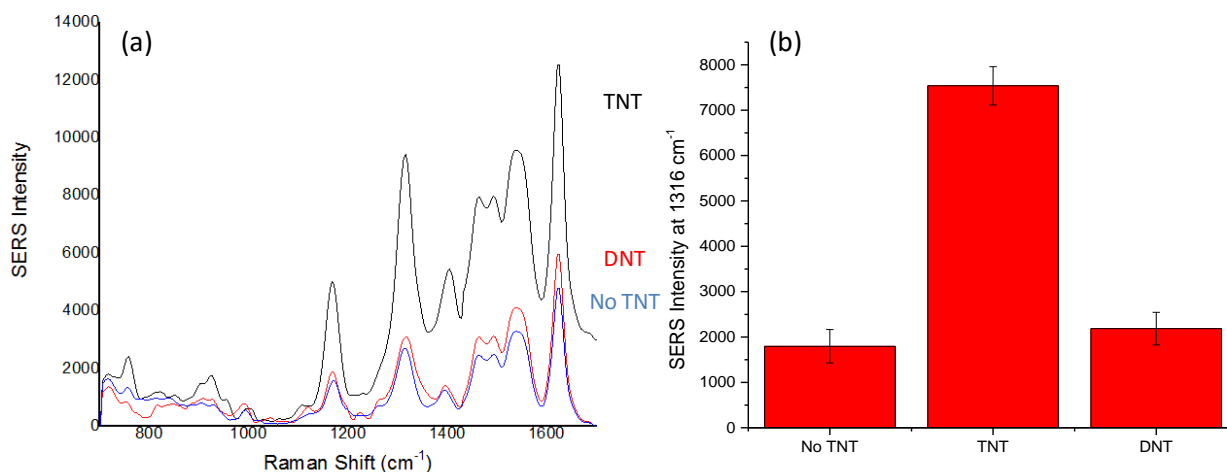
Figure 5.17: (a) SERS spectra of FITC labelled antibody conjugated silver nanoparticles in the presence of HS-PEG-NH$_2$ functionalised Ag@MNPs, with no TNT present (blue), 75 nM DNT (red) and 75 nM TNT (black) collected on a magnet. Spectra shown were the average of 5 measurements of 3 replicate samples obtained using 532 nm laser excitation and a 3 s accumulation time, data set has been baseline corrected. **(b)** Bar chart demonstrating the SERS intensity observed at 1316 cm^{-1} for No TNT, TNT and DNT. Error bars arise from the standard deviation of the replicate samples.

Figure 5.17 (a) shows that when TNT was absent (blue) from the PEG functionalised Ag@MNPs and antibody functionalised silver nanoparticles, a spectrum of FITC was observed suggesting aggregation had occurred. Upon the addition of TNT (black) an increase in the SERS spectrum of over four times the no TNT sample was observed, indicating the Meisenheimer complex had formed and aggregation had occurred. This suggests that the thiol terminated functionalised magnetic nanoparticles were more stable when the Meisenheimer adduct formed, therefore a larger number of nanoparticles were pulled out of the matrix when in the presence of the external magnetic plug, resulting in a large increase in the SERS in the presence of TNT. In Figure 5.17 (a) when DNT was added (red) a small increase in the SERS spectra was observed, indicating that DNT was causing a small amount of aggregation of the nanoparticles. This was further demonstrated in Figure 5.17 (b) in which a bar chart of the SERS intensity at 1316 cm^{-1} was plotted, indicating that TNT can be successfully detected using a magnetic immunoassay and an external electromagnetic field.

The next step of this assay would be to perform a concentration study of TNT, to obtain a limit of detection, however due to time constraints this was not possible.

5.4 Conclusions

In conclusion, FITC modified TNT specific antibodies were functionalised on to silver nanoparticles in combination with an aminated Ag@MNP for the detection of TNT by SERS. It was shown that in the presence of TNT, a Meisenheimer complex can be formed from the lone pair of electrons on an amine group conjugated to Ag@MNPs by nucleophilic attack of the ring in TNT. The FITC modified antibodies also bound to TNT specifically, thus aggregation of the nanoparticles occurred, resulting in an increased SERS spectrum. HMD was investigated as the amine molecule bound to Ag@MNPs. HMD was added to the TNT antibody functionalised nanoparticles and it was observed in the absence of TNT aggregation of the nanoparticles occurred indicating that non-specific binding occurred between the positively charged amine group and the negative nanoparticles. Therefore a blocking agent was investigated to occupy available binding sites on the nanoparticle, the use of HS-PEG-NH$_2$ and BSA were investigated. It was shown that HS-PEG-NH$_2$ was more stable and showed promising results when the Meisenheimer complex was formed and magnetically separated. However only one concentration of TNT was investigated in this assay due to time constraints, therefore a TNT concentration study would have to be investigated in order to obtain an observed limit of detection.

Furthermore, if more time was available the assay could be further optimised so that the magnetic nanoparticles would allow for the assay to be used for TNT detection in more complex sample matrices.

6.Conclusions

Detection of solution based explosives: TNT, RDX and PETN, has been investigated by surface enhanced Raman scattering (SERS). To achieve this, the explosives were adsorbed directly onto the surface of silver nanoparticles and aggregation was induced by the addition of NaCl. This allowed for a unique SERS spectrum of TNT, RDX and PETN to be obtained, with a limit of detection of 120, 100 and 3500 nM. However, it was determined that the SERS response can be greatly influenced by an increase in TNT concentration which was postulated to be due to changes in orientation of the molecule on the nanoparticle surface. As a result, this technique would be challenging when attempting to quantify an unknown concentration of TNT, or when trying to distinguish multiplexed samples in a more complicated matrix due to changes in spectra with TNT concentration. Furthermore, only a very weak SERS spectrum of PETN could be obtained. It was for these reasons that a more sensitive assay was required to be developed allow selective and specific detection of explosives as the direct SERS approach was not sensitive or specific enough.

Antibodies have major selective advantages which, when bound to nanoparticles, offer direct detection of specific target analytes. A FITC modified antibody with a free ITC group was used which allows for the antibody to conjugate to the nanoparticles surface in a 'flat' orientation. This orientation allowed for the target molecule to come in close proximity to the nanoparticles surface, allowing an intrinsic SERS signal of the target molecule to be obtained. Quantitative detection of the explosives, TNT and RDX, was achieved, with nM sensitivity for TNT and pM sensitivity demonstrated for RDX. In addition, PCA was used to allow multiplexed analysis based on unique Raman bands for the two different explosives which could be clearly identified in the SERS spectra. TNT could also be detected in a more complex matrix consisting of natural and synthetic dirt in order to mimic a more realistic matrix in which TNT would be found in the field. Different solvents were explored in order to obtain a solvent which would dissolve the minimum amount of

the dirt components, in order for TNT detection. It was found that THF was the best solvent, TNT could be detected in up to 80% natural dirt, and only 10% synthetic dirt. Furthermore, this assay has been demonstrated to work for a non explosive small molecule to demonstrate the diversity of the assay.

Due to successful detection of TNT, RDX and dioxane using the commercially available FITC modified antibody, an in-house method was investigated to modify a PETN specific antibody with FITC. Preliminary results suggest that, with time, a method could be developed for the conjugation of FITC onto antibodies whilst leaving a free ITC group. This was achieved by using carbodiimide chemistry. Using a direct approach the detection of PETN was found to be successful for a concentration of 50 µl of 200 µM FITC conjugated to the antibody, characterised by RP-HPLC. PETN was detected as low as 100 nM by SERS. Furthermore, with the use of multivariate analysis, it was possible to detect and distinguish all three explosive targets, TNT, RDX and PETN from within a complex matrix i.e. when three antibody conjugated nanoparticle solutions were present.

A final assay was developed which was able to detect TNT via the formation of a Meisenheimer complex with the lone pair of electrons on an amine group by nucleophilic attack of the ring in TNT and using magnetic nanoparticles. However, it was observed that non-specific binding occurred between the positively charged amine group and the negative nanoparticles. Therefore a blocking agent was required to occupy available binding sites on the nanoparticle, in which HS-PEG-NH$_2$ and BSA was investigated. It was shown that HS-PEG-NH$_2$ was more stable and showed promising results for the detection of TNT when the Meisenheimer complex was formed and magnetically separated by SERS.

Overall, it was demonstrated that silver nanoparticles and silver coated magnetic nanoparticles allow for rapid, specific, sensitive and direct detection of small target analytes by SERS in comparison to conventional methods, and therefore should be considered in future applications.

7.Experimental

7.1 Materials

TNT, DNT, RDX and PETN were purchased from LGC standards, UK. The FITC modified antibodies and the unlabelled antibody were purchased from Fitzgerald Antibodies, USA. All other chemicals were purchased from Sigma Aldrich unless otherwise stated.

7.2 Instrumentation

7.2.1 UV-vis Spectroscopy

All UV-vis spectroscopy was carried out on a Varian Cary 3000 Bio UV-Visible spectrophotometer with Win UV scan application version 2.00 software. The instrument was left to warm up and equilibrate for at least 10 minutes. The range of wavelengths scanned was 200-800 nm. All samples (500 µl) were run in 500 µl quartz cuvette.

7.2.2 DLS and Zeta Potential

A Malvern Zetasizer Nano ZS was used to carry out all zeta potential and zeta sizing measurements along with Zetasizer µV and APS version 6.20 software. Approximately 1.7 cm of sample was run in a 1 ml disposable plastic cuvette, with a standard Malvern Dip Cell.

7.2.3 SERS Measurements

SERS of all samples was obtained using a Renishaw plate reader, RenDX, with 532 nm laser excitation from a diode laser. A 96 well plate was placed onto the stage and the instrument's software was used to move the stage automatically so that a spectrum could be recorded from each well. 3 replicate 150 µl samples were analysed for each sample using a 96 well plate, unless otherwise stated. The accumulation time was 5 x 0.5 s using 0.15 mW laser power, unless otherwise stated.

All SERS spectra were normalised against a standard solution of ethanol. Each spectrum was baseline corrected using the asymmetrical least squared smoothing method and then each spectrum was scaled and offset for clarity, unless otherwise stated. [153, 154]

7.2.4 NanoSight

A NanoSight LM20 and accompanying NTA software was used to determine the size and monodispersity of the silver nanoparticles.

7.2.5 Fluorescence Spectroscopy

The FITC fluorescence intensity was determined by exciting at 492 nm for 20 s on the Strategene Mx3005P and measuring the fluorescent emission at 515 nm.

The antibody fluorescence emission was obtained by exciting at 280 nm for 20 s and observing the emission at 360 nm.

7.2.6 AFM

AFM images were obtained on a DPN 5000™ nanofabrication system using ACT silicon probes with a spring constant of 37 N/m and a resonance frequency of 300 kHz. All images were collected in close-contact (or tapping) mode under ambient conditions. Linewise levelling was performed on the images using SPIP™ software and line profiles were taken from the resulting images. SPIP™ was also used to generate 3D images.

7.2.7 SE-HPLC

SE HPLC was performed on a Dionex UVD170U detector fitted with a P680 pump through a HiTrap™ Desalting Column. Eluent used was 100 % H_2O at 1 ml/ min for 5 mins.

7.2.8 RP-HPLC

RP-HPLC was performed on a Dionex UVD170U detector fitted with a P680 pump through a Accucore 150 – C4 HPLC column. Eluent used was A: 0.1 % TFA in acetonitrile/water (2.5 : 97.5 v/v) and B: 0.1 % TFA in acetonitrile / water (90 : 10 v/v). A eluent gradient was applied as shown in the table, at 300 μl / min flow rate:

Time (mins)	% B
0.0	10
15.0	70
15.1	100
16.0	100
16.1	10
19.0	10

7.3   Synthesis of Citrate Reduced Silver Nanoparticles

Silver nanoparticles were synthesised following the citrate reduction method developed by Lee and Meisel.[105] 500 ml of distilled water was heated to 45°C with constant stirring. Silver nitrate (90 mg) was dissolved in 10 ml distilled water and added. Heating was continued until the temperature reached 98°C, then 100 ml of a 1% aqueous solution of sodium citrate was added. The solution was stirred for 90 minutes, maintaining a temperature of 98°C throughout. The colloid was then cooled to room temperature and characterised by UV-vis spectroscopy, DLS and zeta potential.

7.4   SERS of Explosives and Acetonitrile

7.4.1 SERS of Acetonitrile

As TNT, RDX and PETN were dissolved in acetonitrile the SERS spectrum of acetonitrile was obtained. Acetonitrile was purchased from LGC standards, UK (4.4 mM dissolved in acteonitrile), SERS of acetonitrile were performed by adding acetonitrile (100 μl) to silver nanoparticles (150 μl, 0.36 nM) in a 96 well plate.

NaCl (8.8 mM) was added to the 96 well plate to induce aggregation. A 532 nm laser excitation and a 10 s accumulation time was used to obtain a SERS spectrum.

7.4.2 SERS of TNT/RDX/PETN/Dioxane/DNT

A reference spectra of each of the targets was required to ensure the target spectrum was present in the SERS spectrum of the assay developed. TNT, RDX and PETN were purchased from LGC standards, UK (4.4 mM diluted in acetonitrile). Final concentrations of 120 nM, 720 nM, 1.3 μM, 2 μM, 3μM and 3.5 μM (100 μl) of TNT/RDX/PETN were diluted with acetonitrile and added to 150 μl of silver nanoparticles. NaCl (8.8 mM) was then added as an aggregating agent in order to obtain SERS spectra. SERS spectra of TNT/RDX/PETN were obtained by increasing the accumulation time to 10 seconds.

SERS of 2-aminomethyl-1, 4-benzodioxane (dioxane) was obtained by adding 2 μl of dioxane (150 nM) to 150 μl AgNP. The suspension was aggregated with NaCl (8.8 mM) and a SERS spectrum was obtained using an acquisition time of 13 seconds.

The spectrum of 2, 6 – dinitrotoluene (DNT), also purchased from LGC standards, UK (4.4 mM dissolved in acteonitrile), was also obtained to check the specificity of the antibody. SERS of DNT were performed by increasing the accumulation time to 10 seconds.

7.5 Antibody Functionalised Silver Nanoparticles

FITC labelled TNT/RDX/dioxane specific antibodies were purchased from Fitzgerald, USA. The antibody was modified with 4.5 fluorescein isothiocyanate (FITC) groups per an antibody. 20 μl of 2 mg/ml antibody were added to 1 ml of citrate reduced nanoparticles (0.36 nM) and kept at 4°C for 48 hours. The silver nanoparticle-antibody conjugates were then centrifuged (6000 rpm, 20 mins) and resuspended in tris buffer (pH 7.4).

7.6 Fluorescence Spectroscopy

A calibration graph was performed using FITC. 5 replicates of FITC, concentrations of 3, 4, 5, 6 and 7 x 10^{-10} M, 100 µl were measured by fluorescence by exciting at 495 nm for 20 s and measuring the emission at 525 nm. The fluorescent intensity was then plotted against concentration in order to obtain a calibration graph. Next 250 mM of DTT was added to 1 ml of antibody conjugated silver nanoparticles. The solution was then left at 50 ^{o}C in a heating block overnight. The sample was then centrifuged (6000 rpm, 20 mins) so that the now unconjugated antibody is free in solution. Fluorescence was then performed on the supernatant (100 µl), under the same conditions as for FITC.

7.7 Addition of TNT to Antibody Functionalised Silver Nanoparticles

Final concentrations of 1, 10, 50, 75 and 120 nM of TNT/RDX (100 µl) were diluted in acetonitrile and added to 150 µl of antibody conjugated silver nanoparticles. The binding of the small molecule to the antibody proceeded almost immediately and therefore analysis via SERS was carried out directly after addition.

Control samples were analysed to demonstrate the specificity of the assay, therefore the highest concentration of 150 nM DNT (100 µl) diluted in acetonitrile was added to 150 µl antibody conjugated silver nanoparticles. Also a negative control in which 100 µl of acetonitrile was added to 150 µl of antibody conjugated nanoparticles was also observed by SERS.

7.7.1 Enhancement of SERS assay over time

The samples were analysed by SERS every 10 minutes for 100 minutes and the enhancement observed at 1066 cm^{-1} was then plotted against time.

7.8 Conjugation of Unlabelled Antibody to Silver Nanoparticle

TNT specific antibody (unlabelled) was purchased from BBI solutions, UK. 1 ml of citrate reduced silver nanoparticles (0.36 nM) were diluted in PBS buffer (pH 7.4) to an optical density of 1. 80 µl of 1 mg/ml antibody were added to 2 ml of diluted citrate reduced nanoparticles and kept at 4°C for 48 hours. The silver nanoparticle-antibody conjugate was then centrifuged (6000 rpm, 20 mins) and resuspended in 1 ml tris buffer (pH 7.4).

7.9 AFM

All images were collected in close-contact (or tapping) mode under ambient conditions. Antibodies were immobilised on the surface by spotting 2.5 µl of HEPES buffer (10 mM, pH 7.4) for 30 minutes. HEPES buffer was removed from the surface and 2.5 µl of the antibody was spotted and left to dry for 30 min. The surface was then washed 3 times with d.H_2O to remove any unbound antibodies.

7.10 Multiplexing RDX and TNT Specific Antibodies

To prove the selectivity of the assay 75 µl of RDX specific antibody conjugated silver nanoparticles was added to 75 µl of TNT specific antibody conjugated silver nanoparticle solution. Then only RDX or TNT (1 nM, 100 µl) was added to the nanoparticle suspension. Also a negative control in which 100 µl acetonitrile was added to 150 µl antibody functionalised silver nanoparticles was also carried out.

7.11 PCA

As mentioned previously, the data set was baseline corrected using polynomial least squares, and scaled before performing PCA, using Matlab software version R2013a (The MathWorks, Natick, MA, USA). Principal component 1 was then plotted against principal component 2. The loading plots were also plotted to determine correlation.

7.12 SERS of TNT in Solvents

100 µl of TNT (300 nM) was further dissolved in acetone, acetonitrile, dioxane, THF and ethyl acetate, (100 µl) and was added to 150 µl of silver nanoparticles. NaCl (8.8 mM) was added to the solution to aggregate the nanoparticles, to observe a SERS spectrum.

7.13 SERS of Synthetic Dirt

Synthetic dirt was purchased from LGC standards (clean clay sediment No. 2). The synthetic dirt (5 mg) was diluted in each solvent (5 ml). 100 µl of the diluted dirt was then added to 150 µl of silver nanoparticles (0.36 nM) and NaCl (8.8 mM) was added to aggregate the nanoparticles to observe a SERS spectrum of the dirt.

7.14 SERS of Natural Dirt

A cotton swab was used to collect a sample from a nearby plant pot. The cotton swab was then added and mixed to 1 ml of the solvent. 100 µl of the diluted dirt was then added to 150 µl of silver nanoparticles (0.36 nM) and NaCl (8.8 mM) was added to aggregate the nanoparticles to observe a SERS spectrum of the dirt using 532 nm laser excitation and a 10 s accumulation time.

7.15 TNT Assay in Synthetic/Natural Dirt

15 µl of the solvent dissolved dirt was spiked with TNT (50 nM). This sample was then added to 150 µl of antibody conjugated silver nanoparticle (0.36 nM) to make a 10 % (v/v) dirt matrix and was analysed using SERS.

7.16 TNT 'Dirt' Concentration Study

A range of 'dirt' solutions, 0, 2, 5, 10, 20, 30, 50, 80 and 100 % (v/v) were spiked with TNT and added to 150 µl of the antibody conjugated silver nanoparticles. The samples was then analysed in a 96 well plate using 532 nm laser excitation and a 0.5 s accumulation time.

7.17 In-house FITC modified PETN Antibody

Increasing concentrations of FITC (2, 6, 10 and 20 μM) was added to EDC (1.12, 5.6, 11.2, and 19.8 μM). This solution was then added dropwise to sNHS (10.86 μM) and antibody (20 μl, 2 mg/ml) in HEPES buffer (pH 7.4). The sample was left to mix for 4 hrs before being purified by cartridge centrifugation (10 kDa, 6000 rpm, 20 mins).

7.18 BCA Quantification Kit

BCA protein quantification kit purchased from Thermo scientific, USA, was used to quantify the amount of protein in a sample, specifically by measuring the amount of amide bonds present. A BCA working reagent was prepared by mixing solution 'A' with solution 'B', which contained BCA and copper ions which when in the presence of amide bonds the copper was reduced forming a purple complex. Firstly, a BSA calibration graph was obtained by adding increasing concentrations of BSA (0 – 2000 μg/ml) to the working reagent. The samples were then analysed using UV-vis spectroscopy at 562 nm. The FITC modified antibodies were then set to the same optical density and also added to the BCA working reagent to determine if any new amide bonds had been made due to the carbodiimide coupling.

7.19 Meisenheimer Complex

1, 6 hexamethyldiamine (HMD, 20μM) was added to FITC modified antibody functionalised silver nanoparticles (0.36 nM, 150 μl). TNT (50 nM) was added to the assay to form a Meisenheimer complex between the terminal amine group on HMD and the ring in TNT. As TNT was dissolved in acetonitrile, this was used as a control. Acetonitrile was added to a solution of HMD and antibody functionalised silver nanoparticles (0.36 nM, 150 μl) and was analysed by UV-vis spectroscopy every 20 mins for 15 hrs.

7.20 Protein A Functionalised Silver Nanoparticles

Increasing concentrations of protein A (8- 300 μM) were added to 1 ml silver nanoparticle (0.36 nM) solution and was left stirring for 5 mins. A solution of NaCl

(0.17 M, 0.5 mL) was added to the protein A functionalised silver nanoparticles. A UV-Vis spectrum was then obtained of each sample to measure if any aggregation had occurred, demonstrating full monolayer coverage of the silver nanoparticle, as the nanoparticle is stabilised by protein A encapsulation.

7.21 Silver coated Magnetic Nanoparticles

$FeCl_2.4H_2O$ (1.98 g), $FeCl_3.6H_2O$ (5..335 g) and concentrated HCl (821 µl) were added together and made up to 25 ml with distilled water. NaOH (15.058 g) was added to a round-bottom flask along with 250 ml distilled water and heated to 50 °C on a oil bath. The acidified iron salt solution was then added drop-wise with vigorous stirring and a black precipitate formed immediately. Stirring was continued for a further 20 min at 50 °C, then the solution left to settle and cool on a magnet. The black precipitate was washed twice with distilled water, then 125 ml of 0.1 M HNO_3 was added and the solution heated to 95 °C in a round bottom flask, with constant stirring, for 40 min. The resultant reddish-brown solution was centrifuged in triplicate and resuspended in distilled water; this produced the stock maghemite MNPs.

Ag@MNPs were prepared using a glucose-reduction method, 1 ml stock MNPs was added to a round bottom flask along with glucose (0.25 g), water (4 ml), and $AgNO_3$ (1%, 1.5 ml). The mixture was sonicated for 10 min and then heated at 90 °C for 40 mins while rotating. The resultant Ag@MNPs were centrifuged three times and redispersed in sodium citrate (5 mM, 6 ml). Note that magnetic collection of a solution of the synthesised Ag@MNPs resulted in a clear supernatant, indicating that no non-magnetic silver nanoparticles were formed during the silver nitrate reduction.

7.22 HMD Functionalised Ag@MNPs

Increasing concentrations of HMD (2, 6, 10, 20 and 40 µM) was added to Ag@MNPs (500 µl) and was analysed by UV-vis spectroscopy and DLS.

7.22.1 BSA

BSA was used as a non-specific binding agent to occupy the free binding sites on the silver nanoparticle surface, in the hope to prevent non-specific binding. After functionalising the silver nanoparticles with FITC modified antibody, BSA (5 %, 10 µl) was added, and the sample was centrifuged to remove any BSA which was free in solution.

7.23 PEG Functionalised Ag@MNPs

It was thought that HS-PEG-NH$_2$ would form a more stable Meisenheimer complex in comparison to HMD functionalised Ag@MNPs. Therefore, increasing concentrations of HS-PEG-NH$_2$ (0 – 40 µM) was added to Ag@MNPs (500 µl) and was analysed by UV-vis spectroscopy and DLS.

8.References

1. https://www.gov.uk/government/policies/protecting-the-uk-against-terrorism.
2. Home land security, Public Intelligence, https://publicintelligence.net/tag/department-of-homeland-security/.
3. F. Booth, *Trans. Faraday Soc.*, 1953, **49**, 272-281.
4. J. Akhavan, *The chemistry of explosives*, Royal Society of Chemistry, 2011.
5. P. D. SHARMA, *Explosives and Detonators*
6. M. Talawar, A. Agrawal, M. Anniyappan, D. Wani, M. Bansode and G. Gore, *Journal of hazardous materials*, 2006, **137**, 1074-1078.
7. P. Luebcke, P. Dickson and J. Field, *Proceedings of the Royal Society of London. Series A: Mathematical and Physical Sciences*, 1995, **448**, 439-448.
8. M. Suceska, *Test methods for explosives*, Springer Science & Business Media, 2012.
9. G. Baker Jr Samuel, Google Patents, 1936.
10. W. Ling, *Isis*, 1947, 160-178.
11. T. Mashimo, S. Ozaki and K. Nagayama, *Review of scientific instruments*, 1984, **55**, 226-230.
12. R. Echols, R. James and J. Aldstadt, *Analyst*, 1997, **122**, 315-319.
13. I. Cotte-Rodriguez, H. Hernandez-Soto, H. Chen and R. G. Cooks, *Analytical chemistry*, 2008, **80**, 1512-1519.
14. V. Gryaznov, M. Zhernokletov, V. Zubarev, I. Iosilevskii and V. Tortov, *Sov. Phys.-JETP (Engl. Transl.);(United States)*, 1980, **51**.
15. M. E. Walsh and T. F. Jenkins, *Identification of TNT transformation products in soil*, DTIC Document, 1992.
16. T. Norgate and N. Haque, *Journal of Cleaner Production*, 2010, **18**, 266-274.
17. C. Johns, R. A. Shellie, O. G. Potter, J. W. O'Reilly, J. P. Hutchinson, R. M. Guijt, M. C. Breadmore, E. F. Hilder, G. W. Dicinoski and P. R. Haddad, *Journal of Chromatography A*, 2008, **1182**, 205-214.
18. S. R. Jain, *Propellants, Explosives, Pyrotechnics*, 1987, **12**, 188-195.
19. X. S. Song, X. L. Cheng, X. D. Yang and B. He, *Propellants, Explosives, Pyrotechnics*, 2006, **31**, 306-310.
20. J. Clarkson, W. E. Smith, D. N. Batchelder, D. A. Smith and A. M. Coats, *Journal of Molecular Structure*, 2003, **648**, 203-214.
21. F. Arendt, *Contaminated Soil'93: Fourth International KFK/TNO Conference on Contaminated Soil, 3-7 May 1993, Berlin, Germany 3-7 May 1993, Berlin, Germany*, Springer Science & Business Media, 1993.
22. W. Osborne and S. Lawton, *Dermatological Nursing*, 2014, **13**, 46-50.
23. J. Clausen, J. Robb, D. Curry and N. Korte, *Environmental Pollution*, 2004, **129**, 13-21.
24. G. Teleki and A. Chamberlain, *Journal of the Fisheries Board of Canada*, 1978, **35**, 1191-1198.
25. J. Yinon, *TrAC Trends in Analytical Chemistry*, 2002, **21**, 292-301.
26. M. Richardson, *Maritime Studies*, 2004, **2004**, 1-8.
27. A. Kapila, D. Schwendeman, J. Bdzil and W. Henshaw, *Combustion Theory and Modelling*, 2007, **11**, 781-822.

28. D. R. Shankaran, K. V. Gobi, T. Sakai, K. Matsumoto, T. Imato, K. Toko and N. Miura, *Sensors Journal, IEEE*, 2005, **5**, 616-621.
29. S. Vos, in *Chemmatters*, ACS, ACS, 2001, vol. 54, pp. 501-513.
30. P. Torres, L. Mercado, I. Cotte, S. P. Hernández, N. Mina, A. Santana, R. T. Chamberlain, R. Lareau and M. E. Castro, *The Journal of Physical Chemistry B*, 2004, **108**, 8799-8805.
31. J. Chaparro, 2012.
32. T. B. Hansen, *Wages of violence: naming and identity in postcolonial Bombay*, Princeton University Press, 2001.
33. R. W. Kurz and C. K. Bartles, *Journal of Slavic Military Studies*, 2007, **20**, 529-547.
34. B. M. Jenkins, *Terrorists Can Think Strategically-Lessons Learned From the Mumbai Attacks*, DTIC Document, 2009.
35. F. H. Ree, *The Journal of chemical physics*, 1984, **81**, 1251-1263.
36. D. Moore, *Review of scientific instruments*, 2004, **75**, 2499-2512.
37. K. Cabell, *Law & Psychol. Rev.*, 2012, **36**, 259.
38. K. D. Krug, W. F. Aitkenhead, R. F. Eilbert, J. H. Stillson and J. A. Stein, Google Patents, 1997.
39. A. Blake and M. T. Sinclair, *Annals of Tourism Research*, 2003, **30**, 813-832.
40. V. Butler and R. W. Poole, *Rethinking checked-baggage screening*, Reason Public Policy Institute Los Angeles, CA, 2002.
41. G. Harding, *Radiation Physics and Chemistry*, 2004, **71**, 869-881.
42. N. Murray, R. Lacey and P. Mason, 1997.
43. F. Vizard, *Scientific American* 2004.
44. R. G. Ewing, D. A. Atkinson, G. Eiceman and G. Ewing, *Talanta*, 2001, **54**, 515-529.
45. F. Karasek and D. Denney, *Journal of Chromatography A*, 1974, **93**, 141-147.
46. G. A. Eiceman, D. Preston, G. Tiano, J. Rodriguez and J. E. Parmeter, *Talanta*, 1997, **45**, 57-74.
47. M. E. Walsh, *Talanta*, 2001, **54**, 427-438.
48. I. Gazit and J. Terkel, *Applied Animal Behaviour Science*, 2003, **81**, 149-161.
49. K. G. Furton and L. J. Myers, *Talanta*, 2001, **54**, 487-500.
50. C. Technologies, *Morpho and Cascade Technologies to Test a Next Generation*

Security Solution at Glasgow International Airport.
51. M. E. Germain and M. J. Knapp, *Chemical society reviews*, 2009, **38**, 2543-2555.
52. S. Girotti, S. Eremin, A. Montoya, M. Moreno, P. Caputo, M. D'Elia, L. Ripani, F. Romolo and E. Maiolini, *Analytical and bioanalytical chemistry*, 2010, **396**, 687-695.
53. C. Vorbeck, H. Lenke, P. Fischer and H.-J. Knackmuss, *Journal of bacteriology*, 1994, **176**, 932-934.
54. J. B. Roy and R. G. Wilkerson, *Urology*, 1984, **23**, 270-271.
55. K.-A. Kovar and M. Laudszun, 1989.
56. Y. Salinas, R. Martínez-Máñez, M. D. Marcos, F. Sancenón, A. M. Costero, M. Parra and S. Gil, *Chemical society reviews*, 2012, **41**, 1261-1296.

57. L. Pauling, R. B. Corey and H. R. Branson, *Proceedings of the National Academy of Sciences*, 1951, **37**, 205-211.
58. W. Hol, P. T. Van Duijnen and H. Berendsen, *Nature*, 1978, **273**, 443-446.
59. J. S. Richardson, *Proceedings of the National Academy of Sciences*, 1976, **73**, 2619-2623.
60. K. Yue and K. A. Dill, *Proceedings of the National Academy of Sciences*, 1995, **92**, 146-150.
61. M. Zehl and G. Allmaier, *Analytical chemistry*, 2005, **77**, 103-110.
62. P. J. Flory, *Journal of the American Chemical Society*, 1956, **78**, 5222-5235.
63. https://www.thermofisher.com/uk/en/home/life-science/protein-biology/protein-biology-learning-center/protein-biology-resource-library/pierce-protein-methods/chemistry-protein-assays.html.
64. B. J. Underdown and J. M. Schiff, *Annual review of immunology*, 1986, **4**, 389-417.
65. R. Geisberger, M. Lamers and G. Achatz, *Immunology*, 2006, **118**, 429-437.
66. Y. Ohta and M. Flajnik, *Proceedings of the National Academy of Sciences*, 2006, **103**, 10723-10728.
67. P. Parham, *The immune system*, Garland Science, 2014.
68. J. L. Liu, D. Zabetakis, G. Acevedo-Vélez, E. R. Goldman and G. P. Anderson, *Analytica chimica acta*, 2013, **759**, 100-104.
69. P. Sabherwal, M. Shorie, P. Pathania, S. Chaudhary, K. K. Bhasin, V. Bhalla and C. R. Suri, *Analytical Chemistry*, 2014, **86**, 7200-7204.
70. E. R. Goldman, G. P. Anderson, N. Lebedev, B. M. Lingerfelt, P. T. Winter, C. H. Patterson and J. M. Mauro, *Analytical and bioanalytical chemistry*, 2003, **375**, 471-475.
71. E. R. Goldman, I. L. Medintz, J. L. Whitley, A. Hayhurst, A. R. Clapp, H. T. Uyeda, J. R. Deschamps, M. E. Lassman and H. Mattoussi, *Journal of the American Chemical Society*, 2005, **127**, 6744-6751.
72. E. Smith and G. Dent, *Modern Raman spectroscopy: a practical approach*, John Wiley & Sons, 2013.
73. A. Smekal, *Naturwissenschaften*, 1923, **11**, 873-875.
74. C. V. Raman and K. S. Krishnan, *Nature*, 1928, **121**, 501-502.
75. M. Gaft and L. Nagli, *Optical Materials*, 2008, **30**, 1739-1746.
76. D. D. Tuschel, A. V. Mikhonin, B. E. Lemoff and S. A. Asher, *Applied spectroscopy*, 2010, **64**, 425-432.
77. J. Winey and Y. Gupta, *The Journal of Physical Chemistry A*, 1997, **101**, 9333-9340.
78. R. M. Hochstrasser and C. A. Nyi, *The Journal of chemical physics*, 1980, **72**, 2591-2600.
79. M. Fleischmann, P. J. Hendra and A. McQuillan, *Chemical Physics Letters*, 1974, **26**, 163-166.
80. E. Mozes, M. Schwartz and M. Sela, *The Journal of experimental medicine*, 1974, **140**, 349-355.
81. D. L. Jeanmaire and R. P. Van Duyne, *Journal of Electroanalytical Chemistry and Interfacial Electrochemistry*, 1977, **84**, 1-20.
82. M. G. Albrecht and J. A. Creighton, *Journal of the American Chemical Society*, 1977, **99**, 5215-5217.

83. J. A. Creighton, C. G. Blatchford and M. G. Albrecht, *Journal of the Chemical Society, Faraday Transactions 2: Molecular and Chemical Physics*, 1979, **75**, 790-798.
84. A. Stacy and R. Van Duyne, *Chemical Physics Letters*, 1983, **102**, 365-370.
85. G. Das, F. Mecarini, F. Gentile, F. De Angelis, H. M. Kumar, P. Candeloro, C. Liberale, G. Cuda and E. Di Fabrizio, *Biosensors and Bioelectronics*, 2009, **24**, 1693-1699.
86. S. Eustis and M. A. El-Sayed, *Chemical society reviews*, 2006, **35**, 209-217.
87. T. Demeritte, R. Kanchanapally, Z. Fan, A. K. Singh, D. Senapati, M. Dubey, E. Zakar and P. C. Ray, *Analyst*, 2012, **137**, 5041-5045.
88. C. Wang, Y. Chen, T. Wang, Z. Ma and Z. Su, *Chemistry of Materials*, 2007, **19**, 5809-5811.
89. M. P. Chatrathi, J. Wang and G. E. Collins, *Biosensors and Bioelectronics*, 2007, **22**, 2932-2938.
90. L. Q. Chen, S. J. Xiao, L. Peng, T. Wu, J. Ling, Y. F. Li and C. Z. Huang, *The Journal of Physical Chemistry B*, 2010, **114**, 3655-3659.
91. J. Eastman, S. Choi, S. Li, W. Yu and L. Thompson, *Applied physics letters*, 2001, **78**, 718-720.
92. Y. Tan, X. Dai, Y. Li and D. Zhu, *Journal of Materials Chemistry*, 2003, **13**, 1069-1075.
93. C. L. Haynes, A. D. McFarland and R. P. V. Duyne, *Analytical chemistry*, 2005, **77**, 338 A-346 A.
94. S. Nie and S. R. Emory, *science*, 1997, **275**, 1102-1106.
95. S. Link and M. A. El-Sayed, *The Journal of Physical Chemistry B*, 1999, **103**, 4212-4217.
96. P. K. Jain, X. Huang, I. H. El-Sayed and M. A. El-Sayed, *Plasmonics*, 2007, **2**, 107-118.
97. X. Huang, P. K. Jain, I. H. El-Sayed and M. A. El-Sayed, *Lasers in medical science*, 2008, **23**, 217-228.
98. S. Zhu, C. Du and Y. Fu, *Optical Materials*, 2009, **31**, 769-774.
99. K. Gracie, E. Correa, S. Mabbott, J. A. Dougan, D. Graham, R. Goodacre and K. Faulds, *Chemical Science*, 2014, **5**, 1030-1040.
100. M. Y. Ho, N. D'Souza and P. Migliorato, *Analytical chemistry*, 2012, **84**, 4245-4247.
101. G. Padeletti and P. Fermo, *Applied Physics A*, 2003, **76**, 515-525.
102. I. Freestone, N. Meeks, M. Sax and C. Higgitt, *Gold Bulletin*, **40**, 270-277.
103. M. Faraday, *Philosophical Transactions of the Royal Society of London*, 1857, **147**, 145-181.
104. K. Takei, H. Fang, S. B. Kumar, R. Kapadia, Q. Gao, M. Madsen, H. S. Kim, C.-H. Liu, Y.-L. Chueh and E. Plis, *Nano letters*, 2011, **11**, 5008-5012.
105. P. Lee and D. Meisel, *The Journal of Physical Chemistry*, 1982, **86**, 3391-3395.
106. P. K. Jain, K. S. Lee, I. H. El-Sayed and M. A. El-Sayed, *The Journal of Physical Chemistry B*, 2006, **110**, 7238-7248.
107. Y. Chen, K. Munechika and D. S. Ginger, *Nano letters*, 2007, **7**, 690-696.
108. M. Hu, J. Chen, Z.-Y. Li, L. Au, G. V. Hartland, X. Li, M. Marquez and Y. Xia, *Chemical society reviews*, 2006, **35**, 1084-1094.

109. K. A. Willets and R. P. Van Duyne, *Annu. Rev. Phys. Chem.*, 2007, **58**, 267-297.
110. S. Link, Z. L. Wang and M. El-Sayed, *The Journal of Physical Chemistry B*, 1999, **103**, 3529-3533.
111. N. Vigneshwaran, N. M. Ashtaputre, P. V. Varadarajan, R. P. Nachane, K. M. Paralikar and R. H. Balasubramanya, *Materials Letters*, 2007, **61**, 1413-1418.
112. N. Kallay and S. Žalac, *Journal of colloid and interface science*, 2002, **253**, 70-76.
113. J. Turkevich, P. Stevenson and J. Hillier, *A General Discussion of the Faraday Society*, 1951, **11**, 55.
114. L. Barrett, J. A. Dougan, K. Faulds and D. Graham, *Nanoscale*, 2011, **3**, 3221-3227.
115. P. P. Edwards and J. M. Thomas, *Angewandte Chemie International Edition*, 2007, **46**, 5480-5486.
116. N. S. Lee, R. S. Sheng, M. D. Morris and L. M. Schopfer, *Journal of the American Chemical Society*, 1986, **108**, 6179-6183.
117. R. M. Bright, M. D. Musick and M. J. Natan, *Langmuir*, 1998, **14**, 5695-5701.
118. N. Saifuddin, C. Wong and A. Yasumira, *Journal of Chemistry*, 2009, **6**, 61-70.
119. E. L. Holthoff, D. N. Stratis-Cullum and M. E. Hankus, *Sensors*, 2011, **11**, 2700-2714.
120. S. Z. Nergiz, N. Gandra, M. E. Farrell, L. Tian, P. M. Pellegrino and S. Singamaneni, *Journal of Materials Chemistry A*, 2013, **1**, 6543-6549.
121. J. Chen, J. Jiang, X. Gao, G. Liu, G. Shen and R. Yu, *Chemistry-A European Journal*, 2008, **14**, 8374-8382.
122. M. Sanles-Sobrido, L. Rodríguez-Lorenzo, S. Lorenzo-Abalde, Á. González-Fernández, M. A. Correa-Duarte, R. A. Alvarez-Puebla and L. M. Liz-Marzán, *Nanoscale*, 2009, **1**, 153-158.
123. J. G. Skinner and W. G. Nilsen, *J. Opt. Soc. Am.*, 1968, **58**, 113-119.
124. C. Julien, A. Débarre, D. Nutarelli, A. Richard and P. Tchénio, *The Journal of Physical Chemistry B*, 2005, **109**, 23145-23153.
125. R. Aroca, *Surface-enhanced vibrational spectroscopy*, John Wiley & Sons, 2006.
126. K. L. McNesby, J. E. Wolfe, J. B. Morris and R. Pesce-Rodriguez, *Journal of Raman Spectroscopy*, 1994, **25**, 75-87.
127. D. B. Chase, *Journal of the American Chemical Society*, 1986, **108**, 7485-7488.
128. H. Wackerbarth, C. Salb, L. Gundrum, M. Niederkrüger, K. Christou, V. Beushausen and W. Viöl, *Applied optics*, 2010, **49**, 4362-4366.
129. K. Kneipp, Y. Wang, R. R. Dasari, M. S. Feld, B. D. Gilbert, J. Janni and J. I. Steinfeld, *Spectrochimica Acta Part A: Molecular and Biomolecular Spectroscopy*, 1995, **51**, 2171-2175.
130. N. A. Hatab, G. Eres, P. B. Hatzinger and B. Gu, *Journal of Raman Spectroscopy*, 2010, **41**, 1131-1136.
131. S. Botti, S. Almaviva, L. Cantarini, A. Palucci, A. Puiu and A. Rufoloni, *Journal of Raman Spectroscopy*, 2013, **44**, 463-468.

132. C. J. McHugh, A. R. Kennedy, W. E. Smith and D. Graham, *Analyst*, 2007, **132**, 986-988.
133. C. A. Manrique-Bastidas, O. M. Primera-Pedrozo, L. C. Pacheco-Londono and S. P. Hernandez-Rivera, European Symposium on Optics and Photonics for Defence and Security, 2004.
134. nanocomposix, *ZETA POTENTIAL ANALYSIS OF NANOPARTICLES*, https://cdn.shopify.com/s/files/1/0257/8237/files/nanoComposix_Guidelines_for_Zeta_Potential_Analysis_of_Nanoparticles.pdf.
135. D. Graham, D. G. Thompson, W. E. Smith and K. Faulds, *Nature nanotechnology*, 2008, **3**, 548-551.
136. T. A. Taton, C. A. Mirkin and R. L. Letsinger, *science*, 2000, **289**, 1757-1760.
137. K. Faulds, R. E. Littleford, D. Graham, G. Dent and W. E. Smith, *Analytical chemistry*, 2004, **76**, 592-598.
138. A. M. E. Badawy, T. P. Luxton, R. G. Silva, K. G. Scheckel, M. T. Suidan and T. M. Tolaymat, *Environmental science & technology*, 2010, **44**, 1260-1266.
139. M. Kerker, O. Siiman, L. Bumm and D. Wang, *Surface enhanced Raman scattering (SERS) of citrate ion adsorbed on colloidal silver*, Defense Technical Information Center, 1980.
140. D. Begue, P. Carbonnière and C. Pouchan, *The Journal of Physical Chemistry A*, 2005, **109**, 4611-4616.
141. C. M. Ramos, L. F. Alzate, N. M. Hernández, S. P. Hernández and N. Mina, *Journal of Molecular Structure: THEOCHEM*, 2006, **769**, 69-76.
142. E. M. Ali, H. G. Edwards and I. J. Scowen, *Talanta*, 2009, **78**, 1201-1203.
143. R. R. Naik, S. E. Jones, C. J. Murray, J. C. McAuliffe, R. A. Vaia and M. O. Stone, *Advanced Functional Materials*, 2004, **14**, 25-30.
144. I. H. El-Sayed, X. Huang and M. A. El-Sayed, *Cancer letters*, 2006, **239**, 129-135.
145. A. Subramanian and W. H. Velander, *Journal of Molecular Recognition*, 1996, **9**, 528-535.
146. A. K. Trilling, J. Beekwilder and H. Zuilhof, *Analyst*, 2013, **138**, 1619-1627.
147. B. N. Johnson and R. Mutharasan, *Langmuir*, 2012, **28**, 6928-6934.
148. S. J. Kim, K. V. Gobi, R. Harada, D. R. Shankaran and N. Miura, *Sensors and Actuators B: Chemical*, 2006, **115**, 349-356.
149. M. Lynch, C. Mosher, J. Huff, S. Nettikadan, J. Johnson and E. Henderson, *Proteomics*, 2004, **4**, 1695-1702.
150. X. Zhao, F. Pan, B. Cowsill, J. R. Lu, L. Garcia-Gancedo, A. J. Flewitt, G. M. Ashley and J. Luo, *Langmuir*, 2011, **27**, 7654-7662.
151. P. Hildebrandt and M. Stockburger, *Journal of Raman Spectroscopy*, 1986, **17**, 55-58.
152. A. Matschulat, D. Drescher and J. Kneipp, *ACS Nano*, 2010, **4**, 3259-3269.
153. R. Goodacre, R. Burton, N. Kaderbhai, A. M. Woodward, D. B. Kell and P. J. Rooney, *Microbiology*, 1998, **144**, 1157-1170.
154. É. M. Timmins, S. A. Howell, B. K. Alsberg, W. C. Noble and R. Goodacre, *Journal of Clinical Microbiology*, 1998, **36**, 367-374.
155. J. Clarkson, W. E. Smith, D. N. Batchelder, D. A. Smith and A. M. Coats, *Journal of Molecular Structure*, 2003, **648**, 203-214.

156. H. Xu, X. Zhao, C. Grant, J. R. Lu, D. E. Williams and J. Penfold, *Langmuir*, 2006, **22**, 6313-6320.
157. A. P. Le Brun, S. A. Holt, D. S. Shah, C. F. Majkrzak and J. H. Lakey, *Biomaterials*, 2011, **32**, 3303-3311.
158. G. Binnig, C. F. Quate and C. Gerber, *Physical review letters*, 1986, **56**, 930.
159. J. B. Daniel, A. B. William, C. Neal, K. Jennifer and H. T. Neil, *Physical Biology*, 2012, **9**, 021001.
160. C.-Y. Hsu, J.-W. Huang and K.-J. Lin, *Chemical Communications*, 2011, **47**, 872-874.
161. P. T. Charles and A. W. Kusterbeck, *Biosensors and Bioelectronics*, 1999, **14**, 387-396.
162. T. Teslova, C. Corredor, R. Livingstone, T. Spataru, R. L. Birke, J. R. Lombardi, M. Canamares and M. Leona, *Journal of Raman Spectroscopy*, 2007, **38**, 802-818.
163. J. M. Dudik, C. R. Johnson and S. A. Asher, *The Journal of Physical Chemistry*, 1985, **89**, 3805-3814.
164. F. E. Malherbe and H. J. Bernstein, *Journal of the American Chemical Society*, 1952, **74**, 4408-4410.
165. C. A. Tulk, D. D. Klug and J. A. Ripmeester, *The Journal of Physical Chemistry A*, 1998, **102**, 8734-8739.
166. P. Neelakantan, *Proceedings of the Indian Academy of Sciences - Section A*, **57**, 330-336.
167. A. J. Russell, L. J. Trudel, P. L. Skipper, J. D. Groopman, S. R. Tannenbaum and A. M. Klibanov, *Biochemical and Biophysical Research Communications*, 1989, **158**, 80-85.
168. J. Lippincott-Schwartz, *Current Protocols in Cell Biology*, 16.10. 11-16.10. 12.
169. N. Jenkins, R. B. Parekh and D. C. James, *Nature biotechnology*, 1996, **14**, 975-981.
170. R. Jefferis, *Nat Rev Drug Discov*, 2009, **8**, 226-234.
171. Z. Zhou, J. Zhang, Y. Zhang, G. Ma and Z. Su, *Bioconjugate chemistry*, 2015.
172. H. Häkkinen, *Nature chemistry*, 2012, **4**, 443-455.
173. Y. Wang and L. Tang, *Biosensors and Bioelectronics*, 2015, **67**, 18-24.
174. X. Wang, Z. Mei, Y. Wang and L. Tang, *Talanta*, 2014.
175. A. A. Deckert, K. A. Anderson, K. M. Mullaugh and C. Delaney, *The Journal of Physical Chemistry B*, 2004, **108**, 15808-15814.
176. X. Li, Q. Zhang, Z. Li, X. Wang, J. Liu, S. Cui, S. Xu, C. Zhao, C. Chen and K. Guo, *Polymer*, 2016, **84**, 293-303.
177. J. J. Pastuszak and A. Chimiak, *The Journal of Organic Chemistry*, 1981, **46**, 1868-1873.
178. D. Veber, J. Milkowski, S. Varga, R. Denkewalter and R. Hirschmann, *Journal of the American Chemical Society*, 1972, **94**, 5456-5461.
179. J. R. Whitaker and P. E. Granum, *Analytical biochemistry*, 1980, **109**, 156-159.
180. S. Mori and H. G. Barth, *Size exclusion chromatography*, Springer Science & Business Media, 2013.

181. M. Gilar, P. Olivova, A. E. Daly and J. C. Gebler, *Journal of separation science*, 2005, **28**, 1694-1703.
182. J. F. Ken Cook, Valeria Barattini, ed. T. F. Scientific, 2012.
183. K. Gracie, W. Smith, P. Yip, J. Sutter, D. Birch, D. Graham and K. Faulds, *Analyst*, 2014, **139**, 3735-3743.
184. N. Nitin, L. LaConte, O. Zurkiya, X. Hu and G. Bao, *JBIC Journal of Biological Inorganic Chemistry*, 2004, **9**, 706-712.
185. T. Donnelly, W. E. Smith, K. Faulds and D. Graham, *Chemical Communications*, 2014, **50**, 12907-12910.
186. G. Reiss and A. Hütten, *Nature materials*, 2005, **4**, 725-726.
187. J. Dobson, *Drug development research*, 2006, **67**, 55-60.
188. M. Johannsen, U. Gneveckow, L. Eckelt, A. Feussner, N. Waldöfner, R. Scholz, S. Deger, P. Wust, S. Loening and A. Jordan, *International journal of hyperthermia*, 2005, **21**, 637-647.
189. B. Martinez, X. Obradors, L. Balcells, A. Rouanet and C. Monty, *Physical Review Letters*, 1998, **80**, 181.
190. J.-H. Lee, J.-t. Jang, J.-s. Choi, S. H. Moon, S.-h. Noh, J.-w. Kim, J.-G. Kim, I.-S. Kim, K. I. Park and J. Cheon, *Nature nanotechnology*, 2011, **6**, 418-422.
191. A. H. Lu, E. e. L. Salabas and F. Schüth, *Angewandte Chemie International Edition*, 2007, **46**, 1222-1244.
192. S. Dutz, R. Hergt, J. Mürbe, R. Müller, M. Zeisberger, W. Andrä, J. Töpfer and M. Bellemann, *Journal of Magnetism and Magnetic Materials*, 2007, **308**, 305-312.
193. J. Dormann, L. Bessais and D. Fiorani, *Journal of Physics C: Solid State Physics*, 1988, **21**, 2015.
194. S. Sun, C. Murray, D. Weller, L. Folks and A. Moser, *Science*, 2000, **287**, 1989-1992.
195. C. Chinnasamy, A. Narayanasamy, N. Ponpandian, K. Chattopadhyay, H. Guerault and J. Greneche, *Journal of Physics: Condensed Matter*, 2000, **12**, 7795.
196. R. H. Kodama, S. A. Makhlouf and A. E. Berkowitz, *Physical Review Letters*, 1997, **79**, 1393.
197. R. Hergt, S. Dutz and M. Zeisberger, *Nanotechnology*, 2009, **21**, 015706.
198. Q. A. Pankhurst, J. Connolly, S. Jones and J. Dobson, *Journal of physics D: Applied physics*, 2003, **36**, R167.
199. M. Mandal, S. Kundu, S. K. Ghosh, S. Panigrahi, T. K. Sau, S. M. Yusuf and T. Pal, *Journal of Colloid and Interface Science*, 2005, **286**, 187-194.
200. N. A. Frey, S. Peng, K. Cheng and S. Sun, *Chemical Society Reviews*, 2009, **38**, 2532-2542.
201. Z. Wang, P. Xiao and N. He, *Carbon*, 2006, **44**, 3277-3284.
202. T. K. Jain, M. A. Morales, S. K. Sahoo, D. L. Leslie-Pelecky and V. Labhasetwar, *Molecular Pharmaceutics*, 2005, **2**, 194-205.
203. R. C. Huxford, J. Della Rocca and W. Lin, *Current opinion in chemical biology*, 2010, **14**, 262-268.
204. Y. Jiang, H. Zhao, N. Zhu, Y. Lin, P. Yu and L. Mao, *Angewandte Chemie*, 2008, **120**, 8729-8732.
205. K. Qian, H. Liu, L. Yang and J. Liu, *Analyst*, 2012, **137**, 4644-4646.

206.   S. S. Dasary, A. K. Singh, D. Senapati, H. Yu and P. C. Ray, *Journal of the American Chemical Society*, 2009, **131**, 13806-13812.
207.   I. Bjork, B.-A. Petersson and J. Sjoquist, *Eur. J. Biochem.*, 1972, **29**, 579-584.
208.   M. Horisberger and M.-F. Clerc, *Histochemistry*, 1985, **82**, 219-223.
209.   S. D. Flanagan and B. Yost, *Analytical biochemistry*, 1984, **140**, 510-519.
210.   Y. Xiao and S. N. Isaacs, *Journal of immunological methods*, 2012, **384**, 148-151.